RATIONAL DESIGN OF MENE INHIBITORS:
THE DESIGN AND DEVELOPMENT OF NOVEL ANTIBIOTICS

A Dissertation

Presented to the Faculty of the Weill Cornell Graduate School

of Medical Sciences

in Partial Fulfillment of the Requirements for the Degree of

Doctor of Philosophy

by

Christopher Edward Evans

August 2017

Rational Design of MenE Inhibitors:

The Design and Development of Novel Antibiotics

Christopher E. Evans

Cornell University 2017

In order for our society to avoid entering a post-antibiotic era, we need new antibiotics that function through pathways and mechanisms previously untargeted by our current regimen of antibiotics. One such pathway is that of menaquinone biosynthesis. Menaquinone is responsible for electron transport in bacterial respiration and is required for the growth and proliferation of many virulent bacteria such as *Mycobacterium tuberculosis*. Herein, we report efforts in developing a new class of antibiotics, which aim to inhibit menaquinone biosynthesis through targeting of a key enzyme in the biosynthetic pathway, MenE. MenE is an acyl-CoA ligase, which converts *o*-succinyl benzoate (OSB) to OSB-CoA via an OSB-AMP intermediate. Using 5'-*O*-(*N*-acylsulfamoyl) adenosine (acyl-AMS) analogues of the cognate acyl-AMP intermediate, we can effectively inhibit MenE in biochemical assays, but these inhibitors show poor cellular activity as well as unfavorable physicochemical and pharmacological properties, impeding the progression of this inhibitor platform. Utilizing crystal and docking structures, exploration of the structure-activity relationships of the scaffold, and the unique keto-acid/lactol equilibrium of OSB-AMS, we are developing a series of second and third generation OSB-AMS analogues designed to increase cellular activity and progress this inhibitor class.

BIOGRAPHICAL SKETCH

Christopher Evans was born in Casper, Wyoming, on July 8, 1985. He grew up in small towns throughout the northwest United States. After graduating from Columbia Falls High School in Montana, he took five years to travel, work, and meet his future wife Rachel Evans. While working in construction, he began reading textbooks during his lunch break and gradually realized his interest in science was best suited in a different career. Working the night shift in a local manufacturing plant, he began attending Eastern Washington University as a chemistry major. Here, under the guidance of Professor Travis Denton, his passion for the design and development of chemical tools to modify biological systems bloomed. In the laboratory of Professor Denton, he focused his efforts towards the design of biodegradable, sugar-based quaternary ammonium polymers and their testing and application as effective biocides against a variety of bacteria. In 2011, he graduated with a B.S in Chemistry and Biochemistry, and soon after began his graduate studies at the Weill Cornell Graduate School of Medical Sciences. Under the guidance and mentorship of Professor Derek Tan at Memorial Sloan Kettering Cancer Center, his graduate work has focused on the rational design and development of MenE inhibitors as novel antibiotics. Following his graduation, he will be joining the medicinal chemistry team of Cytokinetics, where he will work towards treatments for a variety of neuromuscular diseases.

ACKNOWLEDGMENTS

“There is no such thing as a 'self-made' man. We are made up of thousands of others. Everyone who has ever done a kind deed for us, or spoken one word of encouragement to us, has entered into the make-up of our character and of our thoughts, as well as our success” – George Burton Adams

I would like to thank Prof. Derek Tan for his mentorship and support throughout my time in his lab. Derek has continually given me the independence and freedom to explore my project and follow it wherever it led. The lessons I have learned and skills I have acquired at the bench and at the podium, will forever be a part of who I am as a scientist. I thank also the members of my dissertation committee Prof. Anthony Sauve and Professor Samuel Danishefsky for the years of valuable time, guidance, and support. I am also grateful for Prof. Minkui Luo, Prof. Michael Glickman, and Prof. Yueming Li for being essential and highly valued members of my thesis defense committee. I would like to thank the past and present members of the Tan, Gin, and Danishefsky labs, who have always provided a rich and productive environment with which to work and together have taught me more practical chemistry than I have ever learned in a classroom. A special thanks to the members of the lab of Professor Peter Tonge, who worked together with me on this project and have helped shape it into what it is today. In particular, I would like to thank Dr. Joe Matarlo, for all of the great work, support, and patient explanation for every question I had about his field.

Lastly, I would like to thank my friends and family. I would not be here if not for your love and support throughout my journey, and I will never forget all that you have done for me.

TABLE OF CONTENTS

LIST OF FIGURES

CHAPTER 1

CHAPTER 2

CHAPTER 3

CHAPTER 4

CHAPTER 5

LIST OF TABLES

LIST OF ABBREVIATIONS

Å	angstrom
Ac	acetyl
Ac_2O	acetic anhydride
ADME	absorption distribution metabolism excretion
AMP	adenosine monophosphate
AMS	adenosine monosulfamate
anhyd	anhydrous
aq	aqueous
ATP	adenosine triphosphate
BINAP	2,2'-bis(diphenylphosphino)-1,1'-binaphthyl)
BINOL	1,1'-Bi-2-naphthol
Bn	benzyl
BOM	benzyloxymethyl acetal
Bu	butyl
Bz	benzoyl
ºC	degrees Celsius
c	concentration
CAM	ceric ammonium molybdate
CDC	Centers for Disease Control and Prevention
$CDCl_3$	deuterated chloroform
CH_2Cl_2	methylene chloride
MeCN	acetonitrile
CuKα	copper K-α X-ray energy
dtbpf	1,1'-bis(di-*t*-butylphosphino)ferrocene
DHNA	demethylmenaquinone
DIAD	diisopropyl azodicarboxylate
DIP	Diisopinocampheylborane
DMA	*N*,*N*-dimethylacetamide
DMAP	*N*,*N*-dimethyl-4-aminopyridine
DMF	*N*,*N*-dimethylformamide
DMK	demethylmenaquinone
dppp	1,3-bis(diphenylphosphino)propane
DIPEA	diisopropylethylamine
dr	diastereomeric ratio
EDCI	1-ethyl-3-(3-dimethylaminopropyl)carbodiimide
ent	enantiomer
equiv	equivalents

ESI-MS	electrospray ionization-mass spectrometry
Et	ethyl
Et_2O	diethyl ether
EtOAc	ethyl acetate
g	gram
h	hour
HMDS	hexamethyldisilazane
HRMS	high-resolution mass spectrometry
HPLC	high-performance liquid chromatography
Hz	hertz
IC50	half maximal inhibitory concentration
*i*Pr	isopropyl
IR	infrared
ITC	isothermal titration calorimetry
J	coupling constant
KHMDS	potassium hexamethyldisilazane
LC	liquid chromatography
LDA	lithium diisopropylamide
LiHMDS	lithium hexamethyldisilazane
M	molar
Me	methyl
MeOD	deuterated methanol
MeOH	methanol
mg	milligram(s)
MIC	minimum inhibitory concentration
min	minutes
MK4	menaquinone-4
mL	milliliter(s)
mmol	millimole(s)
MRSA	methicillin-resistant *Staphylococcus aureus*
MS	mass spectrometry
MW	molecular weight
NBS	*N*-bromosuccinimide
NIH	National Institutes of Health
NMR	nuclear magnetic resonance
NMO	*N*-methylmorpholine-N-oxide
NRPS	nonribosomyl peptide synthesis
OSB	*o*-succinylbenzoate

PG	protecting group
Ph	phenyl
Pin	pinacolato
PP_i	inorganic pyrophosphate
ppm	parts per million
R	alkyl group (generic)
RR-TB	rifampicin-resistant *M. tuberculosis*
SAR	structure-activity relationship
satd	saturated
t	time
T	time
TASF	tris(dimethylamino)sulfonium difluorotrimethylsilicate
TB	*M. tuberculosis*
TBAF	tetrabutylammonium fluoride
TBS	*tert*-butyldimethylsilyl
TFA	trifluoroacetic acid
TFAA	trifluoroacetic anhydride
THF	tetrahydrofuran
TMS	trimethylsilane
TLC	thin layer chromatography
TPAP	tetrapropylammonium perruthenate
Ts	tosyl
δ	chemical shift (parts per million)
µ	micro

CHAPTER 1

INHIBITION OF MENAQUINONE BIOSYNTHESIS AS A NOVEL ANTIMICROBIAL TARGET

1.1 The Problem of Antimicrobial Resistance

The proliferation of drug resistant bacteria presents a global health threat that cannot be ignored. The current Centers for Disease Control and Prevention (CDC) report on instances of drug-resistant bacteria in the US show an average rate of 80,000 new reported cases of severe methicillin-resistant *Staphylococcus aureus* (MRSA) infections each year, resulting in 11,000 deaths annually.[1] While the human cost of infection and associated morbidity should not be ignored, the cost to our society and healthcare systems these infections represent is also of great concern. The average treatment cost for a single case of MRSA is $34,657,[2] and when considered with the aforementioned CDC data suggests an annual cost of $2.8 billion to the US healthcare system. It is important to note that this cost addresses only MRSA cases. The CDC estimates at least 2 million people become infected with a variety of bacteria that are resistant antibiotics each year.[1]

A microbe less common in the US but posing a global health threat is drug-resistant *M. tuberculosis* (TB). In the most recent World Health Organization (WHO) global tuberculosis report, they estimate in 2015 there were approximately 10.4 million new cases of TB, 480,000 new cases of multi-drug resistant TB (MDR-TB), and 100,000 new cases of rifampicin-resistant TB (RR-TB), which resulted in an estimated 1.4 million deaths.[3] Therefore, the proliferation of drug-resistant bacteria poses a national and global threat to human lives as well as our economies as a whole.

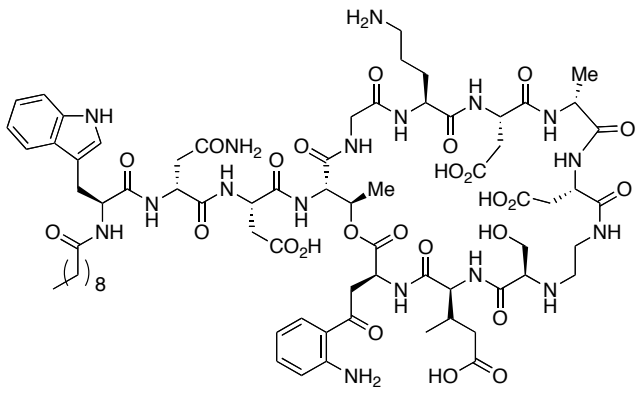

daptomycin

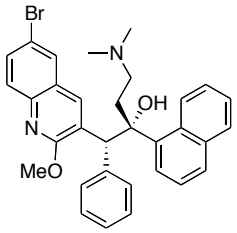

bedaquiline

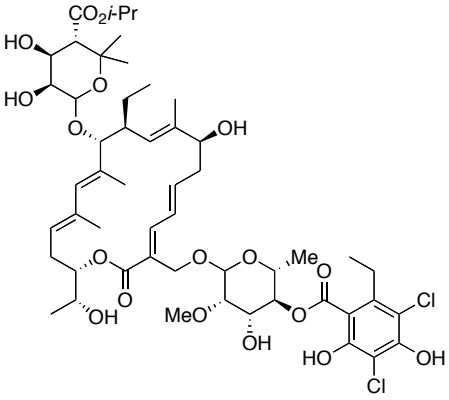

fidaxomicin

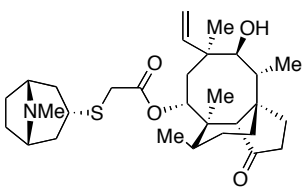

retapamulin

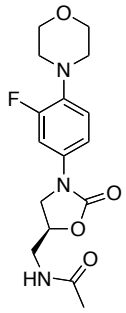

linezolid

Figure 1.1. Structures of recent approved novel antibiotics.

Unfortunately, the increase in drug-resistant microbes has accompanied a sharp decline in the number of companies investigating new antibiotics and consequently, the number of new antibiotics to be introduced to the market.[4-5] From the period of ~1970 to 2005, there were no novel antibiotics introduced to the market. While new antibiotics were reported and approved for use during this time period, they all relied on previously discovered scaffolds and mechanisms of action.[6] Since then, there have been four novel classes of antibiotics to be approved (Figure 1.1):[7]

diarylquinolines (bedaquiline),[8] oxazolidinones (linezolid),[9] lipopeptides (daptomycin),[10] and tiacumicins (fidaxomicin).[11] Another novel antimicrobial agent class released during this time is the pleuromutilins (retapamulin),[12] however these compounds are approved only for topical treatment of skin infections.

Although the recent influx of novel antibiotics is promising and shows a slight reversal of the trends observed in the previous 35 years, these new antibiotics are typically narrow spectrum and carry with them severe toxicity profiles, making them drugs of last resort in most cases.[13-17] Taken together, the increase in the spread of drug-resistant bacteria, the cost in human lives and to our healthcare systems, and relative decline in new antibiotics over the past 60 years, makes it clear that we need new antibiotics that inhibit pathways previously untargeted by our current arsenal.

1.2 Menaquinone Biosynthesis

Menaquinone (vitamin K_2), ubiquinone, and phylloquinone belong to a class of lipid-soluble electron carriers (lipoquinones), and are essential for cellular function for all living organisms (Figure 1.2A).[18-21] Menaquinone acts as a redox-active cofactor for many proteins, including the electron transport chain of many species of bacteria during cellular respiration.[22] Importantly, it is the sole electron carrier for all Gram-positive bacteria, mycobacteria, and all bacteria growing anaerobically.[23-25]

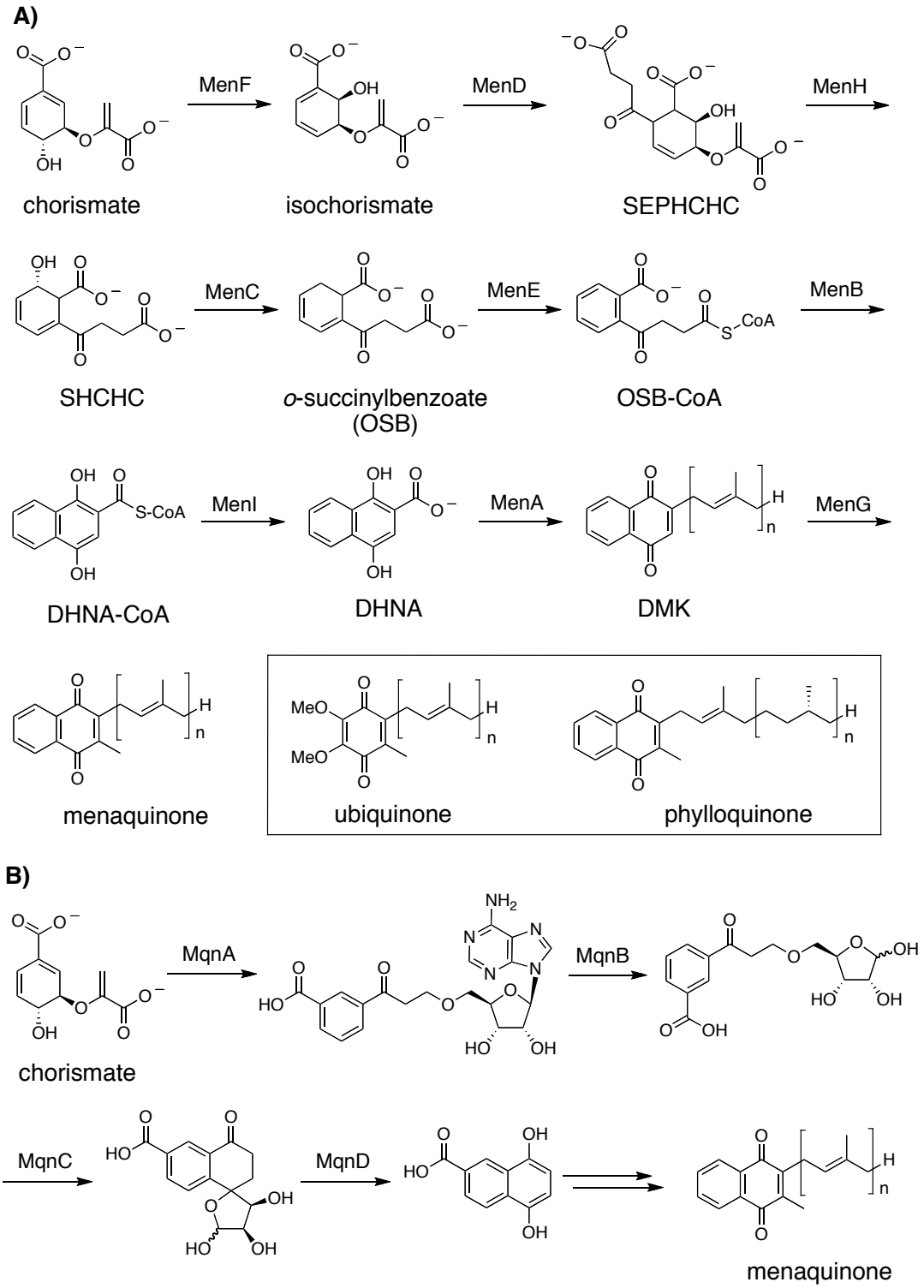

Figure 1.2. Menaquinone biosynthesis A) Canonical menaquinone biosynthetic pathway. B) Alternative biosynthetic pathway (futalosine). Menaquinone n = 4-13, Ubiquinone n = 6-13, Phylloquinone n = 3. SEPHCHC = 2-succinyl-5-enolpyruvyl-6-hydroxy-3-cyclohexene-1-carboxylic acid, SHCHC = 2-succinyl-6-hydroxy-2,4-cyclohexadiene-1-carboxylate, DHNA = 1,4-di-hydroxy-2-naphthoic acid, DMK = demethylmenaquinone.

Menaquinone is commonly produced in bacteria from chorismate, through at least nine distinct enzymes (Figure 1.2A).[20,26-27] Through genetic work by several groups, the main biosynthetic pathway has been shown to be essential for survival and proliferation of bacteria for which it is the sole electron transporter.[23-25] Although some Gram-negative bacteria such as *Helicobacter pylori*, use an alternative biosynthetic pathway to produce menaquinone (futalosine, Figure 1.2B), the two pathways are mutually exclusive with the majority of pathogenic bacteria using the canonical menaquinone biosynthetic pathway.[25,28-29]

Menaquinone is also used in mammals as a cofactor for vitamin K dependent proteins, which are known to play a role in vascular cell migration, angiogenesis, and blood-clotting cascades.[30-31] However, humans lack the necessary *de novo* pathway to produce menaquinone and must acquire it from diet (phylloquinone from plants) and gut flora,[30,32] making menaquinone biosynthesis an attractive target for the development of novel of antibiotics.

Many groups have recognized menaquinone's unique niche in relevant biological systems and have developed inhibitors of the biosynthetic pathway as potential antimicrobial agents. To date, inhibitors of the biosynthetic pathway have been reported for MenD,[33-34] MenC,[35] MenE,[36-40] MenB,[41-43] MenA,[44-47] and MenG.[48] Importantly, these compounds have all shown antimicrobial activity in a variety of bacteria, including *M. tuberculosis*. These findings also provide pharmacological validation of the earlier genetic studies showing menaquinone biosynthesis to be essential and a potential target for future antibiotics.

1.2 MenE: An Acyl-CoA Synthetase

MenE is an acyl-CoA synthetase (ligase) in the menaquinone biosynthetic pathway and has been shown through genetic knockout studies to be essential for the survival and fecundity of *Mycobateria* spp., *Bacillus* spp., and other bacterial species, both pathogenic and nonpathogenic.[49-51] MenE catalyzes the thioesterification of *ortho*-succinylbenzoate (OSB) with CoA through an ordered *bi uni uni bi* ping-pong mechanism in the presence of Mg^{2+} and ATP (Figure 1.3).[37,40] In the first half-reaction, MenE catalyzes the adenylation of OSB with ATP, expelling inorganic pyrophosphate, to form a tightly bound OSB-AMP intermediate. MenE then catalyzes the second half-reaction, binding CoA, which attacks the activated carboxylate of OSB, to form OSB-CoA and release AMP.[41,52-53]

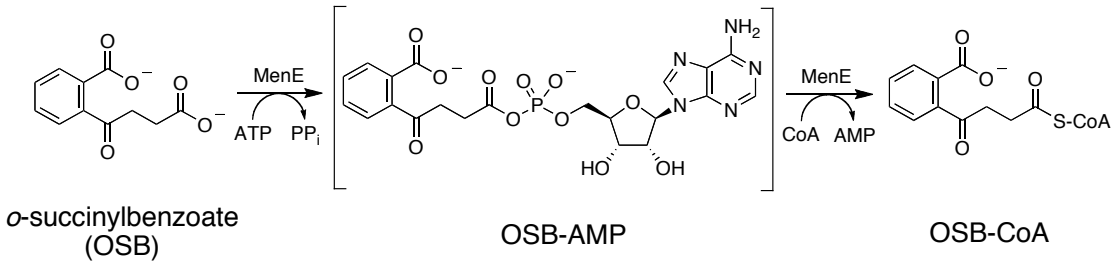

Figure 1.3. MenE mechanism of action. AMP = adenosine monophophate, ATP = adenosine triphosphate, PP_i = inorganic pyrophosphate.

MenE, as an acyl-CoA synthetase, belongs to the ANL (acyl-CoA synthetase, nonribosomal peptide synthetase adenylation domain, luciferase) protein family.[54] Proteins in this family share a similar structure containing a C-terminal "lid" domain connected via a flexible hinge to a much larger N-terminal "hammer and anvil" domain. This general architecture is observed for all members of the ANL family of adenylation enzymes (Figure 1.4).[55-56]

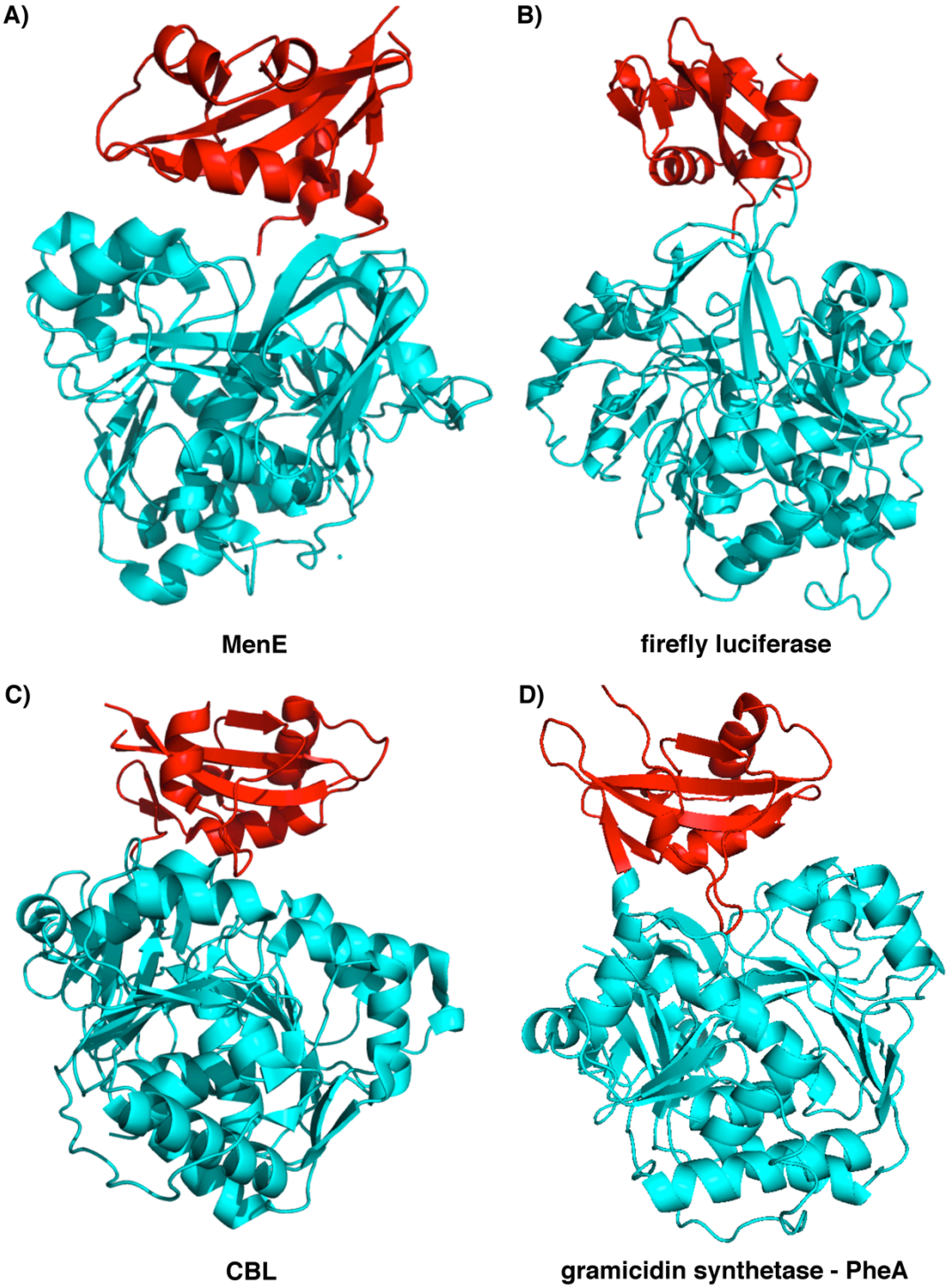

Figure 1.4. ANL family members. C-terminal domain = cyan, N-terminal domain = green. A) MenE, OSB-CoA synthetase, (PDB ID: 3IPL).[57] B) Firefly Luciferase (PDB ID: 1LCI).[55] C) CBL, 4-Chlorobenzoate-CoA synthetase, (PDB ID: 3CW8).[58] D) Gramicidin Synthetase, Phenylalanine-CoA synthetase (PDB ID: 1AMU).[59]

The ANL family is itself a member of the much larger adenylate-forming enzyme superfamily which also includes aminoacyl-tRNA synthetases, E1 activating enzymes, A-ATPases, biotin protein ligase, and NRPS-independent siderophore (NIS) synthetases.[54] The members of this superfamily have large variability in structure, but all catalyze the activation of carboxylic acid substrates through adenylation to form an acyl-AMS intermediate, followed by coupling with nitrogen, oxygen, and sulfur nucleophiles by carbonyl addition–elimination.[56]

1.3 Inhibition of MenE and related cellular activity

Due to the reactivity of the acyl-AMP intermediate, adenylate forming enzymes such as MenE, bind their cognate acyl-AMP intermediate several orders of magnitude more strongly than the corresponding carboxylate and AMP starting materials.[60-62] This tight-binding sequestration by the enzyme of its cognate acyl-AMP intermediate has been exploited successfully by groups using rationally designed inhibitors that mimic the cognate ligand.[63-64] The most successful and widespread inhibitors use the non-hydrolyzable acyl-AMP bioisostere, acyl-5′-*O*-sulfamoyladenosine (acyl-AMS) or acyl-5′-*N*-sulfamoylazadeoxyadenosine (acyl-AMSN).[65]

Acyl-AMS based inhibitors draw inspiration from the natural products ascamycin[66-68] and nucleocidin,[69-70] which themselves have potent antimicrobial activity (Figure 1.5). Synthetic acyl-AMS inhibitors were first pioneered by Ishida and coworkers, where he explored the use L-alanyl-AMS as an inhibitor of alanyl-tRNA synthetases.[71] This inhibition strategy has since been applied to a wide swath of the adenylate-forming enzyme superfamily, including those of the ANL family,[72-74] E1-activating enzymes,[75-77] asparagine

synthetases,[78] and pantothenate synthetases.[79]

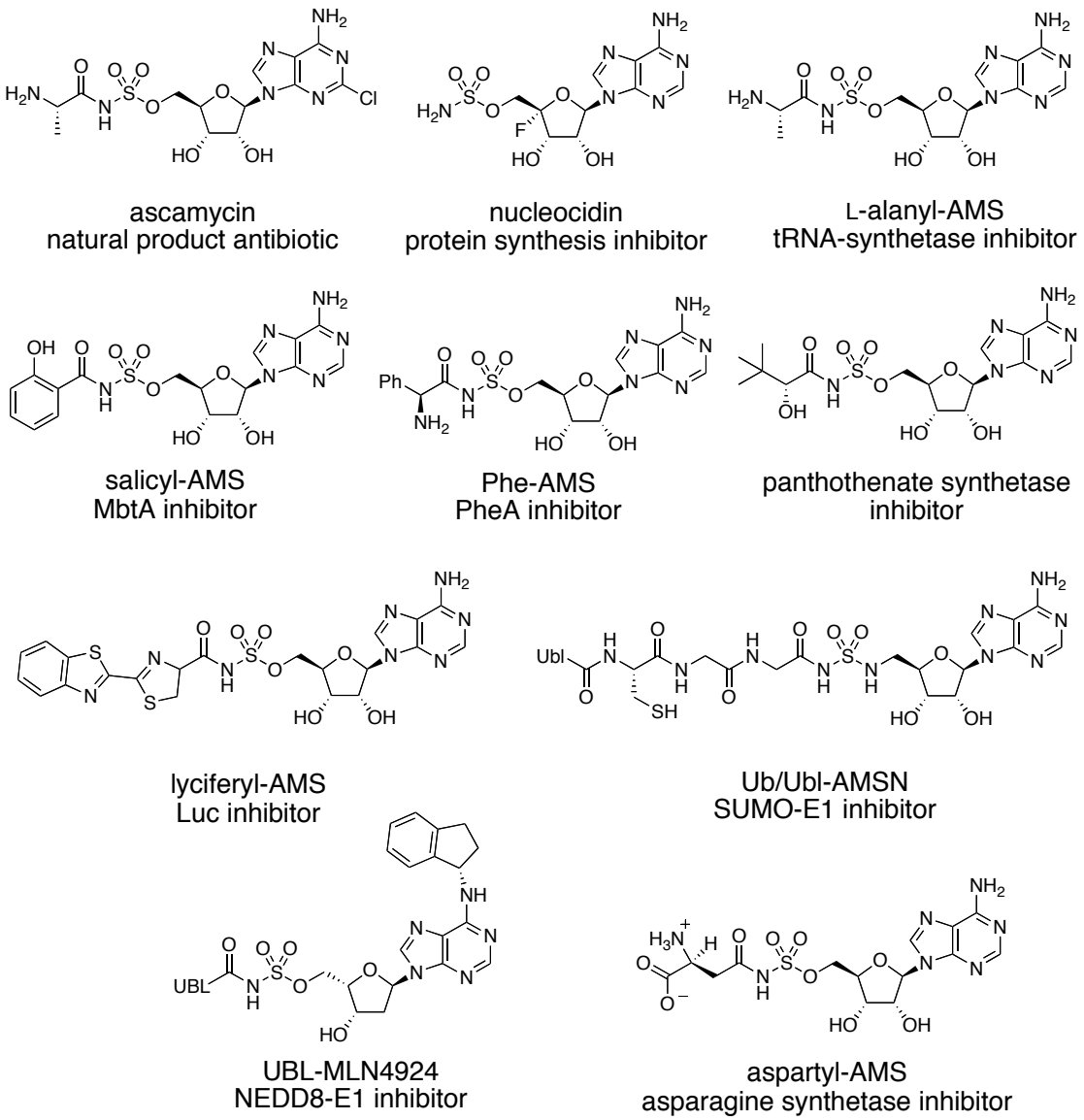

Figure 1.5. Examples of reported acyl-AMS inhibitors for adenylation-forming enzmes.

Work in our laboratory[36-37] and others[40] have used this well established acyl-AMS strategy to target MenE. Mesecar and coworkers reported in 2008, the synthesis of acyl-AMS based OSB-AMP analogue **1** (Figure 1.6), which substituted a trifluoromethyl group in place of the *ortho*-carboxylate of OSB. The reported trifluoromethyl analogue **1** showed modest activity in biochemical

assays (K_i = 108 μM), but no antimicrobial activity was reported.

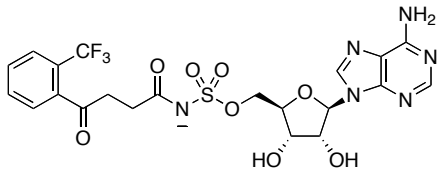

1

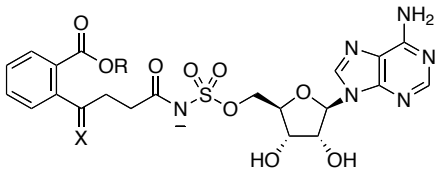

2: OSB-AMS (R = H, X = O)
3: MeOSB-AMS (R = Me, X = O)
4: (R = Me, X = CH_2)

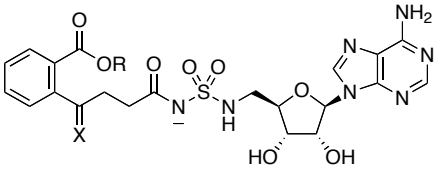

5: OSB-AMSN (R = H, X = O)
6: MeOSB-AMSN (R = Me, X = O)
7: OCPB-AMSN (R = H, X = H,H)
8: MeOCPB-AMSN (R = Me, X = H,H)
9: (R = Me, X = CH_2)

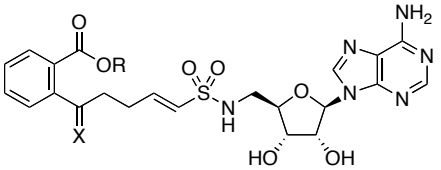

10: OSB-AVSN, (R = H, X = O)
11: MeOSB-AMSN (R = Me, X = O)
12: OCPB-AVSN (R = H, X = O)
13: MeOCPB-AVSN (R = Me, X = O)
14: (R = Me, X = CH_2)

Figure 1.6. Reported OSB-AMP based inhibitors of MenE.

Concurrent to this work, our own laboratory reported the synthesis and inhibitory activity of rationally designed acyl-AMS based analogues of OSB-AMP.[36] These analogues interrogated the structure–activity relationships (SAR) around three key areas of the OSB-AMP scaffold with MenE from *M. tuberculosis* (*mt*MenE), *S. aureus* (*sa*MenE), and *E. coli* (*ec*MenE).[36-37] The first area of focus was the SAR around the free carboxylate of OSB by making both the free-acid (OSB analogues: **2**, **5**, **7**, **10**, **12**, Figure 1.5) and the masking carboxylate as the methyl ester (MeOSB analogues: **3**, **4**, **6**, **8**, **9**, **11**, **13**, **14**). The second area of focus was the SAR around the ketone of the succinyl chain by replacement with an *exo*-methylene (analogues: **4**, **9**, **14**) or elimination completely (desketo analogues: **7**, **8**, **12**, **13**). The final area of focus was the SAR around the acyl-phosphate group (linker region) where

acyl-sulfamoyl analogues (AMS analogues: **2-4**), acyl-sulfamide analogues (AMSN: **5-9**), and vinyl-sulfonamide analogues (AVSN: **10–14**) were synthesized and screened for related biochemical and antimicrobial activity.

Table 1.1. Biochemical activity of reported MenE inhibitors.[36-37,40]

	IC_{50} [μM] of MenE from		
Inhibitor	*M. tuberculosis*	*S. aureus*	*E. coli*
2, OSB-AMS	0.049 ± 0.007	0.060 ± 0.005	0.21 ± 0.16
3, MeOSB-AMS	14.2 ± 3.3	24.6 ± 3.5	38.0 ± 3.0
4, *e*mMeOSB-AMS	n.d	n.d	> 200
5, OSB-AMSN	0.20 ± 0.02	0.24 ± 0.01	0.63 ± 0.14
6, MeOSB-AMSN	23.5 ± 1.0	> 200	34.1 ± 2.8
7, OCPB-AMSN	101 ± 14	85 ± 17	n.d
8, MeOCPB-AMSN	> 200	> 200	> 200
9, *e*mMeOSB-AMSN	n.d	n.d	> 200
10, OSB-AVSN	0.16 ± 0.05	0.33 ± 0.05	0.57 ± 0.06
11, MeOSB-AVSN	117 ± 12	45.7 ± 2.8	5.7 ± 0.7
12, OCPB-AVSN	106 ± 10	54.4 ± 2.3	31.6 ± 5.5
13, MeOCPB-AVSN	> 200	> 200	> 200
14, emMeOSB-AVSN	n.d	n.d	> 200

Assays were performed with *mt*MenE (50 nm), *sa*MenE (100 nm), or *ec*MenE (100 nm). n.d = not determined

OSB-AMS (**2**, Table 1) was found to be a tight-binding, low nM inhibitor of MenE with a K_i^{app} = 5.4 nM.[37] The most drastic SAR observed centered

around the succinyl ketone, where removal of the ketone or substitution to an *exo*-methylene resulted in almost complete loss of inhibition. The SAR at the carboxylate was less dramatic but still showed a 2–3 log decrease in inhibitory activity when the free carboxylate was masked as the methyl ester (OSB vs MeOSB).

SAR in the linker region appears to be far more nuanced and contingent on other factors.[36-37] Substitution of the acyl-AMS group to the acyl-AMSN resulted in little to no change in IC_{50} for MeOSB analogues (MeOSB-AMS **3**, MeOSB-AMSN **6**) against *ec*MenE. However, there was a 3-fold decrease in inhibitory activity for the free-carboxylate analogues (OSB-AMS **2**, OSB-AMSN **5**) with the same enzyme. Likewise, there was 2-fold decrease in inhibitory activity for MeOSB analogues upon substitution of the AMS group (MeOSB-AMS **3**, MeOSB-AMSN **6**) against *mt*MenE, but a 4-fold decrease in inhibitory activity of OSB analogues (OSB-AMS **2**, and OSB-AMSN **5**) with the same enzyme. These results suggest a certain amount of enzyme and scaffold dependence on toleration of substitution at the linker region of OSB-AMS. Whether this is due to an actual conformational shift in the binding between MeOSB and OSB analogues that places the acyl-sulfamoyl group in a more or less tolerant position in the MenE binding pocket or some other mechanism is unknown.

Although OSB-AMS showed low nanomolar inhibition of MenE in biochemical assays, OSB-AMS was shown to have comparatively poor antimicrobial activity. Canonically there are three main factors that determine cellular activity: compound accumulation (influx vs efflux), specificity (on-target binding vs off-target binding [specific and non-specific]), and degradation or metabolism (Figure 1.7B). OSB-AMS has two acidic moieties (Figure 1.7A):

the OSB carboxylate (pK_a = 4.3) and the acyl-sulfonamide (pK_a = 1.5), which at physiological pH will make OSB-AMS a highly polar, di-anionic species. This high polarity is believed to have a significant negative impact on the permeability of OSB-AMS into the bacterial cytosol (influx), and thereby reduce the antimicrobial activity of the compound.

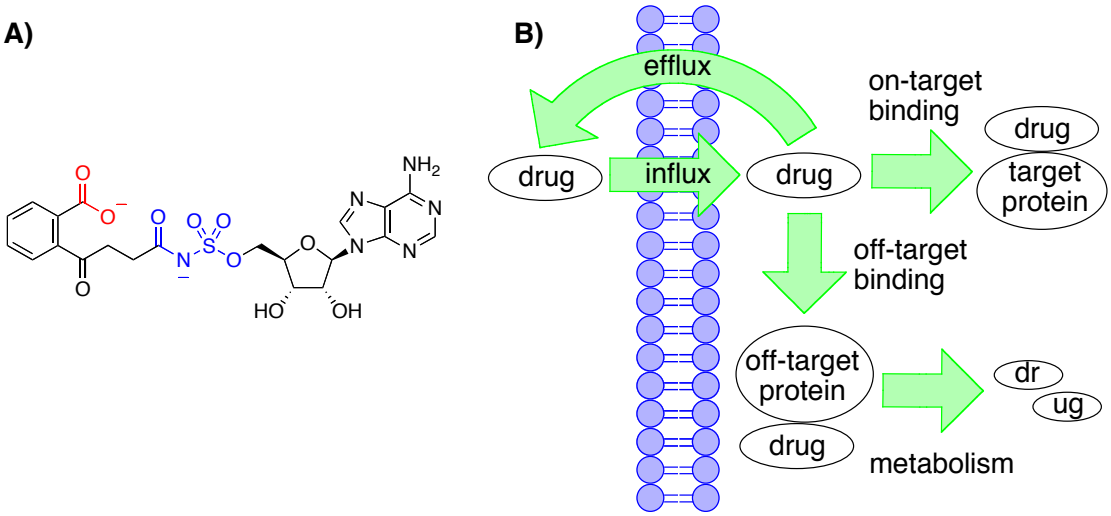

Figure 1.7. Cellular activity modeling of OSB-AMS. A) OSB-AMS at physiological pH, carboxylate (red) pKa = 4.3, acyl-sulfamate (blue) pKa = 1.5. B) Simplified model of factors determining cellular activity.

The extent of this exclusion from the bacterial cytosol has been measured in work conducted by Dr. Tony Davis in our laboratory though use of LC-MS/MS based compound accumulation studies.[80] In Gram–positive cells (*B. subtilis*) OSB-AMS has roughly 24% cellular accumulation at 100 µM and 7% cellular accumulation at 100 µM in mycobacteria (*M. smegmatis*), showing cellular permeability is a factor in the poor antimicrobial activity of OSB-AMS. However, it was noted during the course of the study that in the 1–1000 µM extracellular concentration range, the intracellular concentrations of AMS compounds appear to increase in a linear fashion. Therefore, with *B. subtilis*, we have reported a MIC with OSB-AMS of 113 µM (62.5 µg/mL) which would

indicate an intracellular OSB-AMS concentration of ~27 μM.[39] Likewise, with mycobacteria we have reported a MIC (*M. tuberculosis*) of 227 μM (125 μg/mL), which would indicate an intracellular concentration of ~16 μM. While the nearness of the intracellular concentrations at MIC across species is promising, the ~4-log disparity between intracellular concentrations at MIC and the K_i^{app} and IC_{50} of OSB-AMS for MenE indicates a likelihood of additional factors being involved. One possible factor that also arises from the di-anionic nature of OSB-AMS at physiological pH, is specificity. In our laboratory, a similar acyl-AMS compound (salicyl-AMS) has shown high levels of non-specific plasma protein binding, which is hypothesized to arise primarily from the negatively charged acyl-sulfamoyl group. This correlation between an increase in the negative charge of a compound and an increase in nonspecific protein binding has been noted in the literature.[81-82] Given the highly anionic nature of OSB-AMS at physiological pH, it is possible there are appreciable levels of non-specific binding to proteins which could result in a relative decrease of free-drug able to interact with and inhibit MenE. Thus, to progress this project forward, it is clear a solution to the di-anionic nature of OSB-AMS would need to be addressed.

1.4 Keto-acid/lactol equilibrium

During the synthesis of the OSB-AMS analogues, Dr. Indrajeet Sharma in our laboratory found that OSB-AMS exists in a keto-acid/lactol equilibrium (Figure 1.8).[37] The equilibrium is shifted from the keto-acid to the lactol based on the protonation state of the OSB carboxylate. When the carboxylate is in its deprotonated state, the open-chain keto-acid form predominates. However,

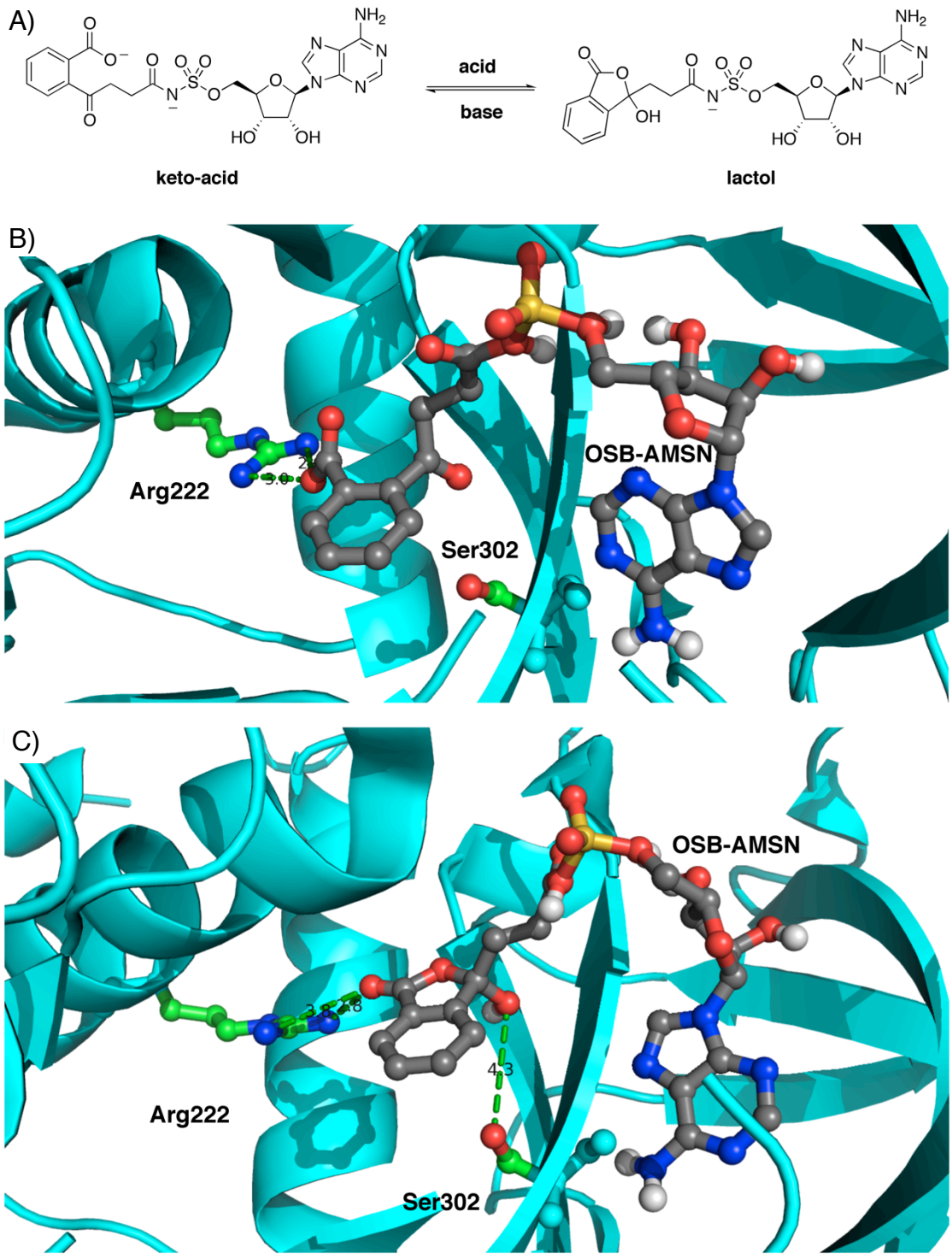

Figure 1.8. The keto-acid/lactol equilibrium. A) Keto-acid/lactol equilibrium of OSB-AMS. B) Keto-acid form of OSB-AMSN docked to *sa*MenE. C) Lactol form of OSB-AMSN docked to *sa*MenE. Key interactions with R222 and S302 shown.

when the carboxylate is protonated to form the carboxylic acid, it cyclizes on the ketone of the succinyl chain, resulting in the cyclic or closed-chain lactol form of OSB. Although at physiological pH the keto-acid form would predominate, there was no direct evidence to determine which form is the active pharmacophore of MenE.

In an attempt to determine which form of OSB-AMS is the active pharmacophore of MenE, docking studies using the unliganded crystal structure of *S. aureus* MenE (saMenE) were performed in collaboration with Dr. Subramanyam Swaminathan (Brookhaven National Laboratories). The study found two key residues (Arg222, Ser302) in the putative binding pocket of OSB, believed to interact with the OSB side-chain. In the docking structure, the free carboxylate of keto-acid form OSB is within 5 Å of Arg222 and the ketone of the succinyl chain within 3 Å of Ser302. The lactol form of OSB docked similarly with the lactol hydroxyl within 3 Å of Ser302. Although, the proximity of the free carboxylate of OSB to Arg222 does suggest the keto-acid form of OSB to be the active pharmacophore, the possibility of the lactol form cannot be eliminated due to the proximity of Ser302, which might favor the lactol form. Likewise, the docking scores from the study gave inconclusive results. Where the keto-acid form of OSB-AMS docked with a score of –7.7 kcal/mol, the lactol form of OSB-AMS docked with a score of –11.43 kcal/mol, suggesting the lactol form to be the active pharmacophore. However, the keto-acid form of OSB-AMSN docked with a score of –11.82 kcal/mol and the lactol form of OSB-AMSN docked with a score of –10.22 kcal/mol, which suggests the keto-acid form to be the active pharmacophore. Thus, the known SAR and docking experiments were not able to provide strong evidence as to the identity of the OSB-AMS pharmacophore of MenE.

1.6 SAR of acyl-AMS based linker analogues

Although the acyl-sulfamoyl group is a well-established bioisostere of the acyl-phosphate, it presents significant stability issues with OSB-AMS based inhibitors as well as presumed negative effects on ADME (absorption, distribution, metabolism, and excretion) of similar acyl-AMS based inhibitors in our laboratory. While we have reported two modifications to the OSB-AMS scaffold in the linker region (AMSN, AVSN), this problem has not yet been fully addressed with inhibitors of MenE. However, groups targeting other adenylate-forming enzymes have investigated alternative bioisosteres of the native acyl-phosphate group.

MbtA is a member of the ANL family and a key enzyme in the non-ribosomal peptide synthesis of the siderophore mycobactin. Courtney Aldrich and coworkers have reported analogues probing the SAR of the salicyl-AMS (Figure 1.8) scaffold originally reported by our laboratory.[64,74,83-89] To address problems of the acyl-sulfamoyl group and investigate the binding pocket at that region, the Aldrich group proposed and made a series of analogues that probed the linker region of MbtA (Figure 1.9).[72,90-91]

Although the changes made in most of the reported analogues were relatively minor, the loss of antimicrobial activity (MIC) was drastic. The only reported analogue to show antimicrobial activity (**15**), had a ~2-log reduction in activity compared to the lead AMS/AMSN compounds, while all other analogues were inactive up to 100 μM (>3-log reduction in activity). These results show the area of the acyl-phosphate group is engaged in multiple interactions with the binding pocket and so is highly intolerant of relatively minor changes to the scaffold. Therefore, although it may be necessary to alter the acyl-sulfamoyl group to improve ADME for acyl-AMS compounds,

substitution at the linker region while retaining activity will be extremely challenging.

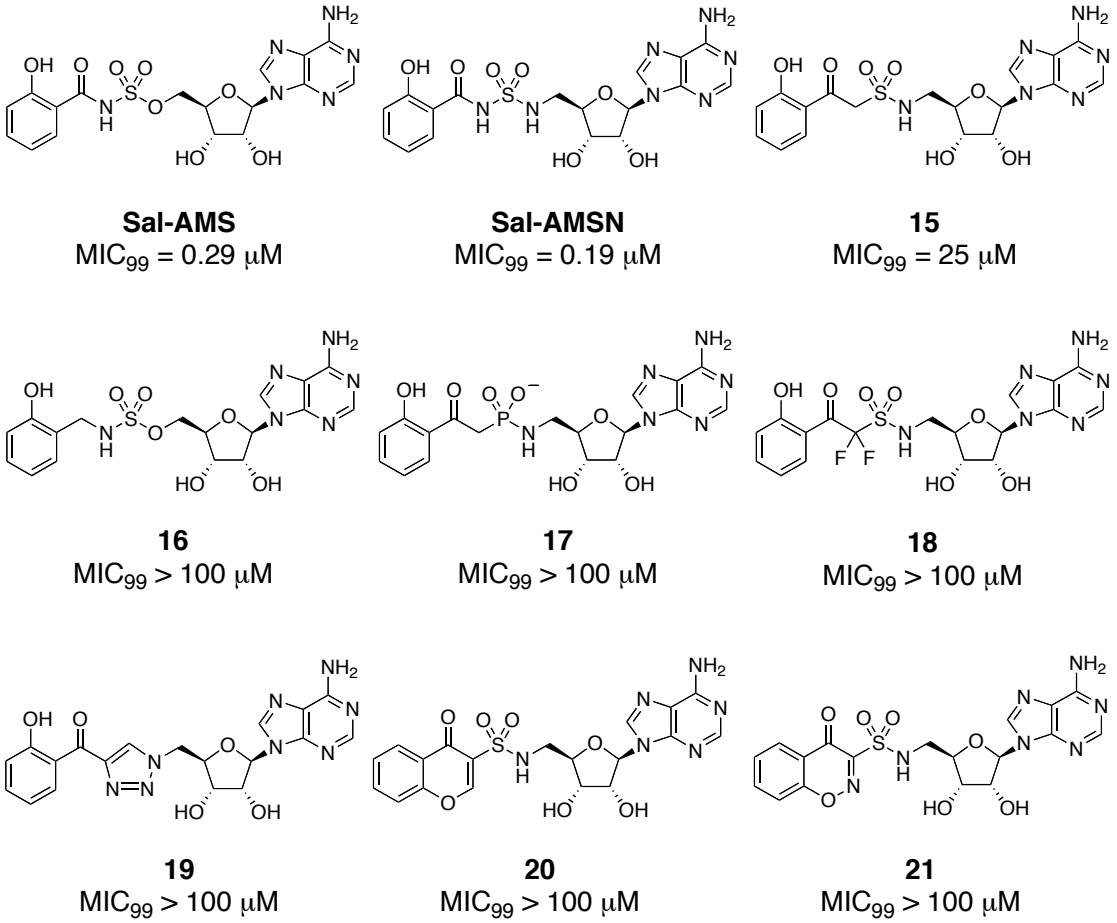

Figure 1.9. Reported linker analogues of Sal-AMS and corresponding activity in antimicrobial assays against *M. tuberculosis*. [64,74,83-89]

1.5 Goals of this work

The previous work by our laboratory had identified OSB-AMS, a tight-binding inhibitor of MenE with low nM inhibition of its biochemical activity. Despite the excellent biochemical activity, OSB-AMS was also shown to have poor antimicrobial activity, which is believed to be due to its di-anionic form at physiological pH. Previous work had provided the necessary validation for MenE as an antibacterial target, but the poor antimicrobial activity of our lead

compound necessitated additional investigation of the scaffold to move the project forward.

The overarching goal of this work is to design and synthesize selective inhibitors of MenE with improved antimicrobial activity while retaining or decreasing cytotoxic activity. To achieve this goal, the project focused on two primary areas of interest that are believed to have a significant negative impact on antimicrobial activity, the OSB carboxylate and the acyl-sulfamoyl group. Secondary objectives to be addressed while working towards our primary objective include: improving our understanding of the MenE binding pocket and the accompanying SAR of our scaffold, and remedying a problem inherent with this scaffold, namely compound stability.

In Chapter 2, we investigate the keto-acid/lactol equilibrium of OSB-AMS and how we might leverage the knowledge from this equilibrium to increase antimicrobial activity. The design, synthesis, biochemical activity, and cellular activity of a series of OSB-AMS analogues using keto-acid and lactol bioisosteres will be addressed. Additionally, we will discuss the first liganded co-crystal structure of MenE (OSB-AMS•MenE) achieved by our collaborators in the laboratory of Prof. Peter Tonge at Stony Brook University. In so doing, we provide interesting and important SAR about the OSB region of OSB-AMS, answer the question of the active pharmacophore of MenE, and discover a difluoroindanediol analogue that shows unusual but improved antimicrobial activity.

In Chapter 3, we investigate the unusual activity of the difluoroindanediol analogue. To do so, we begin with addressing a previously non-stereoselective synthetic route by designing and executing a stereoselective route to the four difluoroindanediol diastereomers. We also will

discuss the computational docking of the four difluoroindanediol diastereomers to the newly acquired OSB-AMS•MenE co-crystal structure. Finally, we will discuss the biochemical and antimicrobial activity of each of the four diastereomers, how it compares to our docking model, and what it means for the future of the difluoroindanediol scaffold.

The Chapter 4, we return to address the final problematic area of the OSB-AMS scaffold, the acyl-sulfamoyl linker. We will discuss the design, synthesis, and activity of a number of rationally designed OSB-AMS analogues designed to mimic key interactions in the MenE binding pocket while improving overall stability of these compounds. We will also discuss the implications this work has toward improvements of the ADME of existing and future acyl-AMP analogues to inhibit adenylation-forming enzymes.

The work herein describes the design and synthesis of novel inhibitors of menaquinone biosynthesis through the inhibition of MenE, an improved docking model for future use of pre-screening proposed inhibitors of MenE, and how this work can guide the future of this and similar projects.

1.6 References

1. *Antibiotic resistance threats in the United States, 2013*; CDC: 2013.

2. Filice, G. A. N., J. A.; Lexau, C.; Lees, C. H.; Bockstedt, L. A.; Como-Sabetti, K.; Lesher, L. J.; Lynfield, R., Excess costs and utilization associated with methicillin resistance for patients with *Staphylococcus aureus* infection. *Infect. Control Hosp. Epidemiol.* **2010,** *31* (4), 365–373.

3. *Global tuberculosis report 2016*; World Health Organization: http://www.who.int/tb/publications/global_report/en/.

4. Taubes, G., The bacteria fight back. *Science* **2008,** *321* (5887), 356–361.

5. Fischbach, M. A.; Walsh, C. T., Antibiotics for emerging pathogens. *Science* **2009,** *325* (5944), 1089–1093.

6. Clatworthy, A. E.; Pierson, E.; Hung, D. T., Targeting virulence: a new paradigm for antimicrobial therapy. *Nat. Chem. Biol.* **2007,** *3* (9), 541–548.

7. Butler, M. S.; Blaskovich, M. A.; Cooper, M. A., Antibiotics in the clinical pipeline in 2013. *J. Antibiot.* **2013,** *66* (10), 571–591.

8. Diacon, A. H.; Donald, P. R.; Pym, A.; Grobusch, M.; Patientia, R. F.; Mahanyele, R.; Bantubani, N.; Narasimooloo, R.; De Marez, T.; van Heeswijk, R.; Lounis, N.; Meyvisch, P.; Andries, K.; McNeeley, D. F., Randomized pilot trial of eight weeks of bedaquiline (TMC207) treatment for multidrug-resistant tuberculosis: long-term outcome, tolerability, and effect on emergence of drug resistance. *Antimicrob. Agents Chemother.* **2012,** *56* (6), 3271–3276.

9. Leach, K. L.; Brickner, S. J.; Noe, M. C.; Miller, P. F., Linezolid, the first oxazolidinone antibacterial agent. *Ann. N.Y. Acad. Sci.* **2011,** *1222* (1), 49–54.

10. Tally, F. P.; DeBruin, M. F., Development of daptomycin for Gram-positive infections. *J. Antimicrob. Chemother.* **2000,** *46* (4), 523–526.

11. Johnson, S., Recurrent Clostridium difficile infection: A review of risk factors, treatments, and outcomes. *J. Infect.* **2009,** *58* (6), 403–410.

12. Jones, R. N.; Fritsche, T. R.; Sader, H. S.; Ross, J. E., Activity of Retapamulin (SB-275833), a novel Pleuromutilin, against selected resistant Gram-positive Cocci. *Antimicrob. Agents Chemother.* **2006,** *50* (7), 2583–2586.

13. Clay, K. D.; Hanson, J. S.; Pope, S. D.; Rissmiller, R. W.; Purdum, P. P.; Iii; Banks, P. M., Brief communication: Severe hepatotoxicity of telithromycin: three case reports and literature review. *Ann. Intern. Med.* **2006,** *144* (6), 415–420.

14. Dixit, D.; Madduri, R. P.; Sharma, R., The role of tigecycline in the treatment of infections in light of the new black box warning. *Expert Rev. Anti Infect. Ther.* **2014,** *12* (4), 397–400.

15. Cox , E.; Laessig , K., FDA approval of bedaquiline — The benefit–risk balance for drug-resistant Tuberculosis. *New Engl. J. Med.* **2014,** *371* (8), 689–691.

16. French, G., Safety and tolerability of linezolid. *J. Antimicrob. Chemother.* **2003,** *51* (suppl_2), 1145–1153.

17. Narita, M.; Tsuji, B. T.; Yu, V. L., Linezolid-associated peripheral and optic neuropathy, lactic acidosis, and serotonin syndrome. *Pharmacother.* **2007,** *27* (8), 1189–1197.

18. Martius, C., The metabolic relationships between the different K vitamins and the synthesis of the ubiquinones. *Am. J. Clin. Nutr.* **1961,** *9* (4), 97–103.

19. Bentley, R.; Meganathan, R., Biosynthesis of vitamin K (menaquinone) in bacteria. *Microbiol. Rev.* **1982,** *46* (3), 241–280.

20. Meganathan, R., Biosynthesis of menaquinone (vitamin K2) and ubiquinone (coenzyme Q): A perspective on enzymatic mechanisms. In *Vitam. Horm.*, Gerald Litwack, T. B., Ed. Academic Press: 2001; Vol. Volume 61, pp 173–218.

21. Meganathan, R.; Kwon, O., Biosynthesis of menaquinone (vitamin K(2)) and ubiquinone (coenzyme Q). *EcoSal Plus* **2009,** *3* (2), 10.1128/ecosalplus.3.6.3.3.

22. Kurosu, M.; Begari, E., Vitamin K2 in electron transport system: are enzymes involved in vitamin K2 biosynthesis promising drug targets? *Molecules* **2010,** *15* (3), 1531–1553.

23. Collins, M. D.; Goodfellow, M.; Minnikin, D. E., Isoprenoid quinones in the classification of coryneform and related bacteria. *Microbiology* **1979,** *110* (1), 127–136.

24. Nahaie, M. R.; Goodfellow, M.; Minnikin, D. E.; Hajek, V., Polar lipid and isoprenoid quinone composition in the classification of Staphylococcus. *Microbiology* **1984,** *130* (9), 2427–2437.

25. Hiratsuka, T.; Furihata, K.; Ishikawa, J.; Yamashita, H.; Itoh, N.; Seto, H.; Dairi, T., An alternative menaquinone biosynthetic pathway operating in microorganisms. *Science* **2008,** *321* (5896), 1670–1673.

26. Truglio, J. J.; Theis, K.; Feng, Y.; Gajda, R.; Machutta, C.; Tonge, P. J.; Kisker, C., Crystal structure of Mycobacterium tuberculosis MenB, a key enzyme in vitamin K2 biosynthesis. *J. Biol. Chem.* **2003,** *278* (43), 42352–42360.

27. Upadhyay, A.; Fontes, F. L.; Gonzalez-Juarrero, M.; McNeil, M. R.; Crans, D. C.; Jackson, M.; Crick, D. C., Partial saturation of menaquinone in *Mycobacterium tuberculosis:* function and essentiality of a novel reductase, MenJ. *ACS Cent. Sci.* **2015,** *1* (6), 292–302.

28. Seto, H.; Jinnai, Y.; Hiratsuka, T.; Fukawa, M.; Furihata, K.; Itoh, N.; Dairi, T., Studies on a new biosynthetic pathway for menaquinone. *J. Am. Chem. Soc.* **2008,** *130* (17), 5614–5615.

29. Dairi, T., An alternative menaquinone biosynthetic pathway operating in microorganisms: an attractive target for drug discovery to pathogenic Helicobacter and Chlamydia strains. *J. Antibiot.* **2009,** *62* (7), 347–352.

30. P Dowd; S W Ham; S Naganathan, a.; Hershline, R., The mechanism of action of vitamin K. *Annu. Rev. Nutr.* **1995,** *15* (1), 419–440.

31. Danziger, J., Vitamin K-dependent proteins, warfarin, and vascular calcification. *Clin. J. Am. Soc. Nephrol.* **2008,** *3* (5), 1504–1510.

32. Nakagawa, K.; Hirota, Y.; Sawada, N.; Yuge, N.; Watanabe, M.; Uchino, Y.; Okuda, N.; Shimomura, Y.; Suhara, Y.; Okano, T., Identification of UBIAD1 as a novel human menaquinone-4 biosynthetic enzyme. *Nature* **2010,** *468* (7320), 117–121.

33. Fang, M.; Toogood, R. D.; Macova, A.; Ho, K.; Franzblau, S. G.; McNeil, M. R.; Sanders, D. A. R.; Palmer, D. R. J., Succinylphosphonate esters are competitive inhibitors of MenD that

show active-site discrimination between homologous α-ketoglutarate-decarboxylating enzymes. *Biochemistry* **2010,** *49* (12), 2672–2679.

34. Fang, M.; Macova, A.; Hanson, K. L.; Kos, J.; Palmer, D. R. J., Using substrate analogues to probe the kinetic mechanism and active Site of *Escherichia coli* MenD. *Biochemistry* **2011,** *50* (40), 8712–8721.

35. Pulaganti, M.; Banaganapalli, B.; Mulakayala, C.; Chitta, S. K.; C. M., A., Molecular modeling and docking studies of *o*-succinylbenzoate synthase of *M. tuberculosis*—a potential target for antituberculosis drug design. *Appl. Biochem. Biotechnol.* **2014,** *172* (3), 1407–1432.

36. Lu, X.; Zhang, H.; Tonge, P. J.; Tan, D. S., Mechanism-based inhibitors of MenE, an acyl-CoA synthetase involved in bacterial menaquinone biosynthesis. *Bioorg. Med. Chem. Lett.* **2008,** *18* (22), 5963–5966.

37. Lu, X.; Zhou, R.; Sharma, I.; Li, X.; Kumar, G.; Swaminathan, S.; Tonge, P. J.; Tan, D. S., Stable analogues of OSB-AMP: potent inhibitors of MenE, the o-succinylbenzoate-CoA synthetase from bacterial menaquinone biosynthesis. *ChemBioChem* **2012,** *13* (1), 129–136.

38. Matarlo, J. S.; Evans, C. E.; Sharma, I.; Lavaud, L. J.; Ngo, S. C.; Shek, R.; Rajashankar, K. R.; French, J. B.; Tan, D. S.; Tonge, P. J., Mechanism of MenE inhibition by acyl-adenylate analogues and discovery of novel antibacterial agents. *Biochemistry* **2015,** *54* (42), 6514–6524.

39. Evans, C. E.; Matarlo, J. S.; Tonge, P. J.; Tan, D. S., Stereoselective synthesis, docking, and biological evaluation of difluoroindanediol-based MenE inhibitors as antibiotics. *Org. Lett.* **2016**, 6384–6387.

40. Tian, Y.; Suk, D.-H.; Cai, F.; Crich, D.; Mesecar, A. D., Bacillus anthracis o-succinylbenzoyl-CoA synthetase: reaction kinetics and a novel inhibitor mimicking Its reaction intermediate. *Biochemistry* **2008,** *47* (47), 12434–12447.

41. Li, X.; Liu, N.; Zhang, H.; Knudson, S. E.; Slayden, R. A.; Tonge, P. J., Synthesis and SAR studies of 1,4-benzoxazine MenB inhibitors: Novel antibacterial agents against *Mycobacterium tuberculosis*. *Bioorg. Med. Chem. Lett.* **2010,** *20* (21), 6306–6309.

42. Li, X.; Liu, N.; Zhang, H.; Knudson, S. E.; Li, H.-J.; Lai, C.-T.; Simmerling, C.; Slayden, R. A.; Tonge, P. J., CoA Adducts of 4-Oxo-4-phenylbut-2-enoates: Inhibitors of MenB from the M. tuberculosis

Menaquinone Biosynthesis Pathway. *ACS Med. Chem. Lett.* **2011,** *2* (11), 818–823.

43. Matarlo, J. S.; Lu, Y.; Daryaee, F.; Daryaee, T.; Ruzsicska, B.; Walker, S. G.; Tonge, P. J., A methyl 4-Oxo-4-phenylbut-2-enoate with in vivo activity against MRSA that inhibits MenB in the bacterial menaquinone biosynthesis pathway. *ACS Infect. Dis.* **2016,** *2* (5), 329–340.

44. Dhiman, R. K.; Mahapatra, S.; Slayden, R. A.; Boyne, M. E.; Lenaerts, A.; Hinshaw, J. C.; Angala, S. K.; Chatterjee, D.; Biswas, K.; Narayanasamy, P.; Kurosu, M.; Crick, D. C., Menaquinone synthesis is critical for maintaining Mycobacterial viability during exponential growth and recovery from non-replicating persistence. *Mol. Microbiol.* **2009,** *72* (1), 85–97.

45. Michio, K.; Dean, C. C., MenA is a promising drug target for developing novel lead molecules to combat *Mycobacterium tuberculosis*. *Med. Chem.* **2009,** *5* (2), 197–207.

46. Li, K.; Schurig-Briccio, L. A.; Feng, X.; Upadhyay, A.; Pujari, V.; Lechartier, B.; Fontes, F. L.; Yang, H.; Rao, G.; Zhu, W.; Gulati, A.; No, J. H.; Cintra, G.; Bogue, S.; Liu, Y.-L.; Molohon, K.; Orlean, P.; Mitchell, D. A.; Freitas-Junior, L.; Ren, F.; Sun, H.; Jiang, T.; Li, Y.; Guo, R.-T.; Cole, S. T.; Gennis, R. B.; Crick, D. C.; Oldfield, E., Multitarget drug discovery for Tuberculosis and other infectious diseases. *J. Med. Chem.* **2014,** *57* (7), 3126–3139.

47. Choi, S.-r.; Frandsen, J.; Narayanasamy, P., Novel long-chain compounds with both immunomodulatory and MenA inhibitory activities against Staphylococcus aureus and its biofilm. *Sci. Rep.* **2017,** *7*, 40077.

48. Sukheja, P.; Kumar, P.; Mittal, N.; Li, S.-G.; Singleton, E.; Russo, R.; Perryman, A. L.; Shrestha, R.; Awasthi, D.; Husain, S.; Soteropoulos, P.; Brukh, R.; Connell, N.; Freundlich, J. S.; Alland, D., A novel small-molecule inhibitor of the *Mycobacterium tuberculosis* demethylmenaquinone methyltransferase MenG Is bactericidal to both growing and nutritionally deprived persister cells. *mBio* **2017,** *8* (1).

49. Akerley, B. J.; Rubin, E. J.; Novick, V. L.; Amaya, K.; Judson, N.; Mekalanos, J. J., A genome-scale analysis for identification of genes required for growth or survival of Haemophilus influenzae. *Proc. Natl. Acad. Sci.* **2002,** *99* (2), 966–971.

50. Chen, W.-H.; Minguez, P.; Lercher, M. J.; Bork, P., OGEE: an online gene essentiality database. *Nucleic Acids Res.* **2012,** *40* (D1), D901–D906.

51. Abicht, H. K.; Gonskikh, Y.; Gerber, S. D.; Solioz, M., Non-enzymic copper reduction by menaquinone enhances copper toxicity in Lactococcus lactis IL1403. *Microbiology* **2013,** *159* (6), 1190–1197.

52. Heide, L.; Arendt, S.; Leistner, E., Enzymatic synthesis, characterization, and metabolism of the coenzyme A ester of o-succinylbenzoic acid, an intermediate in menaquinone (vitamin K2) biosynthesis. *J. Biol. Chem.* **1982,** *257* (13), 7396–400.

53. Suvarna, K.; Stevenson, D.; Meganathan, R.; Hudspeth, M. E. S., Menaquinone (vitamin K2) biosynthesis: localization and characterization of the menA gene from *Escherichia coli*. *J. Bacteriol.* **1998,** *180* (10), 2782–2787.

54. Gulick, A. M., Conformational dynamics in the acyl-CoA synthetases, adenylation domains of non-ribosomal peptide synthetases, and firefly luciferase. *ACS Chem. Biol.* **2009,** *4* (10), 811–827.

55. Conti, E.; Franks, N. P.; Brick, P., Crystal structure of firefly luciferase throws light on a superfamily of adenylate-forming enzymes. *Structure* **1996,** *4* (3), 287–298.

56. Schmelz, S.; Naismith, J. H., Adenylate-forming enzymes. *Curr. Opin. Struct. Biol.* **2009,** *19* (6), 666–671.

57. Crystal structure of o-succinylbenzoic acid-CoA ligase from Staphylococcus aureus FAU - Patskovsky, Y., Toro, R., Dickey, M., Sauder, J.M., Chang, S., Burley, S.K., Almo, *Protein Data Bank*, Structure ID: 3IPL, Aug 25, **2009**; DOI: 10.2210/pdb3ipl/pdb [doi].

58. Reger, A. S.; Wu, R.; Dunaway-Mariano, D.; Gulick, A. M., Structural sharacterization of a 140° domain movement in the two-step reaction catalyzed by 4-chlorobenzoate:CoA ligase. *Biochemistry* **2008,** *47* (31), 8016–8025.

59. Conti, E.; Stachelhaus, T.; Marahiel, M. A.; Brick, P., Structural basis for the activation of phenylalanine in the non-ribosomal biosynthesis of gramicidin S. *J. EMBO* **1997,** *16* (14), 4174–4183.

60. Schimmel, P.; Tao, J.; Hill, J., Aminoacyl tRNA synthetases as targets for new anti-infectives. *The FASEB Journal* **1998,** *12* (15), 1599–1609.

61. Ehmann, D. E.; Shaw-Reid, C. A.; Losey, H. C.; Walsh, C. T., The EntF and EntE adenylation domains of Escherichia coli enterobactin synthetase: Sequestration and selectivity in acyl-AMP transfers to thiolation domain cosubstrates. *Proc. Natl. Acad. Sci.* **2000,** *97* (6), 2509–2514.

62. Keating, T. A.; Suo, Z.; Ehmann, D. E.; Walsh, C. T., Selectivity of the Yersiniabactin synthetase adenylation domain in the two-step process of amino acid activation and transfer to a holo-carrier protein domain. *Biochemistry* **2000,** *39* (9), 2297–2306.

63. Ochsner, U. A.; Sun, X.; Jarvis, T.; Critchley, I.; Janjic, N., Aminoacyl-tRNA synthetases: essential and still promising targets for new anti-infective agents. *Expert Opin. Investig. Drugs* **2007,** *16* (5), 573–593.

64. Benjamin P. Duckworth; Nelson, K. M.; Aldrich, C. C., Adenylating enzymes In *Mycobacterium tuberculosis* as drug targets. *Curr. Top. Med. Chem.* **2012,** *12* (7), 766–796.

65. Cisar, J. S.; Tan, D. S., Small molecule inhibition of microbial natural product biosynthesis-an emerging antibiotic strategy. *Chem. Soc. Rev.* **2008,** *37* (7), 1320–1329.

66. Isono, K. U., Masakazu; Kusakabe, Hiroo; Miyata, Nobuo; Koyama, Tadoyoshi; Ubukata, Makoto; Sethi, Satinder, K.; McCloskey, James, A., Dealanylascamyciin, nucleoside antibiotics from Streptomyces sp. *J. Antibiot.* **1984,** *37* (6), 670–672.

67. Osada, H.; Isono, K., Mechanism of action and selective toxicity of ascamycin, a nucleoside antibiotic. *Antimicrob. Agents Chemother.* **1985,** *27* (2), 230–233.

68. Takahashi, E. B., Teruhiko, A new nucleosidic antibiotic AT-265. *J. Antibiot.* **1982,** *35* (8), 939–947.

69. Waller, C. W.; Patrick, J. B.; Fulmor, W.; Meyer, W. E., The structure of nucleocidin. *J. Am. Chem. Soc.* **1957,** *79* (4), 1011–1012.

70. Florini, J. R.; Bird, H. H.; Bell, P. H., Inhibition of protein synthesis in vitro and in vivo by nucleocidin, an antitrypanosomal antibiotic. *J. Biol. Chem.* **1966,** *241* (5), 1091–1098.

71. Ueda, H.; Shoku, Y.; Hayashi, N.; Mitsunaga, J.-i.; In, Y.; Doi, M.; Inoue, M.; Ishida, T., X-ray crystallographic conformational study of 5′ -O-[N-

(l-alanyl)-sulfamoyl]adenosine, a substrate analogue for alanyl-tRNA synthetase. *Biochim. Biophys. Acta* **1991,** *1080* (2), 126–134.

72. Somu, R. V.; Boshoff, H.; Qiao, C.; Bennett, E. M.; Barry, C. E.; Aldrich, C. C., Rationally designed nucleoside antibiotics that inhibit siderophore biosynthesis of *Mycobacterium tuberculosis*. *J. Med. Chem.* **2006,** *49* (1), 31–34.

73. Finking, R.; Neumüller, A.; Solsbacher, J.; Konz, D.; Kretzschmar, G.; Schweitzer, M.; Krumm, T.; Marahiel, M. A., Aminoacyl adenylate substrate analogues for the inhibition of adenylation domains of nonribosomal peptide synthetases. *ChemBioChem* **2003,** *4* (9), 903–906.

74. Ferreras, J. A.; Ryu, J.-S.; Di Lello, F.; Tan, D. S.; Quadri, L. E. N., Small-molecule inhibition of siderophore biosynthesis in Mycobacterium tuberculosis and Yersinia pestis. *Nat. Chem. Biol.* **2005,** *1* (1), 29–32.

75. Brownell, J. E.; Sintchak, M. D.; Gavin, J. M.; Liao, H.; Bruzzese, F. J.; Bump, N. J.; Soucy, T. A.; Milhollen, M. A.; Yang, X.; Burkhardt, A. L.; Ma, J.; Loke, H.-K.; Lingaraj, T.; Wu, D.; Hamman, K. B.; Spelman, J. J.; Cullis, C. A.; Langston, S. P.; Vyskocil, S.; Sells, T. B.; Mallender, W. D.; Visiers, I.; Li, P.; Claiborne, C. F.; Rolfe, M.; Bolen, J. B.; Dick, L. R., Substrate-assisted inhibition of ubiquitin-like protein-activating enzymes: The NEDD8 E1 inhibitor MLN4924 forms a NEDD8-AMP mimetic in situ. *Mol. Cell* **2010,** *37* (1), 102–111.

76. Lu, X.; Olsen, S. K.; Capili, A. D.; Cisar, J. S.; Lima, C. D.; Tan, D. S., Designed semisynthetic protein inhibitors of Ub/Ubl E1 activating enzymes. *J. Am. Chem. Soc.* **2010,** *132* (6), 1748–1749.

77. Olsen, S. K.; Capili, A. D.; Lu, X.; Tan, D. S.; Lima, C. D., Active site remodelling accompanies thioester bond formation in the SUMO E1. *Nature* **2010,** *463* (7283), 906–912.

78. Koroniak, L.; Ciustea, M.; Gutierrez, J. A.; Richards, N. G. J., Synthesis and characterization of an N-acylsulfonamide inhibitor of human asparagine synthetase. *Org. Lett.* **2003,** *5* (12), 2033–2036.

79. Ciulli, A., Scott; D. E., Ando, M.; Reyes, F.; Saldanha, S. A., Tuck; K. L., ChirgadzeD. Y.; Blundell, T. L.; and Abell, C., Inhibition of *Mycobacterium tuberculosis* pantothenate dynthetase by snalogues of the teaction intermediate. *ChemBioChem* **2008,** *9*, 2606–2611.

80. Davis, T. D.; Gerry, C. J.; Tan, D. S., General platform for systematic quantitative evaluation of small-molecule permeability in bacteria. *ACS Chem. Biol.* **2014,** *9* (11), 2535–2544.

81. Colmenarejo, G., In silico prediction of plasma and tissue protein binding. In *Reference Module in Chemistry, Molecular Sciences and Chemical Engineering*, Elsevier: 2014.

82. Ghafourian, T.; Amin, Z., QSAR models for the prediction of plasma protein binding. *Bioimpacts* **2013,** *3* (1), 21–27.

83. Nelson, K. M.; Viswanathan, K.; Dawadi, S.; Duckworth, B. P.; Boshoff, H. I.; Barry, C. E.; Aldrich, C. C., Synthesis and pharmacokinetic evaluation of siderophore biosynthesis inhibitors for *Mycobacterium tuberculosis*. *J. Med. Chem.* **2015,** *58* (14), 5459–5475.

84. Dawadi, S.; Viswanathan, K.; Boshoff, H. I.; Barry, C. E.; Aldrich, C. C., Investigation and conformational analysis of fluorinated nucleoside antibiotics targeting siderophore biosynthesis. *J. Org. Chem.* **2015,** *80* (10), 4835–4850.

85. Krajczyk, A.; Zeidler, J.; Januszczyk, P.; Dawadi, S.; Boshoff, H. I.; Barry Iii, C. E.; Ostrowski, T.; Aldrich, C. C., 2-Aryl-8-aza-3-deazaadenosine analogues of 5′ -O-[N-(salicyl)sulfamoyl]adenosine: Nucleoside antibiotics that block siderophore biosynthesis in Mycobacterium tuberculosis. *Biorg. Med. Chem.* **2016,** *24* (14), 3133–3143.

86. Gupte, A.; Boshoff, H. I.; Wilson, D. J.; Neres, J.; Labello, N. P.; Somu, R. V.; Xing, C.; Barry, C. E.; Aldrich, C. C., Inhibition of siderophore biosynthesis by 2-triazole substituted analogues of 5′ -O-[N-(salicyl)sulfamoyl]adenosine: antibacterial nucleosides effective against *Mycobacterium tuberculosis*. *J. Med. Chem.* **2008,** *51* (23), 7495–7507.

87. Somu, R. V.; Wilson, D. J.; Bennett, E. M.; Boshoff, H. I.; Celia, L.; Beck, B. J.; Barry, C. E.; Aldrich, C. C., Antitubercular nucleosides that inhibit siderophore biosynthesis: SAR of the glycosyl domain. *J. Med. Chem.* **2006,** *49* (26), 7623–7635.

88. Qiao, C.; Gupte, A.; Boshoff, H. I.; Wilson, D. J.; Bennett, E. M.; Somu, R. V.; Barry, C. E.; Aldrich, C. C., 5‘-O-[(N-Acyl)sulfamoyl]adenosines as antitubercular agents that inhibit MbtA: an adenylation enzyme required for siderophore biosynthesis of the Mycobactins. *J. Med. Chem.* **2007,** *50* (24), 6080–6094.

89. Neres, J.; Labello, N. P.; Somu, R. V.; Boshoff, H. I.; Wilson, D. J.; Vannada, J.; Chen, L.; Barry, C. E.; Bennett, E. M.; Aldrich, C. C., Inhibition of siderophore biosynthesis in *Mycobacterium tuberculosis* with nucleoside bisubstrate analogues: structure–activity relationships of the nucleobase domain of 5′ -O-[N-(salicyl)sulfamoyl]adenosine. *J. Med. Chem.* **2008,** *51* (17), 5349–5370.

90. Vannada, J.; Bennett, E. M.; Wilson, D. J.; Boshoff, H. I.; Barry, C. E.; Aldrich, C. C., Design, synthesis, and biological evaluation of β-ketosulfonamide adenylation inhibitors as potential antitubercular agents. *Org. Lett.* **2006,** *8* (21), 4707–4710.

91. Engelhart, C. A.; Aldrich, C. C., Synthesis of chromone, quinolone, and benzoxazinone sulfonamide nucleosides as conformationally constrained inhibitors of adenylating enzymes required for siderophore biosynthesis. *J. Org. Chem.* **2013,** *78* (15), 7470–7481.

CHAPTER 2

TARGETING OF MENE USING THE KETO-ACID/LACTOL EQUILIBRIUM*

2.1 The keto-acid/lactol equilibrium of OSB-AMS

Work in our laboratory to target MenE has focused on the use of acyl-sulfamoyladenosine bioisosteres of the cognate ligand of MenE, OSB-AMP.[1-2] Through this work, OSB-AMS (**1**, Figure 2.1B) was found to be a low nanomolar, tight-binding inhibitor of MenE across various species.

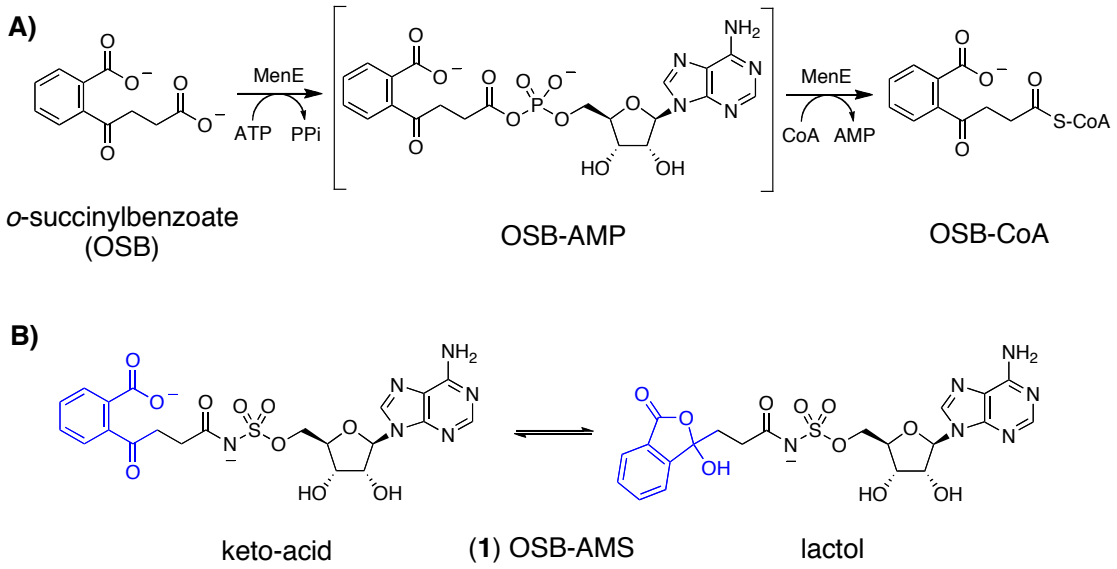

Figure 2.1. OSB-AMS targeting of MenE. A) Catalytic cycle of MenE with cognate bound ligand (OSB-AMP). B) The keto-acid/lactol equilibrium of OSB-AMS

However, although OSB-AMS showed potent biochemical activity against MenE (IC_{50}), in antimicrobial assays OSB-AMS exhibited only mid-micromolar activity (MIC) against a variety of bacteria. We rationalized this

* Adapted from: Matarlo, J. S.; Evans, C. E.; Sharma, I.; Lavaud, L. J.; Ngo, S. C.; Shek, R.; Rajashankar, K. R.; French, J. B.; Tan, D. S.; Tonge, P. J., "Mechanism of MenE Inhibition by Acyl-Adenylate Analogues and Discovery of Novel Antibacterial Agents." *Biochemistry* **2015,** *54*, 6514–6524.

lack of antimicrobial activity to be largely a consequence of the di-anionic nature of OSB-AMS at physiological pH, which would inhibit its ability to diffuse into bacteria efficiently and has negative implications for its pharmacokinetics *in vivo*.

We chose to focus first on addressing to the negatively charged carboxylate region of OSB-AMS. There are a number of known approaches such as prodrugs and other masking strategies that could be used to effectively hide the carboxylate until it enters the cell, which are then removed in the cytoplasm to reveal the more active carboxylate form. However, a more elegant possible solution became available upon the discovery by Dr. Indrajeet Sharma in our laboratory that OSB-AMS exists in a keto-acid/lactol equilibrium (Figure 2.1B).[2] As was discussed in Chapter 1, after examining the structure–activity relationships (SAR) of our existing analogues and subsequent docking experiments, we were unable to determine which form is the active pharmacophore for MenE. We hypothesized that if the lactol form of OSB-AMS is the active pharmacophore, a stable bioisostere of the lactol form would be less polar than OSB-AMS and would therefore more easily pass from the extracellular medium into the bacterial cytosol, leading to increased antimicrobial activity. We further hypothesized that if the keto-acid form of OSB-AMS was the active pharmacophore, stable bioisosteres of the carboxylate that are uncharged at physiological pH, less acidic, or better able to distribute the negative charge would exhibit increased diffusion into the cell and thereby increased antimicrobial activity compared to OSB-AMS.

In this light, we proposed a series of keto-acid and lactol analogues of OSB-AMS (Figure 2.2). Ostensibly this work was to determine which form of OSB-AMS is the active pharmacophore of MenE and explore the SAR in the

OSB binding pocket. However, the overarching goal was that of finding an analogue of OSB-AMS with increased antimicrobial activity.

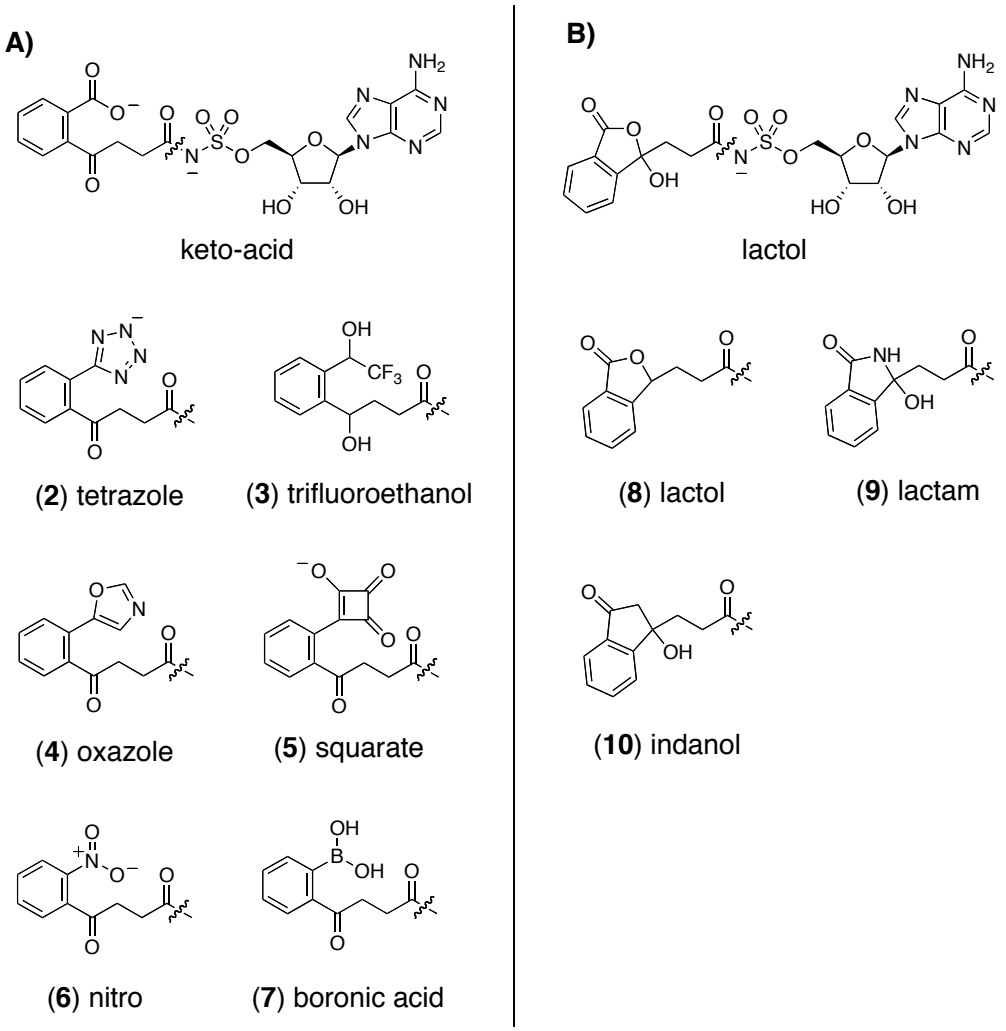

Figure 2.2. Proposed keto-acid and lactol analogues of OSB-AMS.

2.2 Synthesis of proposed analogues

The synthetic strategy we anticipated being able to use for the proposed compounds relied on the general approach used by our laboratory for the synthesis of OSB-AMS based inhibitors.[1-2] The final compounds **11** (Figure 2.3) would be derived from various protected forms of the acyl-AMS derivatives **12**. These in turn could be obtained through EDCI (1-ethyl-3-(3-

dimethylaminopropyl)carbodiimide) coupling of the corresponding protected sulfamoyladenosine scaffold **14** and carboxylic acid **13**. This general approach requires the acyl chain to be in its final form, or a protected version of that form before coupling onto the AMS scaffold. As such, this strategy avoids subjecting the less stable acyl-sulfamate to more steps and potentially damaging conditions than necessary.

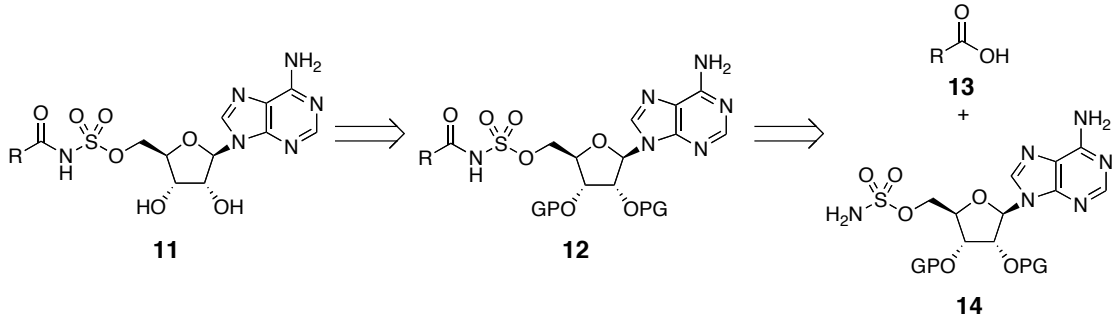

Figure 2.3. Retrosynthetic approach to the synthesis of proposed analogues. PG = protecting group, R = keto-acid and lactol form OSB analogues.

2.2.1 Synthetic routes to proposed analogues using the general approach

The synthesis of the tetrazole analogue **2** proceeded rapidly by first engaging commercially available 2-cyano-bromobenzene (**15**, Figure 2.4) in a cycloaddition reaction with sodium azide to achieve the tetrazole intermediate **16** in high yield. The intermediate **16** was treated with *n*-BuLi, which allowed for lithium–halogen exchange to form the corresponding lithiated species, before being quenched with succinic anhydride to provide the desired acyl side chain **17**. Attempts to optimize this step by first deprotonating the tetrazole with strong bases such as NaH, followed by addition of *n*-BuLi to execute the lithium–halogen exchange failed to appreciably increase the yield. The acyl side chain **17** was then coupled to the protected AMS scaffold **18** and

deprotected to yield the desired tetrazole analogue **2**.

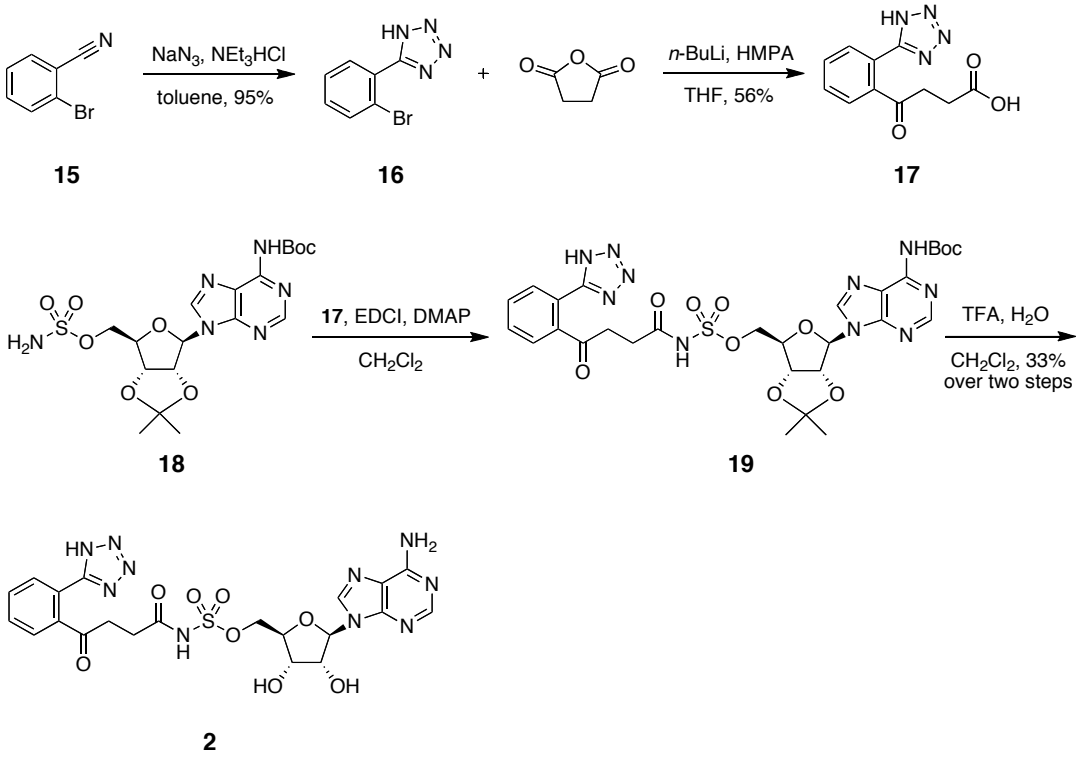

Figure 2.4. Synthesis of tetrazole analogue 2. HMPA = hexamethylphosphoramide, TFA = 2,2,2-trifluoroacetic acid, THF = tetrahydrofuran.

Synthesis of the trifluoroethanol analogue **3** began by converting the commercially available 1,2-dibromobenzene (**20**, Figure 2.5) into the corresponding Grignard with isopropylmagnesium chloride. The Grignard was then quenched with trifluoroacetic anhydride and the newly formed ketone reduced with sodium borohydride to form the desired (2-bromophenyl)-trifluoroethanol intermediate **21**. Protection of the alcohol as the *tert*-butyldimethylsilyl (TBS) ether gave intermediate **22**, to which was added isopropylmagnesium chloride to convert to the corresponding Grignard before being quenched with succinic anhydride. However, the expected succinyl ketone intermediate **23** was not observed in this case. The major product of

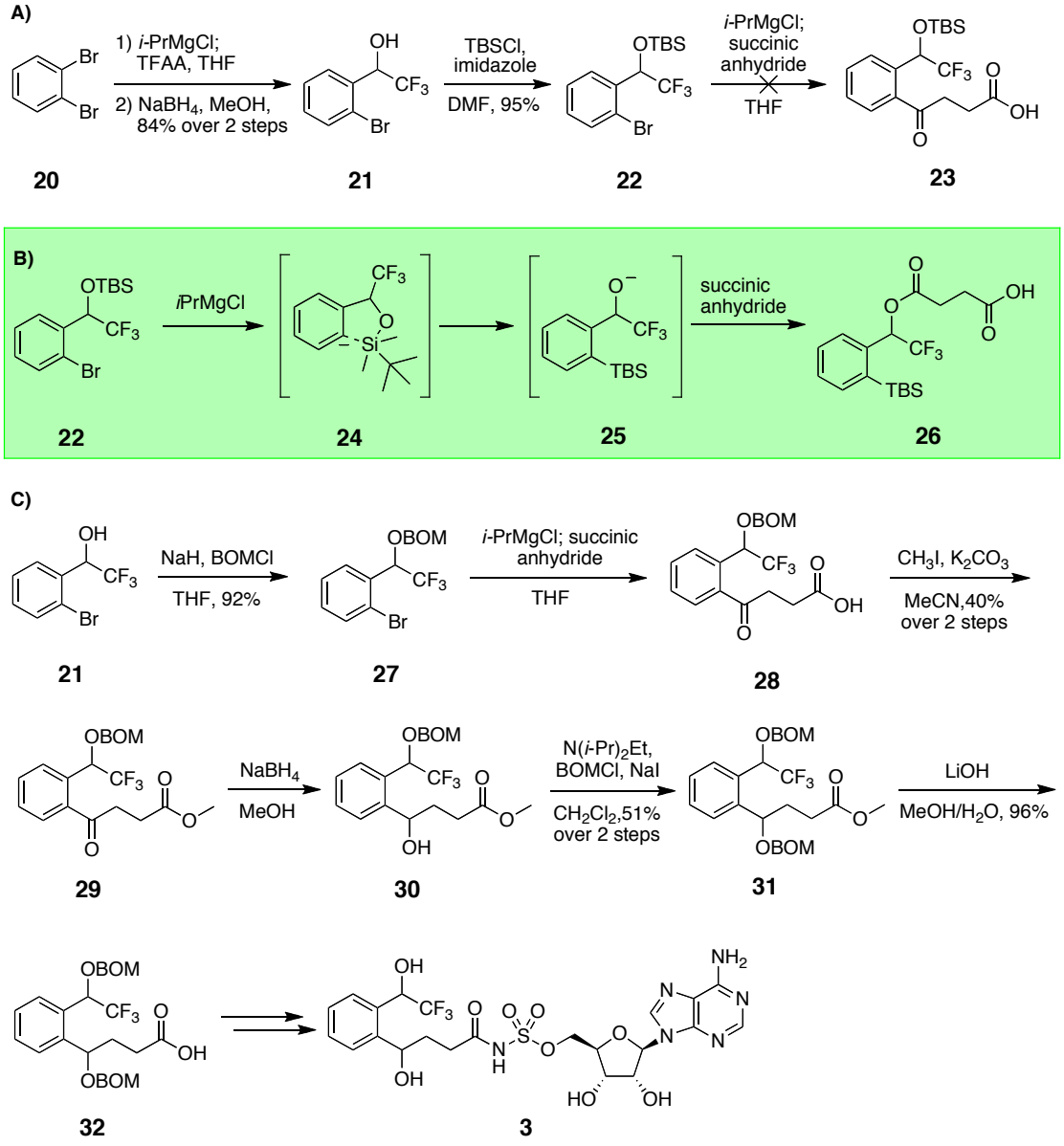

Figure 2.5. Synthesis of trifluoroethanol analogue. A) Original route to trifloroethanol analogue B) Retro-brook rearrangement of intermediate 20. C) Final synthetic route to the trifluoroethanol analogue 3. BOM = benzyl chloromethyl, TBS = tert-butyldimethylsilyl, THF = tetrahydrofuran.

this reaction was the succinyl ester **26**, presumably arising from a retro-Brook rearrangement of the Grignard to form intermediate **25**.[3] Alteration of the solvent, temperature, and other reaction conditions did not result in observation of the desired product. Use of *n*-BuLi in place ofresulted in a significantly increased yield of the undesired retro-Brook rearrangement

product **26**. Therefore, an alternative protecting group that was stable to strongly basic conditions and could be removed under relatively mild conditions was needed.

After screening a number of protecting groups, the benzyloxymethyl acetal (BOM) protecting group was found to be the most able to withstand the subsequent steps and to be removed without destroying the relatively fragile acyl-sulfamate bond of the final product. Using the BOM protected intermediate **27**, we converted **t**o the corresponding Grignard before forming the succinyl ketone intermediate **28** as originally proposed. Although the BOM group was the best suited to our overall needs, we still observed decreased yields due to self-immolation at this step. The carboxylate **28** was protected as the methyl ester **29** before the succinyl ketone was reduced (**30**) and immediately protected to form the bis-BOM ether intermediate **31**. The protection of the carboxylate and immediate carrying forward of the crude reduced product into the protection step, was found to be necessary due to rapid lactonization of the newly formed alcohol onto the free acid or ester of the succinyl chain. The methyl ester was then saponified to give the needed carboxylic acid **32**, which could be carried forward to give the desired trifluoroethanol analogue **3**.

Synthesis of the oxazole analogue **4** proceeded by converting 1,2-dibromobenzene (**20**, Figure 2.6) to the corresponding Grignard, followed by quenching with succinic anhydride and protection of the carboxylate as the methyl ester to provide intermediate **33**. Wilson and coworkers reported the efficient palladium–catalyzed arylation of oxazole with various aryl bromides, chlorides, and triflates with good yields and selectivity.[4] After optimization of the reaction with our scaffold, we were able to achieve the desired protected

oxazole side chain **34** in modest yield. This material was then saponified to give the carboxylic acid **35**, which was carried forward to give the desired oxazole analogue **4**.

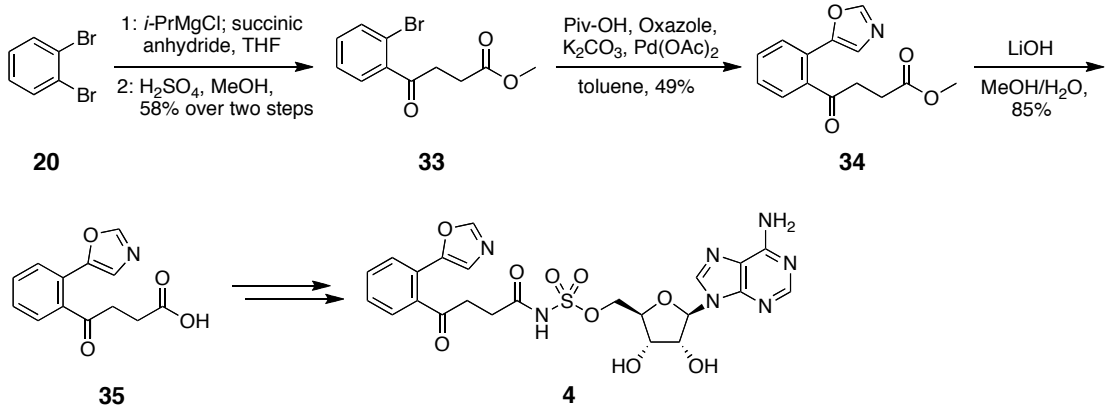

Figure 2.6. Synthesis of oxazole analogue 4. THF = tetrahydrofuran.

Using a similar strategy towards the boronic acid analogue **5**, we converted the aryl bromide intermediate **33** (Figure 2.7) to the corresponding pinacolatoboron intermediate **36** with a Miyaura borylation reaction using bis(pinacolato)diboron (B_2pin_2) before saponification to yield the carboxylic acid **37**. The material was then carried forward as previously described to yield what was expected to be the open-chain boronic acid analogue **5a**. However, we observed the succinyl ketone preferentially coordinates with the boronic acid to form the cyclic boronate complex (**5b**, Figure 2.7). Given work by Jeremy May and others that use the intermolecular coordination of ketones to boronic acids to perform various reactions and observe the coordination step to occur very rapidly,[5] this intramolecular coordination to form a highly favorable five-membered ring is not surprising in retrospect. As such, our originally proposed keto-acid bioisostere is instead an atypical lactol bioisostere.

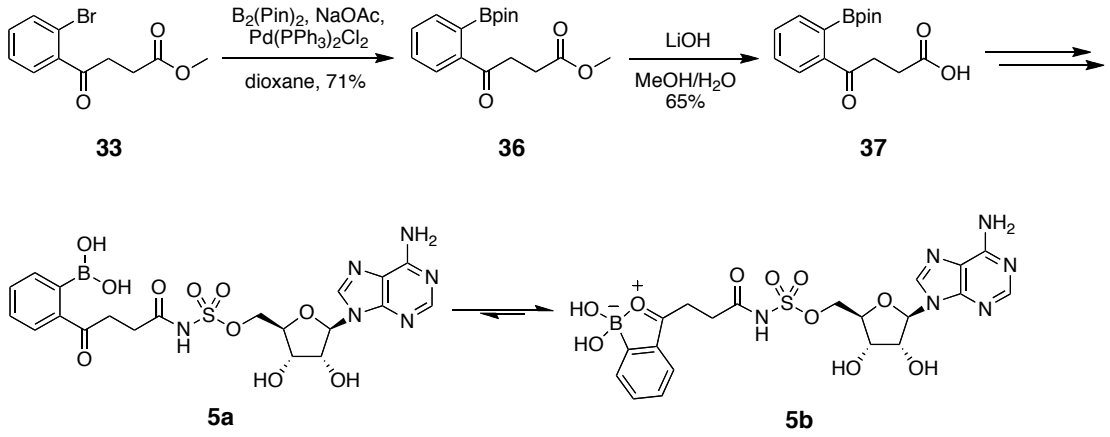

Figure 2.7. Synthesis of boronate analogue 5. Pin = pinacolato.

Synthesis of the nitro analogue **6** (Figure 2.8) began with a Hosomi–Sakurai allylation of commercially available *o*-nitrobenzaldehyde (**38**) to provide the desired olefin intermediate **39**. Hydroboration–oxidation followed by two-step oxidation provided the desired carboxylic acid **41**. The completed acyl-acid **41** was then carried forward to achieve the desired nitro analogue **6**.

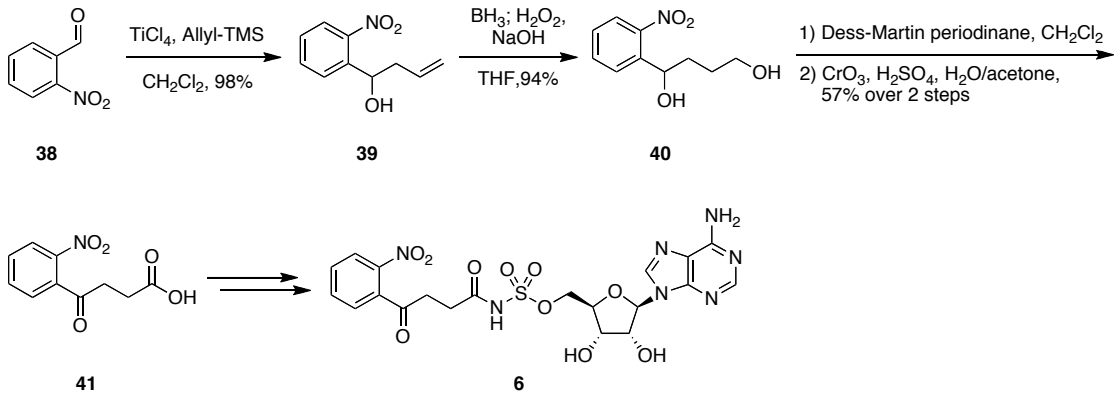

Figure 2.8. Synthesis of nitro analogue 6. THF = tetrahydrofuran, TMS = trimethylsilane.

Two-step oxidation of intermediate **40** was found to be necessary due to the unfavorable kinetics of a one step oxidation, which first oxidizes the primary alcohol to the carboxylic acid. The secondary alcohol then quickly lactonizes on the activated carboxylic acid, blocking further oxidation. While the secondary alcohol almost certainly cyclizes onto the aldehyde during the

Dess–Martin oxidation step to form the hemiacetal, this cyclization is sufficiently reversible to allow for oxidation of the secondary alcohol to the desired ketone.

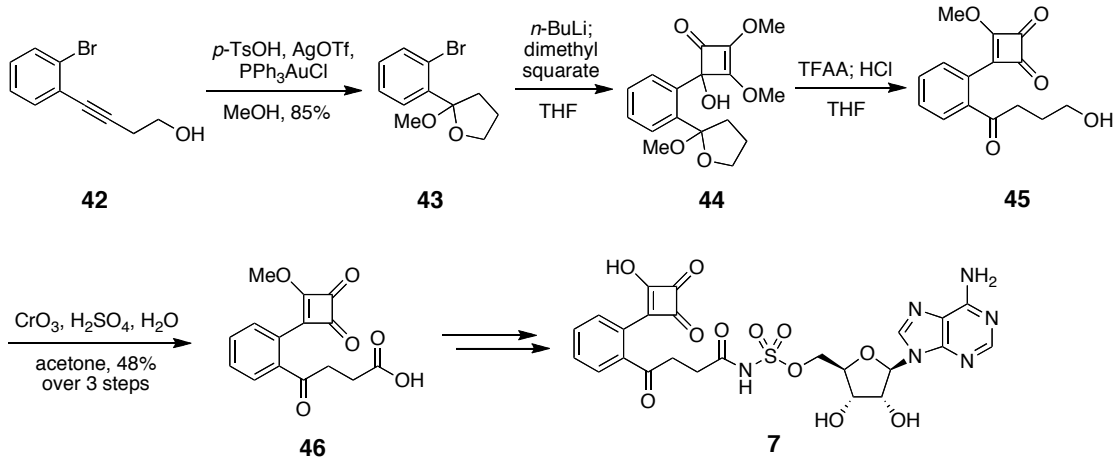

Figure 2.9. Synthesis of squarate analogue 7. TFAA = 2,2,2-trifluoroacetic anhydride, THF = tetrahydrofuran.

The synthesis of squarate analogue **7** began with alkyne intermediate **42** (Figure 2.9) which was obtained by Sonogashira coupling of homopropargyl alcohol to 1,2-dibromobenzene (**20**).[6] Subsequent gold-catalyzed tandem cycloisomerization–hydroalkoxylation of intermediate **42** gave the tetrahydrofuranyl ether product **43**.[7] Lithium–halogen exchange with *n*-BuLi provided the corresponding *ortho*-lithiated species which was quenched with dimethylsquarate to give intermediate **44**. Treatment of the squarate with trifluoroacetic anhydride with concomitant acid catalyzed opening of the tetrahydrofuranyl ether provided the reduced succinyl intermediate **45**. Jones oxidation supplied the desired carboxylic acid **46**, which was then carried forward to provide the desired squarate analogue **7**.

To achieve the lactol analogue **8**, *ortho*-lithiation of benzamide **47** followed by quenching with γ-butyrolactone yielded the reduced succinate

intermediate **48**. Reduction of the ketone with sodium borohydride followed by acid catalyzed lactonization on the *ortho*-benzamide formed the reduced lactone side chain **50**, which was oxidized to the corresponding carboxylic acid **51**. The acid **51** was then carried forward to provide the desired lactol analogue **8**.

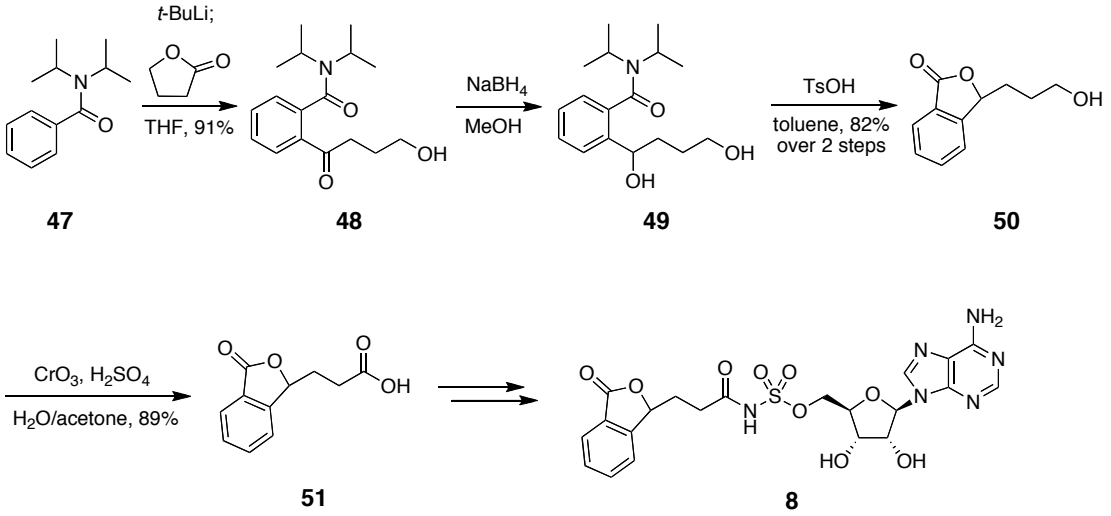

Figure 2.10. Synthesis of lactol analogue 8. THF = tetrahydrofuran

2.2.2 Synthetic route to the lactam analogue 9

One analogue that was not amenable to our general synthetic approach was the lactam analogue **9**. Initial attempts used an OSB diester intermediate **52**, which was treated with ammonia in an effort to form the corresponding benzamide **53**. However, this benzamide was never observed, as it immediately cyclized on the succinyl-ketone to provide the desired lactam scaffold **54**. Upon deprotection of the primary ester to provide the necessary carboxylic acid, we observed immediate formation of the lactam/lactone spirocycle **55** and other decomposition products.

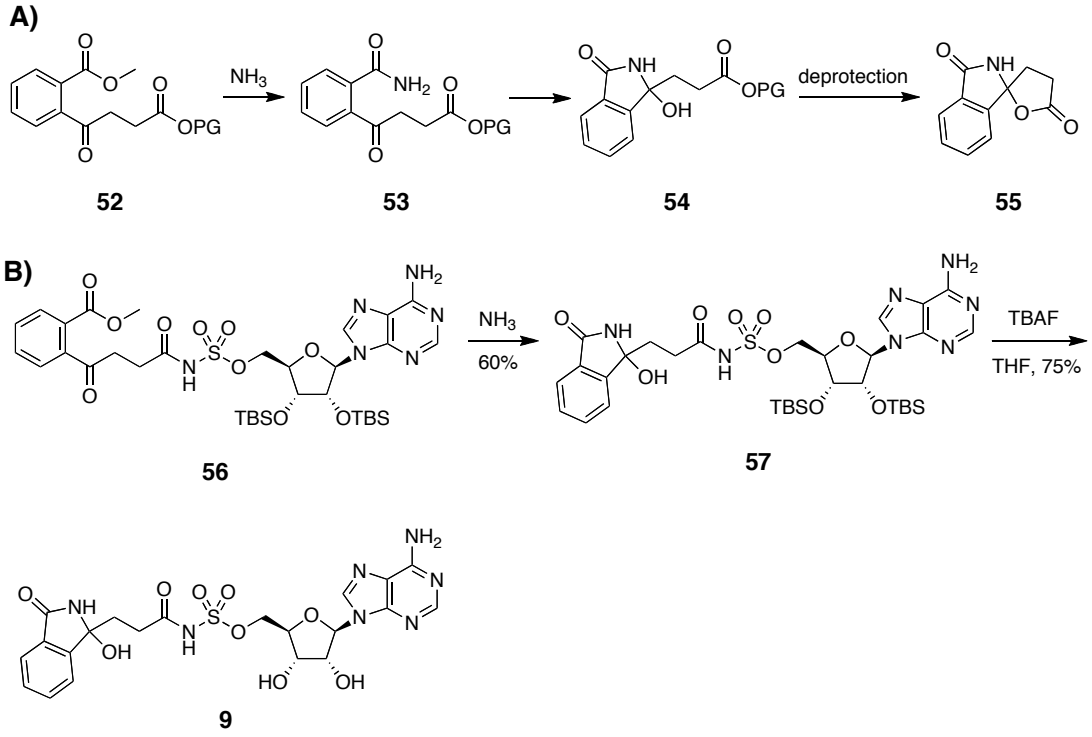

Figure 2.11. Synthesis of the lactam analogue 9. A) Original synthetic route of lactam side-chain. B) Successful route to desired lactam analogue. TBAF = tetrabutylammonium fluoride, THF = tetrahydrofuran.

To avoid spirocyclization, we executed a late-stage modification where the protected MeOSB-AMS scaffold **56** was treated with anhydrous ammonia to produce the desired lactam scaffold intermediate **57**. This intermediate was then deprotected to yield the desired lactam analogue **9**.

2.2.3 Exploration of the hydroxyindanone scaffold and the difluoroindanediol 74

The final lactol analogue proposed was the hydroxyindanone **10**, which substituted a methylene in place of the oxygen of the five-membered lactol ring. Initial success en route to this analogue proceeded via a coupled Heck–aldol annulation cascade with a protected aryl-bromide intermediate **58** (Figure 2.12) to give the desired protected hydroxyindanone scaffold **59**.[8]

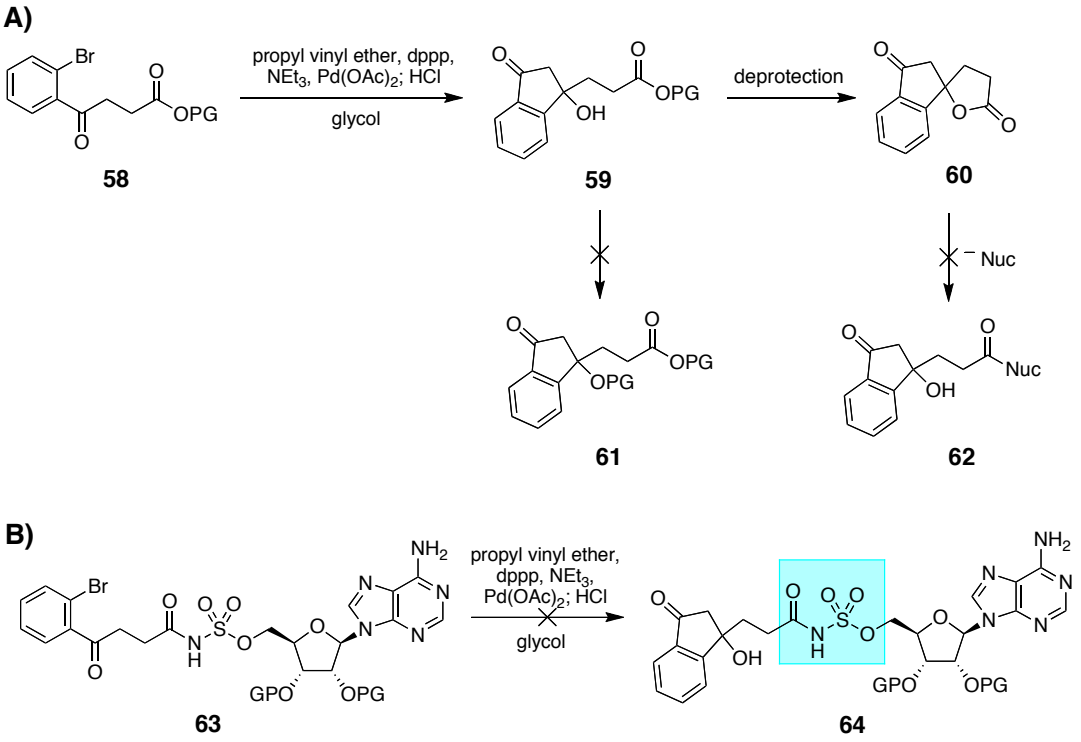

Figure 2.12. Synthetic approaches to the proposed hydroxyinanone analogue. dppp = 1,3-bis(diphenylphosphino)propane, PG = protecting group

However, as was observed with the lactam analogue, once the free carboxylic acid was formed we observed immediate formation of the undesired spirocycle **60**. Attempts to open the spirocycle with various nucleophiles in hopes to form the desired connection through an orthogonal route (**62**) gave only decomposition products. Likewise, attempts to protect the tertiary alcohol (**61**) proved unsuccessful, giving only decomposition products. During this work it became apparent that the intrinsically unstable tertiary-benzylic alcohol is further destabilized by the presence of the acidic *α*-keto protons of the indanone ring, which can deprotonate before rapidly undergoing undesired reaction pathways such as *β*-elimination.

To circumvent the issue of spirocycle formation, we attempted a late stage Heck–aldol with various protected forms of the aryl-bromide-AMS

scaffold **63** (Figure 2.12B). While the majority of the material decomposed along the acyl-sulfamate bond in the reaction conditions, enough desired product was formed to shed light on an important aspect of the scaffold. Upon attempting to isolate the desired product and variations of it, we discovered that the hydroxyindanone motif is intrinsically unstable as a part of the acyl-AMS scaffold. As was mentioned in Chapter 1, the acyl-sulfamate has a pK_a = 1.3, which is sufficiently acidic to induce decomposition of the hydroxyindanone moiety upon concentration. Therefore, to move this analogue forward we needed to address two main issues. The first issue of spirocyclization would require modifications to the proposed acyl chain allowing for formation of the acyl-sulfamate bond. The second issue of self-immolation would require modifications to the proposed hydroxyindanone analogue to increase the stability of the final compound.

As protecting the tertiary alcohol was not favorable to circumvent spirocyclization, we envisioned modifying the route to use an alkyne between the hydroxyindanone and the carboxylic acid (**66**, Figure 2.13). While this would prevent spirocyclization, installation of an alkyne at that position posed additional problems. The protected alkynyl-bromobenzene **65** was unable to undergo the coupled Heck–aldol annulation cascade due to the highly activated alkyne. Likewise, known literature methods of installing an alkyne moiety at the desired position ketone position of the indanone scaffold were not amenable to the reactive *α*-keto protons of either 1,3-indandione (**68**) or 3-hydroxyindanone (**67**). Additionally, we had already established the tertiary alcohol to be highly unstable. The conjugation of an alkynyl group seemed likely to exacerbate the intrinsic instability of this scaffold.

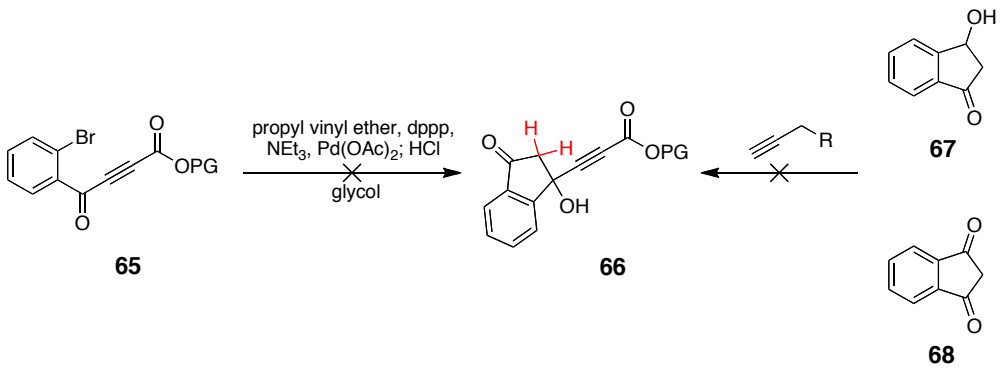

Figure 2.13. Proposed alkynyl intermediate and attempted routes. dppp =1,3-bis(diphenylphosphino)propane

To solve this problem we returned to the second issue of overall compound stability and altering our proposed inhibitor. Historically, when similar hydroxyindanone scaffolds are prepared and used, they contain alkyl substituents at the *α*-keto position.[9-12] This functionally blocks the primary decomposition pathway and allows for a wider breath of chemistries to be performed. Rather than use alkyl substituents, we opted to use fluorine, which would block the *α*-keto position from engaging in unwanted side reactions and inductively increase the stability the tertiary alcohol.

The synthesis of the newly proposed difluorohydroxyindanol analogue began with the fluorination of commercially available 1,3-indanone (**68**, Figure 2.14) to supply the difluoronated intermediate **69**. Treatment with lithiated *tert*-butyl propiolate provided the desired difluorohydroxyindanone scaffold **70**, which was deprotected to give the free carboxylic acid intermediate **71**. This was coupled onto the protected AMS scaffold **18** and the alkyne reduced to give the desired reduced form of the aliphatic chain **73**.

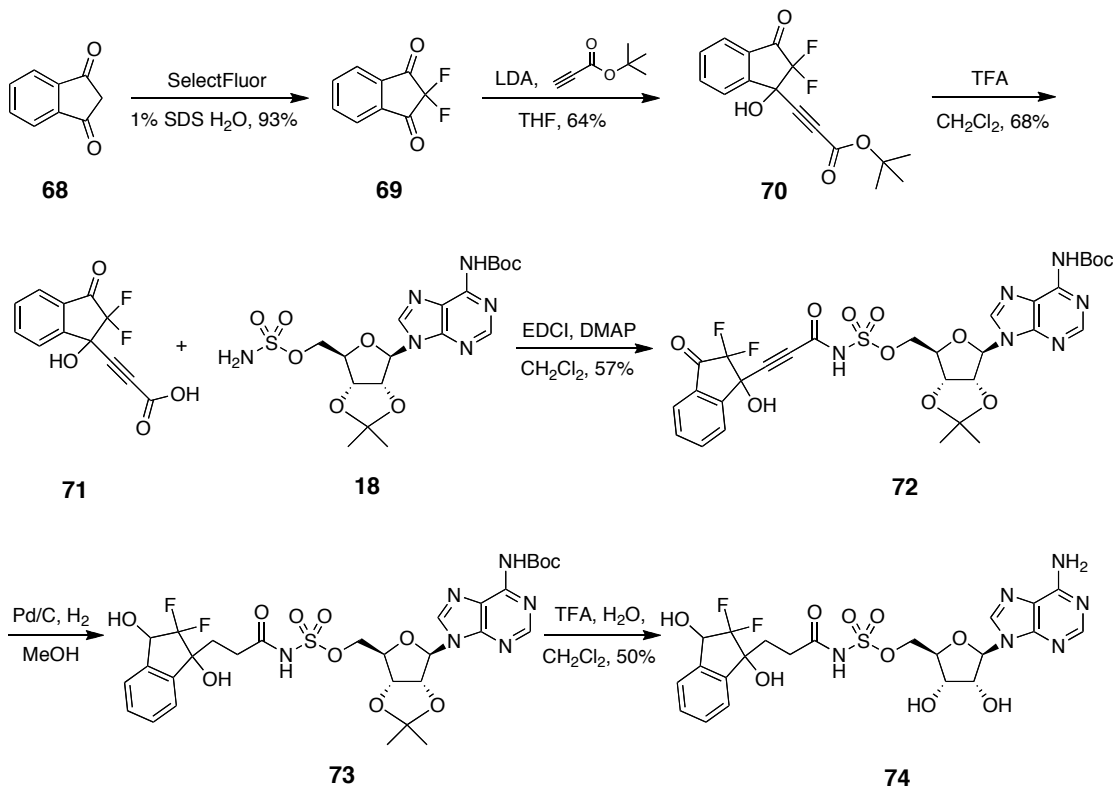

Figure 2.14: Synthesis of difluoroindanediol analogue 74.

Interestingly, all successful attempts to reduce the alkyne resulted in concurrent reduction of the benzylic ketone. A number of different reducing conditions were screened with identical results, and known selective conditions to reduce alkynes such as diimide reduction resulted in decomposition of the acyl-sulfamate group. Attempts to reoxidize the alcohol to the desired ketone also resulted only in decomposition of the starting material. However, upon analysis of the difluoroketone in aqueous media, we observed that it exists as the hydrate, which is consistent with literature reports of α-fluorinated ketones.[13-14] We rationalized therefore that moving forward with the fully reduced analogue would not be unreasonable and in aqueous media could arguably be a better ketone analogue than the larger and bulkier hydrate, so intermediate **73** was deprotected to give the difluoroindanediol

analogue **74**.

2.3 Biochemical activity of keto-acid and lactol analogues

The newly synthesized keto-acid and lactol analogues were tested for inhibitory activity in biochemical assays against *E. coli* MenE (*ec*MenE) by our collaborators in the laboratory of Professor Peter Tonge at Stony Brook University. Briefly, assays were performed using a MenE-MenB coupled assay with percent inhibition determined by the relative decrease in the rate of DHNA (1,4-dihydroxy-2-naphthoic acid) production observed by fluorescence spectroscopy (see experimental section 2.5 for details).[2]

The oxazole (**4**), trifluoroethanol (**3**), and nitro (**6**) analogues of the keto-acid form of OSB-AMS as well as the boronate (**5**), lactol (**8**), and lactam (**9**) analogues of the lactol form of OSB-AMS showed no inhibitory activity up to 100 μM (Table 2.1). The squarate analogue (**7**) was the most potent of the keto-acid and lactol analogues, with an IC_{50} of 0.17 ± 0.05 μM, while the tetrazole analogue (**2**) showed modest activity with an IC_{50} of 2.2 ± 0.4 μM. Interestingly, the difluoroindanediol analogue (**74**) also showed modest inhibitory activity with an observed IC_{50} of 1.5 ± 0.1 μM. While the majority of the SAR indicates that the keto-acid form of OSB-AMS is the active pharmacophore, we could not yet rationalize the activity of the difluoroindanediol analogue.

Table 2.1. Biochemical activity of keto-acid and lactol analogues of OSB-AMS.

Inhibitor		IC_{50} (μM)	pK_a
(**1**) OSB-AMS	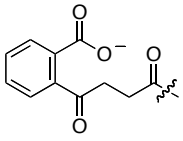	0.025 ± 0.005	4.5
(**2**) tetrazole	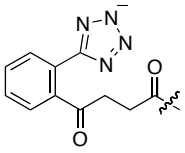	2.2 ± 0.4	3.4
(**3**) trifluoroethanol	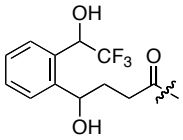	> 100	11.8
(**4**) oxazole	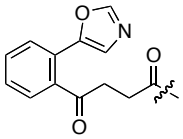	> 100	> 14
(**5**) boronate	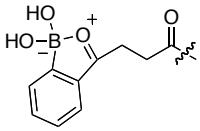	> 100	> 14
(**6**) nitro	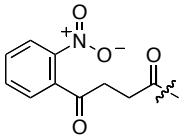	> 100	> 14
(**7**) squarate	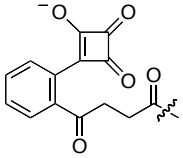	0.17 ± 0.05	1.3
(**8**) lactol	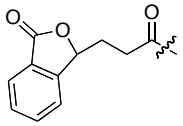	> 100	> 14
(**9**) lactam	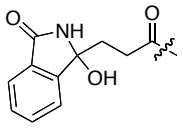	> 100	> 14
(**74**) difluoroindandiol	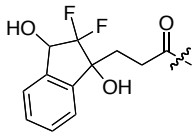	1.5 ± 0.1	11.5

IC_{50} values for inhibition of E. coli MenE (ecMenE). All IC_{50} measurements were performed in triplicate.

After observing that the most active keto-acid analogues carried negative charges at physiological pH [tetrazole (**3**) pK_a = 3.4, squaric acid (**7**) pK_a = 1.3], we measured the pK_a of the difluoroindanediol analogue **74** and determined a pK_a of 11.5. Although this is not sufficiently acidic to be in a deprotonated state at physiological pH, it is within range of deprotonation by the arginine we postulated could interact with the free carboxylate of OSB (arginine pK_a = 12.4). However, upon analyzing the pK_a of the trifluoroethanol analogue (**3**), we found that it has a nearly identical pK_a of 11.8, and so could presumably engage in the same interaction profile. However, it has an IC_{50} > 100-fold worse than that of the difluoroindanediol analogue. Additionally, upon investigating the K_d of the active compounds using isothermal titration calorimetry (ITC), we observed that, unlike the other active compounds (including OSB-AMS), the difluoroindanediol analogue bound with no detectable change in enthalpy and so required fluorescence binding assays to determine the K_d. Given the carboxylate of OSB will exist in a charged state at physiological pH prior to binding MenE, while the difluoroindanediol would exist in an uncharged state prior to binding MenE, if MenE was indeed deprotonating the difluoroindanediol in the binding pocket to form the postulated ionic interaction or is being deprotonated prior to binding, we would expect to see the opposite trend in the enthalpic binding profiles of the two inhibitors.[15-19] Taken together, the asymmetric activity of the trifluoroethanol analogue relative to the difluoroindanediol analogue, the notable decline in binding enthalpy compared to OSB-AMS, and crystallographic evidence (discussed in the next section) suggests the difluoroindanediol analogue has a distinct binding mode from that of OSB-AMS and our keto-acid analogues.

Therefore, although the difluoroindanediol shows modest inhibition of

MenE in biochemical assays, it appears to do so outside the paradigm of the keto-acid and lactol pharmacophore hypothesis. This leaves us with only keto-acid analogues showing activity against MenE, suggesting the keto-acid form of OSB-AMS is the active pharmacophore of MenE. This was confirmed a short time later by work that will be discussed in the next section.

2.3 Studies with the R195K mutant MenE enzyme.

As was discussed in Chapter 1, previous docking studies with the unliganded structure of *S. aureus* MenE found the highly conserved residue Arg222 (*E. coli* = R195, *M. tuberculosis* = R90) could engage in ionic interactions with the free carboxylate of OSB. To investigate the importance and role of this residue while potentially shedding light on the active pharmacophore of MenE, Dr. Joe Matarlo in the laboratory of Professor Peter Tonge replaced the Arg195 residue of *ec*MenE with either a lysine (R195K) or glutamine (R195Q) by site-directed mutagenesis.

Table 2.2. Catalytic and ITC data for the interaction between OSB and OSB-AMS with wild-type and mutant MenE.

ecMenE	K_M^{OSB} (μM)[a]	k_{cat} (min^{-1})[a]	k_{cat}/K_M (μM^{-1} min^{-1})[a]	$K_d^{OSB\text{-}AMS}$ (nM)[b]	ΔG (kcal/mol)[b]
wt	1 ± 0.02	46 ± 0.12	46 ± 0.023	44 ± 11	–10.0
R195K	16 ± 1.4	47 ± 0.33	3 ± 0.2	394 ± 36	–8.8
R195Q		not active		4500 ± 112	–7.3

[a]Kinetic parameters were obtained using the MenE–MenB coupled assay. Measurements were performed in 20 mM $NaHPO_4$ buffer (pH 7.4) containing 150 mM NaCl and 1 mM $MgCl_2$ at 25 °C. All measurements were performed in triplicate. [b]Binding of OSB-AMS to ecMenE determined by ITC. A 1 mM solution of inhibitor [dissolved in 20 mM $NaHPO_4$ buffer (pH 7.4) containing 150 mM NaCl and 1 mM $MgCl_2$ at 25 °C] was titrated in 4 µL increments into the 1.8 mL cell containing a 25 µM solution of ecMenE in the same buffer. The data were fit to a single-binding site model. Measurements were taken in triplicate.

While both *ec*MenE mutants showed no significant alteration to the secondary structure by circular dichroism spectroscopy, testing and analysis of the catalytic activity of the two mutants showed significant changes when compared to the wild-type MenE in MenE-MenB coupled assays. The R195K mutant MenE possessed a catalytic efficiency (k_{cat}/K_M) approximately 15-fold worse than the wild-type MenE and the R195Q mutant showed no catalytic activity with up to 240 μM OSB. Although the turnover rate was nearly identical between the wild-type and the R195K mutant, the binding efficiency of the R195K mutant was ~8-fold worse than that of the wild-type and the R195Q mutant showed a ~100-fold decrease in binding efficiency. Suggesting that the arginine is critically responsible for interactions with OSB in the binding pocket and likely engages the carboxylate in two distinct interactions. The lack of activity with the glutamine mutant also indicates that a negatively charged residue is necessary for optimal substrate recognition, which adds further evidence that the keto-acid is the active pharmacophore of MenE.

In order to fully validate the keto-acid as the active pharmacophore, Dr. Joe Matarlo began work towards a MenE•OSB-AMS cocrystal structure. These efforts met success with the R195K mutant of MenE, resulting in a 2.4 Å resolution OSB-AMS liganded crystal structure of MenE (PDB entry 5C5H). The electron density of the bound OSB-AMS is well defined and models clearly with the keto-acid form of OSB (Figure 2.15). The lactol forms of OSB-AMS are unable to adopt conformations that allow fitting to the electron density of the cocrystalized ligand in either the (*R*)-lactol or (*S*)-lactol forms. Taken together, our combined SAR, enzyme kinetics, and cocrystal structure support the conclusion that the keto-acid form of OSB-AMS is the active pharmacophore.

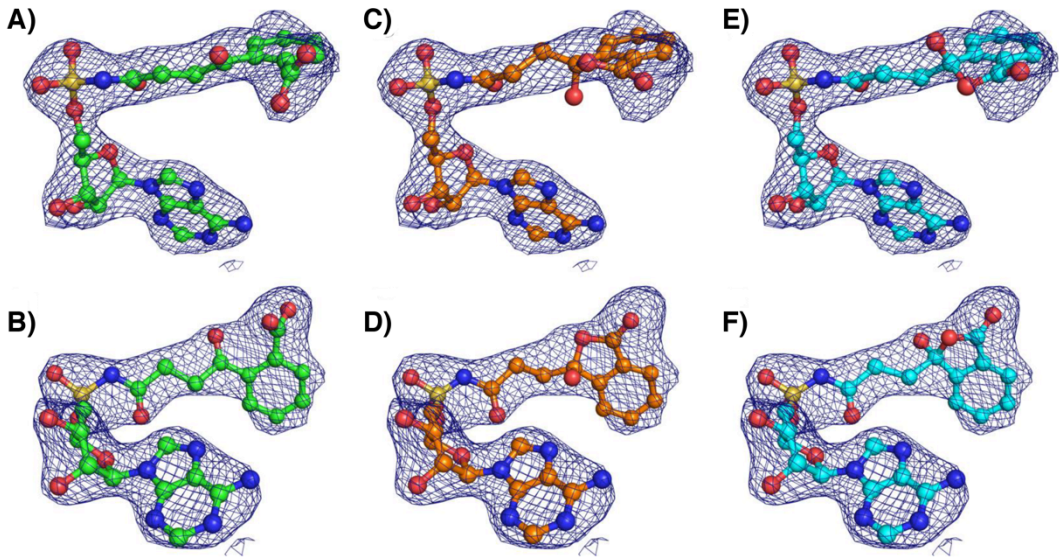

Figure 2.15: Modeling of the lactol isomer of OSB-AMS in the electron density of the ligand in *E. coli* MenE (R195K) active site. The electon density observed in the E. coli Mene (R195) mutant, shown contoured at 2.6 σ. A) Keto-acid form of OSB-AMS (B = rotated 100º on y-axis). C) (S)-lactol form of OSB-AMS (D = C rotated 100º on y-axis). E) (R)-lactol form of OSB-AMS (F = E rotated 100º on y-axis).

Using the crystal structure, we identified a number of highly conserved residues (Ser188, Lys195, Ser222, Thr277) in the OSB binding pocket that would confer binding specificity. While Lys195 (Arg195), Ser188, and Ser222 interact with the free-carboxylate of OSB via two bridging water molecules (Figure 2.16), Thr277 appears to interact directly with the free carboxylate. It is not known whether Arg195 in the wild-type MenE interacts with the free-carboxylate of OSB through these bridging water molecules or if they are eliminated upon binding and the arginine interacts directly with the free-carboxylate. In either case, the crystal structure clearly shows the keto-acid form of OSB-AMS binding to *ec*MenE in much the same conformation predicted in our previously published docking structure of OSB-AMSN to *sa*MenE.[2]

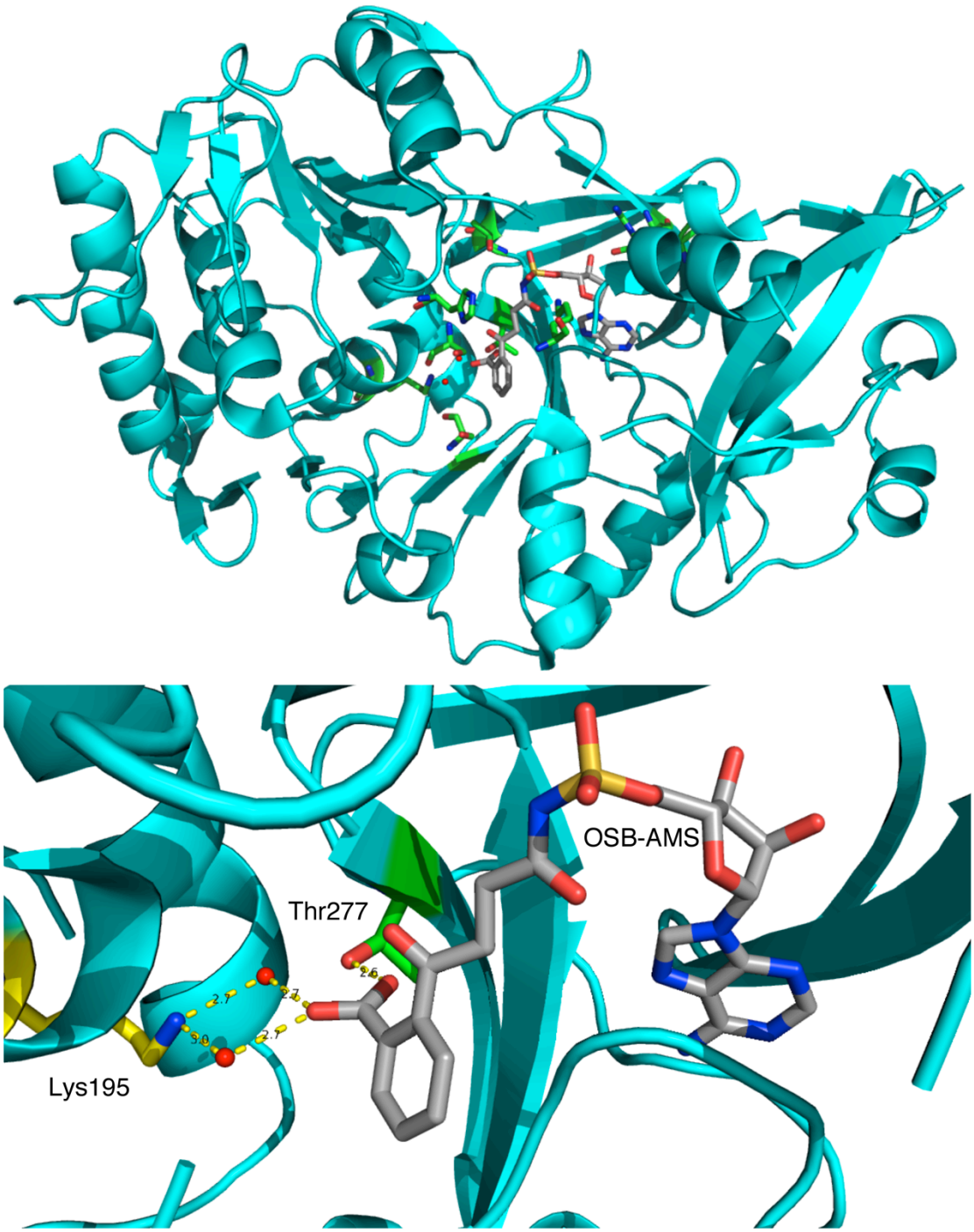

Figure 2.16: X-ray crystal structure of OSB-AMS·MenE (R195K) active site. A) OSB-AMS bound MenE with conserved residues (green). B) MenE binding pocket with interactions and distances between Thr277 (green) and Lys195 (yellow, via bridging waters) with carboxylate of OSB shown.

2.4 Cellular activity of OSB-AMS and the active keto-acid and lactol analogues.

In addition to biochemical assays against MenE, our collaborators in the laboratory of Prof. Peter Tonge tested the keto-acid and lactol analogues in antimicrobial assays against *M. tuberculosis*, methicillin-resistant *Staphylococcus aureus* (MRSA), and *B. subtilis*. OSB-AMS (**1,** Table 3) has an observed MIC of 62.5 μg/mL against *B. subtilis,* 31.25 μg/mL against MRSA, and 25 μg/mL against *M. tuberculosis*. Interestingly, the keto-acid analogues (tetrazole **2** and squarate **7**) showed no antimicrobial activity up to 250 μg/mL, while the difluoroindanediol analogue (**74**) had an MIC of 31.25 μg/mL against *B. subtilis,* 15.6 μg/mL against MRSA, and 15.6 μg/mL against *M. tuberculosis.* Importantly, this increase in toxicity was not observed in mammalian cell lines (Vero).

Table 2.3. Antimicrobial and cytotoxicity of MenE inhibitors.

	MIC (μg/mL)[a]			MIC + MK4 (μg/mL)[b]		Cytotoxicity (μg/mL)[c]
Inhibitor	*B. subtilis*	MRSA	*M. tuberculosis*	MRSA	*M. tuberculosis*	Vero
1	62.5	31.25	125	> 250	> 250	125
2	> 250	> 500	ND	> 500	ND	ND
7	> 250	> 500	ND	> 500	ND	ND
74	31.25	15.6	15.6	> 250	> 250	> 250

[a]MIC values were obtained against *B. subtilis* (ATCC 6057), methicillin-resistant *S. aureus* (ATCC BAA-1762), and *M. tuberculosis* (H37Rv). Inoculum levels for each MIC measurement ranged from 1 Å ~ 10^6 to 2 Å ~ 10^6 cells/mL. All MICs were determined in technical and experimental triplicate. [b]MICs determined with exogenous 10 μg/mL MK4 added to the synthetic growth medium. [c]Cytotoxicity values were obtained against Vero (monkey kidney epithelial) cells. Measurements were performed in technical and experimental triplicate. ND = not determined.

To validate the observed antimicrobial activity is due to inhibition of menaquinone production, assays against MRSA and *M. tuberculosis* were repeated in the presence of menaquinone-4 (MK4, 10 μg/mL). When cells treated with OSB-AMS based inhibitors were coadministered exogenous MK4, we observed rescue of normal cell growth, suggesting that antimicrobial activity arises through inhibition of MenE. To provide additional validation of on-target activity, the laboratory of Professor Peter Tonge used LC-MS/MS analysis of OSB-AMS treated MRSA to quantify levels of endogenous menaquinone. In MRSA treated with sub-lethal doses of OSB-AMS we observed a 3-5-fold decrease in endogenous menaquinone levels over non-treated cells, suggesting further that the observed antimicrobial activity is due to on-target inhibition of menaquinone biosynthesis.

2.4 Discussion and Conclusions

While the initial goal of this work was to determine which form of OSB-AMS is the active pharmacophore of MenE and gain a better understanding of the MenE binding pocket, the overarching goal of the work was to potentially discover an analogue able to exhibit increased antimicrobial activity over our lead compound OSB-AMS. To this end, keto-acid and lactol analogues of OSB-AMS were synthesized and tested in biochemical assays to determine their ability to inhibit MenE. We found the tetrazole (**2**), squarate (**7**), and difluoroindanediol (**74**) analogues of OSB-AMS inhibited MenE in good (squarate: *ec*MenE IC_{50} = 0.17 μM) to modest (tetrazole: *ec*MenE IC_{50} = 2.2 μM, difluoroindanediol: *ec*MenE IC_{50} = 1.5 μM) concentrations. We determined that the difluoroindanediol is likely inhibiting MenE through a

distinct binding mode from OSB-AMS and the other keto-acid analogues, which resulted in only keto-acid form analogues showing appreciable activity in biochemical assays. These results suggested that the keto-acid form of OSB-AMS is the active pharmacophore.

Through the use of MenE mutants (R195K, R195Q), we showed the importance of the previously discovered Arg195 to proper recognition of the OSB substrate. Additionally, the R195K mutant of MenE was cocrystalized with OSB-AMS to show the keto-acid form of OSB-AMS interacting with the R195K side-chain via two bridging water molecules. Taken together, our evidence strongly suggests the keto-acid form of OSB-AMS is the active pharmacophore.

In antimicrobial assays we discovered the keto-acid analogues (tetrazole **2** and squarate **7**) showed no activity (MIC) up to 250 μg/mL, while the difluoroindanediol analogue **74** exhibited antimicrobial activity (MIC) 2–10-fold better than that of OSB-AMS against a variety of bacterial species. Importantly, the difluoroindanediol analogue showed improved antimicrobial activity but exhibited no increase in cytotoxicity against mammalian cells. We observed a rescue of normal cell growth through addition of exogenous menaquinone-4 in bacteria treated with difluoroindanediol and OSB-AMS, and showed menaquinone production in MRSA is inhibited through treatment with OSB-AMS. These results suggest that the active analogues are in fact inhibiting menaquinone production, ostensibly through inhibition of the desired target MenE.

While these results are promising and seem to achieve the goals set out at the beginning of the chapter, the reason for the increased antimicrobial activity of the difluoroindanediol is uncertain. One possible explanation of the

increase activity is the loss of one of the negative charges in the difluoroindanediol analogue relative to OSB-AMS at physiological pH, thereby allowing for higher intracellular concentrations of drug. However, as was noted in Chapter 1, antimicrobial activity of OSB-AMS is only observed with intracellular concentrations ~4-log higher than the IC_{50} of the inhibitor to MenE. If this trend were generally true for all OSB-AMS based inhibitors of MenE, it would imply the difluoroindanediol analogue must have an intracellular concentration of ~15 mM, or roughly 1000-fold higher than the extracellular concentration of drug at the observed MIC. While cells rely on establishment of concentration gradients between the cytosol and the extracellular medium for maintaining membrane potential and uptake of key nutrients from the environment; examples of drugs known to use active-transport in the literature never reach such disparity in concentrations across the membrane.[20-21] Such a disparity would also stand in stark contrast to observed trends observed by our laboratory with acyl-AMS based compounds in published LC-MS/MS based compound accumulation assays.[22] Another possible explanation for the antimicrobial activity is the difluoroindanediol analogue exhibits a level of selectivity for MenE far higher than that of OSB-AMS. However, if we assume the difluoroindanediol is unique from every other polar acyl-AMS based compound and perfectly able to cross the cellular membrane to achieve 100% accumulation in the cells, it would require a specificity ~3-log better for MenE than that of OSB-AMS. While technically possible, given the IC_{50} of the difluoroindanediol is roughly ~3-log less potent than that of OSB-AMS, the likelihood of increased specificity being the cause of the increased activity is remote. The third possibility is the antimicrobial activity of the difluoroindanediol analogue is due to an unknown off-target binding event or

mechanism of action. While we do see rescue of normal cell growth in difluoroindanediol analogue treated MRSA with supplementation of exogenous MK-4, this is not proof that we are in fact inhibiting MenE. Certainly the difluoroindanediol analogue shows promise and warrants further investigation as to the mechanism behind the surprising improvement in antimicrobial activity.

2.5 Experimental Section

A. Materials and Methods

Reagents were obtained from Aldrich Chemical (www.sigma-aldrich.com) or Acros Organics (www.fishersci.com) and used without further purification. Optima or HPLC grade solvents were obtained from Fisher Scientific (www.fishersci.com), degassed with Ar, and purified on a solvent drying system. Reactions were performed in flame-dried glassware under positive Ar pressure with magnetic stirring.

TLC was performed on 0.25 mm E. Merck silica gel 60 F254 plates and visualized under UV light (254 nm) or by staining with potassium permanganate ($KMnO_4$), cerium ammonium molybdenate (CAM), or iodine (I_2). Silica flash chromatography was performed on E. Merck 230–400 mesh silica gel 60. Preparative scale HPLC purification was carried out on a Waters 2545 HPLC with 2996 diode array detector using a Sunfire Prep C18 reverse phase column (10 Å~ 150 mm, 5 µm) with UV detection at 254 nm. Samples were lyophilized using a Labconco Freezone 2.5 instrument.

IR spectra were recorded on a Bruker Optics Tensor 27 FTIR spectrometer with Pike technologies MIRacle ATR (attenuated total reflectance, ZnSe crystal) accessory and peaks reported in cm^{-1}. NMR spectra were recorded on a Bruker Avance III 500 instrument or Bruker Avance III 600 instrument at 24 °C in $CDCl_3$ unless otherwise indicated. Spectra were processed using Bruker TopSpin or nucleomatica iNMR (www.inmr.net) software, and chemical shifts are expressed in ppm relative to TMS (^1H, 0 ppm) or residual solvent signals: $CDCl_3$ (^1H, 7.24 ppm; ^{13}C, 77.23 ppm), CD_3OD (^1H, 3.31 ppm; ^{13}C, 49.15 ppm), D_2O (^1H, 4.80 ppm); coupling constants are expressed in Hz. Mass spectra were obtained at the MSKCC Analytical Core Facility on a Waters Acuity SQD LC-MS by electrospray (ESI) ionization or atmospheric pressure chemical ionization (AP-CI).

Atom numbers shown in chemical structures herein correspond to standard nucleoside numbering system and not to IUPAC nomenclature, which was used solely for each compound. Compounds not cited above are numbered henceforth from **S1**.

B. Tetrazole Analogue (2).

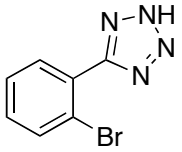

5-(2-Bromophenyl)-2*H*-tetrazole (16). 2-Bromobenzonitrile (**15**) (1 g, 5.494 mmol, 1 equiv), triethylamine hydrochloride (2.269 g, 16.482 mmol, 3.0 equiv), and sodium azide (1.072 g, 16.482 mmol, 3.0 equiv) were suspended in 20 mL toluene and stirred at 100 ºC for 6 h. The reaction was then cooled to rt, filtered through a celite pad, and concentrated under vacuum. The residue was reconstituted in 20 mL water, acidified with 1 M $KHSO_4$, and extracted with EtOAc (5 x 20 mL). The combined organic extracts were dried (Na_2SO_4), filtered, and concentrated by rotary evaporation. Purification by silica flash chromatography (0% → 25% EtOAc in hexanes with 1% AcOH) yielded the title product **16** (1.175 g, 95% yield) as a white solid.

IR (ATR): 2465, 1604, 1574, 1475, 1447, 1435, 1396, 1276, 1247, 1165, 1093, 1056, 1027, 1011, 995, 924, 879, 773, 7485, 712, 643. **^{1}H-NMR** (600 MHz; CD_3OD): δ 7.83 (dd, *J* = 8.0, 0.9 Hz, 1H), 7.69 (dd, *J* = 7.6, 1.5 Hz, 1H), 7.56 (td, *J* = 7.6, 1.2 Hz, 1H), 7.51 (td, *J* = 7.8, 1.7 Hz, 1H). **^{13}C-NMR** (150 MHz; CD_3OD): δ 156.211, 134.966, 133.866, 133.025, 129.233, 127.560, 123.224. **HRMS** (ESI) *m/z* calcd for $C_7H_6BrN_4$ ($[M+H]^+$) 224.9776; found 224.9781.

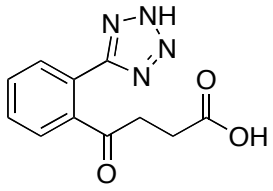

4-(2-(2*H*-Tetrazol-5-yl)phenyl)-4-oxobutanoic acid (17). Aryl bromide **16** (107 mg, 0.475 mmol, 1 equiv) and HMPA (191.5 mg, 1.069 mmol, 2.25 equiv) were dissolved in 0.5 mL THF before being cooled to –78 ºC. *n*-BuLi (0.668 mL, 1.069 mmol, 2.25 equiv, 1.6 M in THF) was added drop wise and the reaction stirred for 1 h at –78 ºC. The reaction was added via cannula to a suspension of succinic anhydride (190 mg, 1.901 mmol, 4.0 equiv) in 2 mL THF at –78 ºC, then stirred for 6 h. The reaction was warmed to rt and quenched with 10 mL 1M HCl before being extracted with EtOAc (5 x 10 mL). The combined organic extracts were dried (Na_2SO_4), filtered, and concentrated by rotary evaporation. Purification by silica flash

chromatography (25% → 75% EtOAc in hexanes, 1% AcOH) yielded the product (**17**) as a white crystalline solid (65 mg, 56%).

IR (ATR): 2964, 2926, 1712, 1402, 1368, 1176, 1102, 991, 778, 756. **^{1}H-NMR** (600 MHz; CD_3OD): δ 7.96–7.95 (m, 1H), 7.72 (dq, *J* = 6.0, 3.0 Hz, 3H), 3.19 (t, *J* = 6.4 Hz, 2H), 2.67 (t, *J* = 6.4 Hz, 2H). **^{13}C-NMR** (150 MHz; CD_3OD): δ 203.563, 176.568, 140.785, 132.760, 132.282, 131.786, 129.928, 124.609, 37.299, 29.125. **HRMS** (ESI) *m/z* calcd for $C_{11}H_9N_4O_3$ ($[M+H]^+$) 269.0651; found 269.0668.

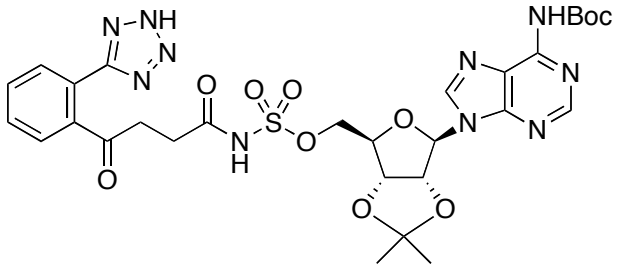

6-*N*-*t*-Butoxycarbonyl-2´,3´-*O*-isopropylidene-5´-*O*-(*N*-[4-(2-(2*H*-tetrazol-5-yl)phenyl)-4-oxobutanoyl]sulfamoyl)adenosine (19). Keto acid **17** (100 mg, 0.406 mmol, 1 equiv), protected 5´-*O*-sulfamoyladenosine **18** (296 mg, 0.609 mmol, 1.5 equiv), prepared as previously described,[2,23] and DMAP (50 mg, 0.406 mmol, 1 equiv) were suspended in 25 mL CH_2Cl_2 and EDCI (311 mg, 1.624 mmol, 4 equiv) added. The reaction was stirred for 3 h at rt before being quenched with 25 mL water and extracted with dichloromethane (5 x 25 mL). The combined organic extracts were dried (Na_2SO_4), filtered through a pad of celite, and concentrated by rotary evaporation to afford the crude protected tetrazole analogue **19** (473 mg, 163% crude yield), which was used without further purification.

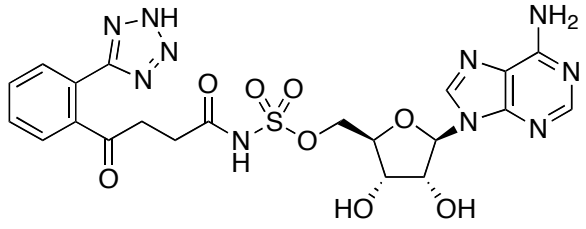

5´-*O*-(*N*-[4-(2-(2*H*-Tetrazol-5-yl)phenyl)-4-oxobutanoyl]sulfamoyl) adenosine (2). Crude protected tetrazole AMS analogue **19** was dissolved in 15 mL DCM and 1 mL H_2O, cooled to 0 ºC. TFA (15 mL) was added and the reaction stirred for 3 h while returning to rt. Concentration by rotary

evaporation, purification by preparative HPLC (5% → 95% MeCN in H_2O with 0.01% TFA), and lyophilization yielded tetrazole analogue **2** as a fluffy white solid (78 mg, 33% over two steps).

IR (ATR): 3321, 3115, 2908, 2824, 1693, 1615, 1479, 1424, 1363, 1201, 1121, 975, 872, 730. **^{1}H-NMR** (600 MHz; CD_3OD): δ 8.45 (s, 1H), 8.33 (s, 1H), 7.95–7.93 (m, 1H), 7.71–7.68 (m, 3H), 6.09 (d, *J* = 5.1 Hz, 1H), 4.62 (t, *J* = 5.1 Hz, 1H), 4.55–4.48 (m, 2H), 4.36 (t, *J* = 4.7 Hz, 1H), 4.32 (q, *J* = 3.8 Hz, 1H), 3.25 (td, *J* = 6.1, 2.4 Hz, 2H), 2.67 (t, *J* = 6.1 Hz, 2H). **^{13}C-NMR** (151 MHz; CD_3OD): δ 203.1, 172.8, 153.1, 150.3, 147.4, 143.2, 140.2, 133.0, 132.5, 131.8, 130.1, 124.2, 120.5, 90.2, 83.7, 75.8, 72.3, 71.7, 36.6, 30.9. **HRMS** (ESI) *m/z* calcd for $C_{21}H_{23}N_{10}O_8S$ ($[M+H]^+$) 575.1421; found 575.1436.

C. Trifluoroethanol analogue (3).

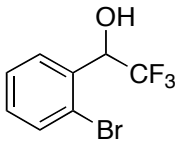

1-(2-Bromophenyl)-2,2,2-trifluoroethanol (21). Isopropylmagnesium bromide (40.75 mL, 52.98 mmol, 1.25 equiv, 1.3 M in THF) was cooled to 0 ºC, 1,2-dibromobenzene (10 g, 42.39 mmol, 1 equiv) was added drop wise and allowed to stir for 1.5 h. The solution was added drop wise via cannula over 30 min to a stirring solution of trifluoroacetic anhydride (32.63 g, 211.9 mmol, 5.0 equiv) in THF (100 mL) at 0 ºC. The reaction was stirred for 30 min, quenched with saturated ammonium chloride (100 mL), diluted with water (200 mL) and extracted with Et_2O (3 x 200 mL). The combined organic extracts were dried (Na_2SO_4), filtered, and concentrated by rotary evaporation. The crude product was dissolved in MeOH (75 mL) and cooled to 0 ºC. $NaBH_4$ (1.9 g, 50.38 mmol, 1.25 equiv) was added in three portions over 15 min. The reaction was stirred for 15 min before being quenched with 1M HCl (250 mL) and extracted with CH_2Cl_2 (4 x 200 mL). The combined organic extracts were dried (Na_2SO_4), filtered, and concentrated by rotary evaporation. Purification by silica flash chromatography (0% → 15% EtOAc in hexanes) yielded the product (**21**) as a clear, colorless oil (8.6 g, 84% over two steps).

IR (ATR): 3377, 1441, 1265, 1173, 1125, 1077, 1026, 874, 830, 757, 730, 701, 674, 624. **^{1}H-NMR** (500 MHz; $CDCl_3$): δ 7.68 (d, *J* = 7.8 Hz, 1H), 7.60 (dd, *J* = 8.0, 0.9 Hz, 1H), 7.40 (td, *J* = 7.6, 0.6 Hz, 1H), 7.28–7.25 (m, 1H), 5.65–5.61

(m, 1H), 2.66 (d, *J* = 4.1 Hz, 1H). **^{13}C-NMR** (126 MHz; $CDCl_3$): δ 133.7, 133.0, 131.0, 129.3, 127.9, 124.3, 123.9, 77.3, 77.0, 76.8, 71.3. **^{19}F-NMR** (471 MHz; $CDCl_3$): δ -77.6. **HRMS** (ESI) *m/z* calcd for $C_8H_5BrF_3O$ ($[M-H]^-$) 252.9481; found 252.9476.

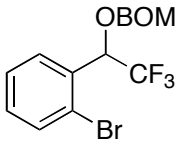

1-(1-((Benzyloxy)methoxy)-2,2,2-trifluoroethyl)-2-bromobenzene (27). NaH (70 mg, 2.940 mmol, 1.5 equiv) was suspended in THF (3 mL), cooled to 0 ºC, and trifluoroethanol analogue **21** (500 mg, 1.960 mmol, 1 equiv) in THF (2 mL) was added drop wise. The reaction was stirred for 15 min, then BOMCl (613 mg, 3.920 mmol, 2.0 equiv) in THF (2 mL) was added drop wise. The reaction was stirred for 4 h, then quenched with saturated ammonium chloride (50 mL), and extracted with CH_2Cl_2 (4 x 50 mL). The combined organic extracts were dried (Na_2SO_4), filtered, and concentrated by rotary evaporation. Purification by silica flash chromatography (0% → 15% EtOAc in hexanes) yielded the product (**27**) as a clear, colorless oil (680 mg, 92%).

IR (ATR): 2956, 2898, 1497, 1472, 1441, 1372, 1272, 1167, 1133, 1041, 980, 906, 846, 734, 699, 677, 626. **^{1}H-NMR** (500 MHz; $CDCl_3$): δ 7.65 (d, *J* = 7.8 Hz, 1H), 7.59 (d, *J* = 8.1 Hz, 1H), 7.38 (t, *J* = 7.6 Hz, 1H), 7.30 (td, *J* = 11.7, 5.8 Hz, 3H), 7.26–7.23 (m, 3H), 5.69 (q, *J* = 6.5 Hz, 1H), 4.87 (d, *J* = 6.9 Hz, 1H), 4.67 (dd, *J* = 16.2, 9.3 Hz, 2H), 4.48 (d, *J* = 11.6 Hz, 1H). **^{13}C-NMR** (126 MHz; $CDCl_3$): δ 136.9, 133.0, 132.7, 131.0, 130.0, 128.5, 128.08, 127.97, 127.82, 124.8, 124.1, 93.1, 73.9, 70.1. **^{19}F-NMR** (471 MHz; $CDCl_3$): δ -75.909. **HRMS** (ESI) *m/z* calcd for $C_{16}H_{14}BrF_3O_2Na$ ($[M+Na]^+$) 397.0027; found 397.0020.

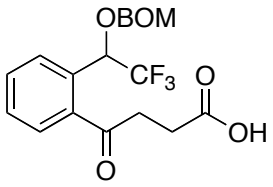

4-Oxo-4-(2-(1-((benzyloxy)methoxy)-2,2,2-trifluoroethyl)phenyl)butanoic acid (28). Isopropylmagnesium chloride (4.1 mL, 5.33 mmol, 2.0 equiv, 1.3 M in THF) was cooled to 0 ºC and arylbromide **27** (1 g, 2.665 mmol, 1 equiv) in THF (2.5 mL) was added drop wise. The reaction was stirred at 0 ºC for 1 h, then added drop wise via cannula to a stirring suspension of succinic

anhydride (800 mg, 7.995 mmol, 3.0 equiv) in THF (10 mL) at 0 ºC. The reaction was stirred for 6 h while returning to rt, then quenched with 1 M HCl and extracted with EtOAc (4 x 100 mL). The combined organic extracts were dried (Na_2SO_4), filtered, and concentrated by rotary evaporation afford the crude acid **28** (1.4 g, 141% crude yield), which was used without further purification.

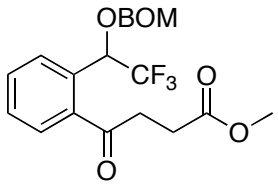

Methyl 4-oxo-4-(2-(1-((benzyloxy)methoxy)-2,2,2-trifluoroethyl)phenyl) butanoate (29). Keto acid **28** from previous step and K_2CO_3 (1.471 g, 10.65 mmol, 4 equiv.) were suspended in 25 mL MeCN before CH_3I (1.511 g, 10.65 mmol, 4 equiv) added. The reaction was heated to 50 ºC for 2 hours, then cooled to room temperature before being diluted with water (100 mL) and extracted with CH_2Cl_2 (4 x 100 mL). The combined organic extracts were dried (Na_2SO_4), filtered, and concentrated by rotary evaporation. Purification by silica flash chromatography (10% → 30% EtOAc in hexanes) yielded the product (**29**) as a clear, colorless oil (440 mg, 40%).

IR (ATR): 2956, 2899, 1734, 1689, 1579, 1438, 1359, 1269, 1218, 1164, 1125, 1040, 978, 845, 735, 987, 628. **^{1}H-NMR** (500 MHz; $CDCl_3$): δ 7.85 (d, *J* = 7.8 Hz, 1H), 7.79 (d, *J* = 7.8 Hz, 1H), 7.60–7.56 (m, 1H), 7.49 (td, *J* = 7.6, 1.2 Hz, 1H), 7.31–7.24 (m, 3H), 7.20 (d, *J* = 6.8 Hz, 2H), 6.16 (q, *J* = 6.7 Hz, 1H), 4.80 (dd, *J* = 62.2, 6.8 Hz, 2H), 4.54 (dd, *J* = 86.9, 11.6 Hz, 2H), 3.68 (s, 3H), 3.25 (ddd, *J* = 18.4, 7.3, 6.1 Hz, 1H), 3.09 (dt, *J* = 18.4, 6.3 Hz, 1H), 2.77–2.65 (m, 2H). **^{13}C-NMR** (126 MHz; $CDCl_3$): δ 201.9, 173.1, 138.3, 137.1, 132.6, 131.9, 129.4, 129.1, 128.51, 128.38, 128.02, 127.83, 124.2, 93.6, 70.6, 69.9, 51.9, 36.3, 28.1. **^{19}F-NMR** (471 MHz; $CDCl_3$): δ -75.685. **HRMS** (ESI) *m/z* calcd for $C_{21}H_{21}F_3O_5Na$ ($[M+Na]^+$) 433.1239; found 433.1238.

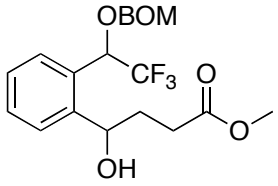

Methyl 4-(2-(1-((benzyloxy)methoxy)-2,2,2-trifluoroethyl)phenyl)-4-hydroxybutanoate (30). Aryl ketone **29** (158 mg, 0.385 mmol, 1 equiv) was

dissolved in MeOH (1 mL) and cooled to 0 ºC and $NaBH_4$ (18 mg, 0.481 mmol, 1.25 equiv) was added. The reaction was stirred for 1 h, then acetone (0.5 mL) was added. The reaction was stirred for 10 min at 0 ºC, then phosphate buffer (10 mL, 0.5 M, pH 7.0) was added. The reaction was stirred for 10 min 0 ºC, then extracted with CH_2Cl_2 (4 x 10 mL). The combined organic extracts were dried (Na_2SO_4), filtered, and reduced to 5 mL in volume by rotary evaporation at 0 ºC. The crude benzyl alcohol **30** solution was used immediately in the next step.

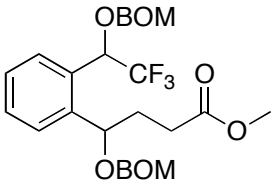

Methyl 4-((benzyloxy)methoxy)-4-(2-(1-((benzyloxy)methoxy)-2,2,2-trifluoroethyl)phenyl)butanoate (31). Crude benzyl alcohol **30** from previous step in 5 mL CH_2Cl_2 was cooled to 0 ºC, then NaI (23 mg, 0.1542 mmol, 0.1 equiv) and BOMCl (241 mg, 1.542 mmol, 4.0 equiv) were added quickly, followed by diisopropylethylamine (199 mg, 1.542 mmol, 4.0 equiv) added drop wise. The reaction stirred for 36 h at 0 ºC, then diluted with saturated sodium bicarbonate (10 mL) and extracted with CH_2Cl_2 (4 x 10 mL). The combined organic extracts were dried (Na_2SO_4), filtered, and concentrated by rotary evaporation. Purification by silica flash chromatography (0% → 10% EtOAc in CH_2Cl_2) yielded the product (**31**) as a clear, colorless oil (125 mg, 62% over 2 steps).

IR (ATR): 3032, 2952, 1735, 1497, 1454, 1381, 1268, 1237, 1162, 1132, 1109, 1027, 979, 907, 844, 765, 736, 698, 625. **^{1}H-NMR** (600 MHz; $CDCl_3$): δ 7.66 (t, *J* = 8.7 Hz, 1H), 7.50 (ddd, *J* = 16.6, 7.7, 1.3 Hz, 1H), 7.43-7.38 (m, 1H), 7.37–7.29 (m, 3H), 7.26 (td, *J* = 4.9, 2.8 Hz, 5H), 7.25–7.20 (m, 2H), 7.13 (dd, *J* = 7.3, 1.9 Hz, 1H), 5.62 (dq, *J* = 28.0, 6.7 Hz, 1H), 5.03 (ddd, *J* = 67.3, 9.9, 3.4 Hz, 1H), 4.83 (dd, *J* = 64.6, 7.0 Hz, 1H), 4.74–4.59 (m, 4H), 4.57–4.50 (m, 1H), 4.48–4.42 (m, 2H), 2.56–2.37 (m, 2H), 2.16–2.06 (m, 1H), 2.01–1.80 (m, 1H). **^{13}C-NMR** (151 MHz; $CDCl_3$): δ 173.6, 141.9, 141.5, 137.9, 137.27, 137.10, 131.2, 130.5, 129.70, 129.66, 128.7, 128.38, 128.36, 128.09, 128.03, 127.85, 127.82, 127.80, 127.66, 127.63, 127.52, 126.5, 124.44, 124.37, 93.17, 93.02, 92.81, 92.69, 73.7, 73.3, 71.3, 71.0, 69.87, 69.83, 51.58, 51.53, 32.8, 32.5, 30.8, 30.1. **^{19}F-NMR** (471 MHz; $CDCl_3$): δ -74.964, -75.855. **HRMS** (ESI) *m/z* calcd for $C_{29}H_{31}F_3O_6Na$ ($[M+Na]^+$) 555.1970; found 555.1984.

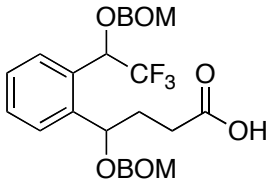

4-((Benzyloxy)methoxy)-4-(2-(1-((benzyloxy)methoxy)-2,2,2-trifluoroethyl)phenyl)butanoic acid (32). Methyl ester **31** (175 mg, 0.329 mmol, 1 equiv) and LiOH (31 mg, 1.314 mmol, 4.0 equiv) were suspended in MeOH:H_2O (4 mL, 9:1) and stirred at 50 ºC for 1 h. The reaction was returned to rt, diluted with 1 M $KHSO_4$ (15 mL) and extracted with EtOAc (4 x 15 mL). The combined organic extracts were dried (Na_2SO_4), filtered, and concentrated by rotary evaporation. Purification by silica flash chromatography (25% → 50% EtOAc in hexanes) yielded the product (**32**) as a white solid (164 mg, 96%).

IR (ATR): 3035, 2954, 2892, 1709, 1499, 1456, 1384, 1270, 1165, 1134, 1040, 982, 910, 846, 767, 738, 670, 651. **^{1}H-NMR** (600 MHz; $CDCl_3$): δ 7.65 (dd, *J* = 14.5, 7.6 Hz, 1H), 7.52–7.47 (m, 1H), 7.43–7.38 (m, 1H), 7.37–7.33 (m, 1H), 7.31–7.21 (m, 8H), 7.19 (dd, *J* = 8.5, 6.7 Hz, 1H), 7.11 (dd, *J* = 7.3, 1.8 Hz, 1H), 5.60 (dquintet, *J* = 15.5, 5.4 Hz, 1H), 5.03 (ddd, *J* = 67.1, 9.8, 3.3 Hz, 1H), 4.80 (dd, *J* = 41.6, 7.0 Hz, 1H), 4.68–4.66 (m, 2H), 4.64–4.60 (m, 1H), 4.59–4.57 (m, 1H), 4.54–4.52 (m, 1H), 4.50–4.42 (m, 2H), 2.56–2.40 (m, 2H), 2.17–2.03 (m, 1H), 1.99–1.80 (m, 1H). **^{13}C-NMR** (151 MHz; $CDCl_3$): δ 179.5, 141.7, 141.3, 137.8, 137.2, 137.0, 131.1, 130.4, 129.7, 128.8, 128.4, 128.17, 128.09, 128.03, 127.90, 127.85, 127.81, 127.69, 127.66, 127.52, 126.6, 124.40, 124.32, 92.99, 92.91, 92.83, 92.70, 73.7, 73.4, 71.12, 71.02, 69.94, 69.79, 32.3, 32.1, 30.8, 30.0. **^{19}F-NMR** (471 MHz; $CDCl_3$): δ -75.044, -75.900. **HRMS** (ESI) *m/z* calcd for $C_{28}H_{29}F_3O_6Na$ ($[M+Na]^+$) 541.1814; found 541.1837.

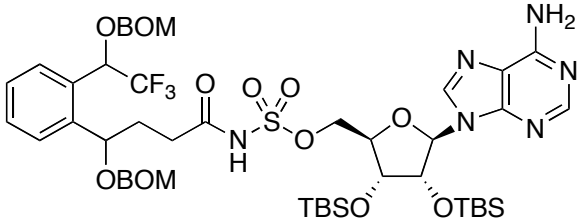

2´,3´-*O*-TBS-5´-*O*-(*N*-[4-((benzyloxy)methoxy)-4-(2-(1-((benzyloxy) methoxy)-2,2,2-trifluoroethyl)phenyl)butanoyl]sulfamoyl)adenosine (S1). Keto acid **32** (164 mg, 0.316 mmol, 1 equiv), protected sulfamoyladenosine **18** (227 mg, 0.395 mmol, 1.25 equiv), prepared as previously described,[2,23] and DMAP (38 mg, 0.316 mmol, 1 equiv) were suspended in CH_2Cl_2 (5 mL) and

EDCI (241 mg, 1.264 mmol, 4 equiv.) added. The reaction was stirred for 6 h, then water (20 mL) added, and extracted with ethyl acetate (5 x 20 mL). The combined organic extracts were dried (Na_2SO_4), filtered, and concentrated by rotary evaporation afford the crude acid **S1** (428 mg, 126% crude yield), which was used without further purification.

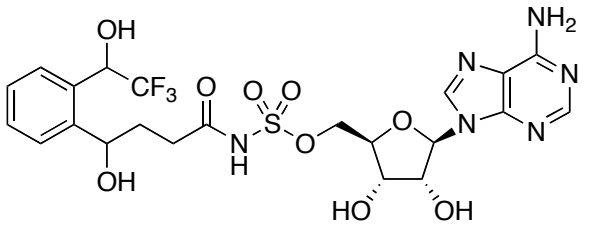

5´-*O*-(*N*-[4-Hydroxy-4-(2-(2,2,2-trifluoro-1-hydroxyethyl)phenyl)butanoyl] sulfamoyl)adenosine (3). Crude product **S1** from the previous step and 10% Pd/C (33 mg, 0.032mmol, 0.1 equiv) were dissolved in MeOH (30 mL) and 1 M HCl (0.3 mL) added. The reaction was stirred under H_2 (balloon) for 12 h at rt, then diluted with CH_2Cl_2 (70 mL), filtered through a pad of celite, and concentrated by rotary evaporation. The residue was suspended in DMF (5 mL) and TASF (260 mg, 0.944 mmol, 3.0 equiv) in DMF (1.5 mL) added. The reaction was stirred for 12 h, then concentration by rotary evaporation, purification by preparative HPLC (5% → 95% MeCN in H_2O with 0.01% TFA), and lyophilization yielded the product (**3**) as a fluffy white solid (42 mg, 22% over three steps).

IR (ATR): 3339, 2504, 1677, 1474, 1429, 1381, 1263, 1199, 1131, 1051, 978, 889, 834, 801, 768, 724, 706, 641, 613. **^{1}H-NMR** (500 MHz; CD_3OD): δ 8.50 (d, *J* = 4.1 Hz, 1H), 8.36 (s, 1H), 7.62–7.60 (m, 1H), 7.56–7.52 (m, 1H), 7.39–7.35 (m, 1H), 7.32–7.29 (m, 1H), 6.11 (dd, *J* = 4.6, 2.1 Hz, 1H), 5.60–5.52 (m, 1H), 5.01 (dd, *J* = 9.2, 3.4 Hz, 1H), 4.64 (dt, *J* = 10.2, 5.0 Hz, 1H), 4.60–4.51 (m, 2H), 4.42 (td, *J* = 5.0, 1.0 Hz, 1H), 4.32 (q, *J* = 4.0 Hz, 1H), 2.62–2.54 (m, 1H), 2.50–2.44 (m, 1H), 2.01–1.96 (m, 1H), 1.83–1.74 (m, 1H). **^{13}C-NMR** (151 MHz; CD_3OD): δ 173.57, 162.11, 147.10, 144.96, 143.42, 133.44, 130.19, 128.97, 128.96, 128.33, 126.71, 126.66, 126.54, 90.46, 83.58, 75.84, 72.32, 71.60, 69.80, 68.24, 34.57, 33.02. **HRMS** (ESI) *m/z* calcd for $C_{22}H_{26}F_3N_6O_9S$ ($[M+H]^+$) 607.1434; found 607.1423.

D. Oxazole analogue (3).

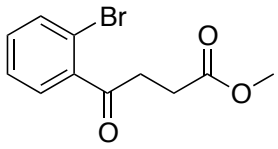

Methyl 4-(2-bromophenyl)-4-oxobutanoate (33). Isopropylmagnesium chloride (7.89 mL, 10.26 mmol, 1.1 equiv, 1.3 M in THF) was cooled to –23 ºC and 1, 2 dibromobenzene (2.2 g, 9.3 mmol, 1 equiv) was added. The reaction was stirred for 45 min, then slowly transferred via cannula to a stirring solution of succinic anhydride (2.799 g, 27.977 mmol, 3.0 equiv) in THF (20 mL) at –23 ºC. The reaction was stirred for 2 h, then quenched with ammonium chloride, acidified with 50 mL 1 M $KHSO_4$, and extracted with dichloromethane (3 x 50 mL). The combined organic extracts were dried (Na_2SO_4), filtered, and concentrated by rotary evaporation. The crude material was dissolved in MeOH (50 mL) and conc. sulfuric acid (92 mg, 0.9326 mmol, 0.1 equiv). The reaction was heated to reflux for 4 h and cooled to room temperature. The reaction was reduced to approximately 10 mL by rotary evaporation, diluted with 50 mL saturated sodium bicarbonate and extracted with dichloromethane (5 x 50 mL). The combined organic extracts were dried (Na_2SO_4), filtered, and concentrated by rotary evaporation. Purification by silica flash chromatography (10% EtOAc in hexanes) yielded the product **(33)** as a clear and colorless oil (1.45 g, 58% yield).

IR (ATR): 2952, 1736, 1703, 1587, 1564, 1467, 1436, 1354, 1020, 1281, 1217, 1167, 1123, 1072, 1048, 1027, 993, 946, 906, 847, 753, 722, 684, 642. **^{1}H-NMR** (600 MHz; $CDCl_3$): δ 7.61 (dd, *J* = 8.0, 1.0 Hz, 1H), 7.49 (dd, *J* = 7.6, 1.7 Hz, 1H), 7.38 (td, *J* = 7.5, 1.1 Hz, 1H), 7.30 (td, *J* = 7.7, 1.7 Hz, 1H), 3.71 (s, 3H), 3.24 (t, *J* = 6.6 Hz, 2H), 2.78 (t, *J* = 6.6 Hz, 2H). **^{13}C-NMR** (150 MHz; $CDCl_3$): δ 202.0, 173.0, 141.2, 133.7, 131.8, 128.8, 127.5, 118.7, 52.0, 37.4, 28.2. **HRMS** (ESI) *m/z* calcd for $C_{11}H_{12}O_3Br$ ($[M+H]^+$) 270.9970; found 270.9979.

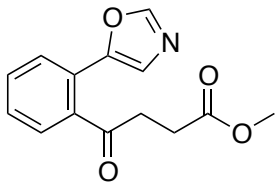

Methyl 4-(2-(5-oxazolyl)phenyl)-4-oxobutanoate (34). Bromobenzene compound **33** (130 mg, 0.4795 mmol, 1 equiv), pivalic acid (20 mg, 0.1918

mmol, 0.4 equiv), oxazole (66 mg, 0.959 mmol, 2.0 equiv), $Pd(OAc)_2$ (11 mg, 0.048 mmol, 0.1 equiv), RuPhos (45 mg, 0.0959 mmol, 0.2 equiv), and K_2CO_3 (199 mg, 1.4385 mmol, 3.0 equiv) were suspended in toluene (2 mL) and stirred at 110 ºC for 14 h. The reaction was cooled to rt, diluted with 5 mL H_2O and extracted with dichloromethane (4 x 5 mL). The combined organic extracts were dried (Na_2SO_4), filtered, and concentrated by rotary evaporation. Purification by silica flash chromatography (15% → 30% EtOAc in hexanes) yielded the title product (**34**) as a clear and colorless oil (60 mg, 49% yield).

IR (ATR): 1737, 1704, 1559, 1516, 1438, 1359, 1319, 1217, 1169, 1076, 1027, 987, 948, 920, 845, 779, 748, 717. **^{1}H-NMR** (600 MHz; $CDCl_3$): δ 7.99–7.97 (m, 1H), 7.71 (s, 1H), 7.55–7.50 (m, 2H), 7.44–7.43 (m, 1H), 7.22 (s, 1H), 3.11 (t, *J* = 6.8 Hz, 2H), 2.82 (t, *J* = 6.8 Hz, 2H). **^{13}C-NMR** (150 MHz; $CDCl_3$): δ 204.638, 173.360, 160.180, 140.929, 139.064, 130.361, 130.002, 128.695, 128.136, 126.696, 123.891, 51.863, 38.086, 28.489. **HRMS** (ESI) *m/z* calcd for $C_{14}H_{13}NO_4Na$ ($[M+H]^+$) 282.0742; found 282.0736.

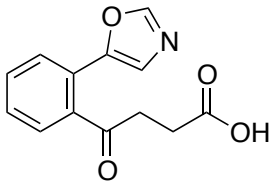

4-(2-(5-Oxazolyl)phenyl)-4-oxobutanoic acid (35). Methyl ester **34** (50 mg, 0.1929 mmol, 1 equiv) and LiOH (14 mg, 0.5787 mmol, 3.0 equiv) were dissolved in MeOH/H_2O (2 mL, 10:1) and stirred at room temperature for 2 h. The reaction was concentrated by rotary evaporation and purified by silica flash chromatography (25% → 50% EtOAc in hexanes with 1% AcOH) to yield the product (35) as an off white solid (40 mg, 85%).

IR (ATR): 1703, 1584, 1560, 1398, 1360, 1220, 1165, 1106, 1075, 991, 916, 824, 778, 731. **^{1}H-NMR** (600 MHz; $CDCl_3$): δ 7.99–7.97 (m, 1H), 7.71 (d, *J* = 0.7 Hz, 1H), 7.53 (qdd, *J* = 7.8, 7.4, 1.6 Hz, 2H), 7.43–7.41 (m, 1H), 7.23 (d, *J* = 0.5 Hz, 1H), 3.11 (t, *J* = 6.7 Hz, 2H), 2.86 (t, *J* = 6.7 Hz, 2H). **^{13}C-NMR** (150 MHz; $CDCl_3$): δ 204.359, 178.129, 160.181, 140.702, 139.153, 130.419, 130.131, 128.625, 128.248, 126.691, 123.891, 37.820, 28.507. **HRMS** (ESI) *m/z* calcd for $C_{13}H_{11}NO_4Na$ ($[M+Na]^+$) 268.0586; found 268.0578.

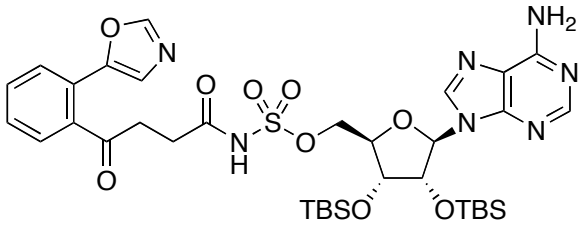

2´,3´-*O*-TBS-5´-*O*-(*N*-[4-(2-(5-oxazolyl)phenyl)-4-oxobutanoyl]sulfamoyl) adenosine (S2). Keto acid **35** (52 mg, 0.212 mmol, 1 equiv), protected 5´-*O*-sulfamoyladenosine **18** (152 mg, 0.265 mmol, 1.25 equiv), prepared as previously described,[2,23] and DMAP (26 mg, 0.212 mmol, 1 equiv) were dissolved in CH_2Cl_2 and EDCI (121 mg, 0.636 mmol, 3 equiv.) added. The reaction was stirred at rt for 4 h, quenched with 20 mL water, extracted with dichloromethane (5 x 20 mL). The combined organic extracts were dried (Na_2SO_4), filtered through a pad of celite, and concentrated by rotary evaporation to afford the crude protected oxazole analogue **S2** (240 mg, 141% crude yield), which was used without further purification.

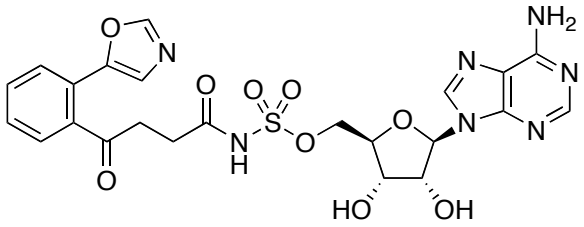

5´-*O*-(*N*-[4-(2-(5-Oxazolyl)phenyl)-4-oxobutanoyl]sulfamoyl)adenosine (4). Crude protected oxazole analogue **S2** from previous step was dissolved in THF (2 mL), cooled to 0 ºC and TBAF (0.3 mL, 0.2991 mmol, 3 equiv, 1.0 M in THF) was added before stirring for 1 h. Concentration by rotary evaporation, purification by preparative HPLC (5% → 95% MeCN in H_2O with 0.01% TFA), and lyophilization yielded the product (**4**) as a white fluffy solid (23 mg, 40% over 2 steps).

IR (ATR): 3325, 3131, 2922, 2824, 1698, 1471, 1421, 1365, 1199, 1135, 979, 886, 831, 721. **^{1}H-NMR** (600 MHz; CD_3OD): δ 8.48 (s, 1H), 8.34 (s, 1H), 7.95 (d, *J* = 0.8 Hz, 1H), 7.91 (dd, *J* = 7.6, 1.0 Hz, 1H), 7.61 (td, *J* = 7.5, 1.5 Hz, 1H), 7.57 (td, *J* = 7.5, 1.3 Hz, 1H), 7.53 (dd, *J* = 7.6, 1.2 Hz, 1H), 7.26 (d, *J* = 0.7 Hz, 1H), 6.10 (d, *J* = 4.9 Hz, 1H), 4.62 (t, *J* = 5.0 Hz, 1H), 4.58 (qd, *J* = 11.0, 3.3 Hz, 2H), 4.40 (t, *J* = 4.8 Hz, 1H), 4.33 (q, *J* = 3.8 Hz, 1H), 3.13 (t, *J* = 6.1 Hz, 2H), 2.71 (t, *J* = 6.3 Hz, 2H). **^{13}C-NMR** (125 MHz; CD_3OD): δ 205.844, 172.740, 161.911, 152.480, 150.178, 164.425, 143.537, 141.614, 141.433, 131.828, 131.740, 129.667, 129.259, 128.355, 125.382, 120.414, 90.289,

83.674, 75.885, 72.276, 71.692, 38.044, 31.082. **HRMS** (ESI) *m/z* calcd for $C_{23}H_{24}N_7O_9S$ ([M+H]$^+$) 574.1356; found 574.1367.

E. Boronate analogue (5).

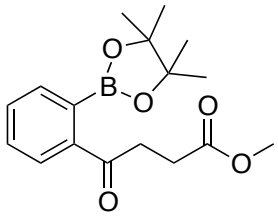

Methyl 4-oxo-4-(2-(4,4,5,5-tetramethyl-1,3,2-dioxaborolan-2-yl)phenyl) butanoate (36). Aryl bromide **33** (290 mg, 1.0697 mmol, 1 equiv), prepared as described above, $B_2(Pin)_2$ (340 mg, 1.3371 mmol, 1.25 equiv), sodium acetate (395 mg, 4.8137 mmol, 4.5 equiv), and $Pd(PPh_3)_2Cl_2$ (75 mg, 0.107 mmol, 0.1 equiv) were suspended in degassed dioxane (10 mL) and stirred at 90 ºC for 14 h. Concentration by rotary evaporation and purification by silica flash chromatography (10% → 20% EtOAc in hexanes) yielded the product (**36**) as a clear semisolid (240 mg, 71%).

IR (ATR): 2977, 1739, 1678, 1598, 1565, 1488, 1438, 1373, 1341, 1300, 1266, 1217, 1147, 1126, 1083, 1035, 962, 858, 755, 653. **^{1}H-NMR** (600 MHz; $CDCl_3$): δ 7.85 (d, J = 7.8, 1H), 7.54–7.53 (m, 2H), 7.44 (ddd, J = 7.8, 5.3, 3.4, 1H), 3.70 (s, 3H), 3.33 (t, J = 7.0, 2H), 2.78 (t, J = 7.0, 2H), 1.42 (s, 12H). **^{13}C-NMR** (150 MHz; $CDCl_3$): δ 199.80, 173.23, 140.43, 132.46, 132.34, 129.01, 127.56, 83.81, 51.84, 33.024, 28.14, 24.88. **HRMS** (ESI) *m/z* calcd for $C_{17}H_{24}BO_5$ ([M+H]$^+$) 319.1717; found 319.1729.

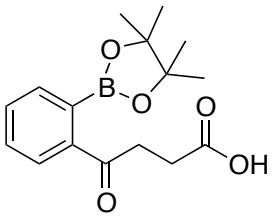

4-Oxo-4-(2-(4,4,5,5-tetramethyl-1,3,2-dioxaborolan-2-yl)phenyl)butanoic acid (37). Methyl ester **36** (80 mg, 0.2514 mmol, 1 equiv.) and LiOH (12 mg, 0.5028 mmol, 2.0 equiv.) were suspended in MeOH/H_2O (2 mL, 10:1) and stirred for 2 h at rt. Concentration by rotary evaporation and purification by

silica flash chromatography (10% → 20% EtOAc in hexanes with 1% AcOH) yielded the product (**37**) as a white oily solid (50 mg, 65%).

IR (ATR): 2982, 1714, 1679, 1604, 1570, 1490, 1378, 1345, 1300, 1200, 1151, 1090, 1040, 965, 683, 758, 674, 654. **^{1}H-NMR** (600 MHz; $CDCl_3$): δ 7.83 (d, *J* = 7.8 Hz, 1H), 7.53 (d, *J* = 4.1 Hz, 2H), 7.44 (dt, *J* = 8.3, 4.1 Hz, 1H), 3.32 (t, *J* = 6.9 Hz, 2H), 2.82 (t, *J* = 6.9 Hz, 2H), 1.42 (s, 11H). **^{13}C-NMR** (150 MHz; $CDCl_3$): δ 199.70, 177.95, 140.37, 132.51, 132.396, 129.05, 128.25, 127.55, 83.88, 32.80, 24.86. **HRMS** (ESI) *m/z* calcd for $C_{16}H_{21}BO_5Na$ ($[M+Na]^+$) 327.1380; found 327.1359.

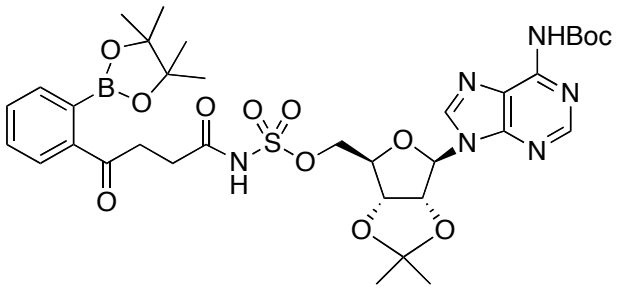

6-*N*-*t*-Butoxycarbonyl-2´,3´-*O*-isopropylidene-5´-*O*-(*N*-[4-oxo-4-(2-(4,4,5,5-tetramethyl-1,3,2-dioxaborolan-2-yl)phenyl)butanoyl]sulfamoyl) adenosine (S3). Keto acid **37** (100 mg, 0.3288 mmol, 1 equiv), protected 5´-*O*-sulfamoyladenosine **18** (240 mg, 0.4932 mmol, 1.5 equiv), prepared as previously described,[2,23] and DMAP (40 mg, 0.3288 mmol, 1 equiv.) were dissolved in CH_2Cl_2 (25 mL) and EDCI (251 mg, 1.315 mmol, 4 equiv) added. The reaction was stirred at rt for 4 h then quenched with water (30 mL) and extracted with dichloromethane (5 x 25 mL). The combined organic extracts were dried (Na_2SO_4), filtered through a pad of celite, and concentrated by rotary evaporation to afford the crude protected analogue **S3** (322 mg, 127% crude yield), which was used without further purification.

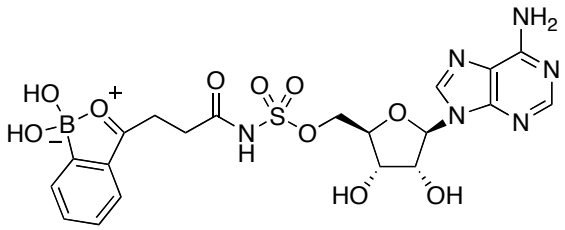

5´-*O*-(*N*-[4-(2-Boronophenyl)-4-oxobutanoyl]sulfamoyl)adenosine (5). Crude protected boronic acid analogue **S3** was dissolved in CH_2Cl_2 (2 mL) and water (0.2 mL) at 0 ºC and TFA (2 mL) added. The reaction was stirred for 1 h

at 0 ºC, then warmed to rt and stirred for 3 h. Concentration by rotary evaporation, purification by preparative HPLC (5% → 95% MeCN in H_2O with 0.01% TFA), and lyophilization yielded the product (**7**) as a fluffy white solid (74 mg, 41%).

IR (ATR): 3376, 2510, 1678, 1377, 1203, 1140, 979, 637. **^{1}H-NMR** (600 MHz; CD_3OD/d-TFA): δ 8.49 (s, 1H), 8.35 (s, 1H), 8.06 (d, *J* = 7.6 Hz, 1H), 7.62 (t, *J* = 7.3 Hz, 1H), 7.51 (td, *J* = 7.7, 1.1 Hz, 1H), 7.39 (d, *J* = 7.1 Hz, 1H), 6.10 (d, *J* = 4.9 Hz, 1H), 4.65 (q, *J* = 5.4 Hz, 1H), 4.63–4.57 (m, 2H), 4.41 (t, *J* = 4.8 Hz, 1H), 4.35 (dt, *J* = 7.3, 3.6 Hz, 1H), 3.42–3.36 (m, 2H), 2.75 (t, *J* = 6.2 Hz, 2H), 1.38 (s, 1H), 1.20 (s, 1H). **^{13}C-NMR** (150 MHz; CD_3OD/d-TFA): δ 203.749, 181.273, 155.558, 153.028, 149.146, 139.987, 138.573, 133.461, 131.048, 128.881, 128.838, 118.600, 87.245, 82.715, 75.504, 74.155, 70.484, 68.321, 32.796, 24.322. **HRMS** (ESI) *m/z* calcd for $C_{20}H_{24}BN_6O_{10}S$ ($[M+H]^+$) 551.1368; found 551.1387.

F. Squaric acid analogue (7).

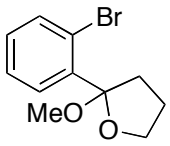

2-(2-Bromophenyl)-2-methoxytetrahydrofuran (43). Alkyne **42** (5.699 g, 25.3197 mmol, 1 equiv) and *p*-toluenesulfonic acid (482 mg, 2.532 mmol, 0.1 equiv) were dissolved in 250 mL MeOH and cooled to 0 ºC. PPh_3AuCl (125 mg, 0.2532 mmol, 0.01 equiv) and AgOTf (65 mg, 0.2532 mmol, 0.01 equiv) was added and the reaction stirred for 2 h at 0 ºC. The reaction was diluted with 500 mL saturated sodium bicarbonate and extracted with dichloromethane (3 x 500 mL). The combined organic extracts were dried (Na_2SO_4), filtered, and concentrated by rotary evaporation. Purification by silica flash chromatography (0% → 10% EtOAc in hexanes) yielded the product (**43**) as a clear and colorless oil (6.5 g, 99%).

IR (ATR): 3063, 2976, 2946, 2885, 2820, 1589, 1567, 1470, 1418, 1266, 1237, 1182, 1134, 1098, 1048, 1020, 936, 852, 755. **^{1}H-NMR** (600 MHz; $CDCl_3$): δ 7.78 (dd, *J* = 7.8, 1.8 Hz, 1H), 7.61 (dd, *J* = 7.9, 1.2 Hz, 1H), 7.30–7.28 (m, 1H), 7.15 (td, *J* = 7.6, 1.8 Hz, 1H), 4.07 (dtd, *J* = 33.1, 8.0, 6.1 Hz, 2H), 3.00 (s, 3H), 2.76 (ddd, *J* = 12.9, 8.5, 4.4 Hz, 1H), 2.21–2.14 (m, 1H), 2.02 (ddd, *J* = 12.9, 9.7, 7.4 Hz, 1H), 1.97–1.91 (m, 1H). **^{13}C-NMR** (150 MHz; $CDCl_3$): δ 139.550, 134.449, 129.415, 129.408, 126.856, 121.129, 108.608, 67.158,

49.615, 38.026, 24.726. **HRMS** (ESI) *m/z* calcd for $C_{11}H_{14}BrO_2$ ($[M+H]^+$) 257.0177; found 257.0158.

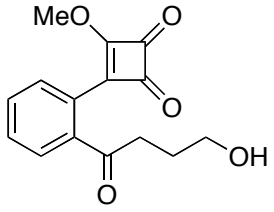

3-(2-(4-Hydroxybutanoyl)phenyl)-4-methoxycyclobut-3-ene-1,2-dione (45). Aryl bromide **43** (145 mg, 0.5639 mmol, 1 equiv) was dissolved in 0.5 mL THF and cooled to –78 ºC. *n*-BuLi (0.4053 mL, 0.6485 mmol, 1.15 equiv, 1.6 M in THF) was added drop wise and the reaction stirred for 1 h. Dimethyl squarate (160 mg, 1.128 mmol, 2.0 equiv) in 1 mL THF was added drop wise at –78 ºC, and the reaction stirred for 1.5 h. Trifluoroacetic anhydride (0.120 mL, 0.8459 mmol, 1.5 equiv) was added drop wise and the reaction stirred for 20 min. The reaction was quenched with 1 M HCl (5 mL) and warmed to 0 ºC before extracting with CH_2Cl_2 (5 x 5 mL). The combined organic extracts were dried (Na_2SO_4), filtered, diluted with 25 mL acetone, and reduced in volume to approximately 10mL by rotary evaporation at 0 ºC. The reaction was diluted with 25 mL acetone and reduced in volume to approximately 5 mL by rotary evaporation at 0 ºC. The crude product **45** in acetone was used immediately in the next step without further purification.

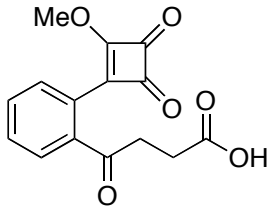

4-(2-(2-Methoxy-3,4-dioxocyclobut-1-enyl)phenyl)-4-oxobutanoic acid (46). Jones reagent was prepared by dissolving CrO_3 (280 mg, 2.8075 mmol, 5.0 equiv) in 1.5 mL H_2O and cooling to 0 ºC. Concentrated sulfuric acid (0.4679 mL, 8.4225 mmol, 15 equiv) was added drop wise and the solution allowed to stir for 15 min. The Jones reagent was added drop wise slowly to the stirring solution of crude alcohol **45** in 5 mL at 0 ºC until the reaction remained a persistent bright red (~30 min). The reaction was stirred for 15 min and quenched with isopropyl alcohol before being diluted with 10 mL water, and extracted with EtOAc (3 x 10 mL). The combined organic extracts were dried (Na_2SO_4), filtered, and concentrated by rotary evaporation.

Purification by silica flash chromatography (50% EtOAc in hexanes with 1% AcOH) yielded the product (**46**) as a white solid (77 mg, 48% over 2 steps).

IR (ATR): 3073, 2964, 1790, 1756, 1691, 1599, 1489, 1454, 1370, 1219, 1169, 11034, 923, 813, 763, 614. **^{1}H-NMR** (600 MHz; $CDCl_3$): δ 7.82 (dd, *J* = 7.6, 0.8 Hz, 1H), 7.73 (dd, *J* = 7.6, 1.0 Hz, 1H), 7.62 (td, *J* = 7.6, 1.2 Hz, 1H), 7.58 (td, *J* = 7.6, 1.2 Hz, 1H), 4.50 (s, 3H), 3.35 (t, *J* = 6.4 Hz, 2H), 2.85 (t, *J* = 6.4 Hz, 2H). **^{13}C-NMR** (150 MHz; $CDCl_3$): δ 201.040, 194.598, 192.453, 191.455, 176.055, 138.487, 131.764, 131.298, 128.863, 128.137, 124.563, 61.708, 35.351, 28.091. **HRMS** (ESI) *m/z* calcd for $C_{15}H_{11}O_6$ ([M-H]$^-$) 287.0556; found 287.0556.

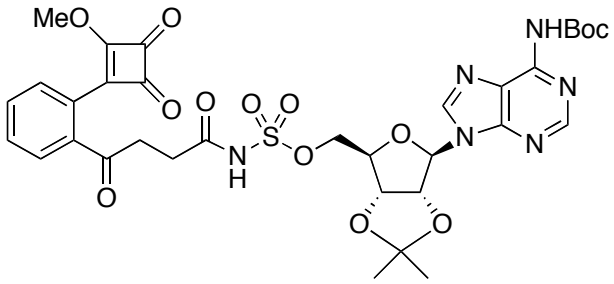

6-*N*-*t*-Butoxycarbonyl-2´,3´-*O*-isopropylidene-5´-*O*-(*N*-[4-(2-(2-methoxy-3,4-dioxocyclobut-1-enyl)phenyl)-4-oxobutanoyl]sulfamoyl)adenosine (S4). Keto acid **46** (69 mg, 0.2394 mmol, 1 equiv), protected 5´-*O*-sulfamoyladenosine **18** (146 mg, 0.2993 mmol, 1.25 equiv), prepared as previously described,[2,23] and DMAP (29 mg, 0.2394 mmol, 1 equiv) were suspended in 1 mL dichloromethane and EDCI (184 mg, 0.9576 mmol, 4.0 equiv) added. The reaction was stirred at rt for 4 hours, quenched with 1 mL water, diluted with 4 mL saturated sodium chloride, and extracted with dichloromethane (5 x 5 mL). The combined organic extracts were dried (Na_2SO_4), filtered through a pad of celite, and concentrated by rotary evaporation to afford the crude protected squarate analogue **S4** (353 mg, 195% crude yield), which was used without further purification.

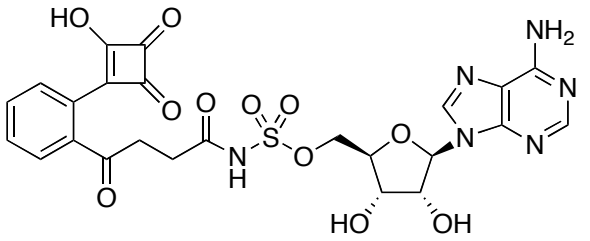

5´-*O*-(*N*-[4-(2-(2-Methoxy-3,4-dioxocyclobut-1-enyl)phenyl)-4-oxobutanoyl]sulfamoyl)adenosine (7). Crude protected squaric acid analogue **S17** was dissolved in 3 mL DCM and 0.2 mL H_2O. TFA (2mL) was added and the reaction heated to 50 ºC for 24 h before being returned to rt. Concentration by rotary evaporation, purification by preparative HPLC (5% → 95% MeCN in H_2O with 0.01% TFA), and lyophilization yielded the product (**4**) as a white fluffy solid (55 mg, 46% over 2 steps).

IR (ATR): 3321, 3124, 2972, 2930, 1696, 1454, 1360, 1205, 1124, 978, 882, 759, 917. **^{1}H-NMR** (600 MHz; DMSO-d_6/D_2O): δ 8.54 (s, 1H), 8.40 (s, 1H), 7.92–7.89 (m, 1H), 7.51 (td, *J* = 7.6, 1.3 Hz, 1H), 7.44 (dd, *J* = 7.7, 1.1 Hz, 1H), 7.33 (td, *J* = 7.5, 1.2 Hz, 1H), 5.98 (d, *J* = 5.1 Hz, 1H), 4.56 (t, *J* = 4.9 Hz, 1H), 4.51 (dd, *J* = 11.0, 3.2 Hz, 1H), 4.44 (dd, *J* = 11.0, 5.4 Hz, 1H), 4.21 (td, *J* = 7.0, 3.7 Hz, 2H), 3.09 (t, *J* = 6.5 Hz, 2H), 2.70 (t, *J* = 6.6 Hz, 2H). **^{13}C-NMR** (150 MHz; DMSO-d_6/D_2O): δ 215.520, 202.677, 195.756, 195.592, 175.892, 170.894, 148.415, 141.365, 137.499, 130.121, 127.738, 127.505, 127.429, 126.619, 125.220, 118.756, 87.782, 81.503, 73.371, 71.326, 69.900, 39.932, 35.952, 29.967. **HRMS** (ESI) *m/z* calcd for $C_{24}H_{23}N_6O_{11}S$ ([M+H]$^+$) 603.1146; found 603.1146.

G. Lactone analogue (8).

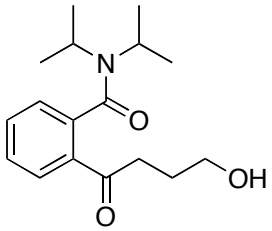

2-(4-Hydroxybutanoyl)-*N*,*N*-diisopropylbenzamide (48). *N*,*N*-Diisopropylbenzamide (**47**) (2 g, 9.742 mmol, 1 equiv.) was dissolved in dry THF (75 mL), cooled to -78 °C, and *t*-BuLi (6.35 mL, 10.81 mmol, 1.11 equiv,

1.7 M in THF) was added. The reaction was stirred for 45 min, then γ-butyrolactone (1.023 g, 11.89 mmol, 1.22 equiv) was added drop wise. The reaction was stirred for 1 h while returning to rt, then quenched with saturated ammonium chloride (75 mL) and extracted with ethyl acetate (5 x 75 mL). The combined organic extracts were dried (Na_2SO_4), filtered, and concentrated by rotary evaporation. Purification by silica flash chromatography (100% EtOAc) yielded the product (**48**) as a clear and colorless oil (2.570 g, 91%).

IR (ATR): 3392, 3063, 2971, 2934, 2876, 2240, 1772, 1689, 1615, 1438, 1370, 1343, 1213, 1163, 1035, 920, 774, 750. **^{1}H-NMR** (500 MHz; $CDCl_3$): δ 7.75 (d, J= 7.68, 1H), 7.49 (t, J=7.46, 1H), 7.40 (t, J= 7.57, 1H), 7.20 (d, J= 7.43, 1H), 3.64 (m, 3H), 3.51 (p, J= 6.78, 1H), 3.04 (t, J= 6.87, 1H), 2.81 (m, 1H), 1.93 (p, J= 6.39, 6.20, 2H), 1.56 (d, J=6.78, 6H), 1.14 (d, J= 6.58, 6H). **^{13}C-NMR** (125 MHz; $CDCl_3$): δ 202.27, 170.52, 138.81, 136.11, 131.64, 128.48, 128.16, 126.15, 61.36, 51.29, 45.75, 36.78, 26.99, 20.26. **HRMS** (ESI) *m/z* calcd for $C_{17}H_{26}NO_3$ ($[M+H]^+$) 292.1913; found 292.1934.

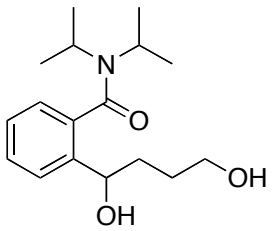

2-(1,4-Dihydroxybutyl)-*N,N*-diisopropylbenzamide (49). Aryl ketone **48** (2 g, 7.035 mmol, 1 equiv) was dissolved in MeOH (80 mL) and $NaBH_4$ (397 mg, 10.5 mmol, 1.5 equiv) added. The reaction was stirred for 12 h at rt, then quenched with 1 M HCl (20 mL), diluted with saturated sodium chloride (75 mL), and extracted with ethyl acetate (5 x 50 mL). The combined organic extracts were dried (Na_2SO_4), filtered, and concentrated by rotary evaporation afford the crude diol **49** (2.99 g, 145% crude yield), which was used without further purification.

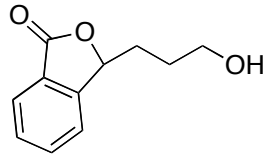

3-(3-Hydroxypropyl)isobenzofuranone (50). Crude diol **49** was dissolved in toluene (230 mL) and *p*-toluenesulfonic acid (12 mg, 0.070 mmol, 0.01 equiv) was added. The reaction was heated to reflux for 24 h, then cooled to rt and concentrated by rotary evaporation. Purification by silica flash

chromatography (100% EtOAc) yielded the product (**50**) as a greasy white solid (1.53 g, 82% over two steps).

IR (ATR): 3426, 3056, 2946, 2875, 2256, 1759, 1614, 1468, 1350, 1288, 1214, 1058, 954, 754, 741. **^{1}H-NMR** (500 MHz; $CDCl_3$): δ 7.88 (d, J=7.69, 1H), 7.68 (t, J= 7.51, 1H), 7.53 (t, J= 7.50, 1H), 7.46 (d, J= 7.50, 1H), 5.55 (q, J= 3.55, 3.98, 3.95, 1H), 3.91 (m, 2H), 2.24 (m, 1H), 1.96 (s, 1H), 1.78 (m, 3H). **^{13}C-NMR** (125 MHz; $CDCl_3$): δ 170.67, 149.89, 134.11, 129.17, 126.02, 125.70, 121.82, 81.26, 62.03, 31.35, 31.21, 27.90. **HRMS** (ESI) *m/z* calcd for $C_{11}H_{12}O_3Na$ ($[M+Na]^+$) 215.0684; found 215.0689.

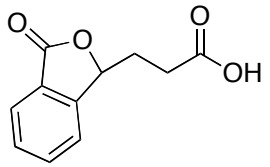

3-(3-Oxo-1,3-dihydroisobenzofuran-1-yl)propanoic acid (51). Alcohol **50** (400 mg, 2.09 mmol, 1 equiv) was dissolved in acetone (20 mL), cooled 0 ºC, then jones reagent (prepared as previously described using CrO_3 (1.044 g, 10.459 mmol, 5 equiv.), H_2O (13.3 mL), and conc. sulfuric acid (1.33 mL)) was added drop wise over 25 min until a deep red color persisted. The reaction was stirred for 20 min, then quenched with isopropyl alcohol, diluted with H_2O (80 mL), and extracted with ethyl acetate (5 x 80 mL). The combined organic extracts were dried (Na_2SO_4), filtered, and concentrated by rotary evaporation. Purification by silica flash chromatography (100% EtOAc with 1% AcOH) yielded the product (**51**) as a greasy white solid (380 mg, 89%).

IR (ATR): 3058, 2931, 2663, 2255, 1760, 1614, 1599, 1467, 1416, 1349, 1288, 1215, 1167, 1085, 1066, 1033, 938, 759, 741. **^{1}H-NMR** (500 MHz; $CDCl_3$): δ 10.59 (Br, 1H), 7.84 (d, J= 7.53, 1H), 7.63 (t, J= 7.53, 1H), 7.48 (t, J=7.53, 1H), 7.40 (d, J= 7.59, 1H), 5.49 (q, J= 3.04, 5.75, 2.49, 1H), 2.56 (m, 1H), 2.43 (m, 2H), 1.92 (m, 1H). **^{13}C-NMR** (125 MHz; $CDCl_3$): δ 178.12, 170.25, 149.06, 134.27, 129.48, 126.03, 125.93, 121.83, 29.70, 29.60, 29.19. **HRMS** (ESI) *m/z* calcd for $C_{11}H_{10}O_4Na$ ($[M+Na]^+$) 229.0477; found 229.0470.

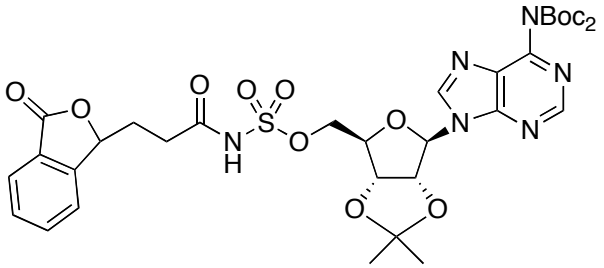

6-*N*-Bis-*t*-butoxycarbonyl-2´,3´-*O*-isopropylidene-5´-*O*-(*N*-[3-(3-oxo-1,3-dihydroisobenzofuran-1-yl)propanoyl]sulfamoyl)adenosine (S5). Propionic acid **51** (40 mg, 0.194 mmol, 1 equiv), protected 5´-*O*-sulfamoyladenosine **18** (141 mg, 0.291 mmol, 1.5 equiv), prepared as previously described,[2,23] and DMAP (24 mg, 0.194 mmol, 1 equiv) dissolved in CH_2Cl_2 (4 mL) and EDCI (511.8 mg, 2.67 mmol, 3 equiv) added. The reaction was stirred 14 h, then quenched with water (25 mL) and extracted with CH_2Cl_2 (5 x 25 mL). The combined organic extracts were dried (Na_2SO_4), filtered, and concentrated by rotary evaporation. Purification by silica flash chromatography (10% MeOH in CH_2Cl_2) yielded the product (**S5**) as a white solid (96 mg, 73%).

IR (ATR): 2982, 2932, 2854, 2254, 1763, 1601, 1579, 1496, 1454, 1371, 1339, 1286, 1257, 1212, 1142, 1112, 1082, 1034, 951, 914, 850, 795, 777, 734, 696, 647. **^{1}H-NMR** (600 MHz; CD_3OD): δ 8.86 (d, J = 1.3, 1H), 8.78 (s, 1H), 7.83 (d, J = 7.7, 1H), 7.74 (td, J = 7.5, 1.0, 1H), 7.62 (dd, J = 7.7, 0.8, 1H), 7.56 (t, J = 7.5, 1H), 6.37 (d, J = 2.9, 1H), 5.63 (dd, J = 8.2, 3.5, 1H), 5.43 (dd, J = 6.1, 2.9, 1H), 5.17 (dd, J = 6.1, 2.6, 1H), 4.57 (td, J = 4.2, 2.7, 1H), 4.31 (qd, J = 10.7, 4.3, 2H), 2.44–2.33 (m, 3H), 1.98–1.93 (m, 1H), 1.59 (s, 3H), 1.37 (s, 19H), 1.35 (s, 3H). **^{13}C-NMR** (150 MHz; CD_3OD): δ 172.52, 154.34, 153.29, 151.62,151.53, 151.1, 146.92, 135.72, 130.48, 130.42, 127.02, 126.33, 123.65, 115.60, 92.21, 85.92, 85.68, 85.53, 83.04, 82.66, 70.10, 35.13, 31.83, 28.05, 27.55, 25.58. **HRMS** (ESI) *m/z* calcd for $C_{34}H_{43}N_6O_{13}S$ ($[M+H]^+$) 775.2609; found 775.2607.

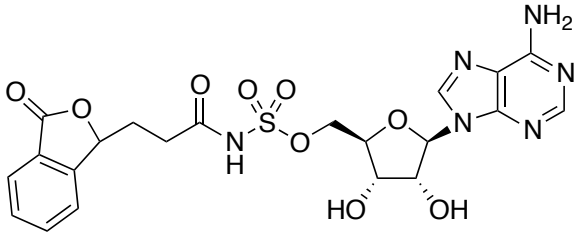

5´-*O*-(*N*-[3-(3-Oxo-1,3-dihydroisobenzofuran-1-yl)propanoyl]sulfamoyl) adenosine (8). Protected lactol analogue **S5** (40 mg, 0.0593 mmol, 1 equiv)

was dissolved in CH_2Cl_2 (1.5 mL) and water (0.25 mL), cooled to 0 º C, and TFA (1.5 mL) added. The reaction was stirred for 1 h at 0 ºC, then allowed to stir for 3 h while returning to rt. Concentration by rotary evaporation, purification by preparative HPLC (5% → 95% MeCN in H_2O with 0.01% TFA), and lyophilization yielded the product (**8**) as a fluffy white solid (28 mg, 88%).

IR (ATR): 3344, 2921, 2852, 1752, 1685, 1603, 1470, 1420, 1364, 1292, 1208, 1140, 1050, 842, 802, 724. **^{1}H-NMR** (600 MHz; CD_3OD): δ 8.51 (s, 1H), 8.17 (s, 1H), 7.82 (d, J = 7.7, 1H), 7.70 (td, J = 7.5, 1.0, 1H), 7.58 (dd, J = 7.7, 0.8, 1H), 7.55 (t, J = 7.5, 1H), 6.07 (d, J = 5.8, 1H), 5.61 (dd, J = 8.3, 3.4, 1H), 4.64 (t, J = 5.4, 1H), 4.38 (dd, J = 5.0, 3.3, 1H), 4.34 (dd, J = 11.7, 3.8, 1H), 4.29 (dt, J = 7.9, 3.6, 2H), 3.34 (s, 1H), 2.46–2.33 (m, 3H), 1.96–1.91 (m, 1H). **^{13}C-NMR** (150 MHz; CD_3OD): δ 181.49, 172.68, 157.32, 153.70, 151.69, 150.89, 141.18, 135.58, 130.37, 126.98, 126.25, 123.60, 120.19, 89.17, 84.65, 82.85, 76.25, 72.34, 69.21, 35.45, 32.28. **HRMS** (ESI) *m/z* calcd for $C_{21}H_{23}O_9N_6S$ ($[M+H]^+$) 535.1247; found 535.1238.

H. Lactam analogue (9).

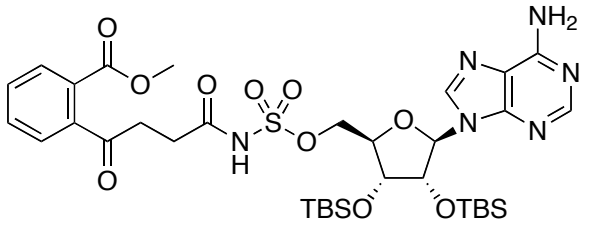

2´,3´-*O*-TBS-5´-*O*-(*N*-[4-(2-methoxycarbonyl)-4-oxobutanoyl]sulfamoyl) adenosine (56). 4-(2-(Methoxycarbonyl)phenyl)-4-oxobutanoic acid (183 mg, 0.774 mmol, 1 equiv), prepared as previously described, [2,23] protected 5´-*O*-sulfamoyladenosine **18** (667 mg, 1.161 mmol, 1.5 equiv), prepared as previously described,[2,23] and DMAP (95 mg, 0.774 mmol, 1 equiv) were dissolved in CH_2Cl_2 (25 mL) and EDCI (594 mg, 3.098 mmol, 4 equiv) added. The reaction was stirred for 12 h, quenched with water (25 mL), and extracted with CH_2Cl_2 (5 x 25 mL). The combined organic extracts were dried (Na_2SO_4), filtered through a pad of celite, and concentrated by rotary evaporation. Purification by silica flash chromatography (0% → 10% MeOH in CH_2Cl_2) yielded the product (**56**) as a white solid (370 mg, 60%).

IR (ATR): 2954, 2931, 2858, 1702, 1654, 1599, 1575, 1473, 1414, 1363, 1285, 1250, 1129, 1095, 1044, 992, 958, 865, 837, 779, 719, 675, 648. **^{1}H-NMR**

(600 MHz; acetone-d_6): δ 8.31 (s, 1H), 8.23 (s, 1H), 7.87 (dd, *J* = 7.7, 0.6 Hz, 1H), 7.66 (td, *J* = 7.5, 1.2 Hz, 1H), 7.58 (qd, *J* = 7.6, 1.0 Hz, 2H), 6.78 (s, 2H), 6.06 (d, *J* = 5.9 Hz, 1H), 5.09 (dd, *J* = 5.8, 4.4 Hz, 1H), 4.77-4.61 (m, 2H), 4.56 (t, *J* = 3.4 Hz, 1H), 4.35 (q, *J* = 3.7 Hz, 1H), 3.83 (s, 3H), 3.19 (t, *J* = 6.5 Hz, 2H), 2.85 (t, *J* = 6.4 Hz, 2H), 0.95 (s, 9H), 0.78 (s, 9H), 0.18 (s, 3H), 0.15 (s, 3H), -0.00 (s, 3H), -0.25 (s, 3H). **^{13}C-NMR** (151 MHz; acetone-d_6): δ 203.9, 167.7, 157.2, 153.7, 150.8, 143.7, 140.8, 133.2, 130.8, 130.4, 129.5, 127.6, 120.89, 120.85, 89.1, 83.5, 75.4, 73.5, 52.9, 37.5, 26.30, 26.15, 18.64, 18.46, -4.23, -4.35, -4.51, -5.0. **HRMS** (ESI) *m/z* calcd for $C_{34}H_{53}N_6O_{10}SSi_2$ ($[M+H]^+$) 793.3082; found 793.3007.

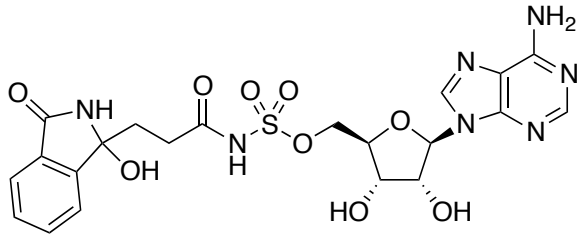

5´-*O*-(*N*-[3-(1-Hydroxy-3-oxoisoindolin-1-yl)propanoyl]sulfamoyl) adenosine (9). Protected MeOSB-AMS **56** (55 mg, 0.0694 mmol, 1 equiv) placed in a 15 mL pressure vessel and cooled to –78 ºC. Anhydrous ammonia (5 mL) was then condensed into the pressure vessel and sealed, then returned to rt and stirred for 2 h. The reaction was then cooled to –78 ºC, placed under cycling nitrogen, and allowed to slowly return to rt to remove the ammonia. The reaction was placed under high vacuum for 30 minutes, then suspended in THF (5 mL) and cooled to 0 ºC. TBAF (0.208 mL, 0.208 mmol, 3.0 equiv, 1.0 M in THF) was added and stirred for 1 h, before phosphate buffer (1 mL, 1M, pH 7.2), and 5 mL toluene were added before being concentrated by rotary evaporation. Purification by silica flash chromatography (10% → 20% MeOH in EtOAc) yielded the product (**10**) as the tetrabutylammonium salt (15 mg, 40% over two steps).

Assignment of **9** as the cyclic lactam isomer, as opposed to the open-chain keto amide isomer, was based on HMBC analysis of the analogous isolated side chain (see below) and correlation of the following diagnostic peaks: succinyl b-hydrogens C3-H_2 (d 2.49-2.23), hemiaminal C4 (d 89.18), lactam NH (DMSO-d_6: d 8.05), side chain OH (DMSO-d_6: d 5.9). This was necessary due to the inherently short half-life of **9** in its protonated sulfamate form, which requires isolation as the corresponding tetrabutylammonium salt, thereby precluding efficient multidimensional NMR analysis.

IR (ATR): 3328, 3190, 2964, 2876, 1707, 1654, 1599, 1471, 1420, 1364, 1298, 1223, 1148, 1088, 944, 884, 835, 801, 747, 718, 642. **^{1}H-NMR** (600 MHz; CD_3OD): δ 8.52 (s, 1H), 8.19 (s, 1H), 7.69–7.67 (m, 1H), 7.62 (tdd, J = 7.4,

2.2, 1.1, 1H), 7.59 (d, J = 7.5, 1H), 7.49 (tt, J = 7.4, 1.1, 1H), 6.09–6.08 (m, 1H), 4.64 (td, J = 5.4, 3.3, 1H), 4.37 (dd, J = 5.0, 3.2, 1H), 4.31-4.23 (m, 3H), 3.24–3.21 (m, 12H), 2.49–2.43 (m, 1H), 2.35–2.23 (m, 2H), 2.13–2.05 (m, 1H), 1.67–1.62 (m, 12H), 1.40 (sextet, J = 7.4, 12H), 1.01 (t, J = 7.4, 18H). **^{13}C-NMR** (150 MHz; CD_3OD): δ 181.98, 171.55, 161.54, 157.35, 153.92, 150.96, 150.59, 141.15, 134.00, 132.45, 130.49, 124.06, 123.49, 120.17, 89.18, 84.72, 76.41, 72.39, 68.88, 59.53, 36.17, 35.24, 24.85, 20.79, 14.02. **HRMS** (ESI) *m/z* calcd for $C_{21}H_{24}N_7O_9S$ ([M+H]$^+$) 550.1356; found 550.1362.

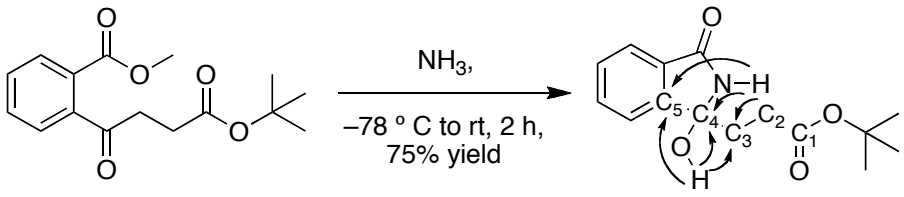

To assign the structure of lactam analogue **9** as the cyclic lactam isomer, as opposed to the corresponding open-chain keto amide isomer, the corresponding OSB side chain analogue, which could be isolated and characterized by multidimensional NMR analysis, was prepared. Thus, the known ketodiester, prepared as previously described,[2,23] was treated with ammonia to afford the lactam product. In acetone-d_6, the hemiaminal C4 (d 87.9) of the product shifted upfield compared to the ketone C4 (d 204.2) of the starting material. In the product, the succinyl β-protons C3-H_2 (d 2.44-2.25) were also shifted upfield compared to those in the starting material (d 3.10). Finally, HMBC correlations were observed between the NH (d 7.83) and C3 (d 35.0), C4 (d 87.9), and C5 (d 149.7), as well as between the OH (d 5.36) and C3, C4, and C5, consistent with the cyclic lactam structure shown and not the open-chain keto amide isomer nor the cyclic imidate isomer. In contrast, the open-chain keto amide isomer would not be expected to show HMBC correlations between the primary carboxamide NH_2 protons and C3 (6-bond), C4 (5-bond), or C6 (4-bond). This preference for the cyclic lactam isomer as opposed to the open-chain keto amide isomer is consistent with literature reports.[24-26]

IR (ATR): 3290, 2979, 2934, 1701, 1616, 1469, 1422, 1368, 1313, 1266, 1154, 1098, 1077, 969, 847, 766, 7337, 699, 630. **^{1}H-NMR** (600 MHz; acetone-d_6): δ 7.83 (s, 1H), 7.65-7.60 (m, 3H), 7.52 (td, *J* = 7.2, 1.2 Hz, 1H), 5.36 (s, 1H), 2.44-2.37 (m, 1H), 2.32-2.25 (m, 2H), 2.15-2.07 (m, 1H), 1.38 (s, 9H). **^{13}C-NMR** (150 MHz; acetone-d_6): δ 172.6, 168.7, 149.7, 133.2, 132.7, 130.1, 123.6, 123.1, 87.9, 80.5, 35.0, 31.1, 28.2. **HRMS** (ESI) *m/z* calcd for $C_{15}H_{20}NO_4$ ([M+H]$^+$) 278.1392; found 278.1405

I. Difluoroindanediol analogue (9).

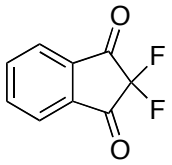

2,2-Difluoro-indene-1,3-dione (69). Selectfluor (24.24 g, 68.43 mmol, 2 equiv), 1,3 indandione **68** (5.0 g, 34.2 mmol, 1.0 equiv) and sodium dodecyl sulfate (99 mg, 0.342 mmol, 0.01equiv) were suspended in water (80 mL). The reaction was heated to 80 ºC for 8 h, then cooled to rt and extracted with Et_2O (5 x 80 mL). The combined organic extracts were dried (Na_2SO_4), filtered, and concentrated by rotary evaporation. Purification by sublimation (200 mTorr, 150 ºC) yielded the product **69** as bright white crystals (5.82 g, 93%).

IR (NaCl, Film): 3479, 3098, 1728, 1583, 1302, 1185, 1090, 1088, 733. **^{1}H-NMR** (500 MHz; $CDCl_3$): δ 8.16 (dtdd, *J* = 5.1, 3.2, 2.3, 0.0 Hz, 2H), 8.11–8.07 (m, 2H). **^{13}C-NMR** (125 MHz; $CDCl_3$): δ 185.923, 139.372, 138.276, 125.088, 102.538. **^{19}F-NMR** (471 MHz; $CDCl_3$): δ –124.843. **HRMS** (ESI) *m/z* calcd for $C_9H_5F_2O_2$ ($[M+H]^+$) 183.0258; found 183.0232.

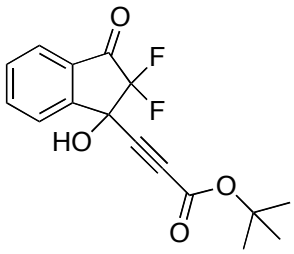

***tert*-Butyl 3-(2,2-difluoro-1-hydroxy-3-oxo-2,3-dihydro-indenyl)propiolate (70).** LiHMDS (13.72 mL, 13.72 mmol, 1.25 equiv, 1.0 M in THF) was cooled to –78 ºC and *t*-butyl propiolate (1.522 g, 12.07 mmol, 1.1 equiv) in THF (10 mL) was added drop wise over 10 min. The reaction was stirred for 1 h, then added via cannula over 30 min to a stirring solution of di-ketone **69** (2 g, 10.98 mmol, 1 equiv) in THF (10 mL) at –78 ºC. The reaction was stirred for 1 h, then quenched with saturated ammonium chloride (50 mL) and extracted with CH_2Cl_2 (5 x 50 mL). The combined organic extracts were dried (Na_2SO_4), filtered, and concentrated by rotary evaporation. Purification by silica flash chromatography (20% EtOAc in hexanes) yielded the product (**70**) as a clear and colorless oil (2.767g, 82%).

IR (ATR): 2988, 2211, 1757, 1712, 1606, 1475, 1401, 1375, 1262, 1221, 1155, 1021, 901, 843, 758, 718, 652. **^{1}H-NMR** (500 MHz; $CDCl_3$): δ 7.93 (dd, *J* = 7.6, 0.9 Hz, 1H), 7.90–7.87 (m, 2H), 7.67 (td, *J* = 7.5, 0.9 Hz, 1H), 4.17 (s, 1H), 1.50 (s, 9H). **^{13}C-NMR** (125 MHz; $CDCl_3$): δ 187.830, 157.996, 151.862, 148.999, 138.156, 131.910, 131.165, 126.282, 125.159, 85.122, 82.060, 77.523, 71.065, 27.933. **^{19}F-NMR** (471 MHz; $CDCl_3$): δ –111.190, –111.762, –125.772, –126.348. **HRMS** (ESI) *m/z* calcd for $C_{16}H_{15}F_2O_4Na$ ($[M+Na]^+$) 331.0758; found 331.0764.

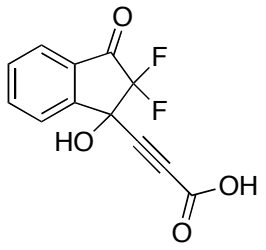

3-(2,2-Difluoro-1-hydroxy-3-oxo-2,3-dihydro-indenyl)propiolic acid (71). *t*-Butyl ester **70** (400 mg, 1.298 mmol, 1 equiv) was dissolved in CH_2Cl_2/H_2O (5 mL, 10:1) and cooled to 0 ºC, then TFA (5 mL) was added. The reaction was stirred for 2 h, then concentrated by rotary evaporation. Purification by silica flash chromatography (10% MeOH in CH_2Cl_2) yielded the product (**71**) as a white semi-solid (225 mg, 69%).

IR (ATR): 3410, 1752, 1690, 1605, 1370, 1277, 1201, 1141, 1082, 1024, 938, 903, 852, 768, 716, 649. **^{1}H-NMR** (500 MHz; DMSO-d6): δ 8.06–8.03 (m, 1H), 7.96–7.94 (m, 2H), 7.80–7.77 (m, 1H). **^{13}C-NMR** (125 MHz; DMSO-d6): δ 188.385, 153.757, 150.586, 138.920, 131.916, 129.758, 126.061, 124.830, 113.974, 83.152, 77.101, 70.006. **^{19}F-NMR** (471 MHz; $CDCl_3$): δ -113.646, -114.207, -128.356, -128.915. **HRMS** (ESI) *m/z* calcd for $C_{24}H_{11}F_4O_8$ ($[2M-H]^-$) 503.0390; found 503.0394.

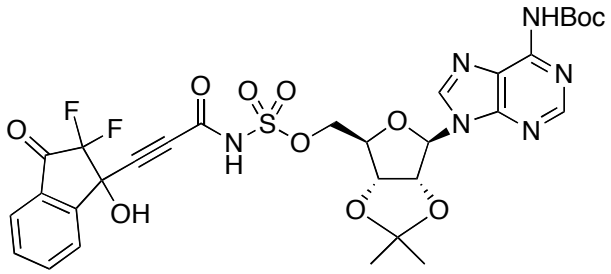

6-*N*-*t*-Butoxycarbonyl-2´,3´-*O*-isopropylidene-5´-*O*-(*N*-[3-(2,2-difluoro-1-hydroxy-3-oxo-2,3-dihydro-indenyl)propioloyl]sulfamoyl)adenosine (72).

Propiolic acid **71** (110 mg, 0.4362 mmol, 1 equiv), protected 5´-*O*-sulfamoyladenosine **18** (265 mg, 0.5452 mmol, 1.25 equiv), prepared as previously described,[2,23] and DMAP (53 mg, 0.4362 mmol, 1.0 equiv.) were dissolved in CH_2Cl_2 (5 mL) and EDCI (335 mg, 1.7448 mmol, 4.0 equiv) was added. The reaction was stirred for 4 h, then quenched with 30 mL water, and extracted with CH_2Cl_2 (5 x 25 mL). The combined organic extracts were dried (Na_2SO_4), filtered, and concentrated by rotary evaporation to afford the crude product **72** (427 mg, 136% crude yield), which was used without further purification.

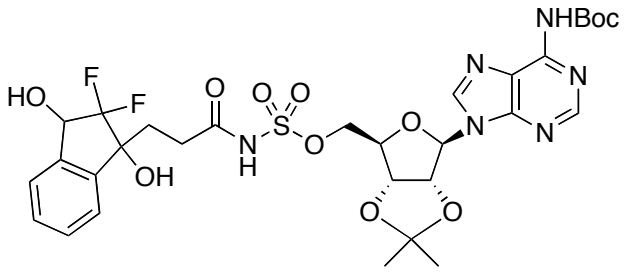

6-*N*-*t*-Butoxycarbonyl-2´,3´-*O*-isopropylidene-5´-*O*-(*N*-[3-(2,2-difluoro-1,3-dihydroxy-2,3-dihydro-1*H*-inden-1-yl)propanoyl]sulfamoyl)adenosine (73). Crude product **72** from previous step and 10% Pd/C (463.5 mg, 0.435 mmol, 1 equiv) were suspended in solution of MeOH/NEt_3 (40 mL, 9:1). The reaction was then stirred vigorously under H_2 balloon for 1 h before being diluted with EtOAc (50 mL), filtered through a celite pad, and concentrated by rotary evaporation to afford the crude product **73** (510 mg, 151% crude yield), which was used without further purification.

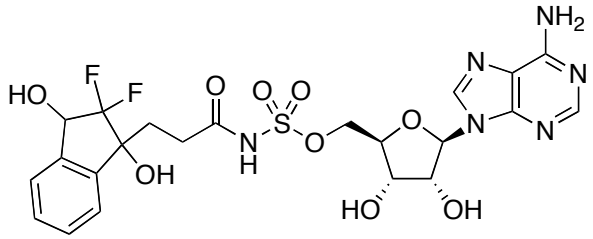

5´-*O*-(*N*-[3-(2,2-Difluoro-1-hydroxy-3-oxo-2,3-dihydro-indenyl)propioloyl] sulfamoyl)adenosine (74). Crude product **73** was suspended in CH_2Cl_2 (5 mL) and water (0.25 mL), then cooled to 0 ºC and TFA (5 mL) added. The reaction was stirred for 1 h at 0 ºC, then allowed to stir for 3 h while returning to rt. Concentration by rotary evaporation, purification by preparative HPLC (5% → 95% MeCN in H_2O with 0.01% TFA), and lyophilization yielded the product (**74**) as a fluffy white solid (71 mg, 28% over 3 steps).

IR (ATR): 3173, 2927, 1693, 1664, 1466, 1415, 1357, 1189, 1134, 1072, 872, 791, 717. **^{1}H-NMR** (500 MHz; CH_3OD): δ 8.47 (s, 1H), 8.35 (d, *J* = 1.8 Hz, 1H), 7.45–7.37 (m, 4H), 6.11–6.09 (m, 1H), 5.13–5.10 (m, 1H), 4.65–4.62 (m, 1H), 4.58–4.50 (m, 2H), 4.42–4.39 (m, 1H), 4.32–4.30 (m, 1H), 2.63 (td, *J* = 7.8, 2.8 Hz, 2H), 2.32–2.13 (m, 2H). **^{13}C-NMR** (150 MHz; CH_3OD): δ 173.449, 150.229, 147.018, 143.991, 143.408, 140.036, 139.286, 130.700, 130.631, 127.093, 126.441, 124.932, 120.495, 90.396, 83.610, 79.622, 75.770, 74.931, 72.261, 71.609, 31.317, 31.146. **^{19}F-NMR** (471 MHz; CH_3OD): δ –120.084, –120.581, –130.679, –131.147. **HRMS** (ESI) *m/z* calcd for $C_{22}H_{25}F_2N_6O_9S$ ($[M+H]^+$) 587.1372; found 587.1349.

J. MenE Biochemical Assay

Enzyme inhibition studies were performed in 20 mM $NaHPO_4$ buffer (pH 7.4) containing 150 mM NaCl and 1 mM $MgCl_2$ using a MenE-MenB coupled assay in which MenE is rate-limiting. IC_{50} values were determined in reaction mixtures containing OSB (60 μM), ATP (240 μM), CoA (240 μM), *mt*MenB (2.5 μM), and varying inhibitor concentrations (5–250 μM). Reactions were initiated by addition of ecMenE (50 nM), and the production of DHNA-CoA was monitored at 392 nm ($\boldsymbol{\varepsilon}^{392}$ = 4000 M^{-1} cm^{-1}).

K. Antimicrobial Assays

Minimum inhibitory concentrations (MICs) were determined using visual growth inspection of cells grown in transparent 96-well plates. *E. coli* , *B. subtilis* (ATCC 6051), MRSA (ATCC BAA-1762), and *M. tuberculosis* (H37Rv) were grown to mid-log phase (OD_{600} of 0.6–0.8) in synthetic broth, or 7H9 with 0.5% glycerol, 0.05% Tween, and 10% OADC medium at 37 ° C in an orbital shaker. A final inoculum concentration of 1–2 x 10^6 cells per well was treated with inhibitor at final concentrations ranging from 0.5 to 500 μg/mL. The MIC was defined as the minimum concentration at which a well showed no obvious growth by visual inspection (MIC-99). Growth rescue studies were performed by supplementing minimal medium (synthetic broth) with 10 μM menaquinone-4 (MK4) and following the same procedure in a 96-well plates. To determine the MK4-rescue MIC, 10% of the solution in each well was plated on synthetic agar plate and allowed to grow for 48 hours in 37 ^{o}C.

Colony forming units (CFUs) were counted and compared to plates with untreated wells. Rescue MICs were defined as the minimum inhibitor concentration at which a plate showed ~90% growth after supplementation with MK4.

2.6 References

1. Lu, X.; Zhang, H.; Tonge, P. J.; Tan, D. S., "Mechanism-based inhibitors of MenE, an acyl-CoA synthetase involved in bacterial menaquinone biosynthesis." *Bioorg. Med. Chem. Lett.* **2008,** *18*, 5963–5966.

2. Lu, X.; Zhou, R.; Sharma, I.; Li, X.; Kumar, G.; Swaminathan, S.; Tonge, P. J.; Tan, D. S., "Stable analogues of OSB-AMP: potent inhibitors of MenE, the o-succinylbenzoate-CoA synthetase from bacterial menaquinone biosynthesis." *ChemBioChem* **2012,** *13*, 129–136.

3. Higashiya, S.; Chung, W. J.; Lim, D. S.; Ngo, S. C.; Kelly; Toscano, P. J.; Welch, J. T., "Synthesis of mono- and difluoroacetyltrialkylsilanes and the corresponding enol silyl ethers." *J. Org. Chem.* **2004,** *69*, 6323–6328.

4. Strotman, N. A.; Chobanian, H. R.; Guo, Y.; He, J.; Wilson, J. E., "Highly regioselective palladium-catalyzed direct arylation of oxazole at C-2 or C-5 with aryl bromides, chlorides, and triflates." *Org. Lett.* **2010,** *12*, 3578–3581.

5. Lundy, B. J.; Jansone-Popova, S.; May, J. A., "Enantioselective conjugate addition of alkenylboronic acids to indole-appended enones." *Org. Lett.* **2011,** *13*, 4958–4961.

6. Xu, H.-D.; Zhang, R.-W.; Li, X.; Huang, S.; Tang, W.; Hu, W.-H., "Rhodium-catalyzed chemo- and regioselective cross-dimerization of two terminal alkynes." *Org. Lett.* **2013,** *15*, 840–843.

7. Belting, V.; Krause, N., "Gold-catalyzed tandem cycloisomerization–hydroalkoxylation of homopropargylic alcohols." *Org. Lett.* **2006,** *8*, 4489–4492.

8. Ruan, J.; Iggo, J. A.; Xiao, J., "Direct synthesis of 1-indanones via Pd-catalyzed olefination and ethylene glycol-promoted aldol-type annulation cascade." *Org. Lett.* **2011,** *13*, 268–271.

9. Partridge, B. M.; Solana González, J.; Lam, H. W., "Iridium-catalyzed arylative cyclization of alkynones by 1,4-iridium migration." *Angew. Chem. Int. Ed.* **2014,** *53*, 6523–6527.

10. Han, X.; Wan, C.; Li, X.; Li, H.; Yang, D.; Du, S.; Xiao, Y.; Qin, Z., "Synthesis and bioactivity of 2′ ,3′ -benzoabscisic acid analogs." *Bioorg. Med. Chem. Lett.* **2015,** *25*, 2438‑2441.

11. Jeong, I.-Y.; Lee, W. S.; Goto, S.; Sano, S.; Shiro, M.; Nagao, Y., "Novel heterocyclic ring-expansion and/or dehydration-hydration reactions of propargylic and allenylic hydroxy γ-lactams in the presence of strong base or Lewis acid." *Tetrahedron* **1998,** *54*, 14437–14454.

12. Bengiat, R.; Gil, M.; Klein, A.; Cohen, O.; Bogoslavsky, B.; Cohen, S.; Dubnikova, F.; Almog, J., "Vasarene and vasarene-analogues: synthesis and characterization of self-assembled, voluminous ligands with specific affinity to M+F– ion-pairs." *Tetrahedron* **2016,** *72*, 2429–2439.

13. Park, C.-M.; Bruncko, M.; Adickes, J.; Bauch, J.; Ding, H.; Kunzer, A.; Marsh, K. C.; Nimmer, P.; Shoemaker, A. R.; Song, X.; Tahir, S. K.; Tse, C.; Wang, X.; Wendt, M. D.; Yang, X.; Zhang, H.; Fesik, S. W.; Rosenberg, S. H.; Elmore, S. W., "Discovery of an orally bioavailable small molecule inhibitor of prosurvival B-cell lymphoma 2 proteins." *J. Med. Chem.* **2008,** *51*, 6902–6915.

14. Hinoshita, M. S., Dai; Hatakenaka, Mizuki; Okada, Etsuji, "Facile and convenient syntheses of fluorine-containing pyrido[2,3-h]quinazolines and 1,7-phenanthrolines by condensation reactions of 6,8-bis(trifluoroacetyl)quinolin-5-amine with carbonyl compounds." *Synthesis* **2011**, 2754–2760.

15. Bülow, A.; Plesner, I. W.; Bols, M., "A large difference in the thermodynamics of binding of isofagomine and 1-deoxynojirimycin to β-glucosidase." *J. Am. Chem. Soc.* **2000,** *122*, 8567–8568.

16. Yin, F.; Cao, R.; Goddard, A.; Zhang, Y.; Oldfield, E., "Enthalpy versus entropy-driven binding of bisphosphonates to farnesyl diphosphate synthase." *J. Am. Chem. Soc.* **2006,** *128*, 3524–3525.

17. Matulis, D. T., M. , "Thermodynamic-structure correlations of sulfonamide inhibitor binding to carbonic anydrase." In *Biocalorimetry 2: Applications of Calorimetry in the Biological Sciences*, Ladbury, E. J. D., L. Michael, Ed. Wiley: 2004; pp 106–132.

18. Velazquez-Campoy, A.; Luque, I.; Todd, M. J.; Milutinovich, M.; Kiso, Y.; Freire, E., "Thermodynamic dissection of the binding energetics of KNI-272, a potent HIV-1 protease inhibitor." *Protein Sci.* **2000,** *9*, 1801–1809.

19. Jogaitė, V.; Zubrienė, A.; Michailovienė, V.; Gylytė, J.; Morkūnaitė, V.; Matulis, D., "Characterization of human carbonic anhydrase XII stability and inhibitor binding." *Biorg. Med. Chem.* **2013,** *21*, 1431–1436.

20. Ishii, H.; Sasaki, Y.; Goshima, Y.; Kanai, Y.; Endou, H.; Ayusawa, D.; Ono, H.; Miyamae, T.; Misu, Y., "Involvement of rBAT in Na+-dependent and -independent transport of the neurotransmitter candidate L-DOPA in Xenopus laevis oocytes injected with rabbit small intestinal epithelium poly A+ RNA." *Biochim. Biophys. Acta* **2000,** *1466*, 61-70.

21. Yamamoto, S.-i.; Kawasaki, T., "Active transport of 5-fluorouracil and its energy coupling in Ehrlich ascites tumor cells." *J. Biochem.* **1981,** *90*, 635–642.

22. Davis, T. D.; Gerry, C. J.; Tan, D. S., "General platform for systematic quantitative evaluation of small-molecule permeability in bacteria." *ACS Chem. Biol.* **2014,** *9*, 2535–2544.

23. Lu, X.; Zhang, H.; Tonge, P. J.; Tan, D. S., "Mechanism-based inhibitors of MenE, an acyl-CoA synthetase involved in bacterial menaquinone biosynthesis." *Bioorganic & medicinal chemistry letters* **2008,** *18*, 5963-6.

24. Yin, Q.; Wang, S.-G.; You, S.-L., "Asymmetric synthesis of tetrahydro-β-carbolines via chiral phosphoric acid catalyzed transfer hydrogenation reaction." *Org. Lett.* **2013,** *15*, 2688–2691.

25. Topliss, J. G.; Konzelman, L. M.; Sperber, N.; Roth, F. E., "Antihypertensive agents. III.1 3-hydroxy-3-phenylphthalimidines." *J. Med. Chem.* **1964,** *7*, 453–456.

26. Hardcastle, I. R.; Liu, J.; Valeur, E.; Watson, A.; Ahmed, S. U.; Blackburn, T. J.; Bennaceur, K.; Clegg, W.; Drummond, C.; Endicott, J. A.; Golding, B. T.; Griffin, R. J.; Gruber, J.; Haggerty, K.; Harrington, R. W.; Hutton, C.; Kemp, S.; Lu, X.; McDonnell, J. M.; Newell, D. R.; Noble, M. E. M.; Payne, S. L.; Revill, C. H.; Riedinger, C.; Xu, Q.; Lunec, J., "Isoindolinone inhibitors of the murine double minute 2 (MDM2)-p53 protein–protein interaction: Structure–activity studies leading to improved potency." *J. Med. Chem.* **2011,** *54*, 1233–1243.

CHAPTER 3

STEREOSELECTIVE SYNTHESIS, DOCKING, AND EVALUATION OF DIFLUOROINDANEDIOL-BASED MENE INHIBITORS*

3.1. Introduction

In our efforts to improve the antimicrobial activity of MenE inhibitor platform, we investigated the keto-acid/lactol equilibrium of OSB-AMS (**1**, Figure 3.1),[1] through the synthesis and evaluation of keto-acid and lactol form bioisosteres of OSB-AMS.[2] In so doing, we discovered the difluoroindanediol analogue **2**, which exhibited a promising but unusual activity profile.

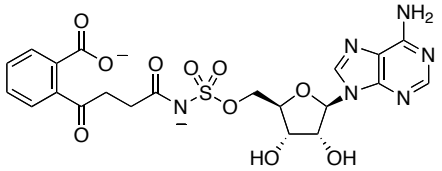

1, OSB-AMS

E. coli MenE IC_{50} = 25 nM
MRSA MIC = 31.25 μg/mL
M. tuberculosis MIC = 125 μg/mL

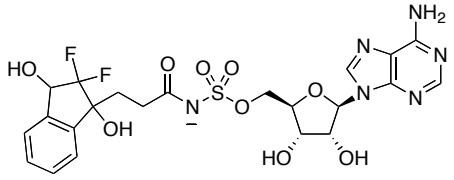

2, difluoroindanediol analogue

*E. coli Men*E IC_{50} = 1.5 mM
MRSA MIC = 15.6 μg/μL
M. *tuberculosis MIC* = 15.6 μg/μL

Figure 3.1. Previously reported analogues OSB-AMS (1) and difluoroindanediol analogue 2, with reported biochemical and antimicrobial activities.

The difluoroindanediol analogue **2** exhibited an IC_{50} against MenE of 1.5 μM in biochemical assays (vs. OSB-AMS MenE IC_{50} = 25 nM), and an antimicrobial activity (MIC) of 15.6 μg/mL against both methicillin-resistant *Staphylococcus aureus* (MRSA) and *M. tuberculosis* (vs. OSB-AMS: MRSA

* Adapted from: Evans, C. E.; Matarlo, J. S.; Tonge, P. J.; Tan, D. S., Stereoselective Synthesis, Docking, and Biological Evaluation of Difluoroindanediol-Based MenE Inhibitors as Antibiotics." *Org. Lett.* **2016**, 6384–6387.

MIC = 31.25 μg/mL, *M. tuberculosis* MIC = 125 μg/mL). We also noted rescue of difluoroindanediol analogue-treated MRSA when coadministered with exogenous menaquinone-4 (MK-4), suggesting that the difluoroindanediol inhibits menaquinone production. However, as was discussed in Chapter 2 (section 2.4), the hypothesis that the difluoroindanediol analogue inhibits cell growth through inhibition of MenE does not align well with our current understanding of OSB-AMS and acyl-AMS inhibitor permeability and selectivity. Therefore, it was necessary to investigate the unusual activity of the difluoroindanediol analogue to gain insight into the mechanism behind this activity and if it can be leveraged to increase the potency of our OSB-AMS based platform.

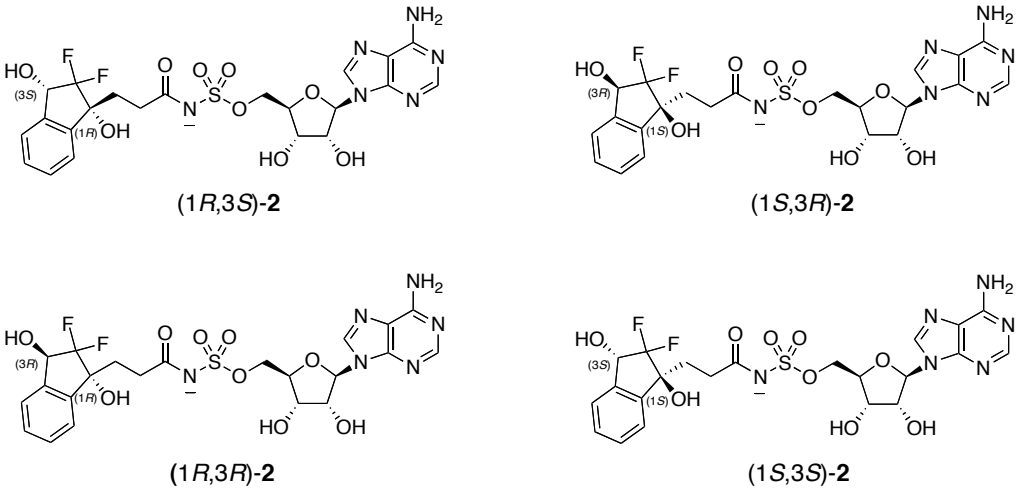

Figure 3.2. Diastereomers of the difluoroindanediol analogue 2.

The original synthetic route to the difluoroindanediol analogue discussed in Chapter 2 resulted in a mixture of four diastereomers around the benzannulated five membered ring of the difluoroindanediol scaffold (Figure 3.2). While this approach allowed for expedient synthesis of the difluoroindanediol analogue to test for initial activity, in order to investigate the

scaffold further it was necessary to synthesize and evaluate the biochemical and antimicrobial activity of each of the diastereomers individually.

3.2. Initial attempts towards the stereoselective synthesis of the diastereomeric difluoroindanediols

Our original synthetic route to the difluoroindanediol analogue involved two main steps that led to the epimeric centers around the difluoroindanediol core. The first stereogenic center at C1 was established through addition of *tert*-butylpropiolate to the 2,2-difluoro-1,3-indandione intermediate **3** (Figure 3.3). The second stereogenic center at C3 was established through a late-stage palladium–catalyzed hydrogenation of the α-difluoroketone intermediate **5**.

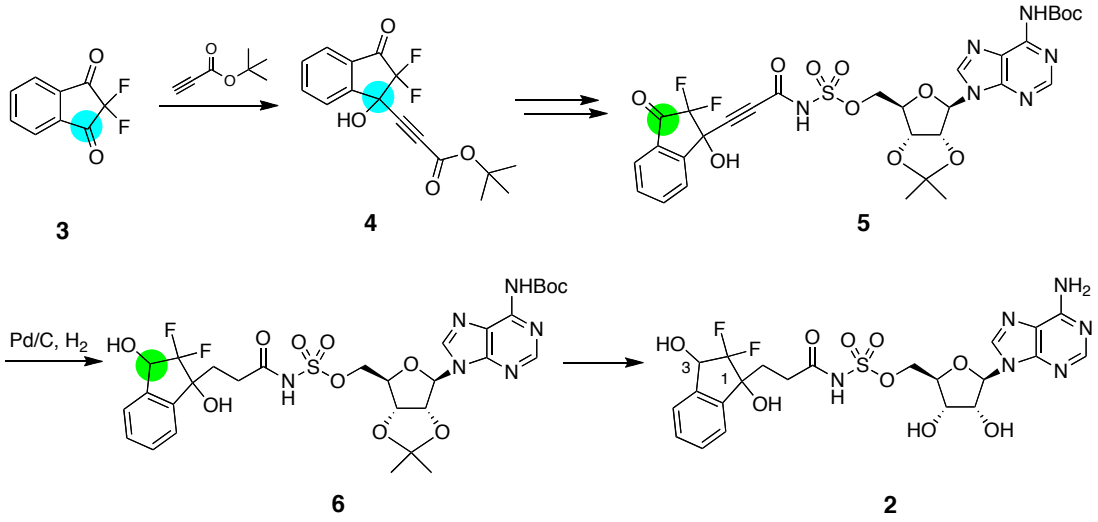

Figure 3.3. Key stereocenter forming steps in original synthesis of the difluoroindanediol analogue 2. Blue circles = C1 position of indanol core at key stereocenter forming step. Green circles = C3 position of indandol core at key stereocenter forming step.

To access the individual diastereomers of the difluoroindanediol analogue in a stereoselective manner, we proposed two alternative

retrosynthetic approaches. In both approaches, the C1 and C3 stereocenters would be in place on the difluoroindanediol acyl chain **8** prior to coupling to the protected AMS scaffold **7**. This would allow access to a greater diversity of chemical transformations without concern for decomposition of the relatively labile acyl-sulfamate bond.

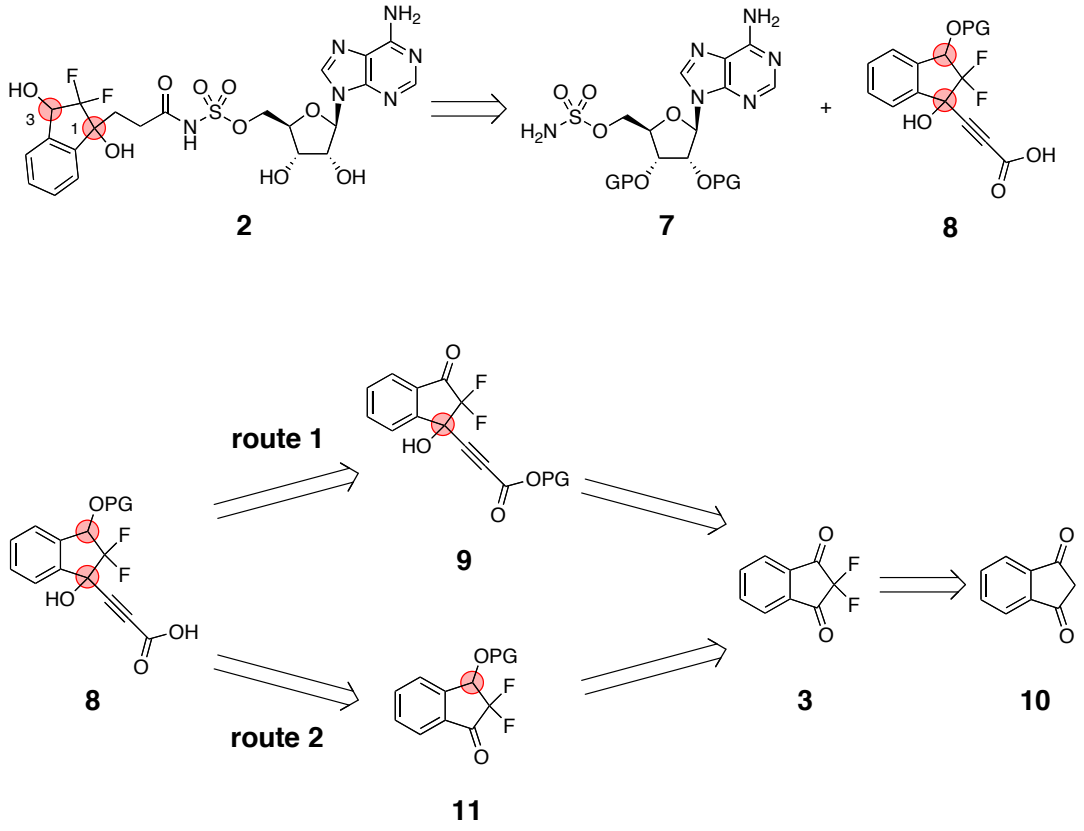

Figure 3.4. Proposed retrosynthetic approaches to diastereomeric difluoroindanediol analogues 2. PG = protecting group. Red circles indicate key stereocenters**.**

In the first approach (route 1, Figure 3.4), the C3 stereochemistry would be set via diastereoselective ketone reduction of intermediate **9**, with absolute stereochemistry at C1 being set by enantioselective alkynylation of 2,2-difluoro-1,3-indandione (**3**). Intermediate **3** can then be quickly and nearly quantitatively obtained from commercially available 1,3-indandione using our

previously published methods.[2] In the second approach (route 2, Figure 3.4), C1 stereochemistry would be set via diastereoselective alkynylation of the protected difluorohydroxyindanone scaffold **11**, with absolute stereochemistry at C3 being established through an enantioselective reduction of the corresponding difluoroindandione **3**. In both routes, the key challenge was the initial establishment of absolute stereochemistry on the highly activated and symmetric 2,2-difluoro-1,3-indandione (**3**).

Work towards the diastereomeric difluoroindanediol analogues in the first approach began by first investigating the key step of the sequence, the alkynylation of the ketone intermediate **3**. Literature reports of enantioselective alkynylation of carbonyls rely on first forming an alkynyl-metal species, typically lithium or zinc, which is coordinated by a chiral ligand to allow for enantioselective addition into the desired carbonyl moiety. There are a wide assortment of chiral ligands reported to catalyze enantioselective alkynylation reactions (Figure 3.5) such as camphorsulfonamide derivatives **12**,[3-4] phenethylamine derivatives **13**,[5-6] napthol derivatives **14**,[7-9] or Schiff base derivatives **14**.[10-11] However, the majority of the reported enantioselective alkynylation reactions focus on addition of an alkyne into an aryl aldehyde. Instances in the literature of ketone alkynylation most often report poor enantioselectivity and/or very limited substrate scope. One notable exception reported by Dr. Lushi Tan and coworkers at Merck Research Laboratories, is a highly enantioselective addition of cyclopropylacetylene (**16**) into trifluoromethylacetophenone **15** en route to the antiretroviral drug, efavirenz.[6] However, using these conditions with difluoroindandione intermediate **3** and related acetylenes **19**, we observed poor chemoselectivity, enantioselectivity, and yields. Additional methods using the other previously described ligand

systems were also screened with identical results, suggesting the α-difluoroketone moiety is not amenable to enantioselective alkynylation. We also explored chiral resolution of the racemic difluorohydroxyindanone intermediate **8** (Figure 3.4), through recrystallization with optically pure chiral amines, or through chromatographic separation of a chiral amine-derived Schiff bases from intermediate **9**. However, both methods failed to provide the suitable enantioenrichment of the corresponding material.

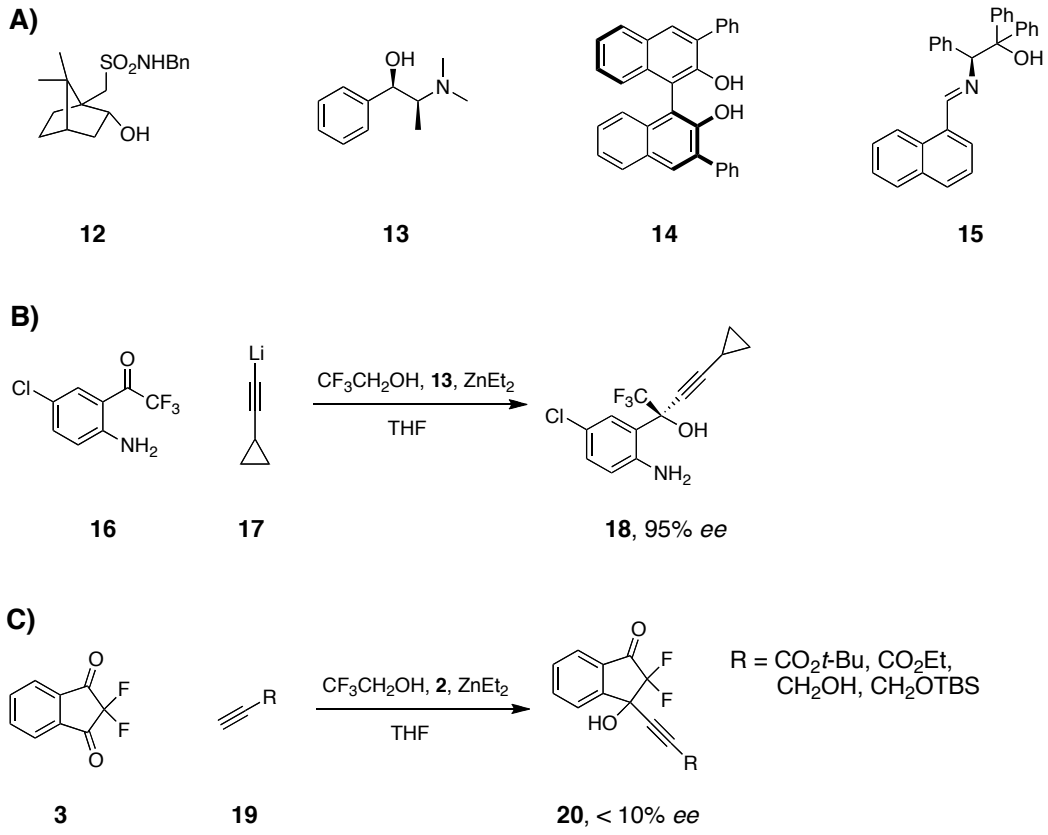

Figure 3.5. Alkynylation of aryl ketones. A) Common chiral ligands for enantioselective alkynylation reactions. B) Reported alkynylation en route to Efavirenz.[6] C) Alkynylation of difluoroindandione **3**. TBS = *tert*-butyldimethylsilyl.

As our scaffold was not amenable to enantioselective alkynylation, we began work towards the diastereomeric difluoroindanediol analogues through our second proposed retrosynthetic approach. This synthetic route relies on a

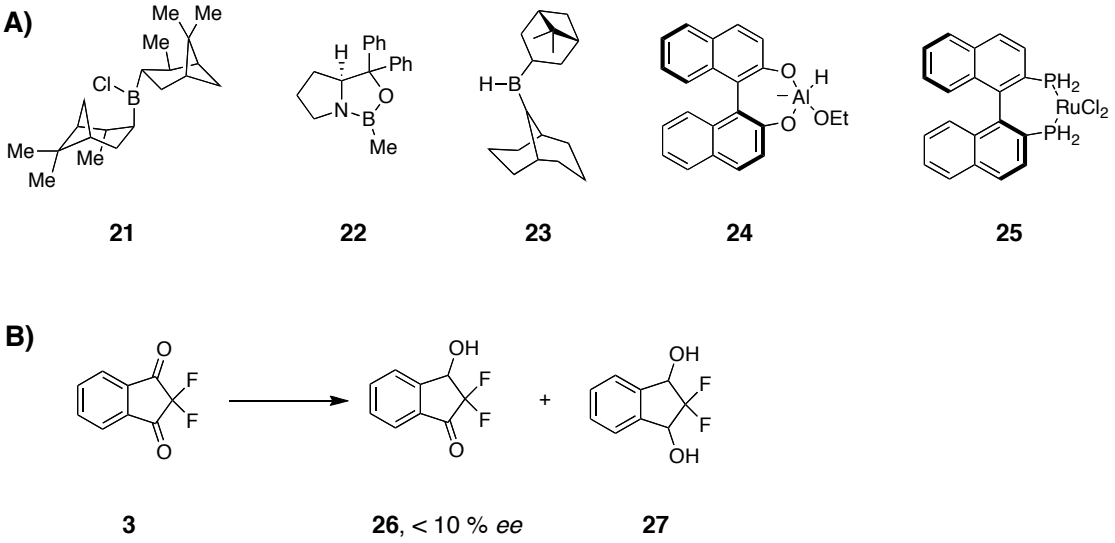

Figure 3.6. Enantioselective reduction of ketones. A) Known chiral systems for enantioselective reduction of aryl-ketones. B) Reduction of difluoroindandione **3** to give reduced product **26** and over-reduced product **27**.

successful enantioselective reduction of the C3 position of difluoroindandione **3**. There are a large number of literature precedents for enantioselective reductions of aryl ketones.[12] Most examples focus on the use of chiral boranes such as DIP-Cl (B-Chlorodiisopinocampheylborane, **21**, Figure 3.6),[13] oxazaborolidine **22**,[14-16] and alpine borane **23**,[16-17] or chiral hydride sources such as BINAL-H (1,1'-Bi-2-naphthol-ethoxy-aluminum hydride, **24**),[18] or transition-metal catalyzed hydrogenations using chiral ligands such as $Ru_2Cl_4[BINAP]_2$ (**25**).[19-22] These systems were screened for enantioselective reduction of the difluoroindandione intermediate **3**. While we consistently observed efficient reduction of the starting material with the reaction conditions screened, the conditions gave no appreciable enantioselectivity as well as poor chemoselectivity, often affording the fully reduced product **27**. Attempts at kinetic resolution of the racemic difluorohydroxyindanone **26** or functionalization with chiral acids to allow for chromatographic separation of

the corresponding diastereomers failed to give the suitable enantioenrichment to proceed with the synthetic route.

3.2. Stereoselective synthesis of the diastereomeric difluoroindanediols.

The results from our initial attempts towards an enantioselective synthesis of the diastereomeric difluoroindanediols indicated that the fluorinated intermediates were unsuitable for enantioselective reactions primarily due to their high reactivity, poor ability to coordinate the chiral ligands, and relative instability. Thus, we next pursued establishment absolute stereochemistry before introduction of fluorine to the indanol scaffold.

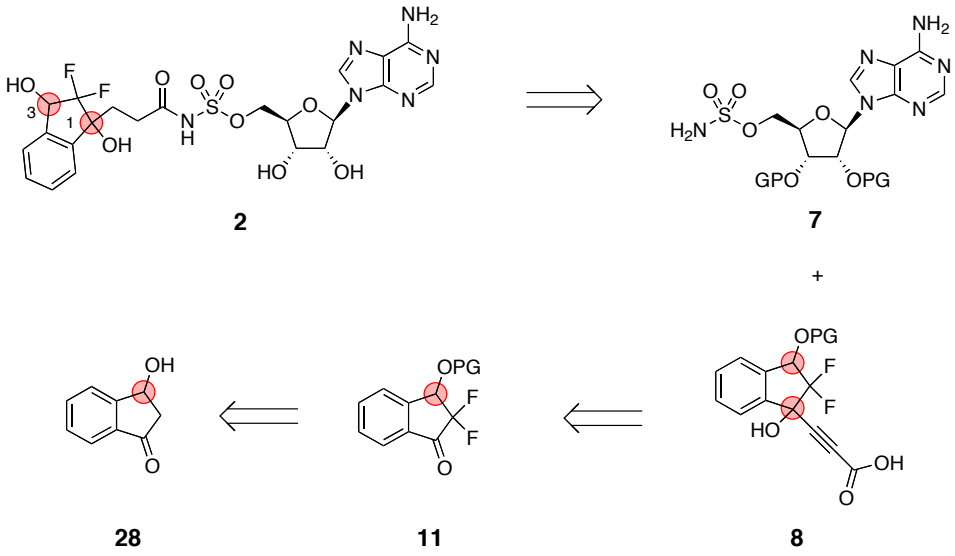

Figure 3.7. Stereoselective retrosynthesis of diastereomeric difluoroindanediol analogues 2. PG = protecting group. Red circles indicate key stereocenters.

Our revised retrosynthetic route retained the concept of stereocenters at C1 and C3 being set before the acyl chain was coupled onto the protected AMS scaffold. Stereochemistry at C1 would be set via a diastereoselective alkynylation of the corresponding protected difluorohydroxyindanone **11**, and absolute stereochemistry at C3 established in 3-hydroxyindanone **28**.

To access both (3*R*)-3-hydroxyindanone (**28**) and (3*S*)-3-hydroxyindanone (**28**) in high enantiopurity, we used a methodology previously reported by Nair and coworkers in which enzymatic kinetic resolution of 3-hydroxyindanone was achieved using Amano Lipase PS (*Burkholderia cepacia*) in vinyl acetate.[23] This method provided 3-hydroxyindanone (3*S*)-(**28**) in 46% yield with > 98% *ee*, and the enantiomeric acetate (3*R*)-**29** in 43% yield and >98% *ee* (Figure 3.8, determined by LCMS with Chiracel OB-H column, E value > 200).[24] With our desired C3 stereochemistry in place, we converted acetate (3*R*)-**29** to silyl ether (3*R*)-**30**. This protection step was necessary to prevent retro-aldol epimerization of the C3 stereocenter and add steric bulk to one side of the five-membered ring. Intermediate (3*R*)-**30** was treated with hexylamine to form the corresponding Schiff base, before fluorination using Selectfluor to provide the α-difluoroketone (3*S*)-**31**. While this method for formation of α-difluoroketones is rarely seen in the literature, more typical methods for installation of fluorine require strong basic conditions such as NaH or lithium hexamethyldisilazide (LiHMDS), which are not compatible with the non-fluorinated hydroxyindanone scaffold. The next key step involved the diastereoselective alkynylation of the α-difluoroketone (3*S*)-**31**. A number conditions using combinations of relevant bases (lithium diisopropylamide [LDA], LiHMDS, NaHMDS, KHMDS, *n*-BuLi), additives (hexamethylphohsphoramide, tetramethylethenediamine) and solvents (hexanes, THF, diethyl ether) were screened for optimal diastereoselective alkynylation of the α-difluoroketone (3*S*)-**31**. Leveraging both the relatively poor nucleophilicity of the alkynyl-lithium species as well as the steric bulk of

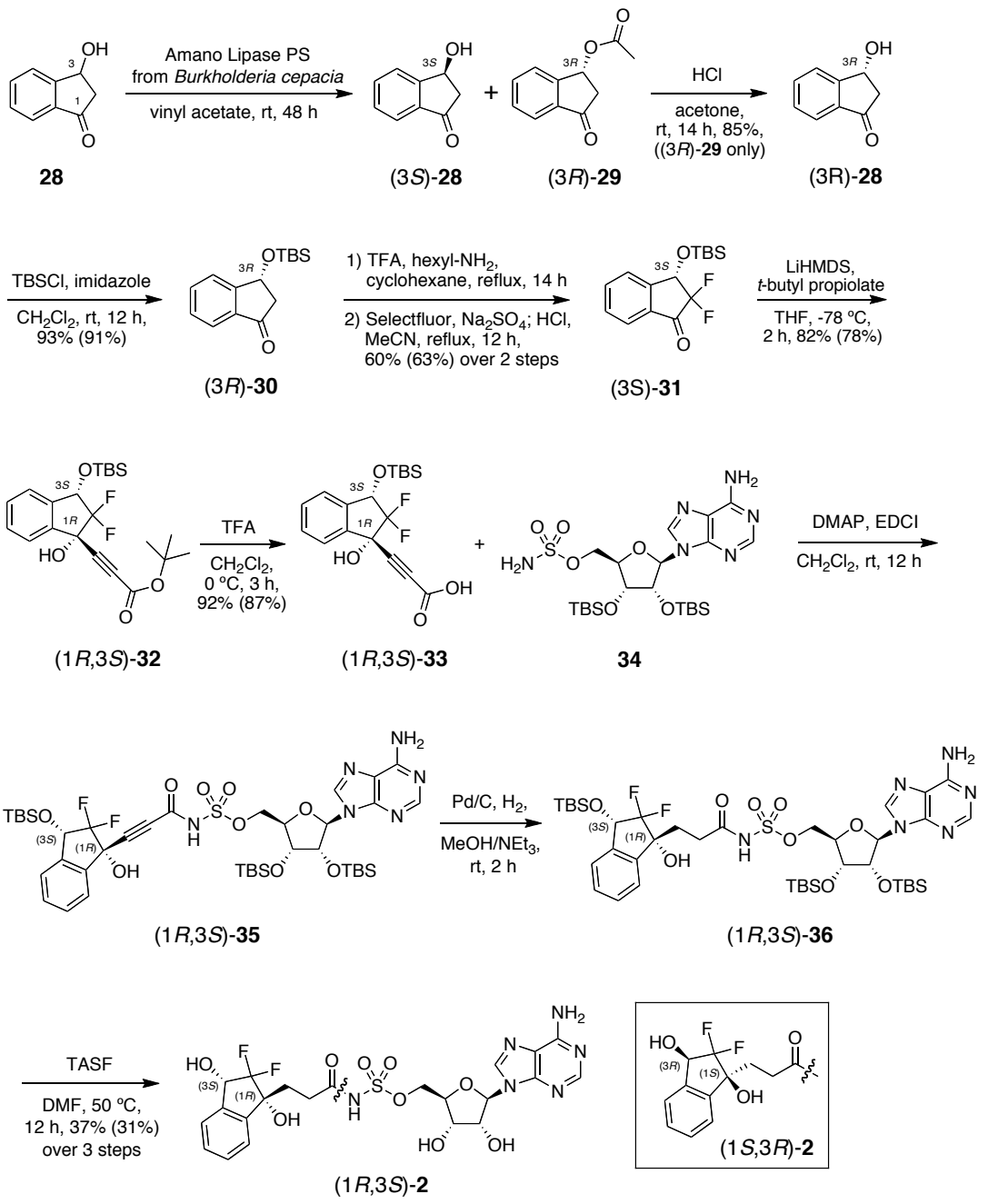

Figure 3.8. Synthesis of *syn*-difluoroindanediol inhibitors (1*R*,3*S*)-2 and (1*S*,3*R*)-2. Yields in parentheses are for synthesis of (1*S*,3*R*)-2, prepared analogously from alcohol (3*S*)-**28**. DMAP = *N*,*N*-dimethyl-4-aminopyridine; EDCI = 1-ethyl-3-(3-dimethylaminopropyl)carbodiimide; HMDS = hexamethyldisilazide; Selectfluor = 1-chloromethyl-4-fluoro-1,4-diazoniabicyclo[2.2.2]octane bis(tetrafluoroborate); TAS-F = tris(dimethylamino)sulfonium difluorotrimethylsilicate; TBS = *t*-butyldimethylsilyl; TFA = 2,2,2-trifluoroacetic acid.

the C3 silyl-ether, we achieved efficient conversion to the *syn*-diol intermediate (1*R*,3*S*)-**32** (>20:1 dr). The *tert*-butyl ester was cleaved to provide the desired

acid (1*R*,3*S*)-**33**, which was desilylated and crystallized to confirm absolute and relative stereochemistry by X-ray crystallographic analysis (CuKα radiation, see experimental section 3.6 for details). The free acid intermediate (1*R*,3*S*)-**33** was coupled to the protected AMS scaffold **34** before hydrogenation of the alkyne and global deprotection provided the *syn*-difluoroindanediol analogue (1*R*,3*S*)-**2**. The alternative *syn*-difluoroindanediol analogue (1*S*,3*R*)-**2** was synthesized analogously from the enantiomeric alcohol (3*S*)-(**28**).

In order to synthesize the *anti*-difluoroindanediol analogue (1*R*,3*R*)-**2**, we began by desilylating the *syn*-diol intermediate (1*R*,3*S*)-**32** (Figure 3.9), to provide the corresponding free-diol (1*R*,3*S*)-**37**. Oxidation to the ketone (1*R*)-**38** followed by reduction with optimized conditions using sodium borohydride provided the anti-diol intermediate (1*R*,3*R*)-**39** (>20:1 dr). In the course of the optimization of this reaction, we observed that rapid addition of reductant or use of an excess of hydride greatly diminished the diastereoselectivity. Thus the diastereoselectivity in this reaction is likely due to a combination of increased sterics on the alkyne facing side of the ring, and the boronate first coordinating with the C1 hydroxyl of (1*R*)-**38** before delivering the hydride from the *syn*-face of the ring to provide the *anti*-diol (1*R*,3*R*)-**39**.[25] The *tert*-butyl ester was cleaved to provide the desired acid (1*R*,3*R*)-**40**, which was coupled to the protected AMS scaffold **34** before hydrogenation of the alkyne and global deprotection provided the *anti*-difluoroindanediol analogue (1*R*,3*R*)-**2**. The alternative *anti*-difluoroindanediol analogue (1*S*,3*S*)-**2** was synthesized analogously from the enantiomeric *syn*-diol intermediate (1*S*,3*R*)-**32**.

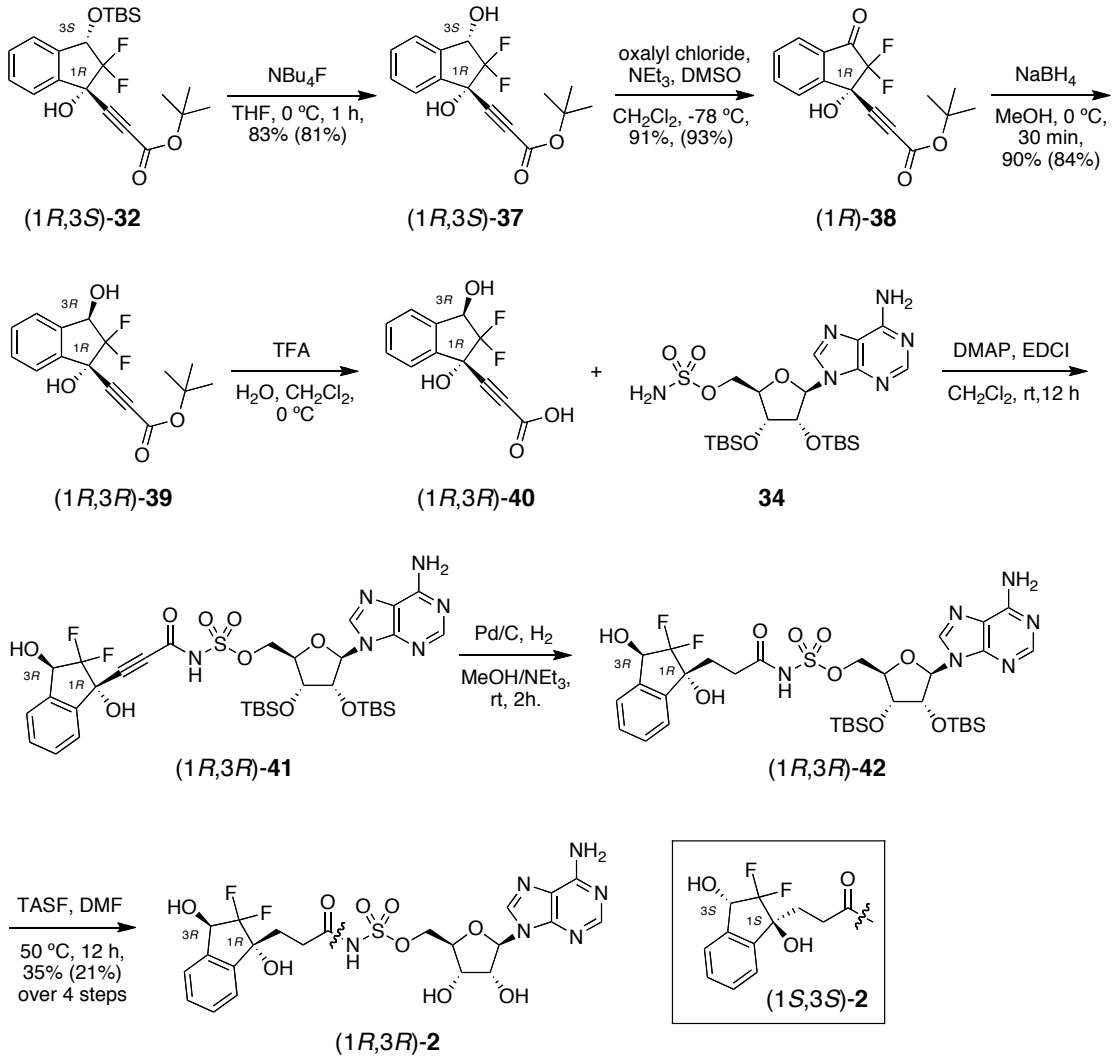

Figure 3.9. Synthesis of anti-difluoroindanediol inhibitors (1*R*,3*S*)-2 and (1*S*,3*R*)-2. Yields in parentheses are for synthesis of (1*S*,3*R*)-2, prepared analogously from alcohol (3*S*)-**28**. DMAP = *N*,*N*-dimethyl-4-aminopyridine; EDCI = 1-ethyl-3-(3-dimethylaminopropyl)carbodiimide; TAS-F = tris(dimethylamino)sulfonium difluorotrimethylsilicate; TBS = *t*-butyldimethylsilyl; TFA = trifluoroacetic acid.

3.3. Computational docking of the diastereomeric difluoroindanediols to the OSB-AMS·MenE cocrystal structure

In parallel to the synthesis of the diastereomeric difluoroindanediols, we investigated *in silico* binding profiles for the individual diastereomers to MenE.

Using Glide (Schrödinger software suite), we docked the four difluoroindanediol diastereomers to our previously published cocrystal structure of OSB-AMS in complex with *E. coli* MenE (Figure 3.10, PDB: 5C5H, see experimental section 3.6 for complete details). As a means to first confirm our docking model was functioning correctly, we docked OSB-AMS to the prepared MenE protein and found it to align nearly perfectly with that of the cocrystalized OSB-AMS (rmsd 0.2 Å). We then proceeded to dock each of the four diasteromeric difluoroindanediols **2**. With each of the four diastereomers, the adenosine region of each molecule docked with high fidelity to the native OSB-AMS cocrystal structure, retaining key interactions with the protein and properly filling the binding pocket (Figure 3.10). In contrast, there were significant levels of variability observed in the sidechain region of the difluoroindanediol diastereomers **2**. Only the *syn*-difluoroindanediol diastereomer (1*R*,3*S*)-**2** fully filled the OSB binding pocket and overlapped well with the structure of the cocrystalized OSB-AMS. The two benzannulated alcohols of the difluoroindanediol sidechain appear poised to engage in a hydrogen bonding network with a conserved water (H_2O-666) and threonine (Thr-277) in the OSB binding pocket, both of which appear to interact with OSB in the MenE cocrystal structure (Figure 3.11). In our docking studies, none of the diastereomers interact with the water molecules responsible for bridging interactions between the free carboxylate of OSB and Lys-195 (Arg-195 in native enzyme). This lack of the theoretical ionic interaction accounts for the difference in enthalpic binding modes observed between the difluoroindanediol

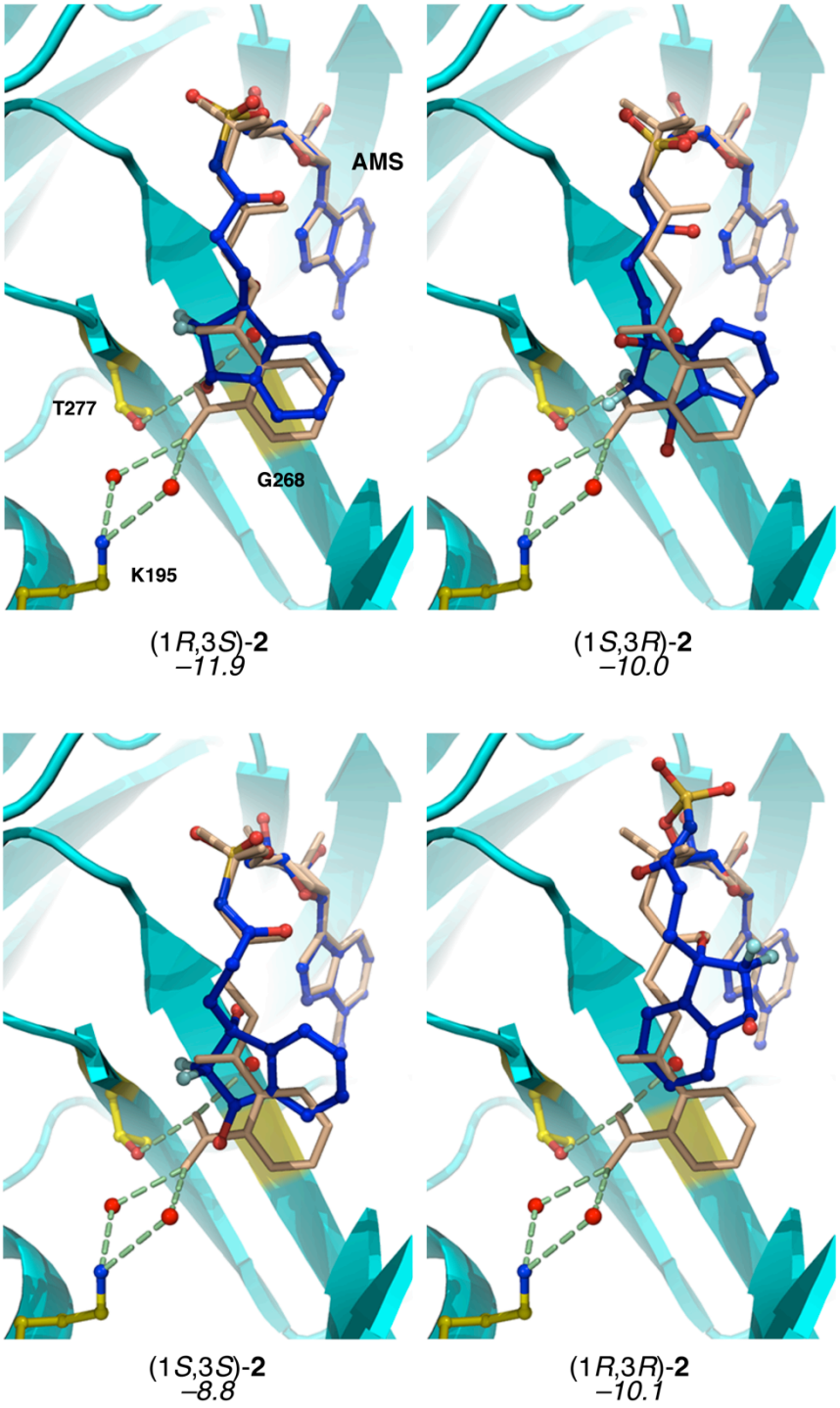

Figure 3.10. Computational docking of diastereomeric difluoroindanediols 2. Difloroindanediols **2** (blue) to E. coli MenE R195K (cyan) (PDB: 5C5H), overlaid with co-crystallized OSB-AMS (beige), with key binding residues (yellow) and conserved waters (red). Schrödinger Glide docking scores shown for each diastereomer (arbitrary units). OSB-AMS docked with a score of **–**13.9.

analogue and OSB-AMS during isothermal calorimetry titration experiments as was discussed during Chapter 2.

As was discussed in Chapter 1, our original docking experiments with the unliganded crystal structure of *S. aureus* MenE identified Ser-302 (Thr-178 in *M. tuberculosis*), whose sidechain was proposed to interact with the succinyl ketone of OSB. While this residue is not conserved across species, and in the case of *E. coli* MenE is a glycine (Gly-268), its location in the docking studies

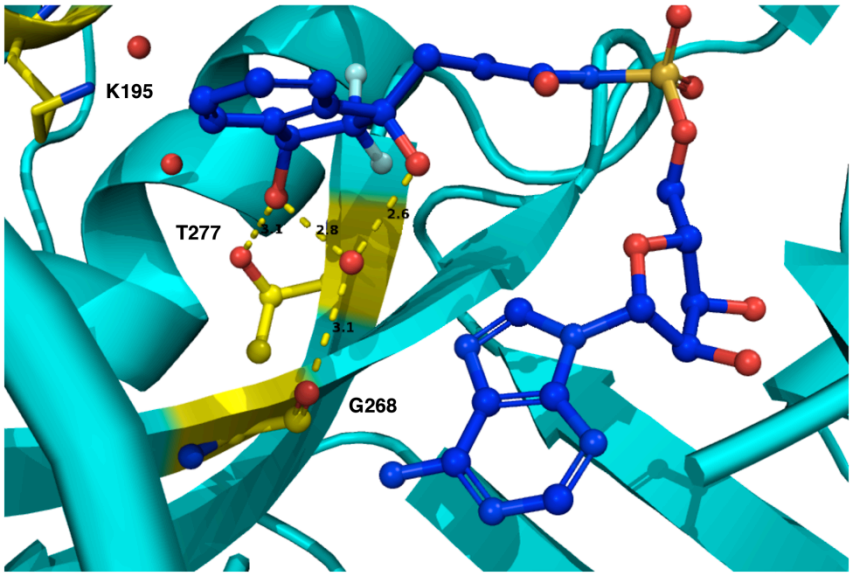

Figure 3.11. Specific interactions between MenE and (1R,3S)-2. Difloroindanediol **2** (blue) to E. coli MenE R195K (cyan) (PDB: 5C5H), with key binding residues (yellow) and conserved waters (red) in the OSB binding pocket.

suggest that the sidechain in *S. aureus* and *M. tuberculosis* may interact with the tertiary alcohol of the difluoroindanediol diastereomer (1*R*,3*S*)-**2**. Whether it would do so in addition to the conserved water or if the sidechain will exclude the molecule of water is unknown.

3.4. Associated biochemical and antimicrobial activity of the diastereomeric difluoroindanediols

The four diastereomeric difluoroindanediol analogues **2** were then tested for biochemical inhibition of *E. coli* MenE by our collaborators in the laboratory of Professor Peter Tonge at Stony Brook University, using our previously discussed MenE-MenB coupled assay (see Chapter 2 for details). In results that closely mirrored the results from our docking studies, the *syn*-difluoroindanediol (1*R*,3*S*)-**2** exhibited the most potent inhibition of MenE (Table 1), while the other three difluoroindanediol diastereomers [(1*S*,3*R*)-**2**, (1*R*,3*R*)-**2**, (1*S*,3*S*)-**2**] failed to inhibit MenE at concentrations up to 200 μM. Importantly, the difluoroindanediol diastereomer (1*R*,3*S*)-**2** had an IC_{50} roughly ¼ that of the mixture of all four diastereomers (synthesized from the original non-stereoselective route), suggesting that the (1*R*,3*S*)-**2** diastereomer is solely responsible for the previously reported inhibition of MenE.

Next, our collaborators evaluated the antimicrobial activity of the diastereometic difluoroindanediols **2** against *B. subtilis*, methicillin resistant *S. aureus* (MRSA), and *M tuberculosis*. However, contrary to our expectations based on our biochemical inhibition results, we observe all four diastereomers exhibited MIC values similar to each other and to the mixture of diastereomers. To test whether the antimicrobial activity of the diastereomeric difluoroindanediols is due to inhibition of menaquinone production, we repeated the antimicrobial assays in the presence of exogenous menaquinone-4 (MK-4, 10 μg/mL). When bacteria were coadministered MK-4 and inhibitor at varying concentrations, we observed a

Table 3.1. Biochemical and antimicrobial activity of difluoroindanediols 2.

entry	inhibitor	MenE IC_{50} [μM][a]	*B. subtilis* MIC [μg/mL][b]	MRSA MIC [ug/mL][b,c]	*M. tuberculosis* MIC [μg/mL][b]
1	**2**[d]	18.3 ± 3.7[e]	15.6 (62.5)	15.6 (62.5)	15.6 (62.5)
2	(1*R*,3*S*)-**2**	5.0 ± 1.0	15.6 (31.2)	15.6 (31.2)	15.6 (62.5)
3	(1*S*,3*R*)-**2**	> 200	15.6 (31.2)	31.2 (31.2)	31.2 (62.5)
4	(1*R*,3*R*)-**2**	> 200	15.6 (15.6)	15.6 (15.6)	15.6 (31.2)
5	(1*S*,3*S*)-**2**	> 200	15.6 (15.6)	15.6 (15.6)	31.2 (31.2)
6	AMS[f]	n.d[g]	3.9 (3.9)	1.9 (1.9)	0.16 (0.32)

[a] *E. coli* MenE. [b] MIC values in parentheses determined with addition of exogenous menaquinone-4 (10 mg/mL). [c] MRSA = methicillin-resistant *S. aureus*. [d] Equimolar mixture of four diastereomers, prepared by the original synthetic route.[2] [e] This IC_{50} is higher than the 1.5 mM that we reported previously,[2] due to batch-to-batch variability of the enyzme; IC_{50} values reported herein were all determined with the same batch of enzyme. [f] 5´-O-sulfamoyl-adenosine. [g] n.d. = not determined.

modest 4-fold increase in the MIC with the mixture of four difluoroindanediol diastereomers and a 2- to 4-fold increase in MIC for the biochemically active diastereomer (1*R*,3*S*)-**2**. Some trace rescue was observed in bacteria co-treated with the other *syn*-difluoroindanediol diastereomer (1*S*,3*R*)-**2**, and no rescue was observed with the two *anti*-difluoroindanediol diastereomers. While this does suggest that the antimicrobial activity of the biochemically active difluoroindanediol diastereomer is at least in part due to inhibition of menaquinone production, it does not explain the nearly identical nature of the antimicrobial activity observed across all the diastereomeric difluoroindanediol analogues.

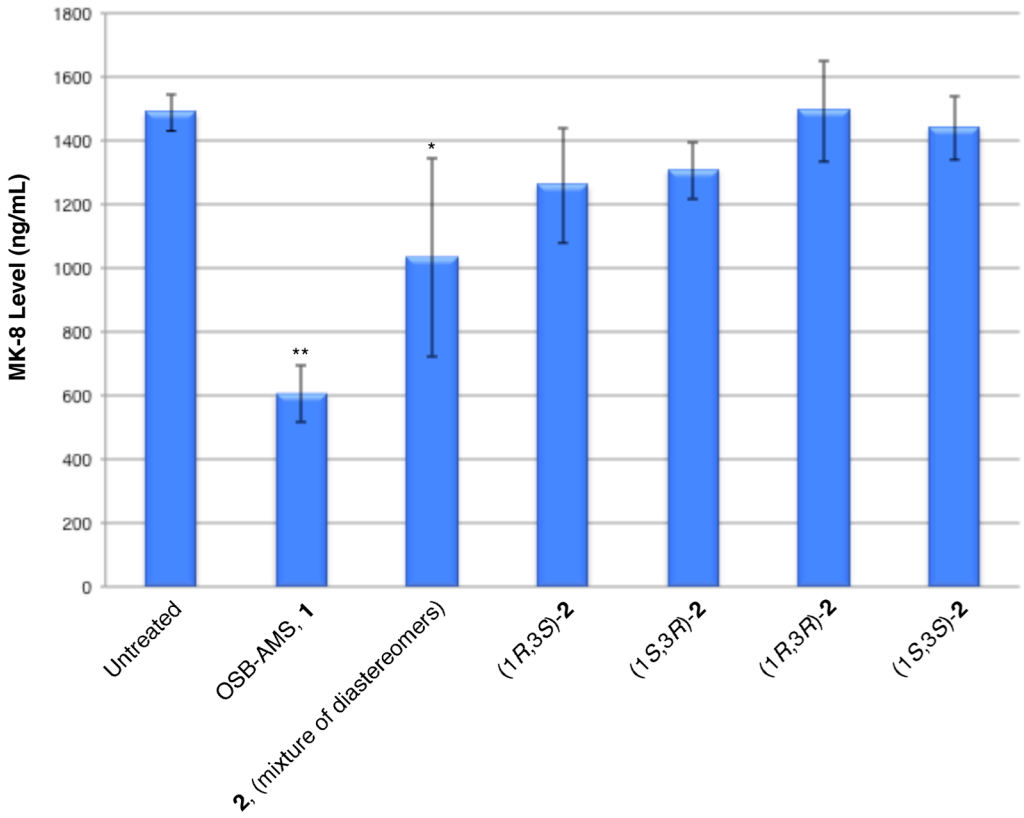

Figure 3.12. Menaquinone-8 levels in methicillin-resistant *Staphylococcus aureus* treated with MenE inhibitors. Standard error shown for two independent experiments. Statistical significance determined using one-tailed *t* test: * $p \leq 0.05$, ** $p \leq 0.01$.

To interrogate the mechanism of action of the diastereomeric difluoroindanediol analogues further, we used LC-MS/MS quantification of endogenous menaquinone levels in MRSA treated with each of the four diastereomeric difluoroindanediol analogues. While OSB-AMS was able induce a 2.5-fold reduction in endogenous menaquinone levels, no individual difluoroindanediol diastereomer was able to reduce endogenous menaquinone levels in a statistically significant manner. Interestingly, the mixture of four diastereomeric difluroindanediols **2** did decrease endogenous menaquinone levels, albeit by a modest 31%, or roughly 10-fold less than that of OSB-AMS.

3.5. Discussion and Conclusions.

To investigate the unusual activity of the difluoroindanediol analogue **2** discovered in Chapter 2, we sought to synthesize each of the four diastereomeric difluoroindanediols and to test their biochemical and antimicrobial activity individually. To this end we first developed a stereoselective synthesis of each of the four diastereomeric difluoroindanediol-based inhibitors. This was achieved through the use of enzymatic kinetic resolution to establish absolute stereochemistry at C3 of the indane scaffold, and diastereoselective alkynylation to establish relative stereochemistry at the C1 position of the scaffold. Docking studies showed the *syn*-difluoroindanediol diastereomer (1*R*,3*S*)-**2** docked to the MenE crystal structure with the best calculated score, as well as being best able to fit into the binding pocket while retaining key interactions with the protein. In biochemical experiments, we identified the difluoroindanediol diastereomer (1*R*,3*S*)-**2** as the only analogue to show inhibition of MenE, which mirrors our docking experiment data. However, in antimicrobial assays all four difluoroindanediol diastereomers exhibited nearly identical MICs against the *B. subtilis*, MRSA, and *M. tuberculosis*, indicating that the antimicrobial mechanism of action of the difluoroindanediol diastereomers is not due to inhibition of MenE. While modest rescue was observed upon supplementation of exogenous MK-4 in MRSA treated with the mixture of difluoroindanediol diastereomers and the difluoroindanediol diastereomer (1*R*,3*S*)-**2**, no appreciable rescue was observed with the other three diastereomers. Finally, there was no statistically significant reduction of endogenous menaquinone production in MRSA treated with any of the four diastereomeric difluoroindanediols.

In beginning this investigation of the diastereomeric difluoroindanediols, we had hoped to find that only one diastereomer was active in antimicrobial assays. This would have lead to an inhibitor with low to sub-μM concentration antimicrobial activity. However, all four diastereomers are essentially equivalent in their antimicrobial activity and do not inhibit production of menaquinone, suggesting the activity of the difluoroindanediol analogue is due primarily to an off-target mechanism of action. The rescue experiments suggest that there is perhaps a more complicated mechanism of action than a simple, single off-target protein inhibition event, and that menaquinone might somehow play a part in this mechanism. This hypothesis is further supported by the fact that the four diastereomers are, within the error of the antimicrobial experiments, equivalently active. These results, when considered in isolation, suggest that if there is an off-target protein, it is not interacting in a specific manner with the difluoroindanediol sidechain. However, if there was such a protein that bound with OSB-AMS type scaffolds in such a promiscuous manner, it is not unreasonable to suppose we would have observed antimicrobial activity with one of the other keto-acid or lactol analogues of OSB-AMS discussed in Chapter 2. Therefore, the evidence suggests that the difluoroindanediol analogue **2** acts through some yet unknown, and possibly complex, mechanism of action. Future investigations with this scaffold will focus on attempting to identify the mechanism of action behind the observed antimicrobial activity through the generation of resistant mutants, pull-down experiments, and other standards of target identification.

3.6. Experimental Section

A. Materials and Methods

Reagents were obtained from Aldrich Chemical (www.sigma-aldrich.com) or Acros Organics (www.fishersci.com) and used without further purification. Optima or HPLC grade solvents were obtained from Fisher Scientific (www.fishersci.com), degassed with Ar, and purified on a solvent drying system. Reactions were performed in flame-dried glassware under positive Ar pressure with magnetic stirring.

TLC was performed on 0.25 mm E. Merck silica gel 60 F254 plates and visualized under UV light (254 nm) or by staining with potassium permanganate ($KMnO_4$), cerium ammonium molybdenate (CAM), or iodine (I_2). Silica flash chromatography was performed on E. Merck 230–400 mesh silica gel 60. Preparative scale HPLC purification was carried out on a Waters 2545 HPLC with 2996 diode array detector using a Sunfire Prep C18 reverse phase column (10 Å~ 150 mm, 5 **μ**m) with UV detection at 254 nm. Samples were lyophilized using a Labconco Freezone 2.5 instrument.

IR spectra were recorded on a Bruker Optics Tensor 27 FTIR spectrometer with Pike technologies MIRacle ATR (attenuated total reflectance, ZnSe crystal) accessory and peaks reported in cm^{-1}. NMR spectra were recorded on a Bruker Avance III 500 instrument or Bruker Avance III 600 instrument at 24 °C in $CDCl_3$ unless otherwise indicated. Spectra were processed using Bruker TopSpin or nucleomatica iNMR (www.inmr.net) software, and chemical shifts are expressed in ppm relative to TMS (^1H, 0 ppm) or residual solvent signals: $CDCl_3$ (^1H, 7.24 ppm; ^{13}C, 77.23 ppm), CD_3OD (^1H, 3.31 ppm; ^{13}C, 49.15 ppm), D_2O (^1H, 4.80 ppm); coupling constants are expressed in Hz. Mass spectra were obtained at the MSKCC Analytical Core Facility on a Waters Acuity SQD LC-MS by electrospray (ESI) ionization or atmospheric pressure chemical ionization (AP-CI).

N.B.: ^1H-NMR chemical shifts in these compounds were found to exhibit significant concentration dependence.

B. Enzymatic Kinetic Resolution of 3-Hydroxy-1-indanone (28).

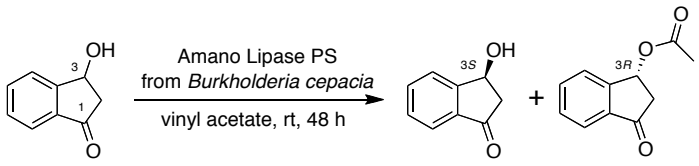

28 (3*S*)-**28** (3*R*)-**29**

Figure 3.13. Enzymatic kinetic resolution of 3-hydroxy-1-indanone (6). The lipase catalyzes acetyl transfer from vinyl acetate to the *R*-alcohol **(*R*)-28** enantioselectively, affording, at ideal 50% conversion, a 1:1 mixture of the *R*-acetate product **(*R*)-29** and the unreacted *S*-alcohol starting material **(*S*)-28**, which are readily separable by silica flash chromatography.

(+)-(*S*)-3-Hydroxy-1-indanone ((*S*)-28) and (–)-(*R*)-3-oxo-1-indanyl acetate ((*R*)-29). Racemic 3-hydroxy-1-indanone (1 g, 6.7 mmol, 1 equiv) prepared as previously described,[26] and Amano Lipase PS from *Burkholderia cepacia* (1.5 g, Sigma Aldrich) were suspended in vinyl acetate (80 mL) and stirred at rt until the reaction had proceeded to 50% conversion as judged by LC-MS analysis (≈48 h). Filtration through a pad of celite, concentration by rotary evaporation, and purification by silica flash chromatography (20 → 60% EtOAc in hexanes) yielded (*S*)-3-hydroxy-1-indanone (**(*S*)-28**) (455 mg, >98% ee, 46% yield) as a red tinged semi-solid and (*R*)-3-oxo-1-indanyl acetate (**(*R*)-29**) (604 mg, >98% ee, 47% yield) as a yellow oil.

Enantiomeric excess was determined by chiral HPLC (Chiralcel: OB-H, 4.6 mm x 150 mm, 5 µm particle size, 5% isopropanol in hexanes, 1 mL/minute), with samples prepared as 1 mg/mL solutions in 10% EtOH/hexanes:[27,†]

(*S*)-6: (*S*)-3-hydroxy-1-indanone	t_{ret} = 25 min
(*R*)-6: (*R*)-3-hydroxy-1-indanone	t_{ret} = 23 min
(*R*)-7: (*R*)-3-oxo-1-indanyl acetate	t_{ret} = 20 min
(*S*)-7: (*S*)-3-oxo-1-indanyl acetate	t_{ret} = 23 min

† *E*=Ln[(1-c)(1-ee)]/Ln[(1-c)(1+ee)]

(*S*)-6: $[\alpha]_D^{19}$: +132.0° (*c* 1, $CHCl_3$). **IR** (ATR): 3393, 2917, 1698, 1605, 1465, 1396, 1332, 1279, 1242, 1211, 1176, 1153, 1099, 1044, 993, 960, 903, 811, 759, 728, 644. **^{1}H-NMR** (500 MHz; $CDCl_3$): δ 7.75-7.68 (m, 3H), 7.51-7.48 (m, 1H), 5.44 (d, *J* = 6.6 Hz, 1H), 3.12 (dd, *J* = 18.9, 6.8 Hz, 1H), 2.62 (dd, *J* = 18.9, 2.9 Hz, 1H), 2.55 (s, 1H). **^{13}C-NMR (**126 MHz; $CDCl_3$): δ 203.5, 155.1, 136.4, 135.4, 129.5, 125.9, 123.3, 68.5, 47.2. **HRMS** (ESI) *m/z* calcd for $C_9H_8O_2Na$ ($[M+Na]^+$) 171.0422; found 171.0419.

(*R*)-7: $[\alpha]_D^{19}$: –11.9° (*c* 1, $CHCl_3$). **IR** (ATR): 3075, 2936, 1718, 1605, 1466, 1433, 1402, 1372, 1341, 1280, 1228, 1164, 1096, 1065, 989, 965, 945, 869, 763, 734, 681, 634, 607. **^{1}H-NMR** (600 MHz; $CDCl_3$): δ 7.78 (d, *J* = 7.7 Hz, 1H), 7.70-7.67 (m, 2H), 7.55-7.52 (m, 1H), 6.36 (dd, *J* = 7.0, 2.6 Hz, 1H), 3.19 (dd, *J* = 19.1, 7.0 Hz, 1H), 2.66 (dd, *J* = 19.1, 2.7 Hz, 1H), 2.14 (s, 3H). **^{13}C-NMR (**151 MHz; $CDCl_3$): δ 202.1, 171.0, 151.5, 137.1, 135.3, 130.0, 126.9, 123.4, 69.9, 43.9, 21.1. **HRMS** (ESI) *m/z* calcd for $C_{11}H_{10}O_3Na$ ($[M+H]^+$) 213.0528; found 213.0522.

C. Synthesis of 1*R*,3*S*-*syn*-Difluoroindanediol (1*R*,3*S*)-2

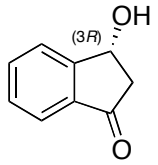

(–)-(*R*)-3-Hydroxy-1-indanone ((*R*)-28). (*R*)-3-Oxo-1-indanyl acetate **(*R*)-29** (550 mg, 2.891 mmol, 1 equiv.) was dissolved in 20 mL acetone then 6 M HCl (20 mL) was added. The mixture was stirred at rt for 14 h, then poured into satd aq $NaHCO_3$ (150 mL) and extracted with CH_2Cl_2 (4 x 75 mL). The combined organic extracts were dried (Na_2SO_4), filtered, and concentrated by rotary evaporation. Purification by silica flash chromatography (30% → 70% EtOAc in hexanes) yielded the alcohol **(*R*)-28** as a pale yellow semi-solid (365 mg, 85%).

$[\alpha]_D^{19}$: –129.1° (*c* 1, $CHCl_3$). **IR** (ATR): 3404, 2914, 1715, 1600, 1466, 1401, 1340, 1275, 1243, 1203, 1152, 1037, 896, 759, 730. **^{1}H-NMR** (600 MHz; $CDCl_3$): δ 7.75-7.68 (m, 3H), 7.51-7.48 (m, 1H), 5.44 (d, *J* = 4.5 Hz, 1H), 3.12 (dd, *J* = 18.9, 6.8 Hz, 1H), 2.63 (dd, *J* = 18.9, 2.9 Hz, 1H), 2.53 (s, 1H).

^{13}C-NMR (151 MHz; $CDCl_3$): δ 203.4, 155.1, 136.4, 135.4, 129.5, 125.9, 123.3, 68.6, 47.2. **HRMS** (ESI) *m/z* calcd for $C_9H_8O_2Na$ ([M+Na]$^+$) 171.0422; found 171.0428.

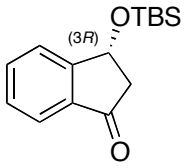

(–)-(*R*)-3-((*t*-Butyldimethylsilyl)oxy)-1-indanone ((*R*)-30). (*R*)-3-Hydroxy-1-indanone (**(*R*)-28**) (310 mg, 2.092 mmol, 1 equiv.) was dissolved in 5 mL CH_2Cl_2 and imidazole (370 mg, 5.439 mmol, 2.6 equiv.) was added. TBSCl (410 mg, 2.719 mmol, 1.3 equiv.) was added and the reaction mixture was stirred at rt for 12 h, then diluted with 50 mL water and extracted with CH_2Cl_2 (4 x 50 mL). The combined organic extracts were dried (Na_2SO_4), filtered, and concentrated by rotary evaporation. Purification by silica flash chromatography (0% → 30% EtOAc in hexanes) yielded the silyl ether **(*R*)-30** as a yellow tinged oil (510 mg, 93%).

$[\alpha]_D^{19}$: –110.3° (*c* 1, $CHCl_3$). **IR** (ATR): 2955, 2930, 2886, 1857, 1720, 1605, 1464, 1390, 1351, 1279, 1254, 1216, 1161, 1106, 1078, 1046, 1006, 961, 933, 856, 837, 809, 776, 759, 741, 720, 668. **^{1}H-NMR** (600 MHz; $CDCl_3$): δ 7.74 (d, *J* = 7.7 Hz, 1H), 7.68-7.66 (m, 1H), 7.61 (d, *J* = 7.6 Hz, 1H), 7.46 (t, *J* = 7.4 Hz, 1H), 5.39 (dd, *J* = 6.6, 3.4 Hz, 1H), 3.07 (dd, *J* = 18.3, 6.7 Hz, 1H), 2.60 (dd, *J* = 18.3, 3.4 Hz, 1H), 0.96 (s, 9H), 0.23 (s, 3H), 0.19 (s, 3H). **^{13}C-NMR (**151 MHz; $CDCl_3$): δ 203.1, 156.0, 136.3, 135.1, 129.0, 125.8, 123.0, 68.9, 47.9, 25.8, 18.2, –4.4, –4.6. **HRMS** (ESI) *m/z* calcd for $C_{15}H_{22}O_2NaSi$ ([M+Na]$^+$) 285.1287; found 285.1280.

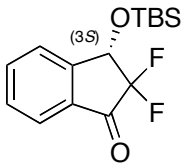

(–)-(*S*)-3-((*t*-Butyldimethylsilyl)oxy)-2,2-difluoro-1-indanone ((*S*)-31). Ketone **(*R*)-30** (266 mg, 1.013 mmol, 1 equiv.) was dissolved in 25 mL toluene, then hexylamine (0.535 mL, 4.052 mmol, 4 equiv.) was added and the reaction mixture was heated to reflux for 14 h. The reaction was then cooled to rt, concentrated by rotary evaporation, and placed under high vacuum (~60

mTorr) for 1 h. The crude imine was dissolved in acetonitrile (10 mL) and Selectfluor (753 mg, 2.125 mmol, 2.1 equiv.) and sodium sulfate (144 mg, 1.012 mmol, 1 equiv.) were added, then the reaction mixture was heated to reflux. The reaction was stirred for 12 h, then cooled to rt, diluted with 1 M HCl (50 mL) and extracted with CH_2Cl_2 (4 x 50 mL). The combined organic extracts were dried (Na_2SO_4), filtered, and concentrated by rotary evaporation. Purification by silica flash chromatography (25% → 75% CH_2Cl_2 in hexanes) yielded the difluoroindanone **(*S*)-31** as a deep yellow tinged oil (180 mg, 60%).

$[\alpha]_D^{19}$: –140.4° (*c* 1, $CHCl_3$). **IR** (ATR): 2956, 2932, 2888, 2860, 1745, 1608, 1472, 1362, 1299, 1256, 1230, 1184, 1143, 1101, 1075, 1007, 927, 895, 838, 780, 740, 698, 670, 648. **^{1}H-NMR** (500 MHz; $CDCl_3$): δ 7.86 (d, *J* = 7.7 Hz, 1H), 7.81 (td, *J* = 7.6, 1.1 Hz, 1H), 7.64 (dd, *J* = 7.8, 0.8 Hz, 1H), 7.57 (t, *J* = 7.5 Hz, 1H), 5.24 (dd, *J* = 12.8, 3.5 Hz, 1H), 0.99 (s, 9H), 0.28 (s, 3H), 0.25 (s, 3H). **^{13}C-NMR (**126 MHz; $CDCl_3$): δ 189.6, 150.4, 137.5, 132.3, 130.4, 126.2, 124.7, 114.9, 71.8, 25.7, 18.4, –4.6, –5.1. **^{19}F-NMR** (471 MHz; $CDCl_3$): δ -116.50 (d, *J* = 279.4 Hz, 1F), -123.44 (d, *J* = 279.8 Hz, 1F). **HRMS (ESI)** m/z calcd for $C_{15}H_{20}O_3F_2SiNa$ ([M+Na]+) 321.1098; found 321.1094.

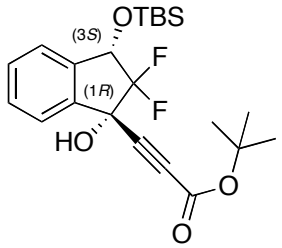

(+)-*t*-Butyl 3-((1*R*,3*S*)-3-(*t*-butyldimethylsilyloxy)-2,2-difluoro-1-hydroxy-1-indanyl)propiolate ((1*R*,3*S*)-32). Lithium bis(trimethylsilyl)amide (6.5 mL, 6.492 mmol, 1.0 M in THF, 1.55 equiv.) was cooled to –78 ºC, then *t*-butyl propiolate (793 mg, 6.283 mmol, 1.5 equiv.) in 3 mL THF was added and the mixture was stirred for 45 min. The solution was then added via cannula over 10 min to ketone (3*R*)-**31** (1.25 g, 4.189 mmol, 1 equiv.) in 5 mL THF at –78 ºC and stirred for 2 h. The reaction was quenched with satd aq NH_4Cl (50 mL), warmed to rt, and extracted with EtOAc (4 x 50 mL). The combined organic extracts were dried (Na_2SO_4), filtered, and concentrated by rotary evaporation. Purification by silica flash chromatography (50% → 100% CH_2Cl_2 in hexanes) yielded the ester **(1*R*,3*S*)-32** as a yellow tinged oil (1.778 g, 82%).

$[\alpha]_D^{19}$: +30.0° (*c* 1, $CHCl_3$). **IR** (ATR): 3394, 2956, 2932, 2888, 2859, 2245, 1762, 1473, 1395, 1371, 1258, 1205, 1153, 1113, 1040, 1013, 909, 888, 839, 791, 751, 732, 695, 672, 657. **^{1}H-NMR** (500 MHz; $CDCl_3$): δ 7.63-7.60 (m, 1H), 7.48-7.44 (m, 2H), 7.39-7.37 (m, 1H), 5.19 (dd, *J* = 8.0, 6.4 Hz, 1H), 1.49 (s, 9H), 0.95 (s, 9H), 0.24 (s, 6H). **^{13}C-NMR (**126 MHz; $CDCl_3$): δ 151.8, 139.4, 139.1, 130.9, 130.3, 124.9, 124.4, 124.2, 84.2, 80.6, 78.2, 74.9, 74.4, 28.0, 25.7, 18.2, –4.6, –4.9. **^{19}F-NMR** (471 MHz; $CDCl_3$): δ -115.04 (d, *J* = 222.3 Hz, 1F), -128.51 (d, *J* = 223.3 Hz, 1F). **HRMS** (ESI) *m/z* calcd for $C_{22}H_{30}O_4F_2SiNa$ ([M+Na]$^+$) 441.1779; found 447.1774.

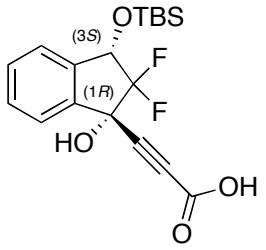

(+)-3-((1*R*,3*S*)-3-(*t*-Butyldimethylsilyloxy)-2,2-difluoro-1-hydroxy-1-indanyl)propiolic acid ((1*R*,3*S*)-33). Ester (1*R*,3*S*)-**32** (485 mg, 1.142 mmol, 1 equiv.) was dissolved in 5 mL CH_2Cl_2 and cooled to 0 ºC, then 5 mL TFA was added and the reaction mixture was stirred for 3 h. Concentration by rotary evaporation at 0 ºC and purification by silica flash chromatography (0% → 20% MeOH in CH_2Cl_2) yielded the acid **(1*R*,3*S*)-33** as a white cotton type solid (245 mg, 58%) as well as the corresponding desilated diol **(1*R*,3*S*)-40** as a white solid (100 mg, 34%).

(1*R*,3*S*)-33: $[\alpha]_D^{19}$: +27.6° (*c* 1, $CHCl_3$). **IR** (ATR): 2957, 2932, 2887, 2860, 2249, 1700, 1472, 1364, 1247, 1150, 1095, 1010, 910, 892, 839, 782, 760, 733, 687, 652, 625. **^{1}H-NMR** (500 MHz; $CDCl_3$): δ 7.62-7.60 (m, 1H), 7.50-7.45 (m, 2H), 7.40-7.38 (m, 1H), 5.18 (dd, *J* = 8.2, 5.8 Hz, 1H), 0.95 (s, 9H), 0.24 (s, 6H). **^{13}C-NMR (**126 MHz; $CDCl_3$): δ 156.1, 139.2, 139.0, 131.2, 130.4, 125.1, 124.5, 124.0, 83.3, 78.5, 75.1, 74.5, 25.7, 18.2, –4.7, –4.9. **^{19}F-NMR** (471 MHz; $CDCl_3$): δ -114.45 (d, *J* = 227.1 Hz, 1F), -128.02 (d, *J* = 224.9 Hz, 1F). **HRMS** (ESI) *m/z* calcd for $C_{18}H_{22}F_2O_4SiNa$ ([M+H]$^+$) 391.1153; found 391.1110.

(1*R*,3*S*)-40: $[\alpha]_D^{19}$: +3.4° (*c* 1, $CHCl_3$). **IR** (ATR): 3374, 2521, 2246, 1698, 1466, 1369, 1271, 1228, 1178, 1159, 1109, 1067, 1001, 910, 886, 582, 796, 758, 731, 682, 656, 632. **^{1}H-NMR** (500 MHz; MeOD): δ 7.56-7.54 (m, 1H), 7.50-

7.46 (m, 3H), 5.19 (t, *J* = 8.6 Hz, 1H). **^{13}C-NMR (**126 MHz; $CDCl_3$): δ 155.6, 141.0, 140.0, 131.6, 131.1, 126.8, 126.0, 124.9, 83.3, 80.4, 75.1, 74.6. **^{19}F-NMR** (471 MHz; $CDCl_3$): δ -118.63 (d, *J* = 224.7 Hz, 1F), -131.89 (d, *J* = 221.8 Hz, 1F). **HRMS** (ESI) *m/z* calcd for $C_{12}H_8F_2O_4Na$ ([M+H]$^+$) 277.0288; found 277.0291.

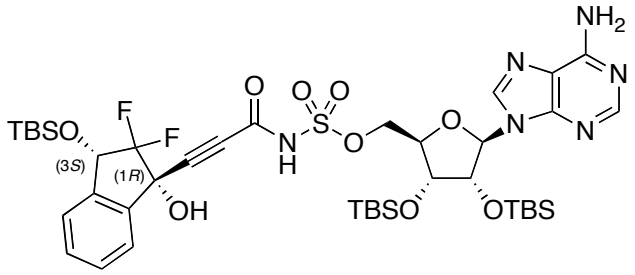

2′,3′-*O*-(*t*-Butyldimethylsilyl)-5′-*O*-(*N*-[3″-((1*R*,3*S*)-3‴-(*t*-Butyldimethyl silyloxy)-2‴,2‴-difluoro-1‴-hydroxy-1‴-indanyl)propioloyl]sulfamoyl) adenosine ((1*R*,3*S*)-35). Propiolic acid **(1*R*,3*S*)-33** (245 mg, 0.665 mmol, 1 equiv), protected 5′-*O*-sulfamoyladenosine **34** (573 mg, 0.997 mmol, 1.5 equiv) prepared as previously described,[28] and DMAP (81 mg, 0.665 mmol, 1.0 equiv.) was dissolved in CH_2Cl_2 (5 mL) and EDCI (510 mg, 2.659 mmol, 4.0 equiv) was added. The reaction was stirred for 12 h, quenched with 25 mL 1 M $KHSO_4$, and extracted with CH_2Cl_2 (5 x 25 mL). The combined organic extracts were dried (Na_2SO_4), filtered, and concentrated by rotary evaporation. The reside was reconstituted in CH_2Cl_2, loaded into a pad of silica and washed with 100 mL CH_2Cl_2, then eluted with 15% MeOH/ CH_2Cl_2 (200 mL) to afford the crude propiolyl-sulfamate **(1*R*,3*S*)-35** (499 mg), which was used without further purification.

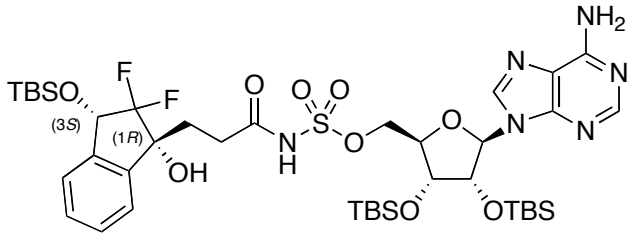

2′,3′-*O*-(*t*-Butyldimethylsilyl)-5′-*O*-(*N*-[3″-((1*R*,3*S*)-3‴-(*t*-Butyldimethyl silyloxy)-2‴,2‴-difluoro-1‴-hydroxy-1‴-indanyl)propanoyl]sulfamoyl) adenosine ((1*R*,3*S*)-36). Crude propiolyl-sulfamate **(1*R*,3*S*)-35** (499 mg, 0.540 mmol, 1 equiv.) from previous step and 10% Pd/C (575 mg, 0.540 mmol, 1 equiv) were suspended in solution of MeOH/NEt_3 (50 mL, 9:1). The

reaction was then stirred vigorously under H_2 balloon for 2 h, then diluted with EtOAc (50 mL), filtered through a celite pad, and concentrated by rotary evaporation to afford the crude propanoyl-sulfamate **(1*R*,3*S*)-36** (500 mg), which was used without further purification.

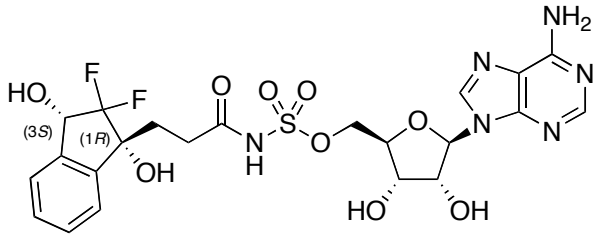

(–)-5´-*O*-(*N*-[3˝-((1*R*,3*S*)-2˝˝,2˝˝-difluoro-1˝˝,3˝˝-dihydroxy-1˝˝-indanyl) propanoyl]sulfamoyl)adenosine ((1*R*,3*S*)-2). Crude propanoyl-sulfamate **(1*R*,3*S*)-36** (500 mg, 0.538 mmol, 1 equiv.) was suspended in DMF (5 mL), then TASF (592 mg, 2.151 mmol, 4.0 equiv.) was added and the reaction mixture was stirred for 12 h at 50 ºC. Concentration by rotary evaporation, purification by preparative HPLC (5% → 30% MeCN in H_2O with 0.1% TFA), and lyophilization yielded the *syn*-difluoroindanediol **(1*R*,3*S*)-2** as a fluffy white solid (144 mg, 37% over 3 steps). *N.B.*: HPLC fractions were stored at 0 °C until just prior to pooling and freezing (dry-ice bath) for lyophilization.

$[\alpha]_D^{19}$: –19.16° (*c* 0.5, MeOH). **IR** (ATR): 3340, 2504, 2245, 2074, 1684, 1558, 1474 1421, 1377, 1201, 1140, 1043, 979, 882, 842, 800, 724, 645. **^{1}H-NMR** (500 MHz; CD_3OD): δ 8.46 (s, 1H), 8.35 (s, 1H), 7.44-7.37 (m, 4H), 6.09 (d, *J* = 4.8 Hz, 1H), 5.12 (dd, *J* = 11.6, 7.5 Hz, 1H), 4.63 (t, *J* = 5.0 Hz, 1H), 4.54-4.48 (m, 2H), 4.39 (t, *J* = 4.9 Hz, 1H), 4.30-4.28 (m, 1H), 2.61 (ddd, *J* = 16.2, 10.0, 5.9 Hz, 1H), 2.47 (ddd, *J* = 16.3, 9.9, 6.1 Hz, 1H), 2.16-2.09 (m, 1H), 1.83 (ddd, *J* = 14.7, 9.4, 5.6 Hz, 1H). **^{13}C-NMR (**126 MHz; CD_3OD): δ 173.2, 150.2, 147.05, 147.03, 143.4, 142.9, 139.3, 130.4, 130.1, 125.2, 124.8, 120.5, 90.3, 83.6, 79.4, 75.8, 74.2, 72.3, 71.6, 49.5, 31.6, 30.9. **^{19}F-NMR** (471 MHz; CD_3OD): δ -128.07 (d, *J* = 225.3 Hz, 1F), -130.99 (d, *J* = 225.2 Hz, 1F). **HRMS** (ESI) *m/z* calcd for $C_{22}H_{25}N_6O_9F_2S$ ($[M+H]^+$) 587.1372; found 587.1364.

D. Synthesis of 1*S*,3*R*-*syn*-Difluoroindanediol (1*R*,3*S*)-2

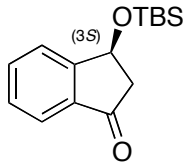

(+)-(*S*)-3-((*t*-Butyldimethylsilyl)oxy)-1-indanone ((*S*)-30). (*S*)-3-Hydroxy-1-indanone **(*S*)-28** (720 mg, 4.859 mmol, 1 equiv.) was dissolved in 10 mL CH_2Cl_2 and imidazole (860 mg, 12.63 mmol, 2.6 equiv.) was added. TBSCl (952 mg, 6.316 mmol, 1.3 equiv.) was added and the reaction mixture was stirred at rt for 12 h, then diluted with 50 mL water and extracted with CH_2Cl_2 (4 x 50 mL). The combined organic extracts were dried (Na_2SO_4), filtered, and concentrated by rotary evaporation. Purification by silica flash chromatography (0% → 30% EtOAc in hexanes) yielded the silyl ether **(*S*)-30** as a yellow tinged oil (1.13 g, 91%).

$[\alpha]_D^{19}$: +109.4° (*c* 1, $CHCl_3$). **IR** (ATR): 2955, 2930, 2886, 2857, 1720, 1606, 1464, 1390, 1361, 1279, 1254, 1216, 1161, 1106, 1079, 1046, 1006, 961, 9334, 857, 837, 809, 776, 759, 719, 668. **^{1}H-NMR** (600 MHz; $CDCl_3$): δ 7.74 (d, *J* = 7.7 Hz, 1H), 7.74 (d, *J* = 7.7 Hz, 1H), 7.68-7.65 (m, 1H), 7.61 (d, *J* = 7.7 Hz, 1H), 7.46 (t, *J* = 7.4 Hz, 1H), 5.39 (dd, *J* = 6.6, 3.4 Hz, 1H), 3.06 (dd, *J* = 18.3, 6.7 Hz, 1H), 2.60 (dd, *J* = 18.3, 3.4 Hz, 1H), 0.96 (s, 9H), 0.23 (s, 3H), 0.19 (s, 3H). **^{13}C-NMR (**151 MHz; $CDCl_3$): δ 203.1, 156.0, 136.3, 135.1, 129.0, 125.8, 123.0, 68.9, 47.9, 25.8, 18.2, -4.4, -4.6. **HRMS** (ESI) *m/z* calcd for $C_{15}H_{23}O_2Si$ ($[M+H]^+$) 263.1467; found 263.1465.

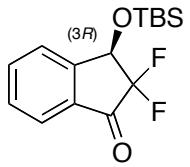

(+)-(*R*)-3-((*t*-Butyldimethylsilyl)oxy)-2,2-difluoro-1-indanone ((*R*)-31). Ketone **(*S*)-30** (1 g, 3.814 mmol, 1 equiv.) was dissolved in 80 mL cyclohexane, then hexylamine (2 mL, 15.25 mmol, 4 equiv.) and trifluoroacetic acid (0.015 mL, 0.19 mmol, 0.05 equiv.) were added and the reaction mixture was heated to reflux for 14 h. The reaction was then cooled to rt, diluted with 75 mL toluene, concentrated by rotary evaporation, and placed under high vacuum (~60 mTorr) for 1 h. The crude imine was dissolved in acetonitrile (50 mL), then Selectfluor (2.83 g, 7.99 mmol, 2.1 equiv.) and sodium sulfate (378

mg, 2.663 mmol, 0.7 equiv.) were added and the reaction mixture was heated to reflux for 12 h. The reaction was cooled to rt, diluted with 1 M HCl (150 mL) and extracted with CH_2Cl_2 (4 x 100 mL). The combined organic extracts were dried (Na_2SO_4), filtered, and concentrated by rotary evaporation. Purification by silica flash chromatography (25% → 75% CH_2Cl_2 in hexanes) yielded the difluoroindanone **(*R*)-31** as a yellow tinged oil (710 mg, 63%).

$[\alpha]_D^{19}$: +138.7° (*c* 3.3, $CHCl_3$). **IR** (ATR): 2958, 2933, 2890, 2862, 1748, 1610, 1474, 1364, 1301, 1258, 1232, 1186, 1145, 1103, 1076, 1008, 929, 897, 840, 782, 741, 700, 672, 650. **^{1}H-NMR** (500 MHz; $CDCl_3$): δ 7.86 (d, *J* = 7.8 Hz, 1H), 7.81 (td, *J* = 7.6, 1.0 Hz, 1H), 7.64 (dd, *J* = 7.8, 0.7 Hz, 1H), 7.57 (t, *J* = 7.5 Hz, 1H), 5.24 (dd, *J* = 12.8, 3.5 Hz, 1H), 0.99 (s, 10H), 0.28 (s, 3H), 0.25 (s, 3H). **^{13}C-NMR (**126 MHz; $CDCl_3$): δ 189.6, 150.4, 137.6, 132.3, 130.4, 126.2, 124.6, 114.93, 114.91, 71.8, 25.68, 18.3, –4.6, –5.1. **^{19}F-NMR** (471 MHz; $CDCl_3$): δ -116.50 (d, *J* = 279.6 Hz, 1F), -123.45 (d, *J* = 279.8 Hz, 1F). **HRMS** (ESI) *m/z* calcd for $C_{15}H_{20}O_3F_2SiNa$ ([M+Na]+) 321.1098; found 321.1103.

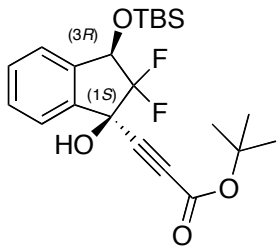

(–)-*t*-Butyl 3-((1*S*,3*R*)-3-(tert-butyldimethylsilyloxy)-2,2-difluoro-1-hydroxy-1-indanyl)propiolate ((1*S*,3*R*)-32). Lithium bis(trimethylsilyl)amide (4.95 mL, 4.95 mmol, 1.0 M in THF, 1.55 equiv.) was cooled to –78 ºC, then *t*-butyl propiolate (604 mg, 4.789 mmol, 1.5 equiv.) in 3 mL THF was added and the reaction mixture was stirred for 45 min. The solution was then added via cannula over 10 min to ketone **(*R*)-31** (953 mg, 3.193 mmol, 1 equiv.) in 5 mL THF at –78 ºC and stirred for 2 h. The reaction was quenched with satd aq NH_4Cl (50 mL), warmed to rt, and extracted with EtOAc (4 x 50 mL). The combined organic extracts were dried (Na_2SO_4), filtered, and concentrated by rotary evaporation. Purification by silica flash chromatography (50% → 100% CH_2Cl_2 in hexanes) yielded the ester **(1*S*,3*R*)-32** as a clear viscous oil (1.05 g, 78%).

$[\alpha]_D^{19}$: –28.1° (*c* 1, $CHCl_3$). **IR** (ATR): 3400, 2956, 2932, 2888, 2860, 2248, 1710, 1473, 1395, 1371, 1258, 1204, 1153, 1114, 1039, 1013, 909, 888, 838, 781, 751, 732, 695, 672, 657. **^{1}H-NMR** (500 MHz; $CDCl_3$): δ 7.63-7.60 (m, 1H), 7.47-7.45 (m, 2H), 7.38-7.37 (m, 1H), 5.19 (dd, *J* = 8.0, 6.3 Hz, 1H), 2.96 (d, *J* = 2.3 Hz, 1H), 1.49 (s, 9H), 0.95 (s, 9H), 0.24 (s, 6H). **^{13}C-NMR (**126 MHz; $CDCl_3$): δ 151.8, 139.5, 139.1, 130.9, 130.3, 124.9, 124.4, 124.2, 84.2, 80.6, 78.2, 74.9, 74.4, 28.0, 25.7, 18.2, –4.65, –4.84. **^{19}F-NMR** (471 MHz; $CDCl_3$): δ -115.05 (d, *J* = 224.7 Hz, 1F), -128.46 (d, *J* = 224.6 Hz, 1F). **HRMS** (ESI) *m/z* calcd for $C_{22}H_{30}O_4F_2SiNa$ ([M+Na]$^+$) 441.1779; found 441.1785.

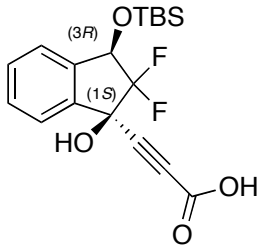

(–)-3-((1*S*,3*R*)-3-(*t*-Butyldimethylsilyloxy)-2,2-difluoro-1-hydroxy-1-indanyl)propiolic acid ((1*S*,3*R*)-33). Ester **(1*S*,3*R*)-32** (950 mg, 2.26mmol, 1 equiv.) was dissolved in 10 mL CH_2Cl_2 and cooled to 0 ºC, then 10 mL TFA was added and the reaction mixture was stirred for 3 h. Concentration by rotary evaporation at 0 ºC and purification by silica flash chromatography (0% → 20% MeOH in CH_2Cl_2) yielded the acid **(1*S*,3*R*)-33** as a white cotton type solid (465 mg, 56%), along with the corresponding desilated congener **(1*S*,3*R*)-40** as a white solid (176 mg, 31%).

(1*S*,3*R*)-33: $[\alpha]_D^{19}$: –27.9° (*c* 1, $CHCl_3$). **IR** (ATR): 2958, 2934, 2893, 2862, 2253, 1701, 1474, 1365, 1249, 1152, 1095, 1010, 912, 893, 841, 783, 764, 733, 688, 653, 626. **^{1}H-NMR** (500 MHz; $CDCl_3$): δ 7.61-7.60 (m, 1H), 7.50-7.45 (m, 2H), 7.40-7.38 (m, 1H), 5.18 (dd, *J* = 8.2, 5.8 Hz, 1H), 0.94 (s, 9H), 0.24 (s, 6H). **^{13}C-NMR (**126 MHz; $CDCl_3$): δ 156.3, 139.2, 139.0, 131.2, 130.5, 125.1, 124.5, 124.0, 83.4, 78.5, 75.1, 74.5, 25.7, 18.2, –4.66, –4.85. **^{19}F-NMR** (471 MHz; $CDCl_3$): 114.45 (d, *J* = 224.6 Hz, 1F), -127.98 (d, *J* = 224.6 Hz, 1F). **HRMS** (ESI) *m/z* calcd for $C_{18}H_{22}O_4F_2NaSi$ ([M+H]$^+$) 391.1153; found 391.1154.

(1*S*,3*R*)-40: $[\alpha]_D^{19}$: –3.6° (*c* 1, $CHCl_3$). **IR** (ATR): 3354, 2502, 2246, 1697, 1466, 1271, 1228, 1178, 1159, 1109, 1066, 1000, 974, 909, 886, 851, 795, 759, 730, 683, 655, 631. **^{1}H-NMR** (500 MHz; MeOD): δ 7.56-7.54 (m, 1H), 7.50-7.46 (m,

3H), 5.18 (t, *J* = 8.6 Hz, 1H). **^{13}C-NMR (**126 MHz; MeOD): δ 155.6, 141.0, 140.0, 131.6, 131.1, 126.9, 126.0, 124.9, 83.3, 80.4, 75.1, 74.5. **^{19}F-NMR** (471 MHz; MeOD): δ -118.67 (d, *J* = 221.5 Hz, 1F), -131.92 (d, *J* = 224.7 Hz, 1F). **HRMS** (ESI) *m/z* calcd for $C_{24}H_{16}O_8F_4$ ([2M-H]$^-$) 507.0703; found 507.0704.

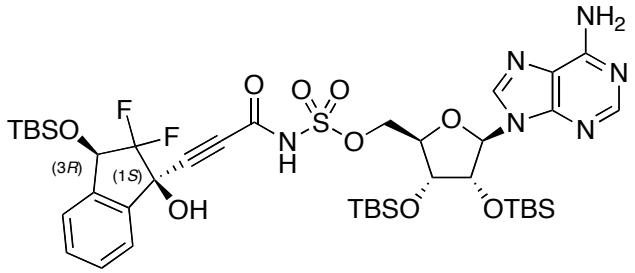

2´,3´-*O*-(*t*-Butyldimethylsilyl)-5´-*O*-(*N*-[3˝-((1*S*,3*R*)-3˝˝-(*t*-Butyldimethyl silyloxy)-2˝˝,2˝˝-difluoro-1˝˝-hydroxy-1˝˝-indanyl)propioloyl]sulfamoyl) adenosine ((1*S*,3*R*)-35). Propiolic acid **(1*S*,3*R*)-33** (250 mg, 0.678 mmol, 1 equiv), protected 5´-*O*-sulfamoyladenosine **34** (585 mg, 1.017 mmol, 1.5 equiv) prepared as previously described,[3] and DMAP (83 mg, 0.678 mmol, 1.0 equiv.) was dissolved in CH_2Cl_2 (5 mL) and EDCI (520 mg, 2.714 mmol, 4.0 equiv) was added. The reaction was stirred for 12 h, then quenched with 25 mL 1 M $KHSO_4$, and extracted with CH_2Cl_2 (5 x 25 mL). The combined organic extracts were dried (Na_2SO_4), filtered, and concentrated by rotary evaporation. The reside was reconstituted in CH_2Cl_2, loaded into a pad of silica and washed with 100 mL CH_2Cl_2, then eluted with 15% MeOH/ CH_2Cl_2 (200 mL) to afford the crude propiolyl-sulfamate **(1*S*,3*R*)-35** (480 mg), which was used without further purification.

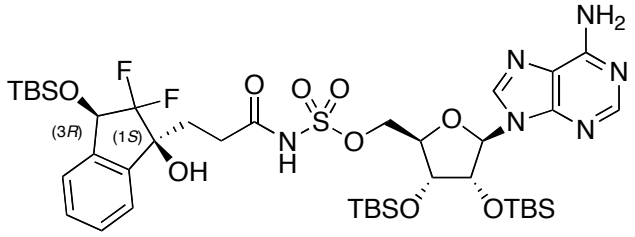

2´,3´-*O*-(*t*-Butyldimethylsilyl)-5´-*O*-(*N*-[3˝-((1*S*,3*R*)-3˝˝-(*t*-Butyldimethyl silyloxy)-2˝˝,2˝˝-difluoro-1˝˝-hydroxy-1˝˝-indanyl)propanoyl]sulfamoyl) adenosine ((1*S*,3*R*)-36). Crude propiolyl-sulfamate **(1*S*,3*R*)-35** (480mg, 0.519 mmol, 1 equiv.) from previous step and 10% Pd/C (552 mg, 0.519 mmol, 1 equiv) were suspended in solution of MeOH/NEt_3 (50 mL, 9:1). The

reaction was then stirred vigorously under H_2 balloon for 2 h, then diluted with EtOAc (50 mL), filtered through a celite pad, and concentrated by rotary evaporation to afford the crude propanoyl-sulfamate **(1*S*,3*R*)-36** (428 mg), which was used without further purification.

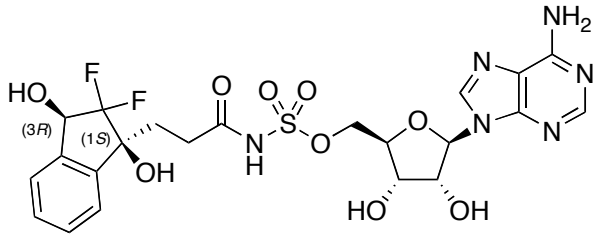

(+)-5′-*O*-(*N*-[3″-((1*S*,3*R*)-2‴,2‴-difluoro-1‴,3‴-dihydroxy-1‴-indanyl)propanoyl]sulfamoyl)adenosine ((1*S*,3*R*)-2). Crude propanoyl-sulfamate **(1*S*,3*R*)-36** (480 mg, 0.461 mmol, 1 equiv.) was suspended in DMF (5 mL), then TASF (507 mg, 1.841 mmol, 4.0 equiv.) was added and the reaction mixture was stirred for 12 h at 50 ºC. Concentration by rotary evaporation, purification by preparative HPLC (5% → 30% MeCN in H_2O with 0.1% TFA), and lyophilization yielded the *syn*-difluoroindanediol **(1*S*,3*R*)-2** as a fluffy white solid (123 mg, 31% over 3 steps). *N.B.*: HPLC fractions were stored at 0 °C until just prior to pooling and freezing (dry-ice bath) for lyophilization.

$[\alpha]_D^{19}$: +5.7° (*c* 0.5, MeOH). **IR** (ATR): 3368, 2512, 2241, 2077, 1687, 1478, 1425, 1379, 1202, 1141, 1045, 980, 882, 803, 726, 645. **^{1}H-NMR** (500 MHz; CD_3OD): δ 8.42 (s, 1H), 8.34 (s, 1H), 7.42-7.36 (m, 4H), 6.07-6.06 (m, 1H), 5.15-5.10 (m, 1H), 4.63-4.60 (m, 1H), 4.54-4.46 (m, 2H), 4.40-4.37 (m, 1H), 4.30-4.27 (m, 1H), 2.66-2.60 (m, 1H), 2.49-2.42 (m, 1H), 2.18-2.12 (m, 1H), 1.81-1.75 (m, 1H). **^{13}C-NMR** (126 MHz; CD_3OD): δ 173.2, 150.2, 147.01, 146.86, 143.4, 142.9, 139.3, 130.4, 130.1, 125.2, 124.9, 120.5, 90.3, 83.6, 79.4, 75.8, 74.2, 72.3, 71.6, 49.9, 31.6, 30.9. **^{19}F-NMR** (471 MHz; CD_3OD): δ -128.11 (d, *J* = 225.3 Hz, 1F), -131.06 (d, *J* = 224.7 Hz, 1F). **HRMS** (ESI) *m/z* calcd for $C_{22}H_{25}N_6O_9F_2S$ ($[M+H]^+$) 587.1372; found 587.1353.

E. Synthesis of 1*R*,3*R*-*anti*-Difluoroindanediol (1*R*,3*S*)-2

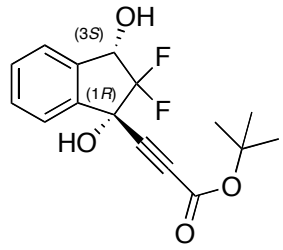

(–)-*t*-Butyl 3-((1*R*,3*S*)-2,2-difluoro-1,3-dihydroxy-1-indanyl)propiolate ((1*R*,3*S*)-37). Silyl ether **(1*R*,3*S*)-32** (470 mg, 1.107 mmol, 1.0 equiv.) was dissolved in 2 mL THF and cooled to 0 ºC, then tetrabutylammonium fluoride (1.217 mL, 1.217 mmol, 1.0 M in THF, 1.1 equiv.) was added, and the reaction mixture was stirred for 1 h. Concentration by rotary evaporation and purification by silica flash chromatography (30% → 60% EtOAc in hexanes) yielded the diol **(1*R*,3*S*)-37** as a white solid (285 mg, 83%).

Enantiomeric excess was confirmed by chiral HPLC (Chiralcel: OB-H, 4.6 mm x 150 mm, 5 µm particle size, 5% isopropanol in hexanes, 1 mL/minute), with samples prepared as 1 mg/mL solutions in 10% EtOH/hexanes:

(1*R*,3*S*)-37: t_{ret} = 17 min, >98% ee

(1*S*,3*R*)-37: t_{ret} = 21 min

$[\alpha]_D^{19}$: –5.3° (*c* 1, $CHCl_3$). **IR** (ATR): 3377, 2984, 2936, 2249, 1707, 1459, 1396, 1372, 1281, 1232, 1152, 1110, 1067, 1003, 909, 838, 798, 754, 732, 682, 660, 649. **^{1}H-NMR** (500 MHz; $CDCl_3$): δ 7.65-7.62 (m, 1H), 7.54-7.48 (m, 3H), 5.11 (dd, *J* = 8.7, 4.0 Hz, 1H), 3.10 (s, 2H), 1.49 (s, 9H). **^{13}C-NMR (**126 MHz; $CDCl_3$): δ 151.8, 139.5, 138.7, 131.3, 130.8, 125.8, 124.8, 123.6, 84.5, 80.9, 77.9, 74.8, 74.3, 28.0. **^{19}F-NMR** (471 MHz; $CDCl_3$): δ -114.40 (d, *J* = 233.2 Hz, 1F), -129.02 (d, *J* = 231.4 Hz, 1F). **HRMS** (ESI) *m/z* calcd for $C_{16}H_{16}O_4F_2Na$ ($[M+H]^+$) 333.0914; found 333.0916.

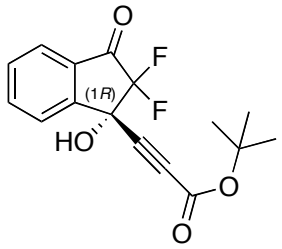

(–)-(*R*)-*t*-Butyl 3-(2,2-difluoro-1-hydroxy-3-oxo-1-indanyl)propiolate ((*R*)-38). DMSO (227 mg, 2.9 mmol, 3.0 equiv.) was dissolved in 4 mL CH_2Cl_2, cooled to –78 ºC, and oxalyl chloride (184 mg, 1.450 mmol, 1.5 equiv.) was added and the reaction mixture was stirred for 10 min. Diol **(1*R*,3*S*)-37** (300 mg, 0.967 mmol, 1.0 equiv.) in 1.5 mL CH_2Cl_2 was added dropwise, then the reaction mixture was stirred for 40 min. Triethylamine (0.675 mL, 4.834 mmol, 5.0 equiv.) was added and the reaction mixture was stirred for 40 min, then removed from the dry-ice bath and stirred for 10 min. The reaction was then quenched with satd aq NH_4Cl (30 mL), extracted with CH_2Cl_2 (4 x 20 mL), the combined organic extracts were dried (Na_2SO_4), filtered, and concentrated by rotary evaporation. Purification by silica flash chromatography (5% → 25% EtOAc in hexanes) yielded the ketoalcohol **(*R*)-38** as a clear oil (272 mg, 91%).

$[\alpha]_D^{19}$: –24.4° (*c* 1, $CHCl_3$). **IR** (ATR): 3410, 2985, 2938, 2244, 1752, 1712, 1604, 1471, 1397, 1372, 1286, 1222, 1193, 1152, 1101, 1041, 1017, 934, 910, 877, 837, 770, 755, 736, 712, 693, 649. **^{1}H-NMR** (500 MHz; $CDCl_3$): δ 7.94-7.88 (m, 3H), 7.68 (td, *J* = 7.5, 1.0 Hz, 1H), 3.59 (s, 1H), 1.51 (s, 9H). **^{13}C-NMR (**126 MHz; $CDCl_3$): δ 187.6, 151.6, 148.8, 138.1, 132.0, 131.3, 126.3, 125.2, 113.5, 85.0, 82.2, 77.1, 71.1, 28.0. **^{19}F-NMR** (471 MHz; $CDCl_3$): δ -111.61 (d, *J* = 269.2 Hz, 1F), -125.99 (d, *J* = 270.5 Hz, 1F). **HRMS** (ESI) *m/z* calcd for $C_{16}H_{14}O_4F_2Cl$ ($[M+Cl]^-$) 343.0549; found 343.0565.

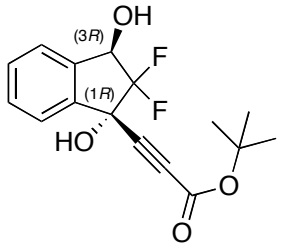

(+)-*t*-Butyl 3-((1*R*,3*R*)-2,2-difluoro-1,3-dihydroxy-1-indanyl)propiolate ((1*R*,3*R*)-39). Ketone **(*R*)-38** (300 mg, 0.941 mmol, 1 equiv.) was dissolved in 5 mL MeOH and cooled to 0 ºC, then $NaBH_4$ (11 mg, 0.282 mmol, 0.3 equiv.) was added in 4 portions over 5 min and the reaction mixture was stirred for 30

min. Acetone (0.1 mL) was added and the reaction mixture was stirred for 10 min, then 1 M phosphate buffer (pH 7.0, 20 mL) was added and the reaction mixture was stirred for an additional 10 min. The reaction was then extracted with EtOAc (4 x 15 mL), the combined organic extracts were dried (Na_2SO_4), filtered, and concentrated by rotary evaporation. Purification by silica flash chromatography (0% → 100% EtOAc in CH_2Cl_2) yielded the *anti*-diol **(1*R*,3*R*)-39** as a white solid (263 mg, 90%).

Enantiomeric excess was confirmed by chiral HPLC (Chiralcel: OB-H, 4.6 mm x 150 mm, 5 µm particle size, 5% isopropanol in hexanes, 1 mL/minute), with samples prepared as 1 mg/mL solutions in 10% EtOH/hexanes:

(1*R*,3*R*)-39: t_{ret} = 21 min, >98% ee

(1*S*,3*S*)-39: t_{ret} = 27 min

$[\alpha]_D^{19}$: +9.6° (*c* 1, $CHCl_3$). **IR** (ATR): 3371, 2983, 2930, 2241, 1684, 1395, 1371, 1230, 1300, 1152, 1111, 1078, 1032, 1003, 913, 834, 752, 731, 649, 574. **^{1}H-NMR** (500 MHz; $CDCl_3$): δ 7.63 (d, *J* = 7.4 Hz, 1H), 7.52-7.49 (m, 2H), 7.48-7.45 (m, 1H), 5.41 (td, *J* = 10.3, 6.4 Hz, 1H), 3.11 (d, *J* = 1.5 Hz, 1H), 2.38 (dd, *J* = 10.7, 2.1 Hz, 1H), 1.51 (s, 9H). **^{13}C-NMR (**126 MHz; $CDCl_3$): δ 151.8, 139.0, 137.6, 131.5, 130.2, 124.94, 124.74, 123.7, 84.6, 80.8, 77.8, 74.17, 74.06, 28.0. **^{19}F-NMR** (471 MHz; $CDCl_3$): δ -123.33 (d, *J* = 225.3 Hz, 1F), -125.61 (d, *J* = 226.3 Hz, 1F). **HRMS** (ESI) *m/z* calcd for $C_{16}H_{16}O_4F_2Na$ ($[M+H]^+$) 333.0914; found 333.0920.

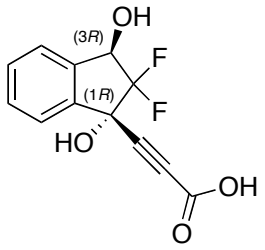

3-((1*R*,3*R*)-2,2-difluoro-1,3-dihydroxy-1-indanyl)propiolic acid ((1*R*,3*R*)-40). Ester **(1*R*,3*R*)-39** (185 mg, 0.593 mmol, 1 equiv.) was dissolved in 5 mL CH_2Cl_2 and cooled to 0 ºC, then 5 mL TFA was added and the reaction mixture was stirred for 3 h. Concentration by rotary evaporation at

0 ºC gave crude acid **(1*R*,3*R*)-40** (170 mg), which was used directly in the next step without further purification.

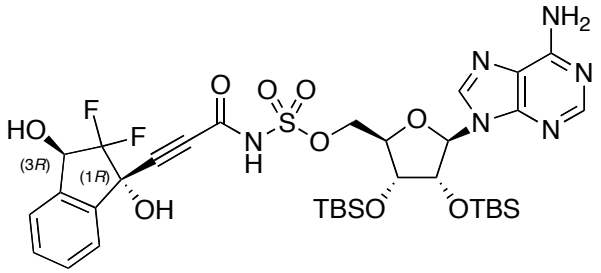

2´,3´-*O*-(*t*-Butyldimethylsilyl)-5´-*O*-(*N*-[3˝-((1*R*,3*R*)-2˝˝,2˝˝-difluoro-1˝˝,3˝˝-dihydroxy-1˝˝-indanyl)propioloyl]sulfamoyl)adenosine ((1*R*,3*R*)-41). Propiolic acid **(1*R*,3*R*)-40** (assumed quantitative yield from previous step: 151 mg, 0.594 mmol, 1 equiv), protected 5´-*O*-sulfamoyladenosine **34** (427 mg, 0.723 mmol, 1.25 equiv) prepared as previously described,[3] and DMAP (73 mg, 0.594 mmol, 1.0 equiv.) was dissolved in CH_2Cl_2:MeCN (5 mL, 2:1) and EDCI (456 mg, 2.376 mmol, 4.0 equiv) was added. The reaction was stirred for 12 h, quenched with 15 mL 1 M $KHSO_4$, and extracted with EtOAc (5 x 15 mL). The combined organic extracts were dried (Na_2SO_4), filtered, and concentrated by rotary evaporation. The reside was reconstituted in CH_2Cl_2, loaded into a pad of silica and washed with 100 mL CH_2Cl_2, then eluted with 15% MeOH/ CH_2Cl_2 (150 mL) to afford the crude propiolyl-sulfamate **(1*R*,3*R*)-40** (294 mg), which was used directly in the next step without further purification.

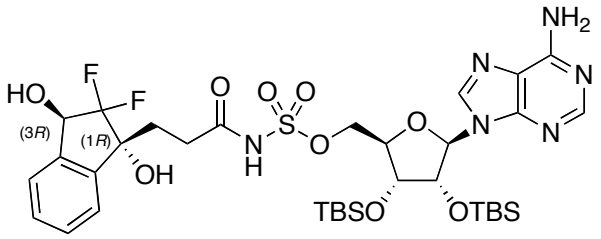

2´,3´-*O*-(*t*-Butyldimethylsilyl)-5´-*O*-(*N*-[3˝-((1*R*,3*R*)-2˝˝,2˝˝-difluoro-1˝˝,3˝˝-dihydroxy-1˝˝-indanyl)propanoyl]sulfamoyl)adenosine ((1*R*,3*R*)-42). Crude propiolyl-sulfamate **(1*R*,3*R*)-41** (294 mg, 0.363 mmol, 1 equiv.) from previous step and 10% Pd/C (386 mg, 0.363 mmol, 1 equiv) were suspended in solution of MeOH/NEt_3 (40 mL, 9:1). The reaction was then stirred vigorously under H_2 balloon for 2 h, then diluted with EtOAc (15 mL), filtered through a celite pad, and concentrated by rotary evaporation to afford the

crude propanoyl-sulfamate **(1*R*,3*R*)-42** (300 mg), which was used directly in the next step without further purification.

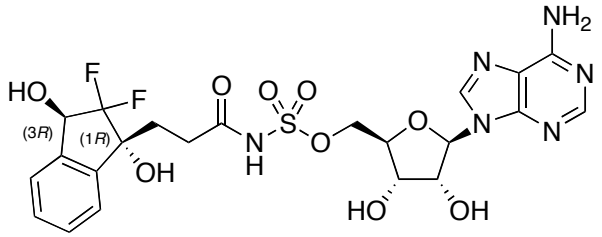

(+)-5´-*O*-(*N*-[3˝-((1*R*,3*R*)-2˝˝,2˝˝-difluoro-1˝˝,3˝˝-dihydroxy-1˝˝-indanyl)propanoyl]sulfamoyl)adenosine ((1*R*,3*R*)-2). Crude propanoyl-sulfamate **(1*R*,3*R*)-42** (300 mg, 0.370 mmol, 1 equiv.) was suspended in DMF (1.5 mL), then TASF (306 mg, 1.109 mmol, 3.0 equiv.) was added and the reaction mixture was stirred for 12 h at 50 ºC. Concentration by rotary evaporation, purification by preparative HPLC (5% → 30% MeCN in H_2O with 0.1% TFA), and lyophilization yielded the *anti*-difluoroindanediol **(1*R*,3*R*)-2** as a fluffy white solid (75 mg, 35% over 4 steps). *N.B.*: HPLC fractions were stored at 0 °C until just prior to pooling and freezing (dry-ice bath) for lyophilization.

$[\alpha]_D^{19}$: +4.0° (*c* 0.5, MeOH). **IR** (ATR): 3343, 2942, 2865, 2509, 2076, 1692, 1473, 1420, 1378, 1198, 1134, 976, 885, 835, 800, 765, 723, 680, 638. **^{1}H-NMR** (500 MHz; CD_3OD): δ 8.47 (s, 1H), 8.34 (s, 1H), 7.45-7.40 (m, 4H), 6.10 (d, *J* = 4.8 Hz, 1H), 5.12 (dd, *J* = 9.7, 5.9 Hz, 1H), 4.64 (t, *J* = 5.0 Hz, 1H), 4.57-4.51 (m, 2H), 4.41 (t, *J* = 4.9 Hz, 1H), 4.31 (q, *J* = 3.9 Hz, 1H), 2.63 (t, *J* = 7.9 Hz, 2H), 2.32-2.13 (m, 2H). **^{13}C-NMR (**126 MHz; CD_3OD): δ 173.4, 150.2, 147.5, 147.3, 143.8, 143.3, 140.0, 130.70, 130.63, 126.4, 124.9, 120.5, 90.3, 83.6, 79.6, 75.8, 74.9, 72.3, 71.6, 49.3, 31.31, 31.13. **^{19}F-NMR** (471 MHz; CD_3OD): δ -120.31 (d, *J* = 230.1 Hz, 1F), -130.90 (d, *J* = 233.2 Hz, 1F). **HRMS** (ESI) *m/z* calcd for $C_{22}H_{25}N_6O_9F_2S$ ($[M+H]^+$) 587.1372; found 587.1370.

F. Synthesis of 1*S*,3*S*-*anti*-Difluoroindanediol (1*R*,3*S*)-2

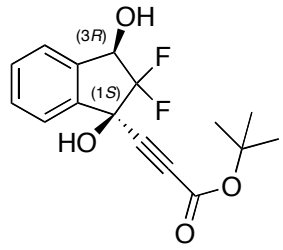

(+)-*t*-Butyl 3-((1*S*,3*R*)-2,2-difluoro-1,3-dihydroxy-1-indanyl)propiolate ((1*S*,3*R*)-37). Silyl ether **(1*S*,3*R*)-32** (681 mg, 1.604 mmol, 1.0 equiv.) was dissolved in 4 mL THF and cooled to 0 ºC, then tetrabutylammonium fluoride (1.764 mL, 1.764 mmol, 1.0 M in THF, 1.1 equiv.) was added and the reaction mixture was stirred for 1 h. Concentration by rotary evaporation and purification by silica flash chromatography (30% → 60% EtOAc in hexanes) yielded the diol **(1*S*,3*R*)-37** as a white solid (405 mg, 81%).

Enantiomeric excess was confirmed by chiral HPLC (Chiralcel: OB-H, 4.6 mm x 150 mm, 5 µm particle size, 5% isopropanol in hexanes, 1 mL/minute), with samples prepared as 1 mg/mL solutions in 10% EtOH/hexanes:

(1*R*,3*S*)-37: t_{ret} = 17 min

(1*S*,3*R*)-37: t_{ret} = 21 min, >98% ee

$[\alpha]_D^{19}$: +5.7° (*c* 1, $CHCl_3$). **IR** (ATR): 3395, 2984, 2936, 2249, 1708, 1459, 1397, 1372, 1281, 1232, 1152, 1110, 1068, 1003, 909, 882, 839, 798, 756, 732, 696, 682, 659, 649. **^{1}H-NMR** (500 MHz; $CDCl_3$): δ 7.64-7.61 (m, 1H), 7.53-7.47 (m, 3H), 5.11 (dd, *J* = 8.7, 4.0 Hz, 1H), 3.05 (s, 2H), 1.48 (s, 9H). **^{13}C-NMR** (126 MHz; $CDCl_3$): δ 151.8, 139.5, 138.7, 131.3, 130.8, 125.8, 124.8, 123.6, 84.6, 80.9, 77.9, 74.8, 74.3, 28.0. **^{19}F-NMR** (471 MHz; $CDCl_3$): δ -114.41 (d, *J* = 228.7 Hz, 1F), -129.08 (d, *J* = 228.8 Hz, 1F). **HRMS** (ESI) *m/z* calcd for $C_{16}H_{16}O_4F_2Na$ ($[M+H]^+$) 374.0914; found 374.1198.

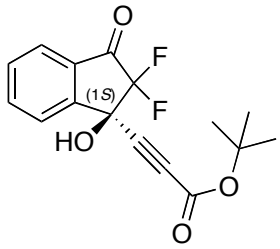

(+)-(*S*)-*t*-Butyl 3-(2,2-difluoro-1-hydroxy-3-oxo-1-indanyl)propiolate ((*S*)-38). DMSO (147 mg, 1.885 mmol, 3.0 equiv.) was dissolved in 2.5 mL CH_2Cl_2, cooled to –78 ºC, and oxalyl chloride (120 mg, 0.943 mmol, 1.5 equiv.) was added and the reaction mixture was stirred for 10 min. Diol **(1*S*,3*R*)-37** (195 mg, 0.628 mmol, 1.0 equiv.) in 1 mL CH_2Cl_2 was added and the reaction mixture was stirred for 40 min. Triethylamine (0.438 mL, 3.142 mmol, 5.0 equiv.) was added and the reaction mixture was stirred for 40 min, then removed from the dry-ice bath and stirred for 10 min. The reaction was then quenched with satd aq NH_4Cl (20 mL), extracted with CH_2Cl_2 (4 x 15 mL), the combined organic extracts were dried (Na_2SO_4), filtered, and concentrated by rotary evaporation. Purification by silica flash chromatography (5% → 25% EtOAc in hexanes) yielded the ketoalcohol **(*S*)-38** as a clear oil (180 mg, 93%).

$[\alpha]_D^{19}$: +25.2° (*c* 1, $CHCl_3$). **IR** (ATR): 3411, 2986, 2939, 2246, 1753, 1713, 1606, 1473, 1398, 1374, 1287, 1223, 1194, 1153, 1103, 1043, 1019, 936, 911, 879, 839, 772, 756, 737, 713, 651. **^{1}H-NMR** (500 MHz; $CDCl_3$): δ 7.94-7.87 (m, 3H), 7.68 (td, *J* = 7.5, 1.1 Hz, 1H), 3.60 (s, 1H), 1.51 (s, 9H). **^{13}C-NMR (**126 MHz; $CDCl_3$): δ 187.6, 151.6, 148.8, 138.1, 132.0, 131.2, 126.3, 125.2, 113.5, 85.0, 82.2, 77.1, 71.1, 28.0. **^{19}F-NMR** (471 MHz; $CDCl_3$): δ -111.50 (d, *J* = 267.2 Hz, 1F), -126.10 (d, *J* = 270.5 Hz, 1F). **HRMS** (ESI) *m/z* calcd for $C_{16}H_{14}O_4F_2Na$ ($[M+H]^+$) 331.0758; found 331.0750.

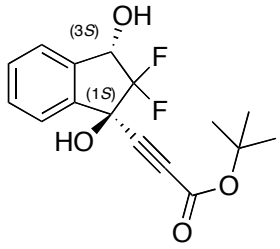

(–)-*t*-Butyl 3-((1*S*,3*S*)-2,2-difluoro-1,3-dihydroxy-1-indanyl)propiolate ((1*S*,3*S*)-39). Ketone **(*S*)-38** (200 mg, 0.649 mmol, 1 equiv.) was dissolved in 3 mL MeOH and cooled to 0 ºC, then $NaBH_4$ (7.4 mg, 0.195 mmol, 0.3 equiv.) was added in 4 portions over 5 min and the reaction mixture was stirred for 30

min. Acetone (0.1 mL) was added and the reaction mixture was stirred for 10 min, then 1 M phosphate buffer (pH 7.0, 15 mL) was added and the reaction mixture was stirred for an additional 10 min. The reaction was then extracted with EtOAc (4 x 10 mL), the combined organic extracts were dried (Na_2SO_4), filtered, and concentrated by rotary evaporation. Purification by silica flash chromatography (0% → 10% EtOAc in CH_2Cl_2) yielded the *anti*-diol **(1*S*,3*S*)-39** as a white solid (170 mg, 84%).

Enantiomeric excess was confirmed by chiral HPLC (Chiralcel: OB-H, 4.6 mm x 150 mm, 5 µm particle size, 5% isopropanol in hexanes, 1 mL/minute), with samples prepared as 1 mg/mL solutions in 10% EtOH/hexanes:

(1*R*,3*R*)-39: t_{ret} = 21 min

(1*S*,3*S*)-39: t_{ret} = 27 min, >98% ee

$[\alpha]_D^{19}$: –9.9° (*c* 1, $CHCl_3$). **IR** (ATR): 3374, 2984, 2938, 2245, 1689, 1466, 1397, 1372, 1305, 1229, 1153, 1110, 1078, 1041, 1008, 911, 893, 837, 795, 756, 732, 696, 648. **^{1}H-NMR** (500 MHz; $CDCl_3$): δ 7.63 (d, *J* = 7.4 Hz, 1H), 7.51-7.45 (m, 3H), 5.40 (td, *J* = 10.4, 6.4 Hz, 1H), 3.18 (s, 1H), 2.42 (dd, *J* = 10.7, 2.5 Hz, 1H), 1.51 (s, 9H). **^{13}C-NMR (**126 MHz; $CDCl_3$): δ 151.8, 139.0, 137.6, 131.4, 130.2, 124.93, 124.73, 123.7, 84.6, 80.8, 77.9, 74.17, 74.05, 28.0. **^{19}F-NMR** (471 MHz; $CDCl_3$): δ -123.25 (d, *J* = 228.4 Hz, 1F), -125.63 (d, *J* = 229.1 Hz, 1F). **HRMS** (ESI) *m/z* calcd for $C_{16}H_{16}O_4F_2Na$ ($[M+H]^+$) 333.0914; found 333.0905.

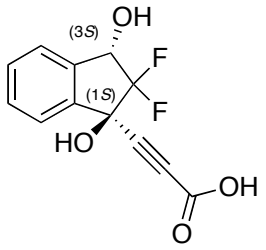

3-((1*S*,3*S*)-2,2-difluoro-1,3-dihydroxy-1-indanyl)propiolic acid ((1*S*,3*S*)-40). Ester **(1*S*,3*S*)-39** (135 mg, 0.435 mmol, 1 equiv.) was dissolved in 5 mL CH_2Cl_2 and cooled to 0 ºC, then 5 mL TFA was added and the reaction mixture was stirred for 3 h. Concentration by rotary evaporation at 0 ºC gave

crude acid **(1*S*,3*S*)-40** (110 mg), which was used directly in the next step without further purification.

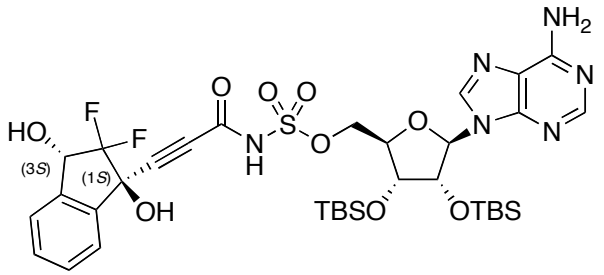

2´,3´-*O*-(*t*-Butyldimethylsilyl)-5´-*O*-(*N*-[3´´-((1*S*,3*S*)-2´´´,2´´´-difluoro-1´´´,3´´´-dihydroxy-1´´´-indanyl)propioloyl]sulfamoyl)adenosine ((1*S*,3*S*)-41). Propiolic acid **(1*S*,3*S*)-40** (assumed quantitative yield from previous step: 110 mg, 0.433 mmol, 1 equiv), protected 5´-*O*-sulfamoyladenosine **34** (373 mg, 0.541 mmol, 1.25 equiv) prepared as previously described,[3] and DMAP (53 mg, 0.433 mmol, 1.0 equiv.) was dissolved in CH_2Cl_2:MeCN (5 mL, 2:1) and EDCI (332 mg, 1.730 mmol, 4.0 equiv) was added. The reaction was stirred for 12 h, then quenched with 15 mL 1 M $KHSO_4$, and extracted with EtOAc (5 x 15 mL). The combined organic extracts were dried (Na_2SO_4), filtered, and concentrated by rotary evaporation. The reside was reconstituted in CH_2Cl_2, loaded into a pad of silica and washed with 100 mL CH_2Cl_2, then eluted with 15% MeOH/ CH_2Cl_2 (150 mL) to afford the crude propiolyl-sulfamate **(1*S*,3*S*)-41** (128 mg), which was used directly in the next step without further purification.

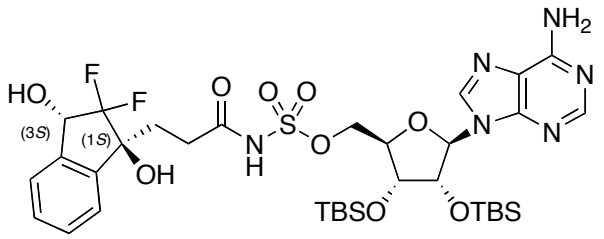

2´,3´-*O*-(*t*-Butyldimethylsilyl)-5´-*O*-(*N*-[3´´-((1*S*,3*S*)-2´´´,2´´´-difluoro-1´´´,3´´´-dihydroxy-1´´´-indanyl)propanoyl]sulfamoyl)adenosine ((1*S*,3*S*)-42). Crude propiolyl-sulfamate **(1*S*,3*S*)-41** (128 mg, 0.158 mmol, 1 equiv.) from previous step and 10% Pd/C (168 mg, 0.158 mmol, 1 equiv) were suspended in solution of MeOH/NEt_3 (15 mL, 9:1). The reaction was then stirred vigorously under H_2 balloon for 2 h, then diluted with EtOAc (15 mL), filtered through a celite pad, and concentrated by rotary evaporation to afford the

crude propanoyl-sulfamate **(1*S*,3*S*)-42** (118 mg), which was used directly in the next step without further purification.

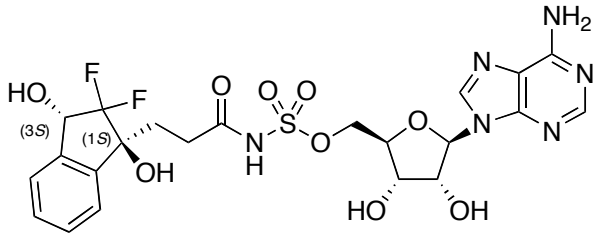

(–)-5´-*O*-(*N*-[3˝-((1S,3S)-2˝˝,2˝˝-difluoro-1˝˝,3˝˝-dihydroxy-1˝˝-indanyl)propanoyl]sulfamoyl)adenosine ((1*S*,3*S*)-2). Crude propanoyl-sulfamate **(1*S*,3*S*)-42** (118 mg, 0.145 mmol, 1 equiv.) was suspended in DMF (1.5 mL), then TASF (120 mg, 0.434 mmol, 3.0 equiv.) was added and the reaction mixture was stirred for 12 h at 50 ºC. Concentration by rotary evaporation, purification by preparative HPLC (5% → 30% MeCN in H_2O with 0.1% TFA), and lyophilization yielded the *anti*-difluoroindanediol **(1*S*,3*S*)-2** as a fluffy white solid (53 mg, 21% over 4 steps). *N.B.*: HPLC fractions were stored at 0 °C until just prior to pooling and freezing (dry-ice bath) for lyophilization.

$[\alpha]_D^{19}$: –6.5° (*c* 0.5, MeOH). **IR** (ATR): 3367, 2502, 2239, 2072, 1693, 1471, 1429, 1380, 1202, 1139, 980, 787, 801, 769, 724, 642. **^{1}H-NMR** (500 MHz; CD_3OD): δ 8.46 (s, 1H), 8.32 (s, 1H), 7.45-7.39 (m, 4H), 6.08 (d, *J* = 4.8 Hz, 1H), 5.11 (dd, *J* = 9.7, 5.8 Hz, 1H), 4.63 (t, *J* = 5.0 Hz, 1H), 4.57-4.50 (m, 2H), 4.40 (t, *J* = 4.9 Hz, 1H), 4.30 (q, *J* = 3.9 Hz, 1H), 2.84 (d, *J* = 8.7 Hz, 1H), 2.63 (ddd, *J* = 9.3, 6.4, 4.7 Hz, 2H), 2.28-2.23 (m, 1H), 2.21-2.15 (m, 1H). **^{13}C-NMR (**126 MHz; CD_3OD): δ 173.5, 150.2, 147.43, 147.40, 143.8, 143.3, 140.0, 130.69, 130.63, 126.5, 125.0, 120.5, 90.3, 83.6, 79.6, 75.8, 74.9, 72.3, 71.6, 49.3, 31.3, 31.1. **^{19}F-NMR** (471 MHz; CD_3OD): δ -120.33 (d, *J* = 233.1 Hz, 1F), -130.94 (d, *J* = 232.3 Hz, 1F). **HRMS** (ESI) *m/z* calcd for $C_{22}H_{25}N_6O_9F_2S$ ($[M+H]^+$) 587.1372; found 587.1366.

G. X-Ray Crystallographic Analysis of *syn*-Diol (1*S*,3*R*)-40

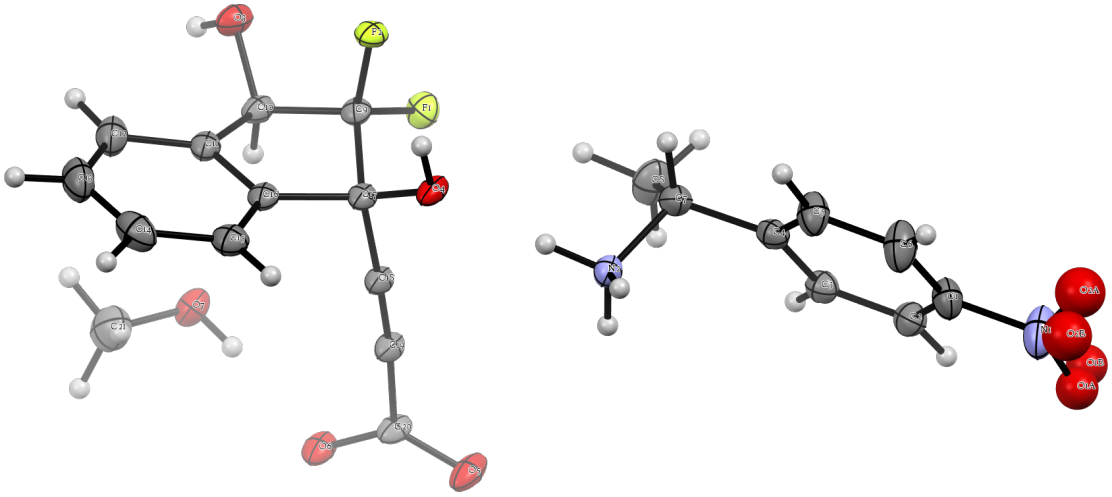

Figure 3.14. X-ray crystal structure of *syn*-diol (1*S*,3*R*)-15 (left) with (*R*)-a-methyl-4-nitrobenzylamine (right, two NO_2 rotamers) and MeOH (lower left).

syn-Diol acid **(1*S*,3*R*)-40** (10 mg, 0.0393 mmol, 1 equiv.) and (*R*)-α-methyl-4-nitrobenzylamine (6.9 mg, 0.0413 mmol, 1.05 equiv., Sigma Aldrich) were placed in a 4 mL glass sample vial and dissolved in 400 µL MeOH. The vial was placed in a 20 mL glass sample vial containing diethyl ether and the 20 mL vial sealed tightly. After 3 days at rt, clear needle shaped crystals were obtained.

A specimen of $[C_8H_{11}N_2O_2][C_{12}H_7F_2O_4]^*CH_3OH$ was used for X-ray crystallographic analysis at the University of Toledo Instrumentation Center at 120 K on a Bruker APEX Duo diffractometer using CuKa radiation (1.54178 Å) for absolute stereochemistry determination. The X-ray intensity data were measured. The integration of the data using a monoclinic unit cell yielded a total of 14285 reflections to a maximum θ angle of 70.88° (0.82 Å resolution), of which 3562 were independent (average redundancy 4.010, completeness = 95.5%, R_{int} = 2.21%, R_{sig} = 2.00%) and 3536 (99.27%) were greater than $2\sigma(F^2)$. The final cell constants of a = 13.014(4) Å, b = 9.450(3) Å, c = 18.211(5) Å, β = 98.828(8)°, volume = 2213.1(11) $Å^3$, are based upon the refinement of the XYZ-centroids of reflections above 20 σ(I).

The structure was solved and refined using the Bruker SHELXTL Software Package, using the space group C 1 2 1, with Z = 4 for the formula unit, $C_{21}H_{22}F_2N_2O_7$. The final anisotropic full-matrix least-squares refinement on F^2 with 377 variables converged at R1 = 3.05%, for the observed data and wR2 = 8.16% for all data. The goodness-of-fit was 1.338. The NO_2 group is disordered over two equally occupied positions (both shown in Figure S8). The largest peak in the final difference electron density synthesis was 0.309 $e^-/Å^3$ and the largest hole was -0.335 $e^-/Å^3$ with an RMS deviation of 0.040 $e^-/Å^3$. On the basis of the final model, the calculated density was 1.358 g/cm^3 and F(000), 944 e^-.

The Flack parameter was determined from Parsons' quotients to be –0.03(5), indicating the correct absolute configuration. This parameter was determined based on 1377 Parsons' quotients, [(I+)-(I-)]/[(I+)+(I-)].[29] Further analysis based on Bayesian Statistics reveal a probability of 1 that the proposed structure is the correct one (P2 and P3 determined by PLATON).[30]

CCDC 1512976 contains the supplementary crystallographic data for this paper. These data can be obtained free of charge from The Cambridge Crystallographic Data Centre via www.ccdc.cam.ac.uk/data_request/cif

H. Docking of Inhibitors to MenE

Protein Preparation. The OSB-AMS•MenE co-crystal structure (PDB: 5C5H) was processed using the Protein Preparation Wizard in the Schrödinger suite (v2015.3). Bond orders were assigned, hydrogen's added, and waters beyond 5 Å were deleted. The protonation and tautomeric states of the protein-ligand complex were generated using EPIK at pH 7.4. Hydrogen bond assignment and optimization was performed with PROPKA to sample hydrogen bonding and orientation of water molecules. Non-bridging waters (< 2 hydrogen bonds) were removed. Geometric refinement was performed using OPLS_2005 force field restrained minimization to a heavy atom convergence of 0.3 Å

Ligand Preparation. Ligand preparation was performed using Ligprep in the Schrödinger suite (v2015.3). Lowest energy conformers were obtained using OPLS_2005 force field optimization. Ionization and tautomeric states were generated using EPIK at pH 7.4.

Grid Generation. Using the Schrödinger suite (v2015.3) receptor grid generator, the receptor-binding site was defined as the area around the co-crystalized ligand with a cube grid of 10 Å side length. Nonpolar parts of the receptor were softened using Van der Waals radius scaling (factor 1.0 with partial cutoff of 0.25). No constraints were defined and rotations allowed for all hydroxyl groups in the defined binding pocket.

Docking Using Soft Receptor. Using Glide (v5.3), ligands were docked to MenE using Glide XP docking precision. Flexible ligand sampling was used and EPIK state penalties applied to docking scores. Post-docking minimization was performed for all poses. See also Figure S1.

I. MenE Biochemical Assay

Enzyme inhibition studies were performed in 20 mM $NaHPO_4$ buffer (pH 7.4) containing 150 mM NaCl and 1 mM $MgCl_2$ using a MenE-MenB coupled assay in which MenE is rate-limiting. IC_{50} values were determined in reaction mixtures containing OSB (60 μM), ATP (240 μM), CoA (240 μM), *mt*MenB (2.5 μM), and varying inhibitor concentrations (5 – 250 μM). Reactions were initiated by addition of ecMenE (50 nM), and the production of DHNA-CoA was monitored at 392 nm ($\boldsymbol{\varepsilon}^{392}$ = 4000 M^{-1} cm^{-1}).

J. Antimicrobial Assays

Minimum inhibitory concentrations (MICs) were determined using visual growth inspection of cells grown in transparent 96-well plates. *E. coli* , *B. subtilis* (ATCC 6051), MRSA (ATCC BAA-1762), and *M. tuberculosis* (H37Rv) were grown to mid-log phase (OD_{600} of 0.6 – 0.8) in synthetic broth, or 7H9 with 0.5% glycerol, 0.05% Tween, and 10% OADC medium at 37 ° C in an orbital shaker. A final inoculum concentration of 1– 2 x 10^6 cells per well was treated with inhibitor at final concentrations ranging from 0.5 to 500 μg/mL. The MIC was defined as the minimum concentration at which a well showed no obvious growth by visual inspection (MIC-99). Growth rescue studies were performed by supplementing minimal medium (synthetic broth) with 10 μM menaquinone-4 (MK4) and following the same procedure in a 96-well plates. To determine the MK4-rescue MIC, 10% of the solution in each well was plated on synthetic agar plate and allowed to grow for 48 hours in 37 ^oC. Colony forming units (CFUs) were counted and compared to plates with untreated wells. Rescue MICs were defined as the minimum inhibitor concentration at which a plate showed ~90% growth after supplementation with MK4.

K. Menaquinone Biosynthesis Assay

The effect of MenE inhibitors on menaquinone levels in *S. aureus* was determined as follows. Cultures of *S. aureus* ATCC BAA-1762 (5 mL of synthetic broth medium with 10% glucose) were incubated overnight in a 37

°C shaker in the presence or absence of OSB-AMS (**1**) or Difluoroindanediol (**2**) below their MICs. The Blight and Dyer (1959) lipid extraction protocol was used to isolate the menaquinone-containing fraction from the cells. Briefly, 0.75 mL of a 1:2 (v/v) $CHCl_3$ /MeOH solvent was added to 0.2 mL of culture. The mixture was vortexed thoroughly, and 0.25 mL of $CHCl_3$ was added followed by further vortexing, after which 0.25 mL of H_2O was added. The mixture was then vortexed and centrifuged at 500g for 5 min at room temperature. The bottom phase was recovered and transferred to a glass vial, and 200 μL was analyzed by APCI LC-MS/MS in positive ion mode using a Thermo TSQ Quantum Access (Thermo-Fisher) triple-quadrupole mass spectrometer. Samples were introduced into the mass spectrometer by flow injection at a rate of 100 μL/min with 2:1 MeOH/$CHCl_3$ solvent. Multiplereaction monitoring (MRM) was performed at 30 eV; and MK8 levels were quantified using a MK9 standard curve (Sigma). Ubiquinone-4 (CoQ4) was used as an internal standard, and experiments were performed in duplicate.

3.7. References

1. Lu, X.; Zhou, R.; Sharma, I.; Li, X.; Kumar, G.; Swaminathan, S.; Tonge, P. J.; Tan, D. S., "Stable analogues of OSB-AMP: potent inhibitors of MenE, the o-succinylbenzoate-CoA synthetase from bacterial menaquinone biosynthesis." *ChemBioChem* **2012,** *13*, 129–136.

2. Matarlo, J. S.; Evans, C. E.; Sharma, I.; Lavaud, L. J.; Ngo, S. C.; Shek, R.; Rajashankar, K. R.; French, J. B.; Tan, D. S.; Tonge, P. J., "Mechanism of MenE inhibition by acyl-adenylate analogues and discovery of novel antibacterial agents." *Biochemistry* **2015,** *54*, 6514–6524.

3. González-López, S.; Yus, M.; Ramón, D. J., "Enantioselective synthesis of (+)-gossonorol and related systems using organozinc reagents." *Tetrahedron: Asymmetry* **2012,** *23*, 611–615.

4. Lu, G.; Li, X.; Jia, X.; Chan, W. L.; Chan, A. S. C., "Enantioselective Alkynylation of Aromatic Ketones Catalyzed by Chiral Camphorsulfonamide Ligands." *Angew. Chem. Int. Ed.* **2003,** *42*, 5057–5058.

5. Jiang, B.; Feng, Y., "Enantioselective alkynylation of a prochiral ketone catalyzed by C2-symmetric diamino diols." *Tetrahedron Lett.* **2002,** *43*, 2975–2977.

6. Tan, L.; Chen, C.-y.; Tillyer, R. D.; Grabowski, E. J. J.; Reider, P. J., "A Novel, Highly Enantioselective Ketone Alkynylation Reaction Mediated by Chiral Zinc Aminoalkoxides." *Angew. Chem. Int. Ed.* **1999,** *38*, 711–713.

7. Tanaka, K.; Ueda, T.; Ichibakase, T.; Nakajima, M., "Enantioselective alkynylation of ketones with trimethoxysilylalkynes using lithium binaphtholate as a catalyst." *Tetrahedron Lett.* **2010,** *51*, 2168–2169.

8. Ueda, T.; Tanaka, K.; Ichibakase, T.; Orito, Y.; Nakajima, M., "Enantioselective alkynylation of carbonyl compounds with trimethoxysilylalkynes catalyzed by lithium binaphtholate." *Tetrahedron* **2010,** *66*, 7726–7731.

9. Cai, H.; Nie, J.; Zheng, Y.; Ma, J.-A., "Lithium Binaphtholate-Catalyzed Enantioselective Enyne Addition to Ketones: Access to Enynylated Tertiary Alcohols." *J. Org. Chem.* **2014,** *79*, 5484–5493.

10. Wang, Q.; Zhang, B.; Hu, G.; Chen, C.; Zhao, Q.; Wang, R., "Asymmetric addition of 1-ethynylcyclohexene to both aromatic and heteroaromatic ketones catalyzed by a chiral Schiff base-zinc complex." *Org. Biomol. Chem.* **2007,** *5*, 1161–1163.

11. Chen, C.; Hong, L.; Xu, Z.-Q.; Liu, L.; Wang, R., "Low Ligand Loading, Highly Enantioselective Addition of Phenylacetylene to Aromatic Ketones Catalyzed by Schiff-Base Amino Alcohols." *Org. Lett.* **2006,** *8*, 2277–2280.

12. Itsuno, S., "Enantioselective Reduction of Ketones." In *Organic Reactions*, John Wiley & Sons, Inc.: 2004.

13. Veeraraghavan Ramachandran, P.; Teodorovic, A. V.; Brown, H. C., "Chiral synthesis via organoboranes. 38. Selective reductions. 48. Asymmetric reduction of trifluoromethyl ketones by B-chlorodiisopinocampheylborane in high enantiomeric purity." *Tetrahedron* **1993,** *49*, 1725–1738.

14. Korenaga, T.; Nomura, K.; Onoue, K.; Sakai, T., "Rational electronic tuning of CBS catalyst for highly enantioselective borane reduction of trifluoroacetophenone." *Chem. Commun.* **2010,** *46*, 8624–8626.

15. Sokeirik, Y. S.; Omote, M.; Sato, K.; Kumadaki, I.; Ando, A., "Synthesis of a Schiff's base chiral ligand with a trifluoromethyl carbinol moiety." *Tetrahedron: Asymmetry* **2006,** *17*, 2654–2658.

16. Corey, E. J.; Cheng, X.-M.; Cimprich, K. A.; Sarshar, S., "Remarkably effective and simple syntheses of enantiomerically pure secondary carbinols from achiral ketones." *Tetrahedron Lett.* **1991,** *32*, 6835–6838.

17. Isabel, E.; Bateman, K. P.; Chauret, N.; Cromlish, W.; Desmarais, S.; Duong, L. T.; Falgueyret, J.-P.; Gauthier, J. Y.; Lamontagne, S.; Lau, C. K.; Léger, S.; LeRiche, T.; Lévesque, J.-F.; Li, C. S.; Massé, F.; McKay, D. J.; Mellon, C.; Nicoll-Griffith, D. A.; Oballa, R. M.; Percival, M. D.; Riendeau, D.; Robichaud, J.; Rodan, G. A.; Rodan, S. B.; Seto, C.; Thérien, M.; Truong, V. L.; Wesolowski, G.; Young, R. N.; Zamboni, R.; Black, W. C., "The discovery of MK-0674, an orally bioavailable cathepsin K inhibitor." *Bioorg. Med. Chem. Lett.* **2010,** *20*, 887–892.

18. Málek, J., "Reductions by Metal Alkoxyaluminum Hydrides." In *Organic Reactions*, John Wiley & Sons, Inc.: 2004.

19. Yu, J.; Duan, M.; Wu, W.; Qi, X.; Xue, P.; Lan, Y.; Dong, X.-Q.; Zhang, X., "Readily Accessible and Highly Efficient Ferrocene-Based Amino-Phosphine-Alcohol (f-Amphol) Ligands for Iridium-Catalyzed Asymmetric Hydrogenation of Simple Ketones." *Chem. Eur. J.* **2017,** *23*, 970–975.

20. Margalef, J.; Slagbrand, T.; Tinnis, F.; Adolfsson, H.; Diéguez, M.; Pàmies, O., "Third-Generation Amino Acid Furanoside-Based Ligands from d-Mannose for the Asymmetric Transfer Hydrogenation of Ketones: Catalysts with an Exceptionally Wide Substrate Scope." *Adv. Synth. Catal.* **2016,** *358*, 4006–4018.

21. Kuroki, Y.; Asada, D.; Iseki, K., "Enantioselective synthesis of 2,2-difluoro-3-hydroxycarboxylates by rhodium-catalyzed hydrogenation." *Tetrahedron Lett.* **2000,** *41*, 9853–9858.

22. Huang, H.; Zong, H.; Bian, G.; Song, L., "Chemo- and Enantioselective Addition and β-Hydrogen Transfer Reduction of Carbonyl Compounds with Diethylzinc Reagent in One Pot Catalyzed by a Single Chiral Organometallic Catalyst." *J. Org. Chem.* **2015,** *80*, 12614–12619.

23. Joly, S.; Nair, M. S., "Efficient enzymatic kinetic resolution of 4-hydroxytetralone and 3-hydroxyindanone." *Tetrahedron: Asymmetry* **2001,** *12*, 2283–2287.

24. Sletten, E. M.; Nakamura, H.; Jewett, J. C.; Bertozzi, C. R., "Difluorobenzocyclooctyne: Synthesis, Reactivity, and Stabilization by β-Cyclodextrin." *J. Am. Chem. Soc.* **2010,** *132*, 11799–11805.

25. Evans, D. A.; Chapman, K. T.; Carreira, E. M., "Directed reduction of .beta.-hydroxy ketones employing tetramethylammonium triacetoxyborohydride." *J. Am. Chem. Soc.* **1988,** *110*, 3560–3578.

26. Ruan, J.; Iggo, J. A.; Xiao, J., "Direct Synthesis of 1-Indanones via Pd-Catalyzed Olefination and Ethylene Glycol-Promoted Aldol-Type Annulation Cascade." *Org. Lett.* **2011,** *13*, 268–271.

27. Chen, C. S.; Fujimoto, Y.; Girdaukas, G.; Sih, C. J., "Quantitative analyses of biochemical kinetic resolutions of enantiomers." *J. Am. Chem. Soc.* **1982,** *104*, 7294–7299.

28. Ferreras, J. A.; Ryu, J.-S.; Di Lello, F.; Tan, D. S.; Quadri, L. E. N., "Small-molecule inhibition of siderophore biosynthesis in Mycobacterium tuberculosis and Yersinia pestis." *Nat. Chem. Biol.* **2005,** *1*, 29–32.

29. Parsons, S.; Flack, H. D.; Wagner, T., "Use of intensity quotients and differences in absolute structure refinement." *Acta Crystallogr. Sect. B* **2013,** *69*, 249-259.

30. Spek, A., "Structure validation in chemical crystallography." *Acta Crystallogr. Sect. D* **2009,** *65*, 148-155.

CHAPTER 4

DOCKING GUIDED DESIGN OF OSB-AMS LINKER ANALOGUES

4.1. Introduction

The use of an acyl-5´-*O*-sulfamoyladenosine (acyl-AMS) motif to mimic the cognate acyl-adenosine monophosphate (acyl-AMP) of adenylate-forming enzymes (Figure 4.1A) has been the primary means by which researchers[1-11] and nature[12-16] have successfully inhibited a variety of targets in the adenylate-forming enzyme superfamily.[17] As was discussed in Chapter 1, although this approach provides excellent biochemical inhibitors of the cognate enzyme, acyl-AMS based inhibitors have several issues associated with the acyl-sulfamate motif that can impede their usefulness as therapeutic lead compounds. The primary problems associated with the acyl-sulfamate are unfavorable physicochemical and pharmacological properties, as well as instability of the acyl-sulfamate itself, which can undergo hydrolysis to release the highly cytotoxic compound, adenosine monosulfamate (AMS).

The acyl-sulfamate of the acyl-AMS scaffold has a pK_a ~1-2, and is therefore in a deprotonated anionic state at physiological pH. This deprotonation confers increased polarity onto what is already a relatively polar and heteroatom rich area of the scaffold. This significant increase in polarity has serious implications for the ADME (absorption, distribution, metabolism, and excretion) of acyl-AMS type inhibitors. High polarity and negative charges have been implicated in poor compound accumulation in bacteria, high levels of non-specific protein binding, and high rates of *in vivo* clearance. [18-22]

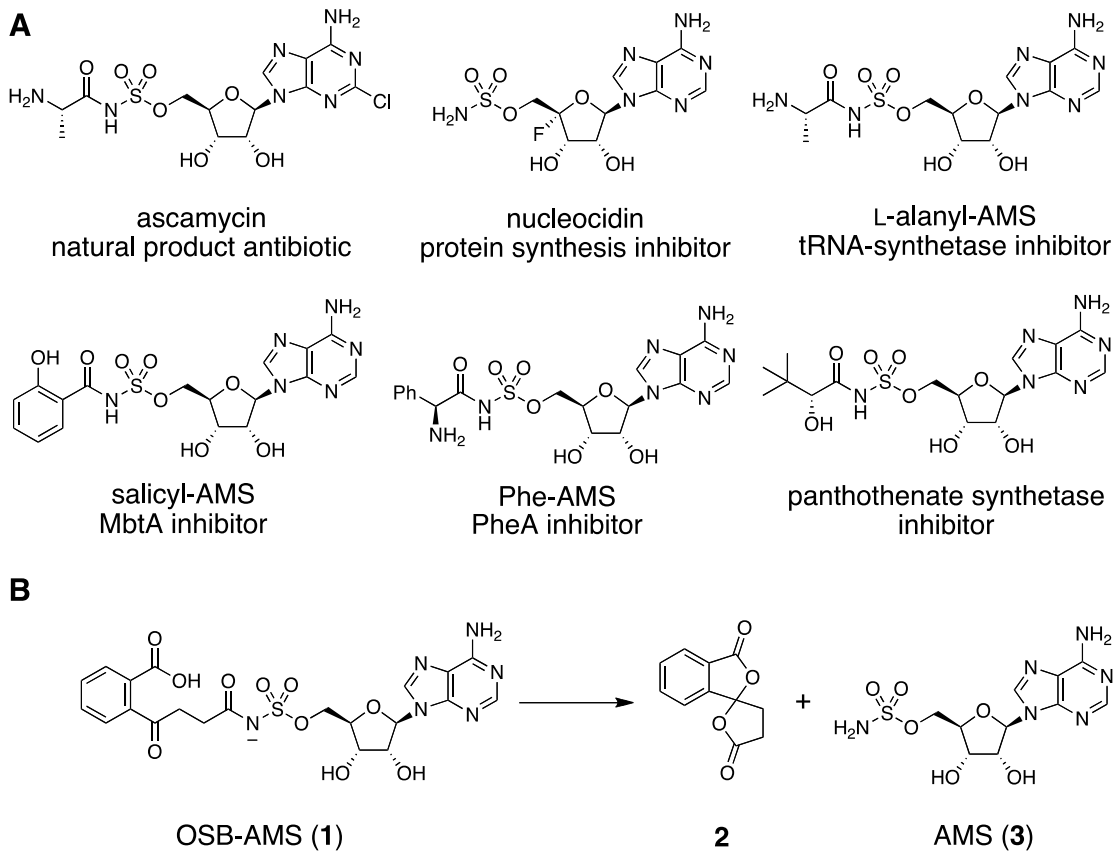

Figure 4.1. Acyl-AMS inhibitors of adenylate-forming enzymes. A) Examples of reported acyl-AMS inhibitors for adenylate-forming enzmes B) Common decomposition pathway of OSB-AMS.

A potentially far more problematic issue with the acyl-sulfamate is overall stability. In some scaffolds the acyl-sulfamate group is relatively stable, but in other derivatives, particularly in the OSB-AMS series of acyl-sulfamate based inhibitors, this group is highly prone to hydrolysis. This lability is largely due to highly favorable cyclization and spirocyclization events that OSB type scaffolds can undergo (Figure 4.1B), cleaving the acyl-sulfamate and releasing free AMS. AMS is a highly cytotoxic compound, typically inducing mammalian cell death in low to sub-nM concentrations.[23] Thus, to move our current line of MenE inhibitors into more favorable drug-like space and decrease the chemical and toxicological liability inherent in the

acyl-AMS motif, an acyl-phosphate bioisostere other than the traditional acyl-sulfamate is needed. However, finding a suitable bioisostere of the OSB-AMP acyl-phosphate is non-trivial. Since the acyl-phosphate is the location at which MenE performs its catalytic activity on the native OSB-AMP scaffold, there are many key interactions in the biding pocket between the scaffold and the enzyme, making this area of the scaffold canonically intolerant to modifications. Aldrich and coworkers describe the most relevant targeted studies to modify the acyl-sulfamate region of an acyl-AMS inhibitor in an attempt to inhibit MbtA, an adenylate-forming enzyme that belongs to the ANL family (Figure 4.2). [2,7,24-30]

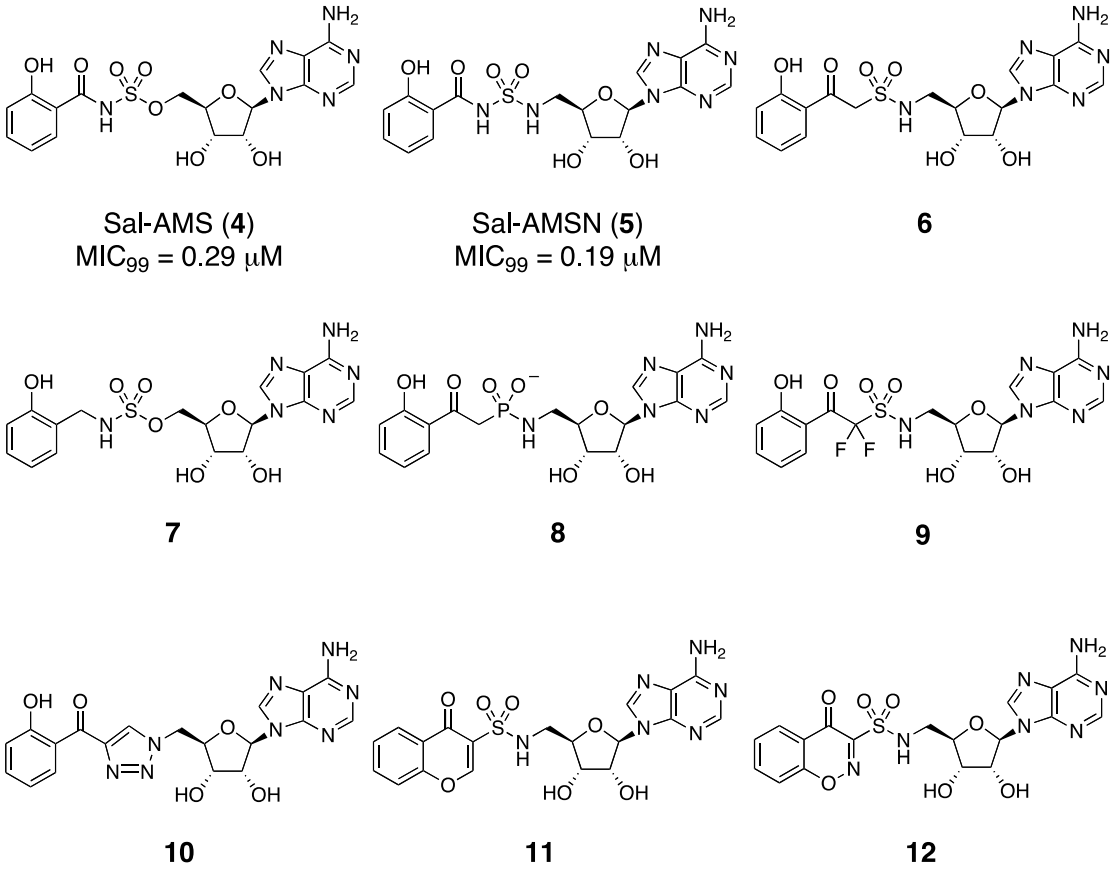

Figure 4.2. Reported linker analogues of salicyl-AMS and corresponding activity in antimicrobial assays. [2,7,24-30]

Their efforts in this area focused on the rational design and synthesis of linker analogues of salicyl-AMS, a compound originally reported by our lab that has potent antimicrobial activity.[2,7,24-30] The Aldrich group reported a number of salicyl-AMS linker analogues, some of which used relatively minor modifications to the acyl-sulfamate group. However, they only report one analogue that retained activity (**6**), albeit at a ~2-log loss in potency verses that of the parent salicyl-AMS compound.

It was clear that an alternative bioisostere of the acyl-phosphate was needed to advance the MenE inhibitor series. However, previously reported efforts in this area suggested that the traditional rational design approach was not an effective strategy to probe the structure–activity relationships (SAR) around this area of the scaffold.

4.2. Docking Guided Design of OSB-AMS Linker Analogues

To find a more effective approach to probing the SAR in the linker region of the MenE binding pocket, we proposed to create a virtual library of rationally designed OSB-AMS linker analogues. We would then dock the analogues into our previously reported OSB-AMS liganded MenE crystal structure,[31] and use the results from the docking study to help prioritize the synthetic targets. This approach would allow us to probe a larger area of chemical space around that region than could quickly be performed by traditional rational design, and if properly executed should increase the relative rate at which we discover active inhibitors of MenE.

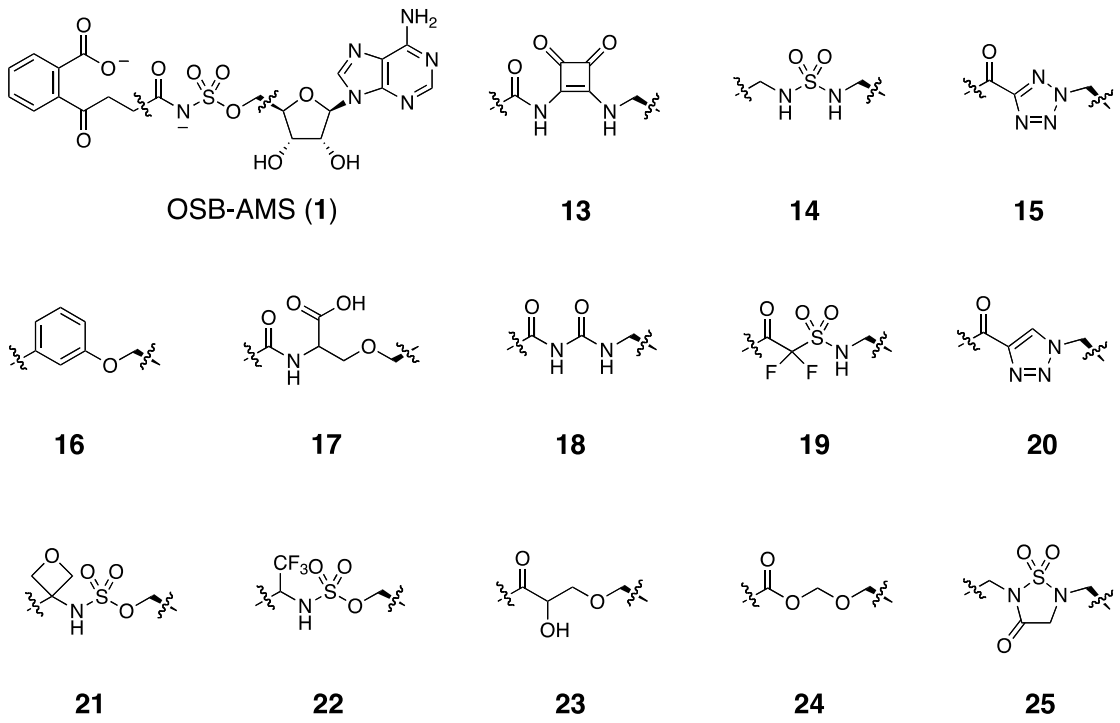

Figure 4.3. Examples of OSB-AMS linker analogues in first-generation virtual library.

We began by first creating a ~70-membered first-generation virtual library of OSB-AMS linker analogues (Figure 4.3). The library was composed of different bioisosteres that ranged greatly in fidelity to the native acyl-phosphate scaffold. While some analogues attempted to retain as many key interactions in the binding pocket as possible (squaramide **13**, sulfamide **14,** acyl-tetrazole **15**), others were envisioned to keep only one or two interactions with MenE but significantly decrease the desolvation-penalty relative to the acyl-sulfamate motif (m-phenol **16**, hydroxy-serine **23**, keto-oxymethyl **24**). Critically, Mescar and coworkers had shown through kinetic studies that extension or shortening of the OSB succinyl chain was not well tolerated,[32] so these analogues aimed to keep a nearly identical distance from the 5'-ribose heteroatom of adenosine (oxygen or nitrogen depending on analogue) to the ketone of OSB.

The analogues were docked to the MenE crystal structure (PDB: 5C5H) using Glide (Schrodinger Software Suite, Table 4.1, see experimental section 4.4 for details), ranked by their Glide docking score, and analogues with a docking score of > –10 kcal/mol removed.

Table 4.1. Docking scores of example OSB-AMS linker analogues.

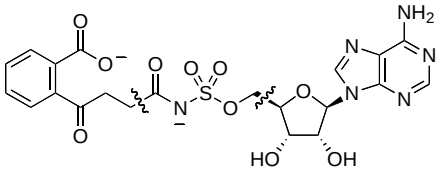

OSB-AMS (**1**)

Entry	Analogue	Docking Score (kcal/mol)	Entry	Analogue	Docking Score (kcal/mol)
13	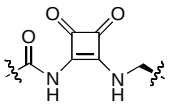	–13.76	19	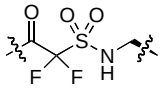	–13.69
14	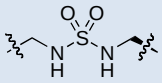	–14.2	20	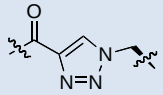	–13.32
15	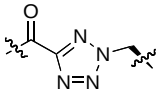	–13.98	21	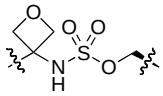	–13.69
16	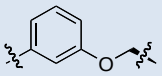	–14.03	22	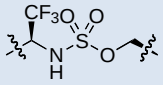	–13.27
17	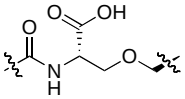	–14.63	23	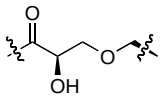	–14.70
18	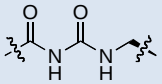	–13.61	24	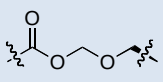	–13.62

OSB-AMS (**1**) docking score = –13.78 kcal/mol.

The list was then inspected to insure that analogues were docking in

reasonable poses with retention of key interactions in the OSB and adenosine binding pockets, and importantly interaction with two key residues (Lys-347, Thr-272) in the linker region of the MenE binding pocket (Figure 4.4).

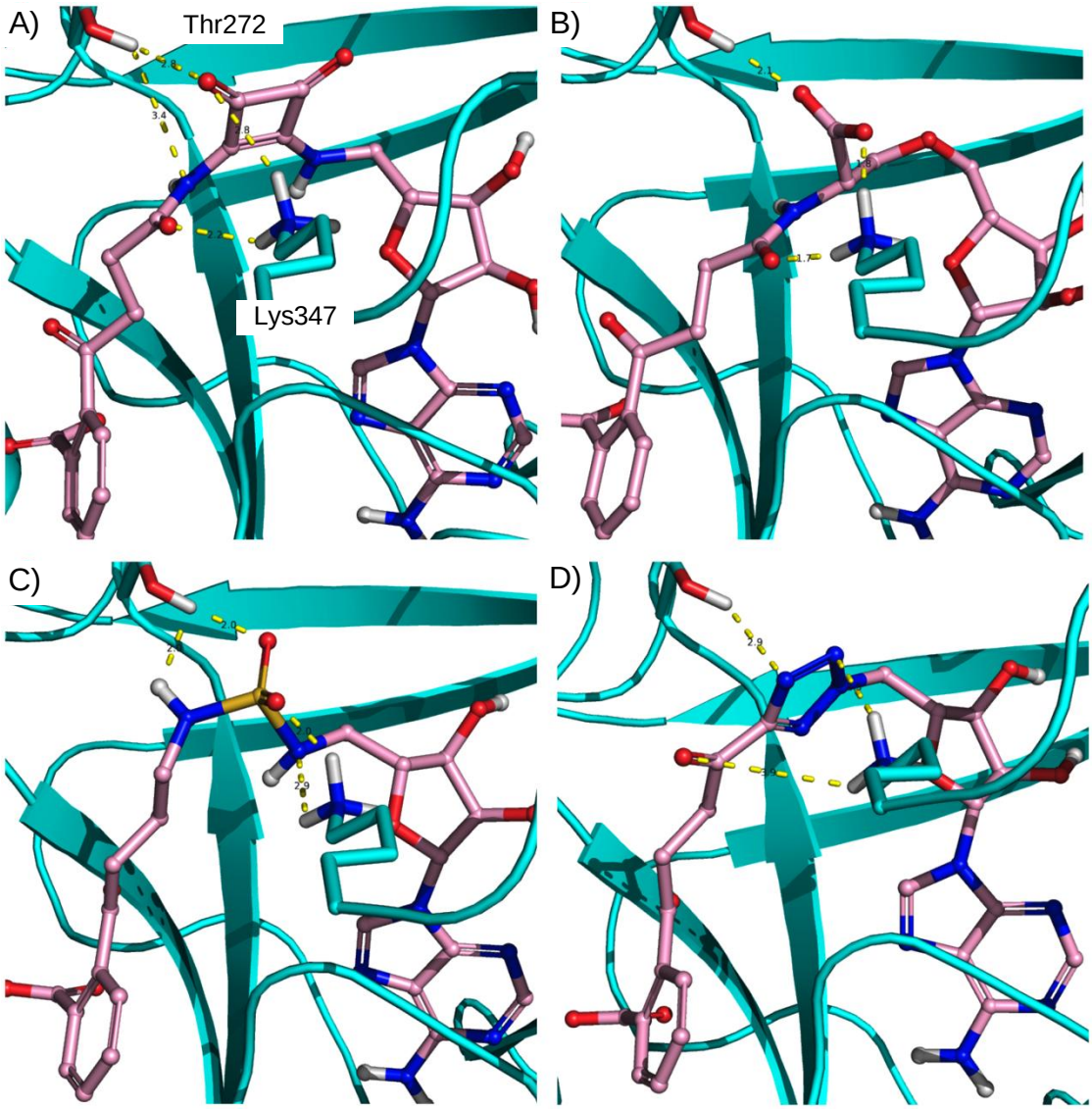

Figure 4.4. Sample of poses from docking study. A) Docking pose of squaramide linker analogue **13**. B) Docking pose of flip-Serine linker analogue **17**. C) Docking pose of alkyl-sulfamide linker analogue **14**. D) Docking pose of acyl-tetrazole linker analogue **15**.

The list was then prioritized based on a combination of docking score, docking pose, ease of functionalization and diversification, likelihood of

increasing favorable physicochemical and pharmacological properties of the platform, and synthetic accessibility. This curated list was used as the starting point for synthesis of linker analogues of OSB-AMS and investigating the linker region of the MenE binding pocket.

4.3. Synthesis of OSB-AMS Linker Analogues

The first analogue to be made was the acyl-squaramide linker analogue. Synthesis of this analogue proceeded by first obtaining the necessary OSB scaffold **28** with an alternate protecting group strategy to that we have reported previosly (Figure 4.5A).[33-34] In parallel, condensation of dimethyl squarate with the protected AMSN scaffold **29**, followed by treatment

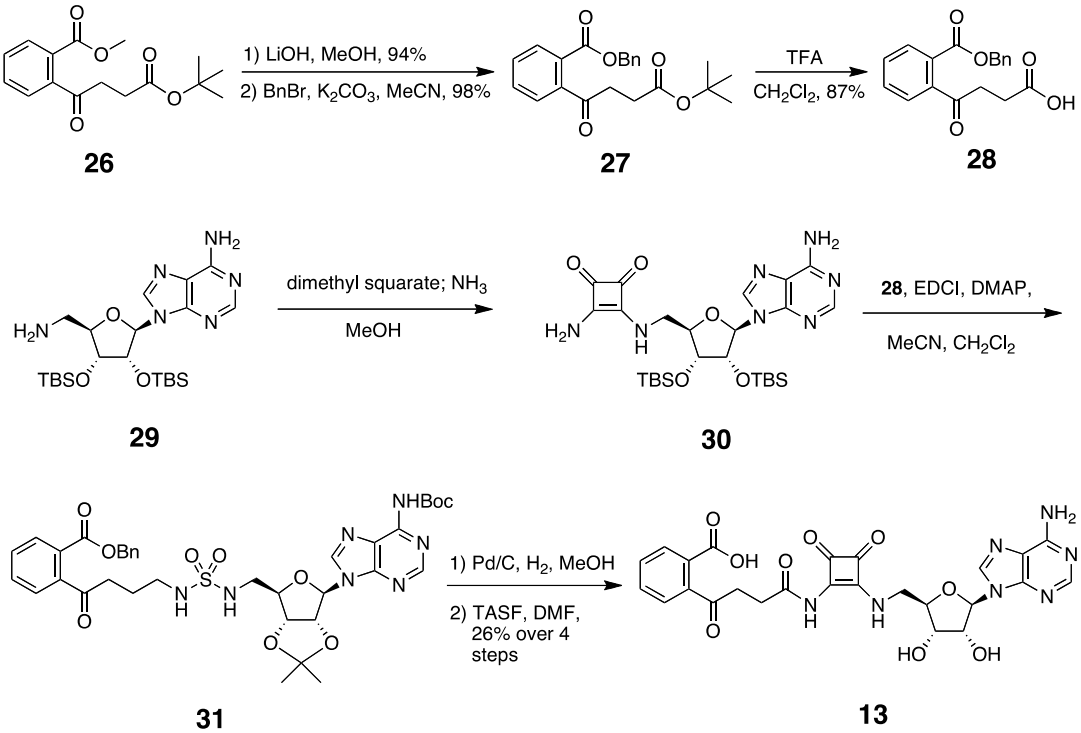

Figure 4.5. Synthesis of squamide linker analogue 13. DMAP = *N*,*N*-dimethylaminopyridine, EDCI = 1-ethyl-3-(3-dimethylaminopropyl)carbodiimide, TFA = trifluoroacetic acid, THF = tetrahydrofuran.

with anhydrous ammonia provided the desired squaramide **30**. Coupling of the squaramide **30** to the prepared OSB scaffold **28**, followed by two-step deprotection provided the desired acyl-squaramide analogue **13**.

Synthesis of the alkyl-sulfamide analogue **14** (Figure 4.6) proceeded by first generating a reduced OSB intermediate **33** and appending it to the Cbz-protected AMSN analogue **34** using Mitsunobu conditions to provide intermediate **35**. This was then deprotected over two steps to generate the desired alkyl-sulfamide analogue **14**.

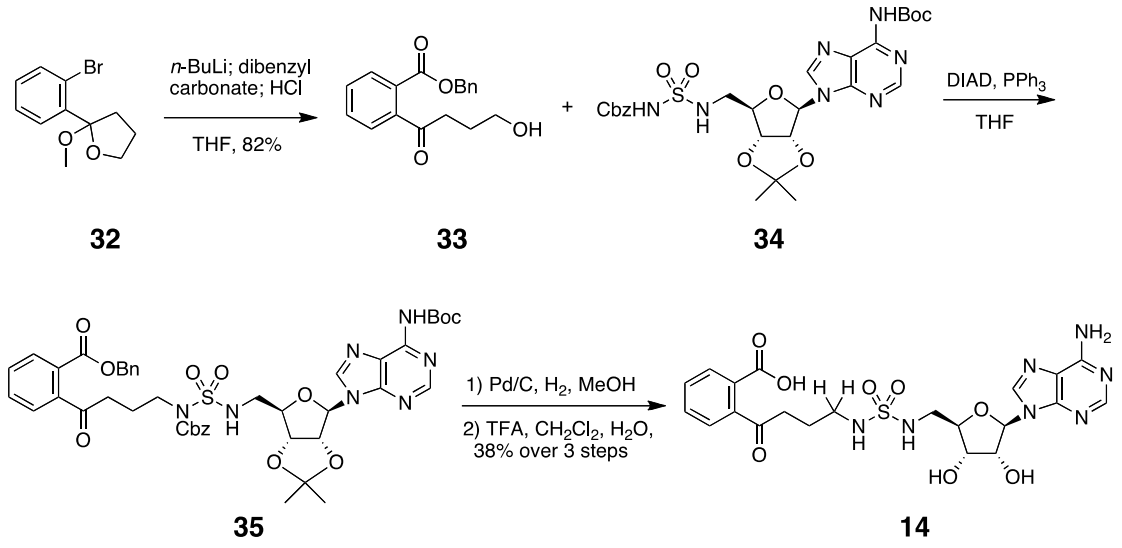

Figure 4.6. Synthesis of alkyl-sulfamide linker analogue 14. DIAD = diisopropyl azodicarboxylate, TFA = trifluoroacetic acid, THF = tetrahydrofuran.

The route to the acyl-tetrazole analogue **44** began by executing a lithium–halogen exchange with the aryl bromide **36**[35] to form the corresponding lithiated species (Figure 4.7). This was then quenched with dimethyl carbonate to form the desired methyl ester, followed by acid catalyzed opening of the tetrahydrofuranyl ring to reveal the keto-alcohol **37**. Intermediate **37** was oxidized to the aldehyde then converted to the cyanohydrin intermediate **38**. To protect both the alcohol and ketone of the

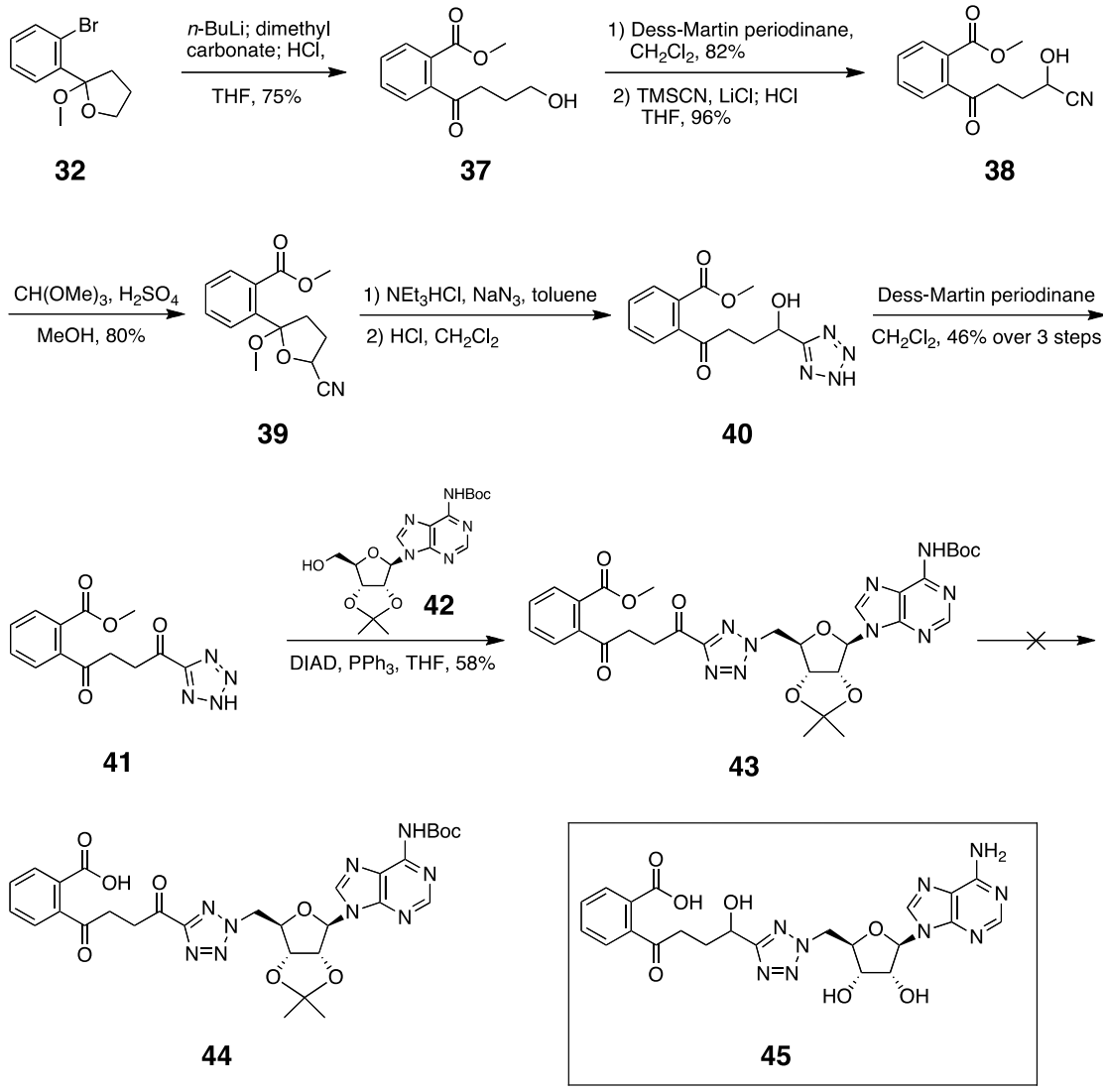

Figure 4.7. Synthetic approach to the acyl-tetrazole linker analogue 42. DIAD = diisopropyl azodicarboxylate, THF = tetrahydrofuran.

succinyl chain, which was found to be necessary during initial exploration of this route, the tetrahydrofuranyl ring was reformed to give the cyclic intermediate **39**. This intermediate was then converted to the desired tetrazole, the tetrahydrofuranyl ring was reopened, and the alcohol oxidized to give the desired acyl-tetrazole fragment **41**. Fragment **41** was appended onto the protected adenosine scaffold **42** using Mitsunobu conditions to give the fully formed, protected acyl-tetrazole analogue **43**. Upon attempting to

deprotect the carboxylate to form the desired free acid intermediate **44**, it was observed that the carbon–carbon bond between the carbonyl and tetrazole was highly labile and prone to addition–elimination reactions with a variety of nucleophiles. We proposed that the reduced form of the analogue, the hydroxy-tetrazole linker analogue **45**, should be hydrolytically stable, as it cannot undergo addition-elimination reactions. The proposed hydroxy-tetrazole analogue was docked into the MenE crystal structure and was found to dock within the parameters previously described in section 4.2 (*S*-hydroxy-tetrazole **45** = –13.81 kcal/mol, *R*-hydroxy-tetrazole **45** = –12.79 kcal/mol).

To achieve the hydroxy-tetrazole analogue, we modified our original route (Figure 4.8) by taking the formed tetrazole fragment **46**, and directly appended the fragment to the adenosine scaffold **42** using Mitsunobu conditions. Acid-catalyzed deprotection removed the isopropylidene and Boc

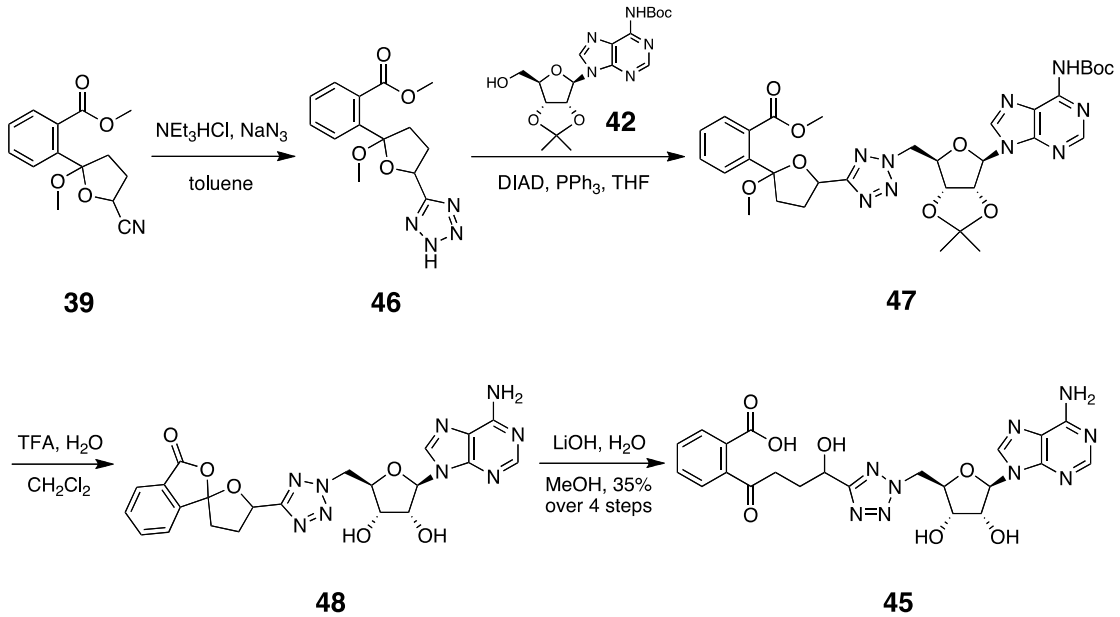

Figure 4.8. Synthesis of hydroxy-tetrazole linker analogue. DIAD = diisopropyl azodicarboxylate, TFA = trifluoroacetic acid, THF = tetrahydrofuran.

protecting groups as expected, but unexpectedly removed the methyl ester of OSB and cyclized to form the spirocycle intermediate **48**. The spirocycle was then opened using lithium hydroxide to provide the desired hydroxy-tetrazole analogue **45**.

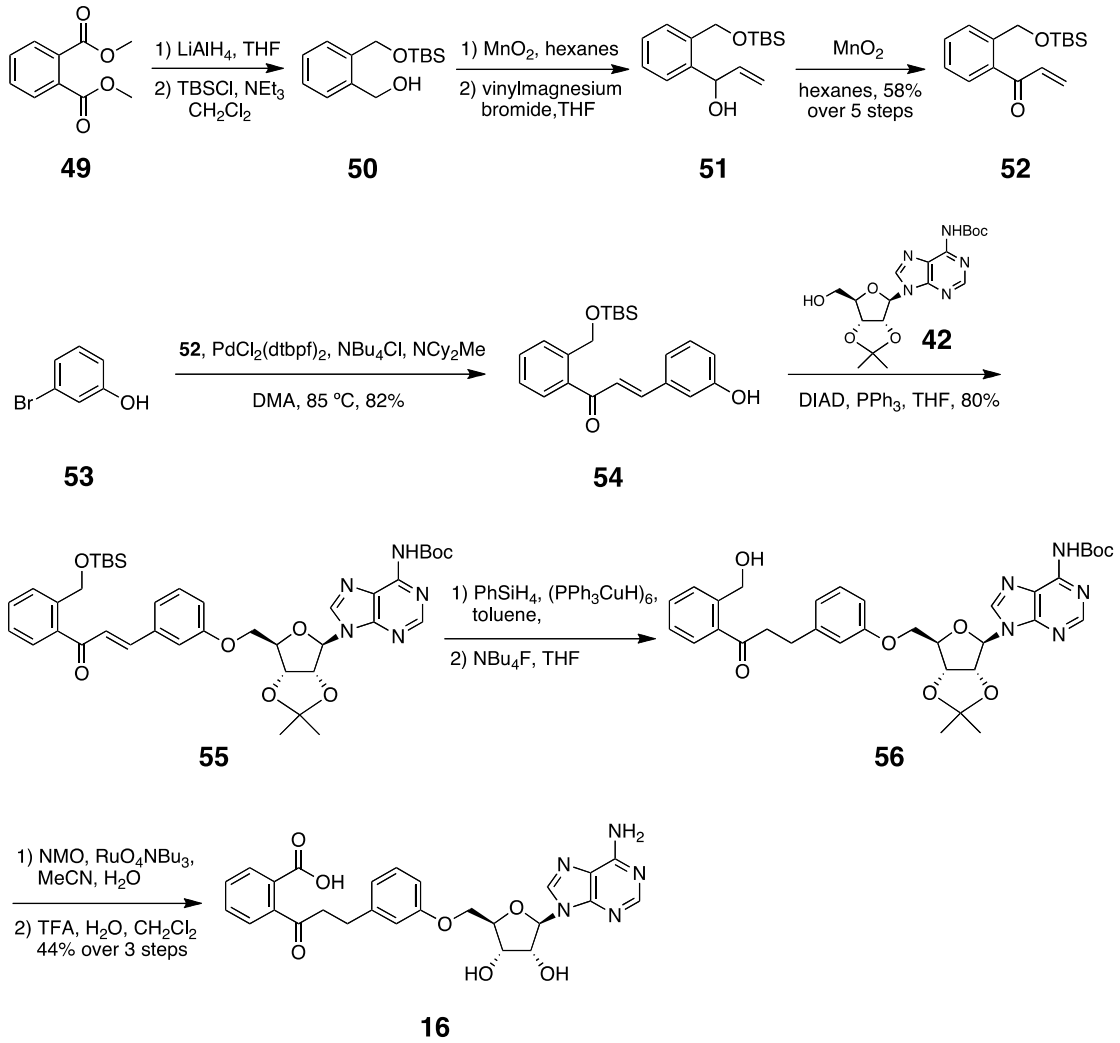

Figure 4.9. Synthesis of phenol linker analogue 16. DIAD = diisopropyl azodicarboxylate, DMA = dimethylacetamide, dtbpf = 1,1'-bis(di-t-butylphosphino)ferrocene, NMO = *N*-methylmorpholine *N*-oxide, TFA = trifluoroacetic acid, THF = tetrahydrofuran.

Synthesis of the phenol linker analogue began by forming the key vinyl ketone fragment **52** over five highly scalable steps from dimethyl phthalate (Figure 4.9). The vinyl ketone **52** efficiently underwent Heck coupling with

m-bromophenol (**53**), followed by a Mitsunobu reaction to append the adenosine scaffold **42** to the free phenol **54**. The olefin was reduced using Stryker's reagent, followed by deprotection of the TBS ether to provide the free alcohol intermediate **56**. This was then oxidized to the desired carboxylate using TPAP and NMO, and finally deprotected to form the desired phenol linker analogue **16**.

4.3. Biochemical Validation of Docking Guided Targeting

Although the synthesis of additional linker analogues from the first-generation library is ongoing, we wanted to gain preliminary validation of our original proposal. Our analogues were tested by our collaborators in the laboratory of Professor Peter Tonge for biochemical inhibition of *E. coli* MenE as previously described (Figure 4.10, see experimental section 4.4 for details).[31,36] Interestingly, while all of the analogues tested showed a significant drop in potency when compared to OSB-AMS, three of the four analogues were active, which is in stark contrast to previous reported efforts in this arena. Perhaps the most unexpected result is that of the phenol linker analogue **16**, which only lost ~2-log potency compared to OSB-AMS, while the more modest modification seen with the acyl-sulfamide analogue **14** resulted in a ~3-log loss of potency versus OSB-AMS. Although use of the MenE docking construct did improve the rate of biochemically active compounds generated, the docking model itself is not perfect. The squaramide linker analogue **13**, which docked with a reasonable score and pose in the MenE binding pocket, had no activity against MenE in biochemical assays.

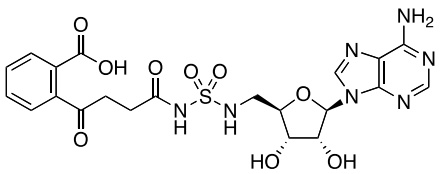

OSB-AMS (1)
ecMenE IC_{50} = 0.025 μM

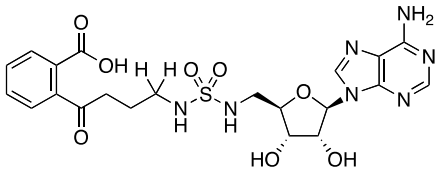

14
ecMenE IC_{50} = 35 μM

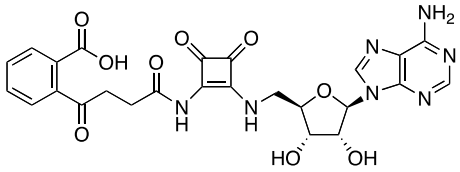

13
ecMenE IC_{50} > 250 μM

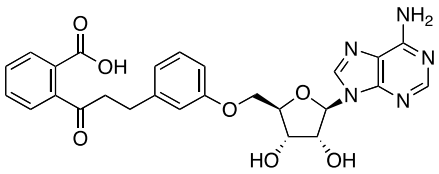

16
ecMenE IC_{50} = 8 μM

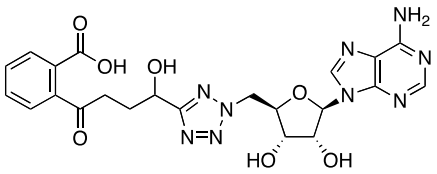

45
ecMenE IC_{50} = 53 μM

Figure 4.10. Biochemical activity of selected OSB-AMS linker analogues.

The activity of the phenolic linker analogue can be rationalized through examination of the docking structure to MenE and consideration of the entropic costs associated with its binding to MenE. The linker region only has one hydrogen-bond acceptor and no traditional hydrogen-bond donor. However, examination of the docking model of the phenolic linker analogue **16** (Figure 4.11) shows that the aromatic ring is in close proximity to a highly conserved residue (Lys-437) and could possibly engage in a cation-π interaction with the lysine sidechain. Additionally, the aromatic linker region, being uncharged and relatively nonpolar, will have a far lower desolvation penalty compared to the more polar and heteroatom rich structures seen in the other analogues.

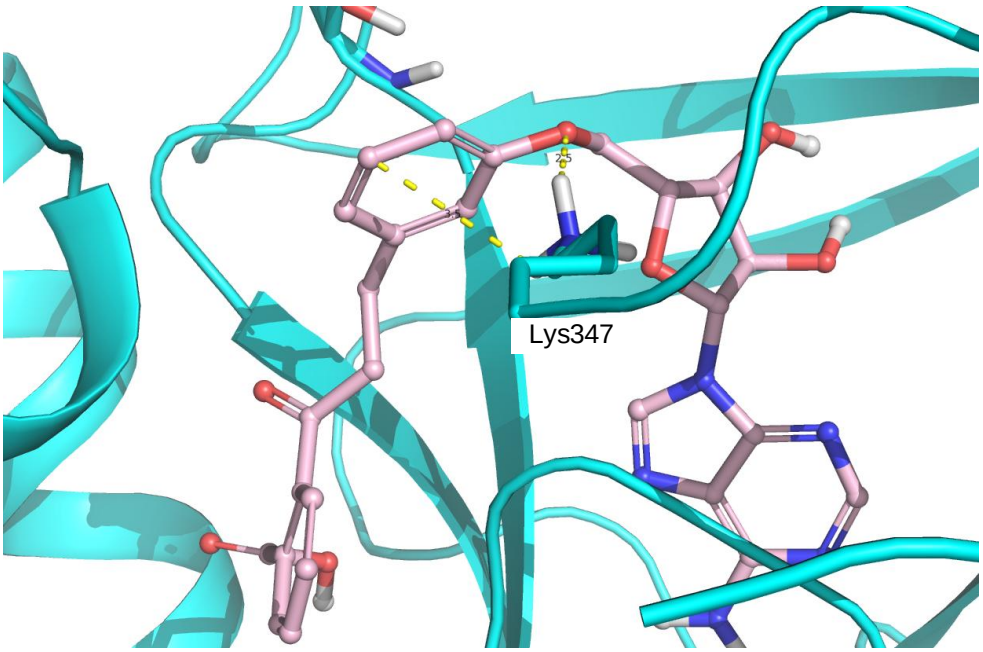

Figure 4.11. Phenolic linker analogue docking pose.

4.3. Exploring the SAR of the Aromatic Linker Analogues of OSB-AMS

Perhaps the most important and promising finding from the preliminary biochemical results is the phenolic linker analogue **16**. This analogue is significantly less polar than that of OSB-AMS at physiological pH and significantly more stable. Given the promise of this analogue in regards to increasing favorable ADME and toxicological liability versus that of OSB-AMS, we decided to investigate the SAR of this analogue further. We proposed a library of analogues that would both alter the electronics of the ring, as well as explore the surrounding space in this region. Furthermore, we hypothesized that the proposed aromatic and heteroaromatic linker analogues could be rapidly generated with the general synthetic route used to achieve the phenolic linker analogue **16** (Figure 4.12).

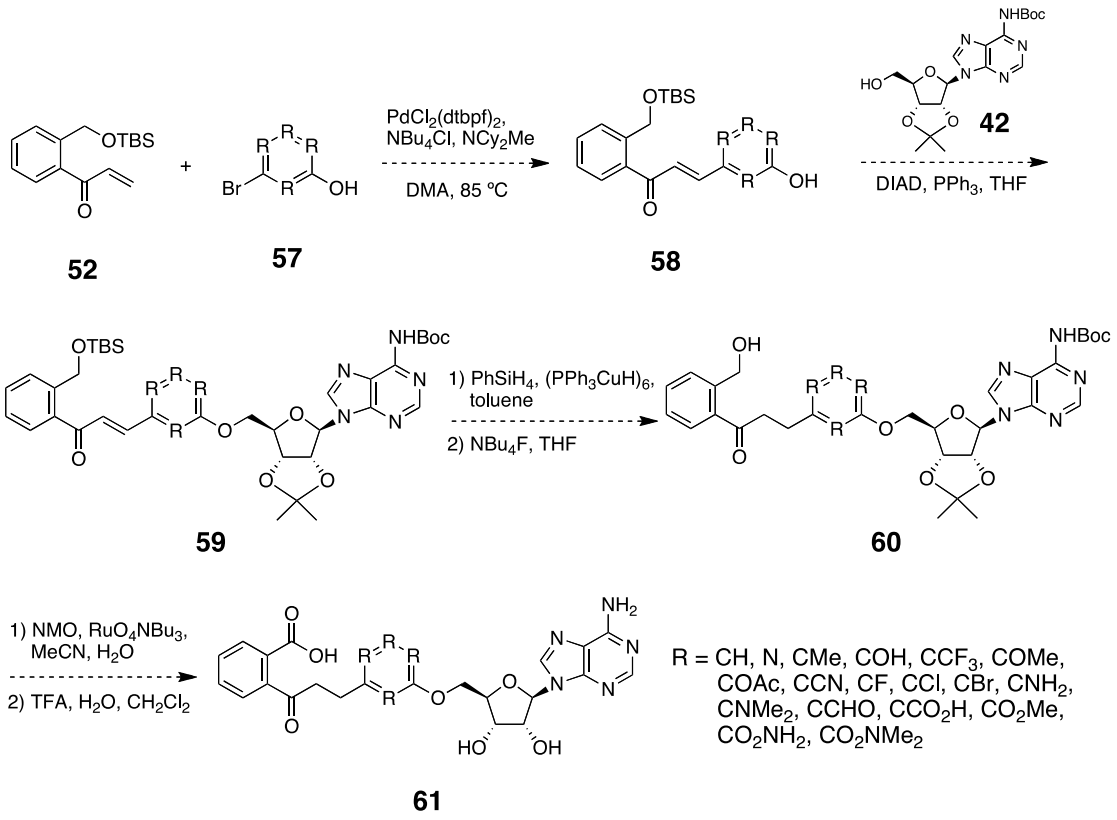

Figure 4.12. Original route to proposed aromatic and heteroaromatic linker analogues DIAD = diisopropyl azodicarboxylate, DMA = dimethylacetamide, dtbpf = 1,1'-bis(di-t-butylphosphino)ferrocene, NMO = *N*-methylmorpholine *N*-oxide, TFA = 2,2,2-trifluoroacetic acid, THF = tetrahydrofuran.

Although the *p*-phenolic linker analogue **62** and 3-(trifluoromethyl)-phenolic linker analogue **63** (Figure 4.13) were synthesized using this approach; electron rich aromatic linker analogues or those functionalized with more sensitive functional groups suffered from very poor yields upon deprotection of the benzyl alcohol and oxidation to the carboxylic acid. To

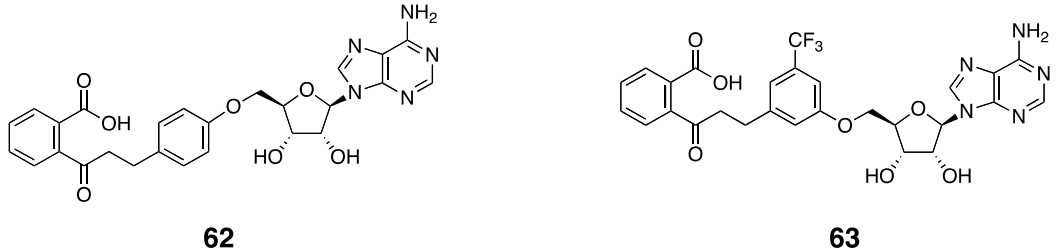

Figure 4.13. Analogues synthesized using the originally proposed synthetic route.

circumvent this issue, our choice of initial Heck coupling partner (**52**) needed to be altered to avoid the late stage desilylation and oxidation steps.

We proposed to use a fully oxidized and protected form of the left-hand fragment (**67**, Figure 4.14), which can be achieved in three steps from a commercially available boronic acid.[33,37-38] This intermediate will allow for the rapid generation of a variety of aromatic and heteroaromatic linker analogues,

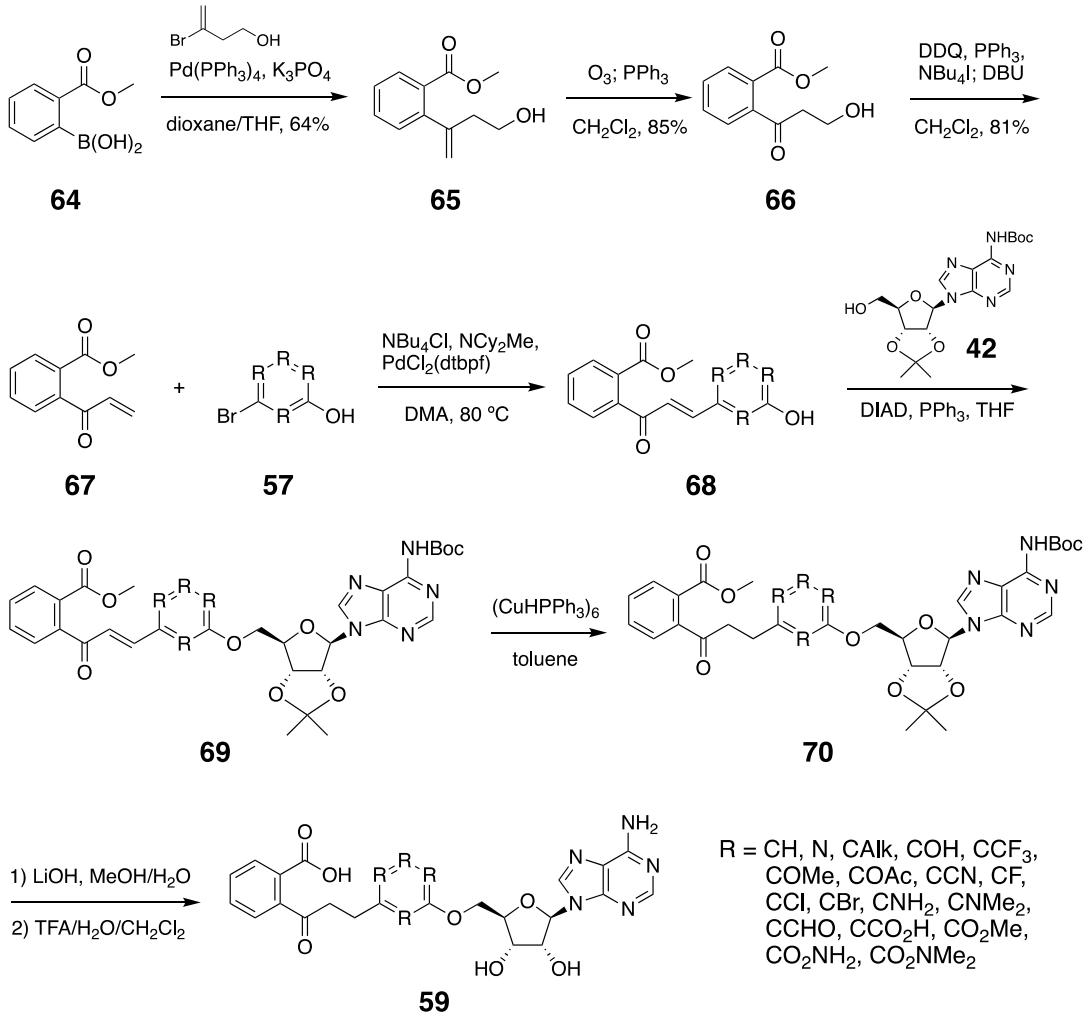

Figure 4.14. Optimized route to proposed aromatic and heteraromatic linker analogues. DBU = 1,8-Diazabicyclo[5.4.0]undec-7-ene, DDQ = 2,3-dichloro-5,6-dicyano-1,4-benzoquinone, DIAD = diisopropyl azodicarboxylate, DMA = dimethylacetamide, dtbpf = 1,1'-bis(di-*t*-butylphosphino)ferrocene, TFA = 2,2,2-trifluoroacetic acid, THF = tetrahydrofuran.

with a larger functional group tolerance than the original route.

To date, the *p*-phenolic linker analogue **62** and 3-(trifluoromethyl)-phenolic linker analogue **63** were tested in biochemical inhibition assays against *E. coli* MenE by our collaborators in the laboratory of Professor Peter Tonge. The *p*-phenolic linker analogue **62** did not show activity against MenE (Figure 4.15), but the 3-(trifluoromethyl)-phenolic linker analogue **63** showed a modest IC_{50} of 26 μM. Although the docking model of the phenolic liker analogue suggest there is sufficient room at the C3 position of the aromatic linker to accommodate the trifluoromethyl substituent, at this time we are unable to determine if the drop in potency with analogue **63** is due to increased steric hindrance from the trifluoromethyl substituent in the binding pocket, or a decreased ability to engage in a cation-π interaction with the conserved Lys-437.

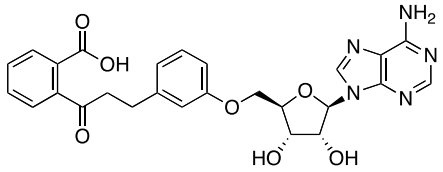

16
MenE IC_{50} = 8 μM

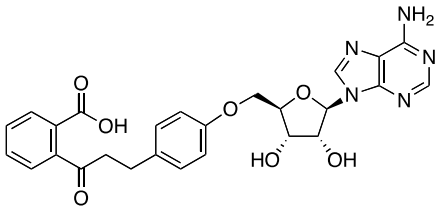

62
MenE IC_{50} > 250 μM

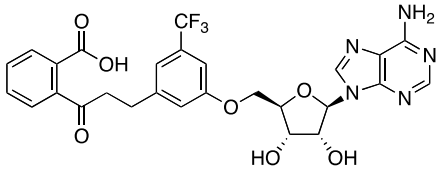

63
MenE IC_{50} = 26 μM

Figure 4.15. Biochemical activity of aromatic linker analogues. Biochemical assays performed using MenE from *E. coli*.

4.3. Conclusions and Discussion

Acyl-AMS based inhibitors, although canonically excellent inhibitors of their cognate adenylate-forming enzymes, have a number of liabilities associated with them that limit their progression as drug candidates. The negatively charged acyl-sulfamate has been implicated in a number of unfavorable physiochemical and ADME properties. Additionally, when the acyl-sulfamate bond is cleaved, highly cytotoxic AMS is released. This cleavage is particularly common in the OSB-AMS class of acyl-sulfamate inhibitors, representing a significant toxicological liability to the progression of these inhibitors beyond use as a tool compounds.

To improve the drug-like properties of our MenE inhibitors and reduce or eliminate the toxicological liability associated with the acyl-AMS motif, we sought to design and synthesize a series of OSB-AMS linker analogues. However, previous work in this area by other groups using a traditional rational design approach, had shown the linker region of acyl-AMS inhibitors to be highly intolerant of modification. To take a different approach, we used the MenE docking construct originally discussed in Chapter 3, to dock a virtual library of OSB-AMS linker analogues. This approach allowed us to probe a far larger area of chemical space in the linker region, and discover a number of analogues that showed inhibitory activity against MenE. The most promising analogue to come from the initial screen was the phenolic linker analogue **16**. Although the analogue had a ~2-log loss in potency versus OSB-AMS, it exhibited greatly increased stability and hydrophobicity, which represents a possible vector for the MenE inhibitors into more favorable drug-like space. Using the newly optimized synthetic route, a large variety of

different aromatic and heteroaromatic linker analogues can be rapidly synthesized, and the SAR around the linker region ascertained with the overarching goal increasing the potency of the inhibitors and achieving a low-nM inhibitor of MenE.

4.4. Experimental Section

A. Materials and Methods

Reagents were obtained from Aldrich Chemical (www.sigma-aldrich.com) or Acros Organics (www.fishersci.com) and used without further purification. Optima or HPLC grade solvents were obtained from Fisher Scientific (www.fishersci.com), degassed with Ar, and purified on a solvent drying system. Reactions were performed in flame-dried glassware under positive Ar pressure with magnetic stirring.

TLC was performed on 0.25 mm E. Merck silica gel 60 F254 plates and visualized under UV light (254 nm) or by staining with potassium permanganate ($KMnO_4$), cerium ammonium molybdenate (CAM), or iodine (I_2). Silica flash chromatography was performed on E. Merck 230–400 mesh silica gel 60. Preparative scale HPLC purification was carried out on a Waters 2545 HPLC with 2996 diode array detector using a Sunfire Prep C18 reverse phase column (10 Å~ 150 mm, 5 µm) with UV detection at 254 nm. Samples were lyophilized using a Labconco Freezone 2.5 instrument.

IR spectra were recorded on a Bruker Optics Tensor 27 FTIR spectrometer with Pike technologies MIRacle ATR (attenuated total reflectance, ZnSe crystal) accessory and peaks reported in cm^{-1}. NMR spectra were recorded on a Bruker Avance III 500 instrument or Bruker Avance III 600 instrument at 24 °C in $CDCl_3$ unless otherwise indicated. Spectra were processed using Bruker TopSpin or nucleomatica iNMR (www.inmr.net) software, and chemical shifts are expressed in ppm relative to TMS (^1H, 0 ppm) or residual solvent signals: $CDCl_3$ (^1H, 7.24 ppm; ^{13}C, 77.23 ppm), CD_3OD (^1H, 3.31 ppm; ^{13}C, 49.15 ppm), D_2O (^1H, 4.80 ppm); coupling constants are expressed in Hz. Mass spectra were obtained at the MSKCC Analytical Core Facility on a Waters Acuity SQD LC-MS by electrospray (ESI) ionization or atmospheric pressure chemical ionization (AP-CI).

B. Synthesis of squaramide linker analogue.

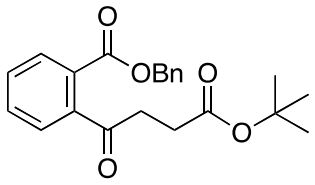

Benzyl 2-(4´-tert-butoxy-4´-oxobutanoyl)benzoate (27). Keto diester **26** (1.64 g, 5.610 mmol, 1 equiv.) prepared as previously described,[33] was dissolved in 5 mL MeOH and 0.5 mL water before LiOH (136 mg, 5.66 mmol, 1.01 equiv.) was added and the reaction stirred for 5 hours. The reaction was concentrated by rotary evaporation and dried under high vacuum before being suspended in 10 mL acetonitrile. K_2CO_3 (1.162 g, 8.413 mmol, 1.5 equiv.) and benzyl bromide (1.438 g, 8.413 mmol, 1.5 equiv.) added and the reaction stirred for 12 hours at room temperature before the reaction was quenched with 50 mL water, extracted with EtOAc (4 x 50 mL). The combined organic extracts were dried (Na_2SO_4), filtered, and concentrated by rotary evaporation. Purification by silica flash chromatography (10% $\rightarrow$ 25% EtOAc in hexanes) yielded the product (**27**) as a clear oil (1.9 g, 92%).

IR (ATR): 2979, 1719, 1575, 1456, 1367, 1270, 1151, 1092, 991, 949, 912, 848, 732, 698, 648. **^{1}H-NMR** (600 MHz; $CDCl_3$): δ 7.92 (dd, *J* = 7.8, 1.1 Hz, 1H), 7.55 (td, *J* = 7.5, 1.2 Hz, 1H), 7.46 (td, *J* = 7.6, 1.2 Hz, 1H), 7.43 (dd, *J* = 7.6, 0.9 Hz, 1H), 7.41-7.39 (m, 2H), 7.38-7.36 (m, 2H), 7.35-7.32 (m, 1H), 5.29 (s, 2H), 3.03 (t, *J* = 6.8 Hz, 2H), 2.57 (t, *J* = 6.8 Hz, 2H), 1.45 (s, 9H). **^{13}C-NMR** (151 MHz; $CDCl_3$): δ 203.9, 172.0, 166.4, 143.2, 135.3, 132.3, 130.0, 129.7, 128.63, 128.54, 128.48, 128.1, 126.4, 80.5, 67.5, 37.7, 29.4, 28.1 **HRMS** (ESI) *m/z* calcd for $C_{22}H_{24}O_5$ ($[M+H]^+$) 369.1702; found 369.1711.

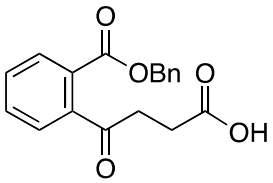

4-(2´-[Benzyloxycarbonyl]phenyl)-4-oxobutanoic acid (28). Keto diester **27** (1.9 g, 5.157 mmol, 1 equiv.) was dissolved in 5 mL CH_2Cl_2 and cooled to

0 ºC before 0.5 mL water and 5 mL TFA was added and the reaction stirred for 3 hours. Concentration by rotary evaporation and purification by silica flash chromatography (40% → 60% EtOAc in hexanes) yielded the product (**28**) as a white solid (1.4 g, 87%).

IR (ATR): 3035, 1706, 1597, 1575, 1498, 1400, 1377, 1272, 1136, 1094, 1041, 991, 956, 912, 735, 698, 648. **^{1}H-NMR** (500 MHz; $CDCl_3$): δ 7.96-7.94 (m, 1H), 7.57 (td, *J* = 7.5, 1.2 Hz, 1H), 7.49 (td, *J* = 7.7, 1.2 Hz, 1H), 7.41-7.37 (m, 5H), 7.36-7.33 (m, 1H), 5.30 (s, 2H), 3.06 (t, *J* = 6.7 Hz, 2H), 2.70 (t, *J* = 6.7 Hz, 2H). **^{13}C-NMR (**126 MHz; $CDCl_3$): δ 203.6, 178.8, 166.3, 142.9, 135.2, 132.5, 130.1, 129.9, 128.69, 128.63, 128.59, 128.0, 126.3, 67.6, 37.4, 28.0. **HRMS** (ESI) *m/z* calcd for $C_{18}H_{16}O_5$ ($[M+H]^+$) 312.0998; found 312.1005.

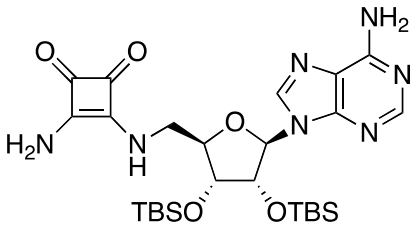

2´,3´-*O*-*t*-Butyldimethylsilyl-5´-*N*-(3-amino-cyclobut-3-ene-1,2-dione) aminodeoxyadenosine (30). Protected adenosine analogue **29** (180 mg, 0.364 mmol, 1 equiv.) prepared as previously described,[36,39] was suspended in 5 mL MeOH before dimethoxysquarate (103 mg, 0.727 mmol, 2.0 equiv.) was added. The reaction was stirred for 4 hours before the reaction was cooled to 0 ºC and anhydrous ammonia slowly bubbled into the solution for 15 min. The reaction was stirred for 1 hour while returning to room temperature before being filtered through a pad of celite and solvent removed by rotary evaporation. The residue was reconstituted in 15% MeOH in EtOAc, filtered though a pad of silica, and the pad washed with 100 mL 15% MeOH in EtOAc. The eluent was concentrated by rotary evaporation to give the crude product (**30**) as a yellow tinged solid (172 mg), which was used without further purification.

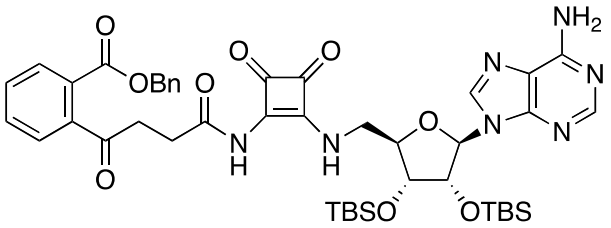

2´,3´-*O*-*t*-Butyldimethylsilyl-5´-*N*-(*N*-[4´´-(2´´-[benzyloxycarbonyl]phenyl)-4-oxobutanoyl]-(3-amino-cyclobut-3-ene-1,2-dione))aminodeoxy adenosine (31). Carboxylic acid **28** (87 mg, 0.280 mmol, 1.1 equiv.), protected AMSq **30** (165 mg, 0.280 mmol, 1 equiv) and DMAP (34 mg, 0.280 mmol, 1.0 equiv.) were dissolved in CH_2Cl_2:MeCN (5 mL, 50:50) before EDCI (214 mg, 1.118 mmol, 4.0 equiv) was added. The reaction was stirred for 12 h, then quenched with 20 mL 1M $KHSO_4$, and extracted with CH_2Cl_2 (5 x 20 mL). The combined organic extracts were dried (Na_2SO_4), filtered, and concentrated by rotary evaporation. The reside was reconstituted in 5% MeOH in EtOAc (~20 mL), filtered though a pad of silica and the pad washed with 100 mL 5% MeOH in EtOAc. Eluent was then concentrated by rotary evaporation to afford the crude product **31** (125 mg), which was used without further purification.

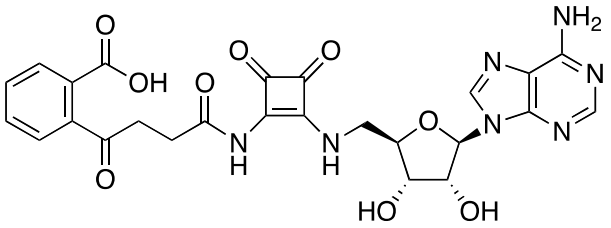

5´-*N*-(*N*-[4´´-(2´´(carboxyl)phenyl)-4´´-oxobutanoyl]-(3-amino-cyclobut-3-ene-1,2-dione))aminodeoxyadenosine (13). Crude protected OSB-AMSq **31** (125 mg, 0.538 mmol, 1 equiv.) and 10% Pd/C (15 mg, 0.014 mmol, 0.1 equiv.) were suspended in MeOH (14 mL) before being stirred under H_2 balloon for 4h. The reaction was then filtered through a celite pad and concentrated by rotary evaporation before being dried under high vacuum. The residue was suspended in DMF (3 mL) and TASF (108 mg, 0.394 mmol, 2.5 equiv.) added before being stirred for 12 h at 50 ºC. Concentration by rotary evaporation, purification by preparative HPLC (5% $\rightarrow$ 95% MeCN in H_2O with 0.01% TFA), and lyophilization yielded the product (**13**) as a fluffy white solid (52 mg, 23% over 4 steps).

IR (ATR): 3364, 2487, 1803, 1698, 1601, 1537, 1447, 1204, 1143, 1124, 980, 895, 801, 768, 724, 702, 638. **^{1}H-NMR** (600 MHz; MeOD): δ 8.45 (s, 1H), 8.33 (s, 1H), 7.85-7.84 (m, 1H), 7.74-7.71 (m, 1H), 7.61-7.57 (m, 2H), 6.06 (d, *J* = 4.7 Hz, 1H), 4.72 (t, *J* = 5.0 Hz, 1H), 4.41 (t, *J* = 5.1 Hz, 1H), 4.24 (q, *J* = 4.7 Hz, 1H), 4.07 (ddd, *J* = 46.9, 14.3, 4.9 Hz, 2H), 2.99-2.86 (m, 2H), 2.66-2.63 (m, 2H). 13C-NMR (151 MHz; MeOD): δ 189.6, 183.8, 174.5, 173.6, 170.1, 160.9, 153.32, 153.31, 150.2, 147.79, 147.78, 147.78, 147.76, 147.74, 147.73, 143.6, 120.7, 90.5, 85.0, 75.4, 72.2, 49.6, 46.0, 38.7, 30.9. **HRMS** (ESI) *m/z* calcd for $C_{25}H_{24}N_7O_9$ ($[M+H]^+$) 566.1636; found 566.1627.

C. Synthesis of sulfamide linker analogue.

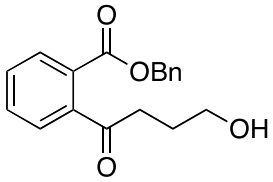

Benzyl 2-(4-hydroxybutanoyl)benzoate (33). Aryl bromide **32** (1 g, 3.889 mmol, 1 equiv.) prepared as previously described,[33] was suspended in 4 mL THF and cooled to -78 ºC before *n*-BuLi (3.038 mL, 4.861 mmol, 1.6 M in THF, 1.25 equiv.) was added. After 1 h, the reaction was transferred via cannula over 5 min to a stirring solution of benzyl chloroformate (1.326g, 7.778 mmol, 2 equiv.) in 5 mL THF at -78 ºC before being stirred for 2 h while returning to room temperature. The reaction was then quenched with HCl (20 mL, 1M) and stirred for 10 min before being extracted with EtOAc (4 x 25 mL), organics combined, dried (Na_2SO_4), filtered, and concentrated by rotary evaporation. Purification by silica flash chromatography (40% → 60% EtOAc in hexanes) yielded the product (**33**) as a clear oil (950 mg, 82%).

IR (ATR): 3393, 3068, 3036, 2954, 2886, 1716, 1599, 1577, 1500, 1457, 1406, 1378, 1274, 1139, 1101, 1079, 1004, 961, 915, 755, 701, 649. **^{1}H-NMR** (600 MHz; $CDCl_3$): δ 7.95-7.94 (m, 1H), 7.57 (td, *J* = 7.5, 1.1 Hz, 1H), 7.48 (td, *J* = 7.7, 1.0 Hz, 1H), 7.40 (dt, *J* = 13.8, 7.0 Hz, 4H), 7.36-7.33 (m, 2H), 5.32 (s, 2H), 3.70 (t, *J* = 6.0 Hz, 2H), 2.88 (t, *J* = 6.8 Hz, 2H), 2.19 (s, 1H), 1.92 (quintet, *J* = 6.4 Hz, 2H). **^{13}C-NMR (**151 MHz; $CDCl_3$): δ 206.0, 166.6, 143.7, 135.3, 132.5, 130.1, 129.7, 128.67, 128.55, 128.54, 128.0, 126.2, 67.6, 61.7, 39.4, 26.6. **HRMS** (ESI) *m/z* calcd for $C_{18}H_{18}O_4Na([M+H]^+)$ 321.1103; found 321.1110.

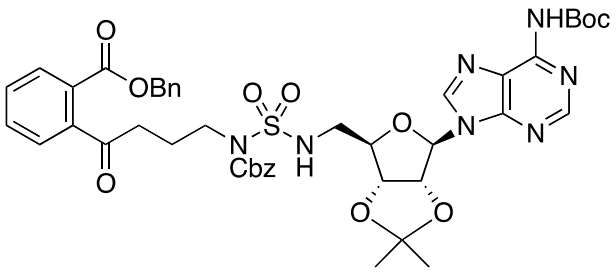

6-*N*-*t*-Butoxycarbonyl-2´,3´-*O*-isopropylidene-5´-*N*-(*N*-[benzyloxycarbonyl]-[benzyl 2-(4-hydroxybutanoyl)]sulfamoyl)aminodeoxyadenosine (35). Triphenylphosphine (105 mg, 0.402 mmol, 1.5 equiv.) in 1 mL THF was added drop wise to a stirring solution of DIAD (81 mg, 0.402 mmol, 1.5 equiv.) in 5 mL THF at 0 ºC. After 10 min, alcohol **33** (80 mg, 0.268 mmol, 1 equiv.) in 1 mL THF was added dropwise followed by protected adenosine analogue **34** (266 mg, 0.364 mmol, 1 equiv.) prepared as previously described,[33] in 1 mL THF. The reaction was allowed to stir for 14 h while returning to rt before 1 mL MeOH was added and the solvent was removed by rotary evaporation. The resulting residue was reconstituted in diethyl ether, filtered through a pad of silica, the pad washed with 100 mL diethyl ether, and the solvent removed by rotary evaporation to give the crude product **35** (350 mg, 145%), which was used without further purification.

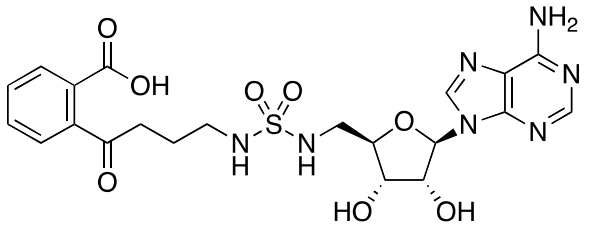

5´-*N*-(*N*-[4´´-(2´´´-[Carboxyl]phenyl)-4-oxobutane]sulfamoyl)amino deoxyadenosine (14). Crude intermediate **35** from the previous step (assumed quantitative yield) and 10% Pd/C (28 mg, 0.027 mmol, 0.1 equiv.) were suspended in MeOH (5 mL). The reaction was stirred vigorously under H_2 balloon for 12 h, then diluted with EtOAc (5 mL), filtered through a celite pad, and concentrated by rotary evaporation. The crude material was then reconstituted in CH_2Cl_2 (15 mL) and cooled to 0 ºC before water (0.5 mL) and TFA (15 mL) added and the reaction stirred for 3 h. Concentration by rotary evaporation, purification by preparative HPLC (5% $\rightarrow$ 30% MeCN in H_2O with

0.1% TFA), and lyophilization yielded the product **14** as a fluffy white solid (51 mg, 38% over 3 steps).

IR (ATR): 3393, 3068, 3036, 2954, 2886, 1716, 1599, 1577, 1500, 1457, 1406, 1378, 1274, 1139, 1101, 1079, 1004, 961, 915, 755, 701, 649. **^{1}H-NMR** ((600 MHz; D_2O): δ 8.13 (s, 1H), 8.05 (s, 1H), 7.42 (dd, *J* = 7.7, 1.2 Hz, 1H), 7.35 (td, *J* = 7.5, 1.2 Hz, 1H), 7.23 (td, *J* = 7.5, 1.1 Hz, 1H), 7.16 (dd, *J* = 7.5, 0.9 Hz, 1H), 5.85 (d, *J* = 6.4 Hz, 1H), 4.68 (dd, *J* = 6.3, 5.5 Hz, 1H), 4.30 (dd, *J* = 5.4, 3.2 Hz, 1H), 4.25 (q, *J* = 3.4 Hz, 1H), 3.29-3.22 (m, 3H), 2.96-2.88 (m, 2H), 2.73 (td, *J* = 7.3, 1.6 Hz, 2H), 1.72 (quintet, *J* = 7.2 Hz, 2H). **^{13}C-NMR** (151 MHz; D_2O): δ 175.8, 155.6, 152.4, 148.3, 141.1, 138.6, 137.0, 131.0, 129.5, 127.8, 126.4, 119.3, 117.3, 115.4, 88.8, 83.6, 72.8, 71.1, 48.9, 44.0, 41.8, 39.0, 23.6. **HRMS** (ESI) *m/z* calcd for $C_{21}H_{26}N_7O_8S$ ($[M+H]^+$) 536.1564; found 536.1539.

D. Synthesis of hydroxyl-tetrazole linker analogue.

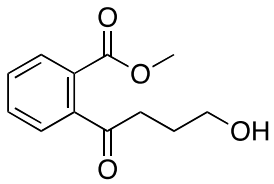

Methyl 2-(4-hydroxybutanoyl)benzoate (37). Aryl bromide **36** (3 g, 11.66 mmol, 1 equiv.) prepared as previously described,[36] was suspended in 10 mL THF and cooled to -78 ºC before *n*-BuLi (5.127 mL, 12.82 mmol, 2.5 M in hexanes, 1.1 equiv.) was added. After 1 h, the reaction was transferred via cannula over 5 min to a stirring solution of dimethyl carbonate (2.1, 23.32 mmol, 2 equiv.) in 5 mL THF at -78 ºC, and stirred for 2 h while returning to room temperature. The reaction was then quenched with HCl (20 mL, 1M) and stirred for 10 min before being extracted with EtOAc (4 x 25 mL), organics combined, dried (Na_2SO_4), filtered, and concentrated by rotary evaporation. Purification by silica flash chromatography (25% → 100% EtOAc in hexanes) yielded the product (**37**) as a clear oil (1.95 g, 75%).

IR (ATR): 3400, 2954, 2883, 1720, 1597, 1575, 1486, 1436, 1406, 1370, 1285, 1195, 1136, 1098, 1054, 963, 914, 830, 764, 737, 709, 781, 647. **^{1}H-NMR** (600 MHz; $CDCl_3$): δ 7.92 (dt, *J* = 7.8, 0.5 Hz, 1H), 7.58 (td, *J* = 7.5,

0.9 Hz, 1H), 7.50 (td, *J* = 7.7, 1.0 Hz, 1H), 7.35 (dt, *J* = 7.6, 0.5 Hz, 1H), 3.90 (s, 3H), 3.79 (t, *J* = 6.0 Hz, 2H), 2.94 (t, *J* = 6.7 Hz, 2H), 2.02 (quintet, *J* = 6.3 Hz, 2H). **^{13}C-NMR (**151 MHz; $CDCl_3$): δ 206.2, 167.2, 143.7, 132.5, 130.0, 129.7, 128.0, 126.2, 61.8, 52.7, 39.4, 26.7. **HRMS** (ESI) *m/z* calcd for $C_{12}H_{15}O_4$ ($[M+H]^+$) 223.0970; found 223.0966.

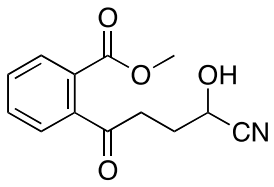

Methyl 2-(4-cyano-4-hydroxybutanoyl)benzoate (38). Dess-Martin periodinane (2.146 g, 5.061 mmol, 1.25 equiv.) was added to a stirring solution of intermediate **37** (900 mg, 4.049 mmol, 1 equiv.) and sodium bicarbonate (1.36 g, 16.19 mmol, 4.0 equiv.) in CH_2Cl_2 (15 mL). After 1 h, the reaction was poured into a solution of saturated sodium thiosulfate (50 mL) saturated sodium bicarbonate (25 mL), and stirred vigorously for 10 min before being extracted with CH_2Cl_2 (4 x 50 mL), organics combined, dried (Na_2SO_4), filtered, and concentrated by rotary evaporation. TMSCN (421.6 mg, 4.250 mmol, 1.05 equiv) and LiCl (17.16 µg, 0.405 µmol, 0.0001 equiv. 0.3 M in THF) were added to the crude aldehyde and the reaction stirred vigorously for 2h. The reaction was then quenched by addition of 6 M HCl (20 mL) and stirred for 10 min before being extracted with EtOAc (4 x 25 mL), organics combined, dried (Na_2SO_4), filtered, and concentrated by rotary evaporation. Purification by silica flash chromatography (30% → 50% EtOAc in hexanes) yielded the product (**38**) as a clear oil (790 mg, 79%).

IR (ATR): 3434, 3070, 3002, 2954, 2848, 2253, 1793, 1711, 1597, 1576, 1487, 1436, 1409, 1371, 1285, 1203, 1165, 1138, 1093, 994, 960, 913, 830, 802, 761, 736, 708, 681, 648. **^{1}H-NMR** (600 MHz; $CDCl_3$): δ 7.97 (dd, *J* = 7.8, 0.7 Hz, 1H), 7.62 (td, *J* = 7.5, 1.2 Hz, 1H), 7.53 (td, *J* = 7.7, 1.1 Hz, 1H), 7.33 (dd, *J* = 7.6, 0.7 Hz, 1H), 4.81 (s, 1H), 4.03 (s, 1H), 3.92 (s, 3H), 3.14 (ddd, *J* = 18.8, 8.9, 4.9 Hz, 1H), 2.98 (ddd, *J* = 18.8, 6.3, 5.0 Hz, 1H), 2.43 (ddt, *J* = 14.2, 9.3, 4.8 Hz, 1H), 2.25 (dddd, *J* = 14.4, 7.8, 6.5, 5.0 Hz, 1H). **^{13}C-NMR (**151 MHz; $CDCl_3$): δ 205.9, 167.1, 143.3, 133.0, 130.21, 130.03, 127.5, 125.9, 119.8, 60.2, 53.0, 38.3, 29.4. **HRMS** (ESI) *m/z* calcd for $C_{19}H_{17}O_4Na$ ($[M+Na]^+$) 346.1055; found 346.1041.

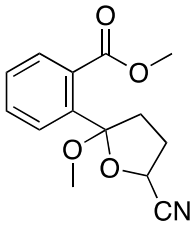

Methyl 2-(5-cyano-2-methoxytetrahydrofuran-2-yl)benzoate (39). Trimethyl orthoformate (858 mg, 8.088 mmol, 4.0 equiv.) and concentrated sulfuric acid (19.8 mg, 0.202 mmol, 0.1 equiv.) were added to a stirring solution of cyanohydrin intermediate **38** (500 mg, 2.022 mmol, 1 equiv.) in MeOH (20 mL) before being heated reflux. After 12 h, the reaction was cooled to room temperature, poured into saturated sodium bicarbonate (50 mL), extracted with EtOAc (4 x 50 mL), organics combined, dried (Na_2SO_4), filtered, and concentrated by rotary evaporation. Purification by silica flash chromatography (10% $\rightarrow$ 30% EtOAc in hexanes containing 1% NEt_3) yielded the product (**39**) as a clear oil (425 mg, 80%).

IR (ATR): 2999, 2948, 2837, 1729, 1434, 1295, 1268, 1191, 1131, 1099, 1076, 1031, 960, 928, 874, 827, 784, 762, 738, 703, 651. **^{1}H-NMR** (600 MHz; $CDCl_3$): δ 7.54 (dt, *J* = 7.9, 0.6 Hz, 1H), 7.48-7.43 (m, 1H), 7.42-7.36 (m, 2H), 4.89-4.86 (m, 1H), 3.88 (d, *J* = 11.6 Hz, 3H), 3.15 (s, 3H), 2.63-2.49 (m, 3H), 2.38-2.20 (m, 1H). **^{13}C-NMR (**151 MHz; $CDCl_3$): δ 170.5, 136.4, 132.4, 130.1, 128.5, 128.1, 127.2, 119.3, 110.9, 66.0, 52.4, 50.7, 40.1, 30.8. **HRMS** (ESI) *m/z* calcd for $C_{14}H_{15}O_4NNa$ ([M+Na]$^+$) 284.0899; found 284.0903.

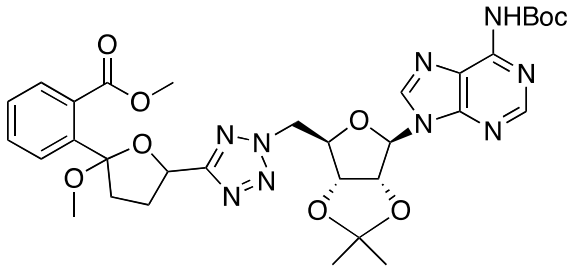

6-*N*-*t*-Butoxycarbonyl-2´,3´-*O*-isopropylidene-5´-*N*-(*N*-2´´-[methyloxy carbonyl] - [benzyl-(2-methoxy-5-[2*H*-tetrazol-5-yl] tetrahydrofuran-2-yl)]) aminodeoxyadenosine (47). Intermediate **39** (206 mg, 0.788 mmol, 1 equiv.), sodium azide (153.7 mg, 2.365 mmol, 3.0 equiv.), and triethylammonium hydrochloride (325.5 mg, 2.365 mmol, 3.0 equiv.) were suspended in toluene (15 mL) and stirred at 100 ºC for 4 h. The reaction was

then cooled to room temperature, diluted with 30 mL acetone, filtered through a pad of celite and the filtrate concentrated by rotary evaporation. The residue was dissolved in EtOAc (50 mL) and washed with saturated ammonium chloride (2 x 25 mL), dried (Na_2SO_4), filtered, and concentrated by rotary evaporation to give the crude tetrazole intermediate **46**. The crude tetrazole **46** was then suspended in THF (15 mL) with protected adenosine **42** (321 mg, 0.789 mmol, 1 equiv.) prepared as previously described,[33] and resin bound PPh_3 (969 mg, 1.182 mmol, 1.5 equiv. 32% w/w) before being cooled to 0 ºC and diisopropyl azodicarboxylate (239 mg, 1.182 mmol, 1.5 equiv) added. The reaction was allowed to stir for 14 h while returning to room temperature before being quenched with water (1 mL), filtered through a pad of celite and the filtrate concentrated by rotary evaporation to yield the crude product **47** as a yellow solid (680 mg).

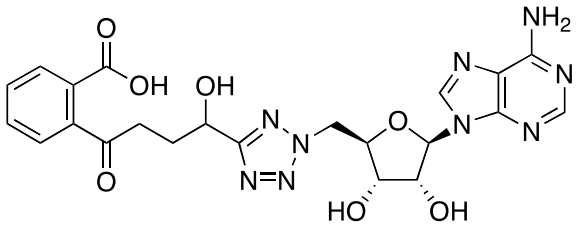

5´-*N*-(*N*-[4´´-([2´´´-(Carboxyl)phenyl]4-hydroxy)2*H*-tetrazol-5-yl]butanoyl) aminodeoxyadenosine (45). Intermediate **47** was reconstituted in CH_2Cl_2 (20 mL) and cooled to 0 ºC before TFA (20 mL) and water (1 mL) added and the reaction stirred for 4 h while returning to room temperature before being concentrated by rotary evaporation and dried under high vacuum for 4h to give the crude spirocycle product **48**. The residue was then dissolved in MeOH (25 mL) and water (3 mL) before LiOH (75 mg, 3.152 mmol, 4.0 equiv.) added and the reaction stirred at room temperature for 12 h. Concentration by rotary evaporation, purification by preparative HPLC (5% $\rightarrow$ 45% MeCN in H_2O with 0.1% TFA), and lyophilization yielded the product **45** as a fluffy white solid (145 mg, 35% over 4 steps).

IR (ATR): 3350, 1751, 1694, 1509, 1468, 1428, 1324, 1289, 1202, 1138, 1062, 1033, 898, 831, 801, 767, 723, 700, 643. **^{1}H-NMR** (600 MHz; D_2O): δ 8.00 (d, *J* = 4.9 Hz, 1H), 7.84 (s, 1H), 7.46 (d, *J* = 7.6 Hz, 1H), 7.39 (q, *J* = 7.8 Hz, 1H), 7.30-7.25 (m, 1H), 7.19 (dd, *J* = 23.4, 7.7 Hz, 1H), 5.92 (t, *J* = 3.0 Hz, 1H), 5.11 (dtd, *J* = 29.2, 12.4, 4.7 Hz, 2H), 5.01 (dt, *J* = 15.2, 6.6 Hz, 1H), 4.59-4.56 (m, 1H), 4.50 (dq, *J* = 9.7, 4.8 Hz, 2H), 2.79-2.72 (m, 2H), 2.19-2.09

(m, 2H). **^{13}C-NMR (**151 MHz; D_2O): δ 208.3, 175.96, 175.80, 167.51, 167.48, 163.1, 162.9, 160.2, 155.29, 155.29, 152.6, 148.4, 139.5, 138.34, 138.30, 138.15, 138.13, 137.18, 137.17, 137.16, 137.01, 136.98, 131.09, 131.08, 131.01, 131.00, 130.99, 129.35, 129.31, 127.80, 127.76, 126.51, 126.49, 126.36, 126.34, 126.34, 119.2, 118.60, 118.57, 117.3, 115.3, 113.4, 88.30, 88.24, 80.63, 80.55, 73.07, 73.02, 70.05, 69.98, 64.5, 53.25, 53.12, 29.82, 29.76. **HRMS** (ESI) *m/z* calcd for $C_{22}H_{22}O_7N_9$ ($[M+H]^+$) 524.1642; found 524.1630.

E. Synthesis of *m*-phenolic linker analogue.

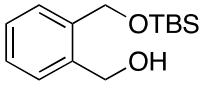

(2-((*tert*-Butyldimethylsilyloxy)methyl)phenyl)methanol (50). Dimethyl phthalate (20 g, 102.9 mmol, 1 equiv.) in THF (50 mL) was added dropwise to a stirring solution of lithium aluminum hydride (4.880 g, 128.6 mmol, 1.25 equiv.) in ether (200 mL) at 0 ºC before being allowed to return to room temperature. After 36 h the reaction was cooled to 0 ºC before water (5 mL), aqueous NaOH (5 mL, 3.75 M), and water (15 mL) were added sequentially and the reaction stirred for 15 min. $MgSO_4$ (5 g) was then added and the reaction stirred for 15 min while returning to room temperature before being filtered through a pad of celite and the solvent removed by rotary evaporation. The crude diol (11.3 g, 81.78 mmol, 1 equiv.) and TBSCl (12.94 g, 85.86 mmol, 1.05 equiv) were dissolved in dichloromethane (150 mL) and cooled to 0 ºC before triethylamine (45.64 mL, 327.1 mmol, 4 equiv) was added and the reaction returned to room temperature. After 14 h the reaction was quenched with 150 mL saturated ammonium chloride, the organic layer removed, the aqueous layer extracted with dichloromethane (3 x 150 mL), organics combined, dried (Na_2SO_4), filtered, and concentrated by rotary evaporation to give the crude alcohol **50** (17.6 g) which was used without further purification.

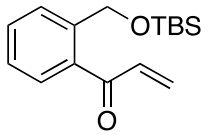

1-(2-((*tert*-Butyldimethylsilyloxy)methyl)phenyl)prop-2-en-1-one (52). Crude alcohol **50** (17.6 g, 69.72 mmol, 1 equiv) was suspended in hexanes (500 mL) before MnO_2 (90 g, 1.045 mol, 15 equiv.) was added and the reaction stirred for 14 h. The reaction was then filtered through a pad of celite and the solvent removed by rotary evaporation. The crude aldehyde (15.3 g, 61.10 mmol, 1 equiv.) was dissolved in THF (60 mL) and cooled to 0 ºC before vinylmagnesium bromide (91.65 mL, 91.65 mmol, 1 M in THF, 1.5 equiv) was added dropwise over 30 min. After 1 h, the reaction was quenched with saturated ammonium chloride (200 mL), extracted with EtOAc (3 x 200 mL), organics combined, dried (Na_2SO_4), filtered, and concentrated by rotary evaporation. The crude alcohol was suspended in hexanes (500 mL) before MnO_2 (53 g, 610.4 mmol, 10 equiv.) was added and the reaction stirred for 8 h. The reaction was then filtered through a pad of celite and the solvent removed by rotary evaporation. Purification by silica flash chromatography (0% $\rightarrow$ 20% EtOAc in hexanes) yielded the product (**52**) as a clear oil (16.2 g, 58% over 5 steps).

IR (ATR): 2957, 2932, 2888, 2859, 1674, 1609, 1575, 1474, 1404, 1364, 1298, 1258, 1230, 197, 1130, 1081, 994, 966, 840, 817, 779, 755, 671. **^{1}H-NMR** (600 MHz; $CDCl_3$): δ 7.74 (dd, *J* = 7.8, 0.7 Hz, 1H), 7.56 (dd, *J* = 7.7, 1.2 Hz, 1H), 7.51 (td, *J* = 7.6, 1.3 Hz, 1H), 7.33-7.31 (m, 1H), 6.87 (dd, *J* = 17.4, 10.6 Hz, 1H), 6.20 (dd, *J* = 17.4, 1.4 Hz, 1H), 5.96 (dd, *J* = 10.6, 1.4 Hz, 1H), 4.95 (s, 2H), 0.94 (s, 9H), 0.10 (s, 6H). **^{13}C-NMR (**151 MHz; $CDCl_3$): δ 195.2, 142.4, 135.7, 135.2, 131.5, 130.8, 128.8, 127.1, 126.3, 63.0, 26.0, 18.4, -5.4. **HRMS** (ESI) *m/z* calcd for $C_{16}H_{25}O_2Si$ ($[M+H]^+$) 277.1624; found 277.1631.

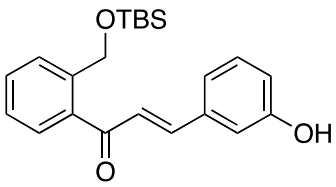

(*E*)-1-(2-((*tert*-Butyldimethylsilyloxy)methyl)phenyl)-3-(3-hydroxyphenyl) prop-2-en-1-one (54). Vinyl ketone **52** (300 mg, 1.085 mmol, 1.2 equiv.), 3-bromophenol **(53) (**156 mg, 0.904 mmol, 1 equiv.), NBu_4Cl (25 mg, 0.0904 mmol, 0.1 equiv.), and $PdCl_2$(dtbpf) (59 mg, 0.0904 mmol, 0.1 equiv) were suspended in DMA (2.7mL) before NCy_2Me (265 mg, 1.356 mmol, 1.5 equiv.) was added and the reaction stirred vigorously at 85 ºC in a sealed tube for 16 h. The reaction was cooled to room temperature before being diluted with 8 mL water and extracted with Et_2O (4 x 8 mL), organics combined, dried (Na_2SO_4), filtered, and concentrated by rotary evaporation. Purification by silica flash chromatography (10% $\rightarrow$ 30% EtOAc in hexanes) yielded the product (**54**) as a white solid (274 mg, 82%).

IR (ATR): 3354, 2955, 2929, 2892, 2857, 1625, 1600, 1472, 1452, 1361, 1257, 1160, 112, 1084, 1022, 997, 983, 839, 816, 778, 740, 677, 610. **^{1}H-NMR** (600 MHz; $CDCl_3$): δ 7.75-7.74 (m, 1H), 7.60 (dd, J = 7.6, 1.1 Hz, 1H), 7.53 (td, J = 7.6, 1.2 Hz, 1H), 7.46 (d, J = 16.0 Hz, 1H), 7.35 (t, J = 7.3 Hz, 1H), 7.28-7.25 (m, 1H), 7.18 (d, J = 16.0 Hz, 1H), 7.13 (d, J = 7.7 Hz, 1H), 7.05 (t, J = 2.0 Hz, 1H), 6.89 (ddd, J = 8.1, 2.5, 0.7 Hz, 1H), 5.41 (s, 1H), 4.96 (s, 2H), 0.92 (s, 9H), 0.09 (s, 6H). **^{13}C-NMR (**151 MHz; $CDCl_3$): δ 195.4, 156.1, 145.6, 142.0, 136.30, 136.20, 131.3, 130.2, 128.4, 127.2, 126.4, 126.2, 121.3, 117.9, 114.7, 63.0, 26.0, 18.4, -5.3. **HRMS** (ESI) *m/z* calcd for $C_{22}H_{27}O_3Si$ ($[M+H]^+$) 367.1729; found 367.1743.

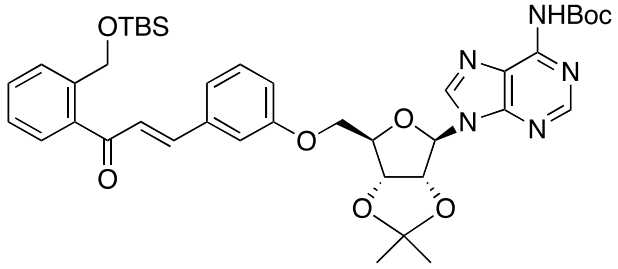

6-*N*-*t*-Butoxycarbonyl-2´,3´-*O*-isopropylidene-5´-*O*-([*E*]-1-[2-([*tert*-butyldimethylsilyloxy]methyl)phenyl]-3-(3-hydroxyphenyl) prop-2-en-1-one)adenosine (55). DIAD (103 mg, 0.509 mmol, 1.5 equiv.) was added

dropwise to a stirring solution of phenol **54** (125 mg, 0.339 mmol, 1 equiv.), protected adenosine **42** (138 mg, 0.339 mmol, 1 equiv.), and resin bound PPh_3 (417 mg, 0.509 mmol, 32 % by weight, 1.5 equiv.) in THF (4 mL) at 0 ºC before being allowed to return to room temperature. After 14 h, the reaction was quenched with water (0.2 mL) and filtered through a pad of celite, the pad washed with EtOAc, and solvent removed by rotary evaporation. Purification by silica flash chromatography (40% → 60% EtOAc in hexanes) yielded the product (**55**) as a white solid (205 mg, 80%).

IR (ATR): 2932, 2858, 1752, 1700, 1620, 1586, 1528, 1464, 1370, 1326, 1303, 1232, 1213, 1146, 1083, 1012, 945, 911, 840, 776, 734, 670, 646. **^{1}H-NMR** (600 MHz; $CDCl_3$): δ 8.78 (s, 1H), 8.09 (s, 1H), 7.92 (s, 1H), 7.75 (d, *J* = 7.8 Hz, 1H), 7.61 (dd, *J* = 7.6, 1.1 Hz, 1H), 7.53 (td, *J* = 7.6, 1.2 Hz, 1H), 7.46 (t, *J* = 13.3 Hz, 1H), 7.36 (td, *J* = 7.5, 0.6 Hz, 1H), 7.27 (t, *J* = 4.0 Hz, 2H), 7.19-7.15 (m, 2H), 7.01 (t, *J* = 1.8 Hz, 1H), 6.79 (dd, *J* = 8.1, 2.4 Hz, 1H), 6.26 (d, *J* = 2.3 Hz, 1H), 5.48 (dd, *J* = 6.2, 2.3 Hz, 1H), 5.18 (dd, *J* = 6.2, 3.0 Hz, 1H), 4.96 (s, 2H), 4.75-4.66 (m, 2H), 4.29 (dd, *J* = 10.2, 4.0 Hz, 1H), 4.18 (dd, *J* = 10.1, 4.9 Hz, 1H), 1.67 (s, 3H), 1.55 (s, 9H), 1.49 (s, 3H), 1.43 (s, 3H), 0.93 (s, 9H), 0.09 (s, 6H). **^{13}C-NMR (**151 MHz; $CDCl_3$): δ 194.8, 158.4, 153.2, 150.4, 150.0, 149.5, 145.0, 142.1, 141.2, 136.3, 131.3, 130.2, 128.4, 127.2, 126.51, 126.40, 122.3, 122.0, 116.7, 114.7, 113.8, 113.3, 91.6, 85.5, 84.7, 82.4, 81.8, 68.1, 63.0, 28.21, 28.16, 27.3, 26.0, 25.4, 18.4, -5.3. **HRMS** (ESI) *m/z* calcd for $C_{40}H_{52}N_5O_8Si$ ($[M+H]^+$) 758.3585; found 758.3561.

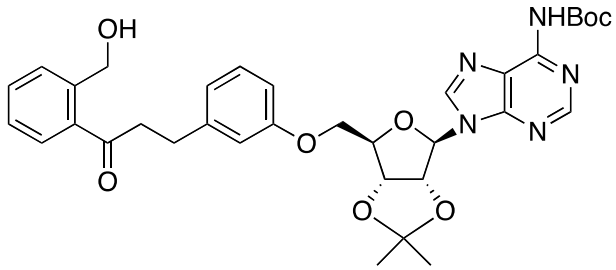

6-*N*-*t*-Butoxycarbonyl-2´,3´-*O*-isopropylidene-5´-*O*-(1-[2-(hydroxymethyl) phenyl]-3-(3-hydroxyphenyl) prop-2-en-1-one)adenosine (56). Phenylsilane (28.5 mg, 263.8 µmol, 2 equiv.) was added to a stirring solution of intermediate **55** (100 mg, 131.9 µmol, 1 equiv.) and Strykers catalyst (23 mg, 11.9 µmol, 0.09 equiv.) in toluene (2 mL). After 16 h, the reaction was quenched with saturated ammonium chloride (5 mL) and stirred for 5 min before 10% ammonium hydroxide (5 mL) was added and the reaction stirred

for an additional 5 min. The reaction was then extracted with Et_2O (4 x 10 mL), organics combined, dried (Na_2SO_4), filtered, concentrated by rotary evaporation, and dried under high vacuum for 1 h. The reside was reconstituted in THF (3 mL) and cooled to 0 ºC before TBAF (264 µL, 264 µmol, 1M in THF, 2 equiv.) was added and the reaction stirred for 1 h. $CaCO_3$ (132 mg, 1.315 mmol, 10 equiv.) and MeOH (3 mL) was added and the reaction stirred for 15 min before sulfonic acid resin (Dowex 50WX8, 200 mg) was added and the reaction stirred for an additional 10 min. The reaction was then filtered through a pad of celite and concentrated by rotary evaporation to give the crude product **56** (86 mg, 101% yield).

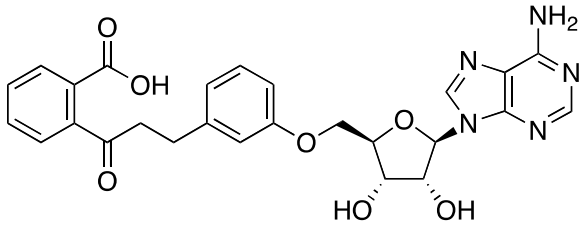

5´-*O*-([2-(Carboxyl)phenyl]3-(3-hydroxyphenyl)propanoyl)adenosine (16). Water (24 mg, 1.33 mmol, 10 equiv.), NMO (156 mg, 1.33 mmol, 10 equiv.) and TPAP (4.8 mg, 13 µmol, 0.1 equiv.) were added to a stirring solution of crude intermediate **56** (86 mg, 133.1 µmol, 1 equiv.) in MeCN (2 mL) before being stirred at room temperature for 14 h. The reaction was then quenched with isopropanol and 1 M $KHSO_4$ (1 mL) was added before the reaction was diluted with water (10 mL), extracted with EtOAc (4 x 10 mL), organics combined, dried (Na_2SO_4), filtered, concentrated by rotary evaporation. The residue was reconstituted in CH_2Cl_2 (5 mL) and cooled to 0 ºC before TFA (5 mL) and water (0.1 mL) added and the reaction stirred for 4 h while returning to room temperature. Concentration by rotary evaporation, purification by preparative HPLC (5% $\rightarrow$ 45% MeCN in H_2O with 0.1% TFA), and lyophilization yielded the product **16** as a fluffy white solid (30 mg, 44% over 4 steps).

IR (ATR): 3320, 2946, 2837, 1757, 1697, 1607, 1492, 1447, 1424, 1290, 1262, 1204, 1141, 1103, 1030, 900, 842, 802, 771, 726, 701, 644. **^{1}H-NMR** (600 MHz; MeOD): δ 8.40 (s, 1H), 8.29 (s, 1H), 7.80-7.77 (m, 1H), 7.70-7.69 (m, 1H), 7.58-7.55 (m, 2H), 7.12-7.09 (m, 1H), 6.73-6.69 (m, 2H), 6.10 (d, *J* = 4.5 Hz, 1H), 4.67 (t, *J* = 4.7 Hz, 1H), 4.44 (dd, *J* = 5.9, 3.7 Hz, 1H), 4.35 (dt, *J* = 4.7, 3.0 Hz, 1H), 4.28-4.26 (m, 1H), 4.17-4.14 (m, 1H), 2.69-2.28 (m, 4H).

^{13}C-NMR (151 MHz; $CDCl_3$): δ 160.1, 153.1, 150.2, 147.36, 147.33, 144.27, 144.25, 144.25, 143.0, 130.74, 130.72, 122.45, 122.42, 122.37, 120.4, 115.66, 115.63, 113.2, 90.5, 85.1, 76.4, 71.9, 68.3, 49.9, 49.6, 31.1. **HRMS** (ESI) *m/z* calcd for $C_{26}H_{26}N_5O_7$ ($[M+H]^+$) 520.1832; found 520.1824.

E. Synthesis of *p*-phenolic linker analogue.

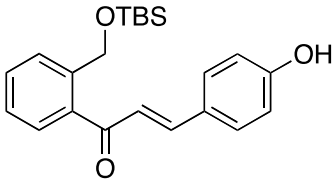

(*E*)-1-(2-((*tert*-butyldimethylsilyloxy)methyl)phenyl)-3-(4-hydroxyphenyl) prop-2-en-1-one (S1). Vinyl ketone **52** (300 mg, 1.085 mmol, 1.2 equiv.), 4-bromophenol (156 mg, 0.904 mmol, 1 equiv.), NBu_4Cl (25 mg, 0.0904 mmol, 0.1 equiv.), and $PdCl_2$(dtbpf) (59 mg, 0.0904 mmol, 0.1 equiv) were suspended in DMA (2.7mL) before NCy_2Me (265 mg, 1.356 mmol, 1.5 equiv.) was added and the reaction stirred vigorously at 85 ºC in a sealed tube for 16 h. The reaction was cooled to room temperature before being diluted with 8 mL water and extracted with Et_2O (4 x 8 mL), organics combined, dried (Na_2SO_4), filtered, and concentrated by rotary evaporation. Purification by silica flash chromatography (10% → 30% EtOAc in hexanes) yielded the product (**S1**) as a white solid (270 mg, 81%).

IR (ATR): 3332, 2957, 2931, 2887, 2858, 1626, 1580, 1514, 1473, 1443, 1364, 1336, 1282, 1258, 1215, 1171, 1128, 1085, 1025, 985, 941, 911, 834, 777, 734, 671, 631. **^{1}H-NMR** ((600 MHz; $CDCl_3$): δ 7.72 (d, *J* = 7.8 Hz, 1H), 7.56 (dd, *J* = 7.6, 0.9 Hz, 1H), 7.52 (td, *J* = 7.6, 1.0 Hz, 1H), 7.47-7.43 (m, 3H), 7.35 (td, *J* = 7.5, 0.4 Hz, 1H), 7.05 (d, *J* = 15.9 Hz, 1H), 6.87-6.84 (m, 2H), 6.59 (s, 1H), 4.94 (s, 2H), 0.91 (s, 9H), 0.08 (s, 6H). **^{13}C-NMR (**151 MHz; $CDCl_3$): δ 196.5, 158.7, 146.7, 141.4, 136.7, 131.0, 130.6, 128.2, 127.3, 127.0, 126.5, 123.6, 116.1, 62.9, 26.0, 18.4, -5.4. **HRMS** (ESI) *m/z* calcd for $C_{22}H_{27}O_3Si$ ($[M+H]^+$) 367.1729; found 367.1727.

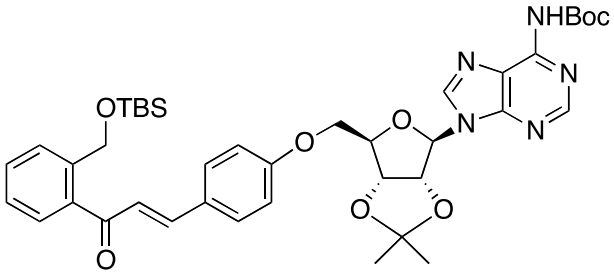

6-*N*-*t*-Butoxycarbonyl-2´,3´-*O*-isopropylidene-5´-*O*-([*E*]-1-[2-([*tert*-butyldimethylsilyloxy]methyl)phenyl]-3-(4-hydroxyphenyl)prop-2-en-1-one)adenosine (S2). DIAD (189 mg, 0.936 mmol, 1.5 equiv.) was added dropwise to a stirring solution of phenol **S1** (230 mg, 0.624 mmol, 1 equiv.), protected adenosine **42** (254 mg, 0.624 mmol, 1 equiv.), and resin bound PPh_3 (767 mg, 0.936 mmol, 32 % by weigh, 1.5 equiv.) in THF (6 mL) at 0 ºC before being allowed to return to room temperature. After 14 h, the reaction was quenched with water (0.2 mL) and filtered through a pad of celite, the pad washed with EtOAc, and solvent removed by rotary evaporation. Purification by silica flash chromatography (40% $\rightarrow$ 60% EtOAc in hexanes) yielded the product (**S2**) as a white solid (310 mg, 66%).

IR (ATR): 2989, 2954, 2931, 2857, 2247, 1751, 1705, 1658, 1609, 1511, 1463, 1423, 1384, 1369, 1327, 1304, 1251, 1213, 1174, 1144, 1081, 1017, 982, 909, 836, 776, 729, 668, 645. **^{1}H-NMR** ((600 MHz; $CDCl_3$): δ 8.79 (s, 1H), 8.09 (s, 1H), 8.05 (s, 1H), 7.74 (d, *J* = 7.8 Hz, 1H), 7.60 (dd, *J* = 7.6, 1.1 Hz, 1H), 7.52 (td, *J* = 7.6, 1.2 Hz, 1H), 7.49-7.44 (m, 3H), 7.35 (t, *J* = 7.5 Hz, 1H), 7.09 (d, *J* = 15.9 Hz, 1H), 6.79-6.76 (m, 2H), 6.25 (d, *J* = 2.2 Hz, 1H), 5.52 (dd, *J* = 6.2, 2.2 Hz, 1H), 5.19 (dd, *J* = 6.2, 2.9 Hz, 1H), 4.95 (s, 2H), 4.72 (dd, *J* = 7.4, 4.3 Hz, 1H), 4.30 (dd, *J* = 10.2, 4.1 Hz, 1H), 4.18 (dd, *J* = 10.2, 4.9 Hz, 1H), 1.67 (s, 3H), 1.56 (s, 9H), 1.43 (s, 3H), 0.92 (s, 9H), 0.09 (s, 6H). **^{13}C-NMR (**151 MHz; $CDCl_3$): δ 195.1, 159.9, 153.2, 150.26, 150.06, 149.6, 145.1, 141.8, 141.3, 136.6, 131.0, 130.2, 128.25, 128.23, 127.1, 126.3, 124.2, 122.2, 114.74, 114.66, 91.7, 85.5, 84.6, 82.4, 81.8, 68.0, 62.9, 28.1, 27.2, 26.0, 25.4, 18.4, -5.3. **HRMS** (ESI) *m/z* calcd for $C_{40}H_{52}N_5O_8Si$ ($[M+H]^+$) 758.3585; found 758.3576.

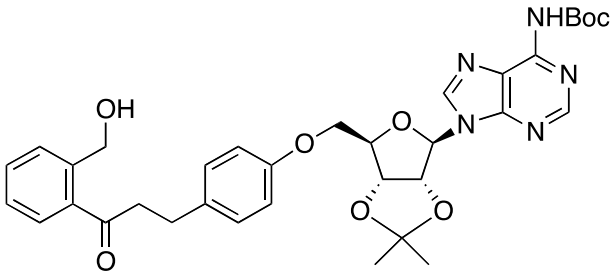

6-*N*-*t*-Butoxycarbonyl-2´,3´-*O*-isopropylidene-5´-*O*-(1-[2-(hydroxymethyl) phenyl]-3-(3-hydroxyphenyl) prop-2-en-1-one)adenosine (S3). Phenylsilane (96 mg, 699.2 µmol, 2 equiv.) was added to a stirring solution of intermediate **S2** (265 mg, 349.6 µmol, 1 equiv.) and Strykers catalyst (62 mg, 31.5 µmol, 0.09 equiv.) in toluene (5 mL) and room temperature. After 16 h, the reaction was quenched with saturated ammonium chloride (10 mL) and stirred for 5 min before 10% ammonium hydroxide (10 mL) was added and the reaction stirred for an additional 5 min. The reaction was then extracted with Et_2O (4 x 20 mL), organics combined, dried (Na_2SO_4), filtered, concentrated by rotary evaporation, and dried under high vacuum for 1 h. The reside was reconstituted in THF (5 mL) and cooled to 0 ºC before TBAF (697 µM, 697 µmol, 1M in THF, 2 equiv.) was added and the reaction stirred for 1 h. $CaCO_3$ (349 mg, 3.486 mmol, 10 equiv.) and MeOH (3 mL) was added and the reaction stirred for 15 min before sulfonic acid resin (dowex 50WX8, 500 mg) was added and the reaction stirred for an additional 10 min. The reaction was then filtered through a pad of celite and concentrated by rotary evaporation to give the crude product **S3** (202 mg, 90% yield).

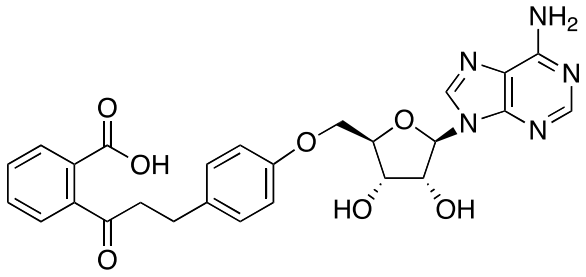

5´-*O*-([2-(Carboxyl)phenyl]3-(3-hydroxyphenyl)propanoyl)adenosine (62). Water (56 mg, 3.128 mmol, 10 equiv.), NMO (366 mg, 3.128 mmol, 10 equiv.) and TPAP (11 mg, 31 µmol, 0.1 equiv.) were added to a stirring solution of crude intermediate **S3** (202 mg, 312.8 µmol, 1 equiv.) in MeCN (5 mL) before being stirred at room temperature for 14 h. The reaction was then quenched with isopropanol and 1 M $KHSO_4$ (1 mL) was added before the

reaction was diluted with water (20 mL), extracted with EtOAc (4 x 20 mL), organics combined, dried (Na_2SO_4), filtered, concentrated by rotary evaporation, and dried under high vacuum 1 h. The residue was reconstituted in CH_2Cl_2 (8 mL) and cooled to 0 ºC before TFA (8 mL) and water (0.8 mL) added and the reaction stirred for 4 h while returning to room temperature. Concentration by rotary evaporation, purification by preparative HPLC (5% $\rightarrow$ 45% MeCN in H_2O with 0.1% TFA), and lyophilization yielded the product **62** as a fluffy white solid (65 mg, 36% over 4 steps).

IR (ATR): 3323, 2921, 2869, 1750, 1690, 1614, 1512, 1424, 1292, 1242, 1203, 1140, 1050, 980, 898, 827, 801, 769, 724, 699, 642. **^{1}H-NMR** (600 MHz; MeOD): δ 8.45 (s, 1H), 8.33 (s, 1H), 7.84-7.83 (m, 1H), 7.77-7.76 (m, 1H), 7.64-7.63 (m, 2H), 7.04-7.03 (m, 2H), 6.87-6.85 (m, 2H), 6.14 (d, *J* = 4.6 Hz, 1H), 4.72 (t, *J* = 4.8 Hz, 1H), 4.49 (t, *J* = 4.8 Hz, 1H), 4.40 (q, *J* = 3.9 Hz, 1H), 4.32-4.30 (m, 1H), 4.20 (dd, *J* = 10.9, 3.3 Hz, 1H), 2.72-2.65 (m, 1H), 2.48-2.29 (m, 3H). **^{13}C-NMR (**151 MHz; $CDCl_3$): δ 158.3, 153.38, 153.37, 150.2, 147.71, 147.70, 142.8, 136.7, 135.9, 135.20, 135.19, 135.19, 135.18, 131.7, 130.5, 120.46, 120.45, 115.7, 90.5, 85.1, 76.4, 71.9, 68.5, 50.0, 49.6, 30.2. **HRMS** (ESI) *m/z* calcd for $C_{26}H_{26}N_5O_7$ ($[M+H]^+$) 520.1832; found 520.1809.

F. Synthesis of *m*-(3-trifluoromethyl)phenolic linker analogue.

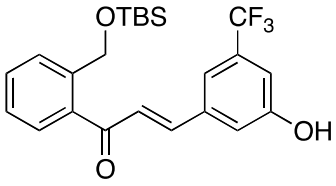

(*E*)-1-(2-((*tert*-butyldimethylsilyloxy)methyl)phenyl)-3-(3-hydroxy-5-(trifluoromethyl) phenyl)prop-2-en-1-one (S4). Vinyl ketone **52** (300 mg, 1.085 mmol, 1.2 equiv.), 3-bromo-5-trifluoromethylphenol (218 mg, 0.904 mmol, 1 equiv.), NBu_4Cl (25 mg, 0.0904 mmol, 0.1 equiv.), and $PdCl_2$(dtbpf) (59 mg, 0.0904 mmol, 0.1 equiv) were suspended in DMA (2.7 mL) before NCy_2Me (265 mg, 1.356 mmol, 1.5 equiv.) was added and the reaction stirred vigorously at 85 ºC in a sealed tube for 16 h. The reaction was cooled to room temperature before being diluted with 8 mL water and extracted with Et_2O (4 x

8 mL), organics combined, dried (Na_2SO_4), filtered, and concentrated by rotary evaporation. Purification by silica flash chromatography (10% → 30% EtOAc in hexanes) yielded the product (**S4**) as a white solid (290 mg, 74%).

IR (ATR): 3372, 2955, 291, 2885, 2858, 1601, 1449, 1369, 1310, 1258, 1219, 1173, 1130, 1098, 1024, 981, 911, 839, 815, 778, 736, 690, 669, 620. **^{1}H-NMR** ((500 MHz; $CDCl_3$): δ 7.73 (d, *J* = 7.8 Hz, 1H), 7.61 (d, *J* = 7.6 Hz, 1H), 7.54 (t, *J* = 7.5 Hz, 1H), 7.46 (d, *J* = 16.0 Hz, 1H), 7.38-7.35 (m, 2H), 7.23 (d, *J* = 16.0 Hz, 2H), 7.12 (s, 1H), 6.08 (s, 1H), 4.96 (s, 2H), 0.92 (s, 9H), 0.09 (s, 6H). **^{13}C-NMR (**126 MHz; $CDCl_3$): δ 195.1, 156.6, 143.8, 142.0, 137.0, 136.0, 132.8, 131.7, 128.5, 127.60, 127.52, 126.6, 123.5, 118.1, 117.3, 114.4, 63.1, 26.0, 18.4, -5.4. **^{19}F-NMR (**126 MHz; $CDCl_3$): δ –63.0. **HRMS** (ESI) *m/z* calcd for $C_{23}H_{28}O_3F_3Si$ ($[M+H]^+$) 437.1760; found 437.1739.

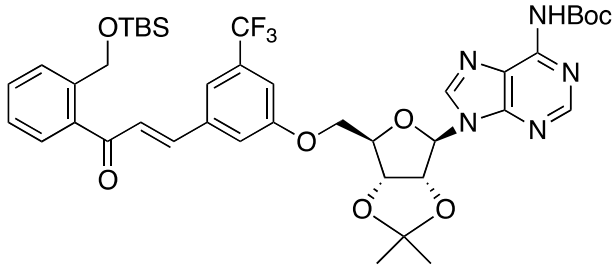

6-*N*-*t*-Butoxycarbonyl-2´,3´-*O*-isopropylidene-5´-*O*-([*E*]-1-[2-([*tert*-butyldimethylsilyloxy]methyl)phenyl]-3-(3-hydroxy-5-(trifluoromethyl) phenyl) prop-2-en-1-one)adenosine (S5). DIAD (125 mg, 0.619 mmol, 1.5 equiv.) was added dropwise to a stirring solution of phenol **S4** (270 mg, 0.619 mmol, 1 equiv.), protected adenosine **42** (126 mg, 0.309 mmol, 1 equiv.), and resin bound PPh_3 (507 mg, 0.619 mmol, 32 % by weigh, 1.5 equiv.) in THF (6 mL) at 0 ºC before being allowed to return to room temperature. After 14 h, the reaction was quenched with water (0.2 mL) and filtered through a pad of celite, the pad washed with EtOAc, and solvent removed by rotary evaporation. Purification by silica flash chromatography (40% → 60% EtOAc in hexanes) yielded the product (**S5**) as a white solid (215 mg, 84%).

IR (ATR): 2982, 2955, 2934, 2857, 2244, 1753, 1717, 1666, 1610, 1521, 1464, 1359, 1326, 1300, 1233, 1173, 1133, 1104, 1080, 1020, 977, 911, 587, 839, 815, 778, 734, 689, 646. **^{1}H-NMR** ((600 MHz; $CDCl_3$): δ 8.76 (s, 1H), 8.04 (s, 1H), 7.92 (s, 1H), 7.76 (d, *J* = 7.7 Hz, 1H), 7.63 (d, *J* = 7.6 Hz, 1H), 7.55 (td, *J* = 7.6, 0.9 Hz, 1H), 7.44 (d, *J* = 16.0 Hz, 1H), 7.39 (dd, *J* = 13.8, 5.5

Hz, 2H), 7.26 (s, 1H), 7.22 (d, *J* = 16.0 Hz, 1H), 7.15 (s, 1H), 7.03 (s, 1H), 6.22 (d, *J* = 2.2 Hz, 1H), 5.52 (dd, *J* = 6.2, 2.2 Hz, 1H), 5.21 (dd, *J* = 6.2, 3.3 Hz, 1H), 4.96 (s, 2H), 4.70-4.68 (m, 1H), 4.29 (ddd, *J* = 48.5, 10.0, 4.9 Hz, 2H), 1.67 (s, 3H), 1.55 (s, 9H), 1.44 (s, 3H), 0.93 (s, 9H), 0.09 (s, 6H). **^{13}C-NMR (**126 MHz; $CDCl_3$): δ 194.1, 158.7, 153.2, 150.27, 150.16, 149.5, 142.9, 142.3, 141.4, 137.3, 135.9, 132.8, 131.6, 128.5, 127.9, 127.3, 126.5, 123.4, 122.4, 118.0, 117.1, 114.9, 113.0, 91.4, 85.3, 84.4, 82.4, 81.7, 68.5, 63.0, 28.1, 27.2, 26.0, 25.4, 18.4, -5.3. **^{19}F-NMR (**126 MHz; $CDCl_3$): δ –63.0. **HRMS** (ESI) *m/z* calcd for $C_{41}H_{51}N_5O_8F_3Si$ ($[M+H]^+$) 826.3459; found 826.3453.

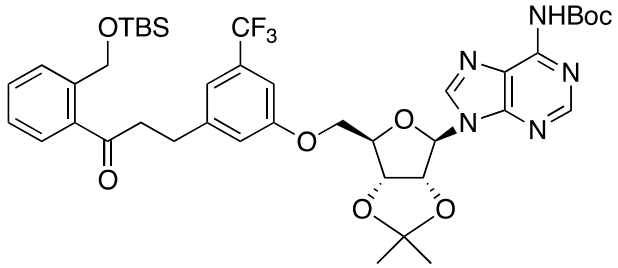

6-*N*-*t*-Butoxycarbonyl-2´,3´-*O*-isopropylidene-5´-*O*-(1-[2-(hydroxymethyl) phenyl]-3-(3-hydroxy-5-(trifluoromethyl)phenyl)prop-2-en-1-one) adenosine (S6). Phenylsilane (56 mg, 521 µmol, 2 equiv.) was added to a stirring solution of intermediate **S5** (215 mg, 260.3 µmol, 1 equiv.) and Strykers catalyst (51 mg, 26.0 µmol, 0.09 equiv.) in toluene (5 mL) and room temperature. After 16 h, the reaction was quenched with saturated ammonium chloride (10 mL) and stirred for 5 min before 10% ammonium hydroxide (10 mL) was added and the reaction stirred for an additional 5 min. The reaction was then extracted with Et_2O (4 x 20 mL), organics combined, dried (Na_2SO_4), filtered, concentrated by rotary evaporation. Purification by silica flash chromatography (50% → 100% EtOAc in hexanes) yielded the product (**S6**) as a white solid (207 mg, 96%).

IR (ATR): 2982, 2956, 2933, 2902, 2858, 2245, 1753, 1681, 1610, 1587, 1522, 1463, 1359, 1329, 1233, 1172, 1144, 1128, 1105, 1080, 1107, 972, 911, 854, 839, 814, 777, 734, 702, 670, 646. **^{1}H-NMR** ((600 MHz; $CDCl_3$): δ 8.78 (s, 1H), 8.05 (s, 1H), 7.95 (s, 1H), 7.82 (d, *J* = 7.8 Hz, 1H), 7.73-7.71 (m, 1H), 7.55-7.52 (m, 1H), 7.34-7.31 (m, 1H), 7.10 (s, 1H), 6.84 (s, 2H), 6.23 (d, *J* = 2.2 Hz, 1H), 5.50 (dd, *J* = 6.2, 2.3 Hz, 1H), 5.17 (dd, *J* = 6.2, 3.1 Hz, 1H), 5.00 (s, 2H), 4.68 (q, *J* = 3.9 Hz, 1H), 4.23 (ddd, *J* = 55.1, 10.1, 4.6 Hz, 2H), 3.25 (t, *J* = 7.6 Hz, 2H), 3.02 (t, *J* = 7.5 Hz, 2H), 1.66 (s, 3H), 1.55 (s, 9H), 1.43 (s,

3H), 0.95 (s, 9H), 0.11 (s, 6H). **^{13}C-NMR (**126 MHz; $CDCl_3$): δ 201.4, 158.3, 153.2, 150.3, 150.1, 149.5, 144.2, 143.3, 141.3, 134.5, 132.3, 132.1, 128.7, 126.9, 126.4, 123.8, 122.3, 118.4, 118.2, 114.8, 109.0, 91.6, 85.3, 84.5, 82.4, 81.7, 68.2, 63.5, 41.8, 30.0, 28.1, 27.3, 26.0, 25.4, 18.4, -5.3. **^{19}F-NMR (**126 MHz; $CDCl_3$): δ –62.7. **HRMS** (ESI) *m/z* calcd for $C_{41}H_{53}N_5O_8F_3Si$ ($[M+H]^+$) 828.3610; found 828.3616.

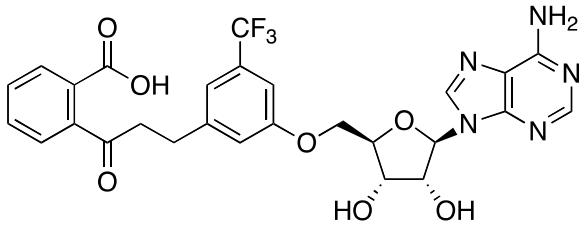

5´-*O*-([2-(Carboxyl)phenyl]3-(3-hydroxy-5-(trifluoromethyl)phenyl) propanoyl)adenosine (63). TBAF (786 µL, 786.0 µmol, 1M in THF, 3 equiv.) was added to intermediate **S6** (217 mg, 260.3 µmol, 1 equiv.) in THF (5 mL) at 0 ºC before and stirred for 1 h. $CaCO_3$ (349 mg, 3.486 mmol, 10 equiv.) and MeOH (3 mL) was added and the reaction stirred for 15 min before sulfonic acid resin (Dowex 50WX8, 500 mg) was added and the reaction stirred for an additional 10 min. The reaction was then filtered through a pad of celite and concentrated by rotary evaporation. The residue was reconstituted in MeCN (5 mL) before water (45 mg, 2.5 mmol, 10 equiv.), NMO (295 mg, 2.521 mmol, 10 equiv.), and TPAP (8.9 mg, 25 µmol, 0.1 equiv.) were added and stirred at room temperature for 14 h. The reaction was then quenched with isopropanol and 1 M $KHSO_4$ (1 mL) was added before the reaction was diluted with water (20 mL), extracted with EtOAc (4 x 20 mL), organics combined, dried (Na_2SO_4), filtered, concentrated by rotary evaporation, and dried under high vacuum 1 h. The residue was reconstituted in CH_2Cl_2 (8 mL) and cooled to 0 ºC before TFA (8 mL) and water (0.8 mL) added and the reaction stirred for 4 h while returning to room temperature. Concentration by rotary evaporation, purification by preparative HPLC (5% → 45% MeCN in H_2O with 0.1% TFA), and lyophilization yielded the product **63** as a fluffy white solid (46 mg, 31% over 4 steps).

IR (ATR): 3346, 2509, 2247, 2076, 1756, 1693, 1608, 1455, 1353, 1320, 1289, 1245, 1205, 1126, 1055, 982, 898, 842, 802, 767, 726, 703, 644. **^{1}H-NMR** ((600 MHz; MeOD): δ 8.43 (s, 1H), 8.34 (s, 1H), 7.84-7.81 (m, 1H), 7.72-7.68 (m, 1H), 7.60-7.57 (m, 2H), 7.05-6.96 (m, 3H), 6.14 (d, *J* = 4.4 Hz,

1H), 4.76 (t, *J* = 4.7 Hz, 1H), 4.53 (t, *J* = 5.0 Hz, 1H), 4.43-4.38 (m, 2H), 4.28 (dd, *J* = 10.8, 3.5 Hz, 1H), 2.89-2.50 (m, 4H). **^{13}C-NMR (**126 MHz; MeOD): δ 160.4, 153.13, 153.05, 153.03, 150.1, 147.1, 145.77, 145.71, 145.65, 143.22, 143.18, 132.9, 131.58, 131.43, 125.4, 124.1, 120.5, 119.4, 118.9, 110.4, 90.7, 84.8, 76.0, 71.8, 68.8, 49.3, 31.0. **^{19}F-NMR (**126 MHz; MeOD): δ –64.07. **HRMS** (ESI) *m/z* calcd for $C_{27}H_{25}N_5O_7F_3$ ($[M+H]^+$) 588.1706; found 588.1681.

G. MenE Biochemical Assay

Enzyme inhibition studies were performed in 20 mM $NaHPO_4$ buffer (pH 7.4) containing 150 mM NaCl and 1 mM $MgCl_2$ using a MenE-MenB coupled assay in which MenE is rate-limiting. IC_{50} values were determined in reaction mixtures containing OSB (60 μM), ATP (240 μM), CoA (240 μM), *mt*MenB (2.5 μM), and varying inhibitor concentrations (5 − 250 μM). Reactions were initiated by addition of ecMenE (50 nM), and the production of DHNA-CoA was monitored at 392 nm (ε^{392} = 4000 M^{-1} cm^{-1}).

H. Docking of Inhibitors to MenE

Protein Preparation. The OSB-AMS•MenE co-crystal structure (PDB: 5C5H) was processed using the Protein Preparation Wizard in the Schrödinger suite (v2017.2). Bond orders were assigned, hydrogen's added, and waters beyond 5 Å were deleted. The protonation and tautomeric states of the protein-ligand complex were generated using EPIK at pH 7.4. Hydrogen bond assignment and optimization was performed with PROPKA to sample hydrogen bonding and orientation of water molecules. Non-bridging waters (< 2 hydrogen bonds) were removed. Geometric refinement was performed using OPLS_3 force field restrained minimization to a heavy atom convergence of 0.3 Å

Ligand Preparation. Ligand preparation was performed using Ligprep in the Schrödinger suite (v2017.2). Lowest energy conformers were obtained using OPLS_3 force field optimization. Ionization and tautomeric states were generated using EPIK at pH 7.4.

Grid Generation. Using the Schrödinger suite (v2017.2) receptor grid generator, the receptor-binding site was defined as the area around the co-crystalized ligand with a cube grid of 10 Å side length. Nonpolar parts of the receptor were softened using Van der Waals radius scaling (factor 1.0 with partial cutoff of 0.25). No constraints were defined and rotations allowed for all hydroxyl groups in the defined binding pocket.

Docking Using Soft Receptor. Using Glide (v7.2), ligands were docked to MenE using Glide XP docking precision. Flexible ligand sampling was used and EPIK state penalties applied to docking scores. Post-docking minimization was performed for all poses.

Table 4.2.1 Docking scores of OSB-AMS linker analogues. OSB-AMS (**1**) docking score = –13.78 kcal/mol.

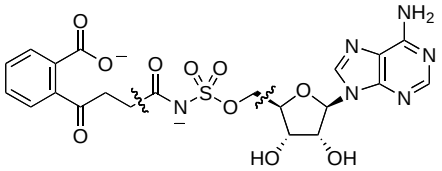

OSB-AMS (**1**)

Entry	Analogue	Docking Score (kcal/mol)	Entry	Analogue	Docking Score (kcal/mol)
13	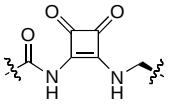	–13.76	22	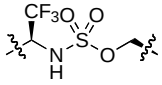	–13.27
14	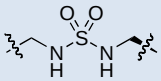	–14.2	23	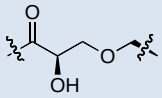	–14.70
15	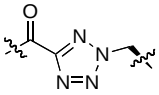	–13.98	24	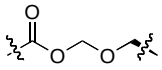	–13.62
16	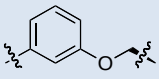	–14.03	S7	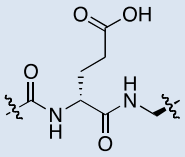	–15.27
17	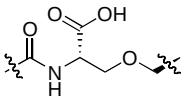	–14.63	S8	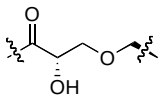	–15.25
18	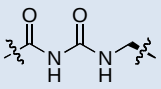	–13.61	S9	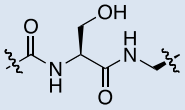	–14.94
19	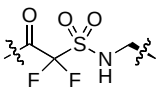	–13.69	S11	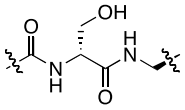	–14.55
20	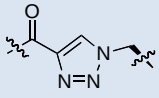	–13.32	S12	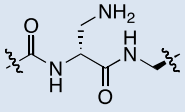	–14.50
21	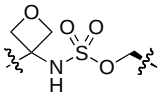	–13.69	S13	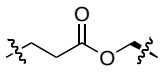	–14.48

Table 4.2.2 Docking scores of OSB-AMS linker analogues. OSB-AMS (**1**) docking score = –13.78 kcal/mol.

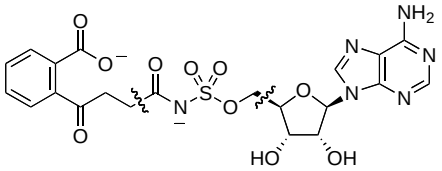

OSB-AMS (**1**)

Entry	Analogue	Docking Score (kcal/mol)	Entry	Analogue	Docking Score (kcal/mol)
S14	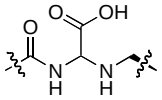	–14.48	S23	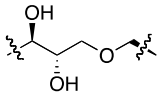	–14.05
S15	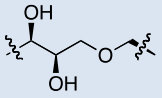	–14.42	S24	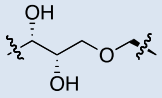	–14.05
S16	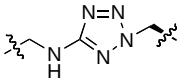	–14.32	S25	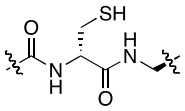	–13.98
S17	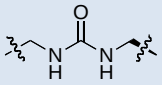	–14.28	S26	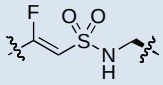	–13.95
S18	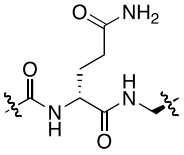	–14.22	S27	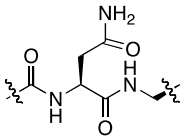	–13.91
S19	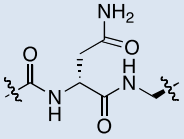	–14.22	S28	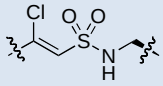	–13.85
S20	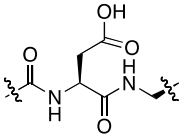	–14.09	S29	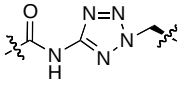	–13.73
S21	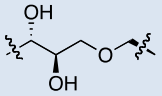	–14.08	S30	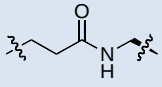	–13.71
S22	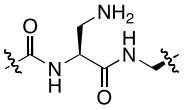	–14.08	S31	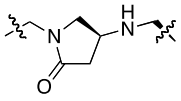	–13.63

Table 4.2.3 Docking scores of OSB-AMS linker analogues. OSB-AMS (**1**) docking score = –13.78 kcal/mol.

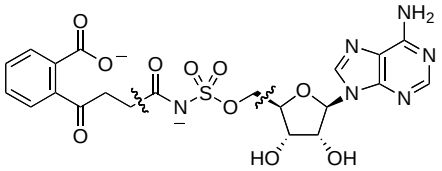

OSB-AMS (**1**)

Entry	Analogue	Docking Score (kcal/mol)	Entry	Analogue	Docking Score (kcal/mol)
S32	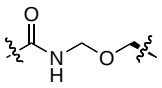	–13.62	S41	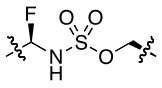	–13.30
S33	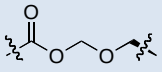	–13.62	S42	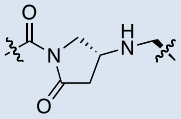	–13.30
S34	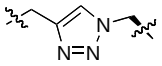	–13.60	S43	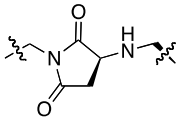	–13.29
S35	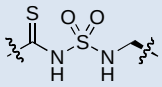	–13.54	S44	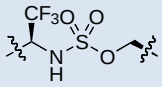	–13.27
S36	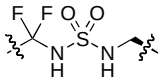	–13.53	S45	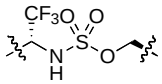	–13.26
S37	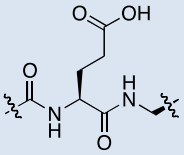	–13.45	S46	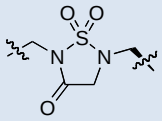	–13.19
S38	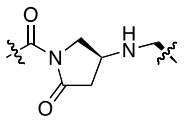	–13.38	S47	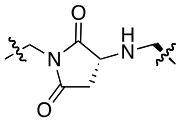	–13.18
S39	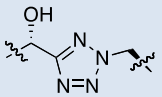	–13.36	S48	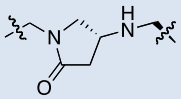	–13.17
S40	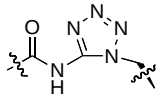	–13.31	S49	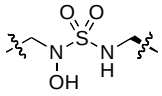	–13.01

Table 4.2.4 Docking scores of OSB-AMS linker analogues. OSB-AMS (**1**) docking score = –13.78 kcal/mol.

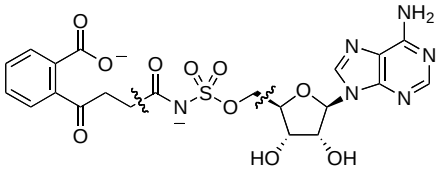

OSB-AMS (**1**)

Entry	Analogue	Docking Score (kcal/mol)	Entry	Analogue	Docking Score (kcal/mol)
S50	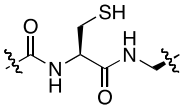	–12.98	S58	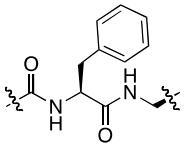	–11.90
S51	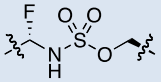	–12.95	S59	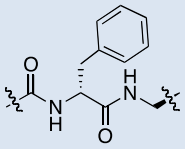	–10.76
S52	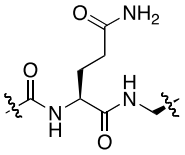	–12.91	S60	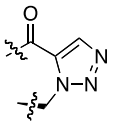	> –10
S53	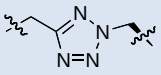	–12.84	S61	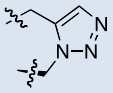	> –10
S54	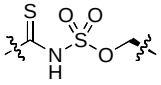	–12.83	S62	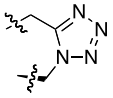	> –10
S55	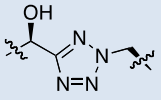	–12.79	S63	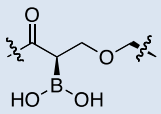	> –10
S56	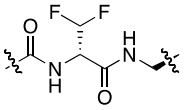	–12.55	S64	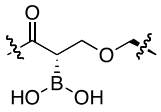	> –10
S57	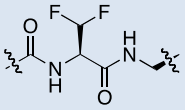	–12.42	S65	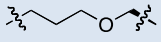	> –10

Table 4.2.5 Docking scores of OSB-AMS linker analogues. OSB-AMS (**1**) docking score = –13.78 kcal/mol.

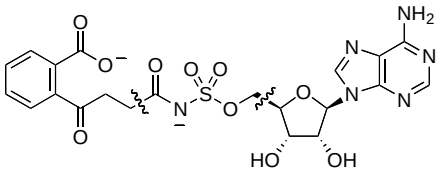

OSB-AMS (**1**)

Entry	Analogue	Docking Score (kcal/mol)	Entry	Analogue	Docking Score (kcal/mol)
S66	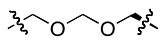	> –10			
S67	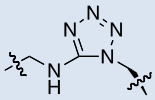	> –10			
S68	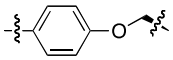	> –10			
S69	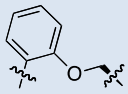	> –10			
S70	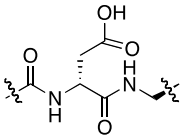	> –10			
S71	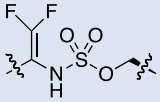	> –10			
S72	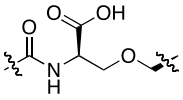	> –10			
S73	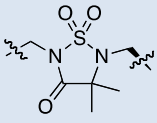	> –10			

4.5. References

1. Ochsner, U. A.; Sun, X.; Jarvis, T.; Critchley, I.; Janjic, N., Aminoacyl-trna synthetases: Essential and still promising targets for new anti-infective agents. *Expert Opin. Investig. Drugs* **2007,** *16* (5), 573–593.

2. Benjamin P. Duckworth; Nelson, K. M.; Aldrich, C. C., Adenylating enzymes in *mycobacterium tuberculosis* as drug targets. *Curr. Top. Med. Chem.* **2012,** *12* (7), 766–796.

3. Cisar, J. S.; Tan, D. S., Small molecule inhibition of microbial natural product biosynthesis-an emerging antibiotic strategy. *Chem. Soc. Rev.* **2008,** *37* (7), 1320–1329.

4. Ueda, H.; Shoku, Y.; Hayashi, N.; Mitsunaga, J.-i.; In, Y.; Doi, M.; Inoue, M.; Ishida, T., X-ray crystallographic conformational study of 5′ -o-[n-(l-alanyl)-sulfamoyl]adenosine, a substrate analogue for alanyl-trna synthetase. *Biochim. Biophys. Acta* **1991,** *1080* (2), 126–134.

5. Somu, R. V.; Boshoff, H.; Qiao, C.; Bennett, E. M.; Barry, C. E.; Aldrich, C. C., Rationally designed nucleoside antibiotics that inhibit siderophore biosynthesis of *mycobacterium tuberculosis*. *J. Med. Chem.* **2006,** *49* (1), 31–34.

6. Finking, R.; Neumüller, A.; Solsbacher, J.; Konz, D.; Kretzschmar, G.; Schweitzer, M.; Krumm, T.; Marahiel, M. A., Aminoacyl adenylate substrate analogues for the inhibition of adenylation domains of nonribosomal peptide synthetases. *ChemBioChem* **2003,** *4* (9), 903–906.

7. Ferreras, J. A.; Ryu, J.-S.; Di Lello, F.; Tan, D. S.; Quadri, L. E. N., Small-molecule inhibition of siderophore biosynthesis in mycobacterium tuberculosis and yersinia pestis. *Nat. Chem. Biol.* **2005,** *1* (1), 29–32.

8. Brownell, J. E.; Sintchak, M. D.; Gavin, J. M.; Liao, H.; Bruzzese, F. J.; Bump, N. J.; Soucy, T. A.; Milhollen, M. A.; Yang, X.; Burkhardt, A. L.; Ma, J.; Loke, H.-K.; Lingaraj, T.; Wu, D.; Hamman, K. B.; Spelman, J. J.; Cullis, C. A.; Langston, S. P.; Vyskocil, S.; Sells, T. B.; Mallender, W. D.; Visiers, I.; Li, P.; Claiborne, C. F.; Rolfe, M.; Bolen, J. B.; Dick, L. R., Substrate-assisted inhibition of ubiquitin-like protein-activating enzymes: The nedd8 e1 inhibitor mln4924 forms a nedd8-amp mimetic in situ. *Mol. Cell* **2010,** *37* (1), 102–111.

9. Lu, X.; Olsen, S. K.; Capili, A. D.; Cisar, J. S.; Lima, C. D.; Tan, D. S., Designed semisynthetic protein inhibitors of ub/ubl e1 activating enzymes. *J. Am. Chem. Soc.* **2010,** *132* (6), 1748–1749.

10. Olsen, S. K.; Capili, A. D.; Lu, X.; Tan, D. S.; Lima, C. D., Active site remodelling accompanies thioester bond formation in the sumo e1. *Nature* **2010,** *463* (7283), 906–912.

11. Koroniak, L.; Ciustea, M.; Gutierrez, J. A.; Richards, N. G. J., Synthesis and characterization of an n-acylsulfonamide inhibitor of human asparagine synthetase. *Org. Lett.* **2003,** *5* (12), 2033–2036.

12. Waller, C. W.; Patrick, J. B.; Fulmor, W.; Meyer, W. E., The structure of nucleocidin. *J. Am. Chem. Soc.* **1957,** *79* (4), 1011–1012.

13. Florini, J. R.; Bird, H. H.; Bell, P. H., Inhibition of protein synthesis in vitro and in vivo by nucleocidin, an antitrypanosomal antibiotic. *J. Biol. Chem.* **1966,** *241* (5), 1091–1098.

14. Isono, K. U., Masakazu; Kusakabe, Hiroo; Miyata, Nobuo; Koyama, Tadoyoshi; Ubukata, Makoto; Sethi, Satinder, K.; McCloskey, James, A., Dealanylascamyciin, nucleoside antibiotics from streptomyces sp. *J. Antibiot.* **1984,** *37* (6), 670–672.

15. Osada, H.; Isono, K., Mechanism of action and selective toxicity of ascamycin, a nucleoside antibiotic. *Antimicrob. Agents Chemother.* **1985,** *27* (2), 230–233.

16. Takahashi, E. B., Teruhiko, A new nucleosidic antibiotic at-265. *J. Antibiot.* **1982,** *35* (8), 939–947.

17. Gulick, A. M., Conformational dynamics in the acyl-coa synthetases, adenylation domains of non-ribosomal peptide synthetases, and firefly luciferase. *ACS Chem. Biol.* **2009,** *4* (10), 811–827.

18. Davis, T. D.; Gerry, C. J.; Tan, D. S., General platform for systematic quantitative evaluation of small-molecule permeability in bacteria. *ACS Chem. Biol.* **2014,** *9* (11), 2535–2544.

19. Colmenarejo, G., In silico prediction of plasma and tissue protein binding. In *Reference module in chemistry, molecular sciences and chemical engineering*, Elsevier: 2014.

20. Ghafourian, T.; Amin, Z., Qsar models for the prediction of plasma protein binding. *Bioimpacts* **2013,** *3* (1), 21–27.

21. Alex, A., Physicochemical profiling (solubility, permeability and charge state). *Curr. Top. Med. Chem.* **2001,** *1* (4), 277–351.

22. Yin, J.; Wang, J., Renal drug transporters and their significance in drug–drug interactions. *Acta Pharmaceutica Sinica B* **2016,** *6* (5), 363–373.

23. Bloch, A.; Coutsogeorgopoulos, C., Inhibition of protein synthesis by 5'-sulfamoyladenosine. *Biochemistry* **1971,** *10* (24), 4394–4398.

24. Nelson, K. M.; Viswanathan, K.; Dawadi, S.; Duckworth, B. P.; Boshoff, H. I.; Barry, C. E.; Aldrich, C. C., Synthesis and pharmacokinetic evaluation of siderophore biosynthesis inhibitors for *mycobacterium tuberculosis*. *J. Med. Chem.* **2015,** *58* (14), 5459–5475.

25. Dawadi, S.; Viswanathan, K.; Boshoff, H. I.; Barry, C. E.; Aldrich, C. C., Investigation and conformational analysis of fluorinated nucleoside antibiotics targeting siderophore biosynthesis. *J. Org. Chem.* **2015,** *80* (10), 4835–4850.

26. Krajczyk, A.; Zeidler, J.; Januszczyk, P.; Dawadi, S.; Boshoff, H. I.; Barry Iii, C. E.; Ostrowski, T.; Aldrich, C. C., 2-aryl-8-aza-3-deazaadenosine analogues of 5′ -o-[n-(salicyl)sulfamoyl]adenosine: Nucleoside antibiotics that block siderophore biosynthesis in mycobacterium tuberculosis. *Biorg. Med. Chem.* **2016,** *24* (14), 3133–3143.

27. Gupte, A.; Boshoff, H. I.; Wilson, D. J.; Neres, J.; Labello, N. P.; Somu, R. V.; Xing, C.; Barry, C. E.; Aldrich, C. C., Inhibition of siderophore biosynthesis by 2-triazole substituted analogues of 5′ -o-[n-(salicyl)sulfamoyl]adenosine: Antibacterial nucleosides effective against *mycobacterium tuberculosis*. *J. Med. Chem.* **2008,** *51* (23), 7495–7507.

28. Somu, R. V.; Wilson, D. J.; Bennett, E. M.; Boshoff, H. I.; Celia, L.; Beck, B. J.; Barry, C. E.; Aldrich, C. C., Antitubercular nucleosides that inhibit siderophore biosynthesis: Sar of the glycosyl domain. *J. Med. Chem.* **2006,** *49* (26), 7623–7635.

29. Qiao, C.; Gupte, A.; Boshoff, H. I.; Wilson, D. J.; Bennett, E. M.; Somu, R. V.; Barry, C. E.; Aldrich, C. C., 5‘-o-[(n-acyl)sulfamoyl]adenosines as antitubercular agents that inhibit mbta: An adenylation enzyme required for siderophore biosynthesis of the mycobactins. *J. Med. Chem.* **2007,** *50* (24), 6080–6094.

30. Neres, J.; Labello, N. P.; Somu, R. V.; Boshoff, H. I.; Wilson, D. J.; Vannada, J.; Chen, L.; Barry, C. E.; Bennett, E. M.; Aldrich, C. C., Inhibition of siderophore biosynthesis in *mycobacterium tuberculosis* with nucleoside bisubstrate analogues: Structure−activity relationships

of the nucleobase domain of 5′ -o-[n-(salicyl)sulfamoyl]adenosine. *J. Med. Chem.* **2008,** *51* (17), 5349–5370.

31. Evans, C. E.; Matarlo, J. S.; Tonge, P. J.; Tan, D. S., Stereoselective synthesis, docking, and biological evaluation of difluoroindanediol-based mene inhibitors as antibiotics. *Org. Lett.* **2016**, 6384–6387.

32. Tian, Y.; Suk, D.-H.; Cai, F.; Crich, D.; Mesecar, A. D., Bacillus anthracis o-succinylbenzoyl-coa synthetase: Reaction kinetics and a novel inhibitor mimicking its reaction intermediate. *Biochemistry* **2008,** *47* (47), 12434–12447.

33. Lu, X.; Zhang, H.; Tonge, P. J.; Tan, D. S., Mechanism-based inhibitors of mene, an acyl-coa synthetase involved in bacterial menaquinone biosynthesis. *Bioorg. Med. Chem. Lett.* **2008,** *18* (22), 5963–5966.

34. Lu, X.; Zhou, R.; Sharma, I.; Li, X.; Kumar, G.; Swaminathan, S.; Tonge, P. J.; Tan, D. S., Stable analogues of osb-amp: Potent inhibitors of mene, the o-succinylbenzoate-coa synthetase from bacterial menaquinone biosynthesis. *ChemBioChem* **2012,** *13* (1), 129–136.

35. Matarlo, J. S.; Lu, Y.; Daryaee, F.; Daryaee, T.; Ruzsicska, B.; Walker, S. G.; Tonge, P. J., A methyl 4-oxo-4-phenylbut-2-enoate with in vivo activity against mrsa that inhibits menb in the bacterial menaquinone biosynthesis pathway. *ACS Infect. Dis.* **2016,** *2* (5), 329–340.

36. Matarlo, J. S.; Evans, C. E.; Sharma, I.; Lavaud, L. J.; Ngo, S. C.; Shek, R.; Rajashankar, K. R.; French, J. B.; Tan, D. S.; Tonge, P. J., Mechanism of mene inhibition by acyl-adenylate analogues and discovery of novel antibacterial agents. *Biochemistry* **2015,** *54* (42), 6514–6524.

37. Lancefield, C. S.; Ojo, O. S.; Tran, F.; Westwood, N. J., Isolation of functionalized phenolic monomers through selective oxidation and c-o bond cleavage of the β-o-4 linkages in lignin. *Angew. Chem. Int. Ed.* **2015,** *54* (1), 258–262.

38. Iranpoor, N.; Firouzabadi, H.; Aghapour, G.; Vaez zadeh, A. R., Triphenylphosphine/2,3-dichloro-5,6-dicyanobenzoquinone as a new, selective and neutral system for the facile conversion of alcohols, thiols and selenols to alkyl halides in the presence of halide ions. *Tetrahedron* **2002,** *58* (43), 8689–8693.

39. Kotch, F. W.; Sidorov, V.; Lam, Y.-F.; Kayser, K. J.; Li, H.; Kaucher, M. S.; Davis, J. T., Water-mediated association provides an ion pair receptor. *J. Am. Chem. Soc.* **2003,** *125* (49), 15140–15150.

CHAPTER 5

CONCLUSIONS AND FUTURE DIRECTIONS

5.1. Conclusions

A series of keto-acid and lactol analogues of OSB-AMS were designed and synthesized to determine the active pharmacophore for MenE and discover an analogue that exhibited increased antimicrobial activity (Figure 5.1A).[1]

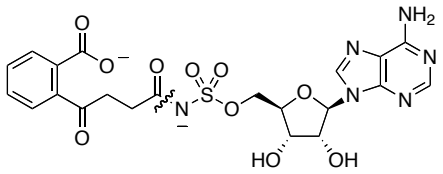

(**1**) OSB-AMS

A)

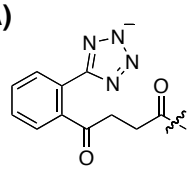

(**2**) tetrazole
IC_{50} = 2.2 μM

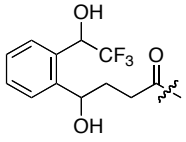

(**3**) trifluoroethanol
IC_{50} = 125 μM

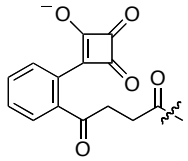

(**4**) squarate
IC_{50} = 0.17 μM

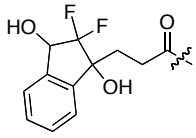

(**5**) difluoroindanediol
IC_{50} = 1.5 μM

B)

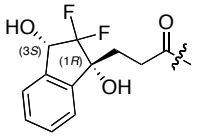

(1*R*,3*S*)-**5**

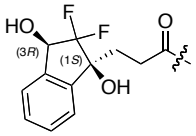

(1*S*,3*R*)-**5**

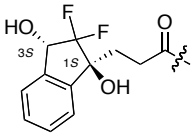

(1*S*,3*S*)-**5**

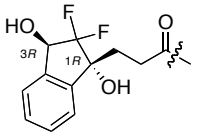

(1*R*,3*R*)-**5**

Figure 5.1. Selected analogues of OSB-AMS A) Biochemically active keto-acid and lactol analogues of OSB-AMS, IC50s reported against E. coli MenE. B) The four diastereomers of the difluoroindanediol analogue.

En route to a proposed indanol analogue, we discovered that the indanol motif was not sufficiently acid stable and degraded in the presence of

the relatively acidic acyl-sulfamate. We modified the proposed structure by substituting fluorine at the α-keto position, which inductively stabilized the tertiary alcohol of the indanol motif and allowed for the synthesis of the difluoroindanediol analogue **5**. Ultimately, this analogue, although only a low-*μ*M inhibitor of MenE in biochemical assays, was the only analogue to have improved antimicrobial activity versus OSB-AMS. While the initial rescue studies using exogenous menaquinone (MK-4) suggested that the mechanism of action of the difluoroindanediol analogue was inhibition of menaquinone, the high similarity between the active concentrations of drug in biochemical and antimicrobial assays suggested that the mechanism of action was not through inhibition of MenE. To elucidate the mechanism of action of the difluoroindanediol analogue, we designed and executed a stereoselective synthesis of the four diastereomeric difluoroindanediol analogues (Figure 5.1B) and tested their individual activities against MenE.[2] In so doing, we discovered that only one of the four diastereomers was active against MenE in biochemical assays (Table 5.1). Docking studies suggested that the active diastereomer is best suited to fill the OSB binding pocket, and retain key interactions in the binding pocket. Interestingly, this docking is through direct interaction with a conserved threonine rather than the bridging waters with which the carboxylate of OSB interacts. Upon testing the diastereomers in antimicrobial assays, we discovered that all four diastereomers are equipotent against a variety of bacteria and showed no inhibition of menaquinone biosynthesis in LC-MS/MS studies examining the levels of endogenous menaquinone in methicillin-resistant *S. aureus* (MRSA). This indicated that, although the analogues have modest activity against bacteria, the primary mechanism of action is not inhibition of menaquinone biosynthesis and is

instead an unknown mechanism of action. Future work with the difluoroindanediol scaffold should investigate the mechanism of action through generation and sequencing of resistant mutants and pull-down studies using functionalized difluoroindanediol derivatives.

Table 5.1. Biochemical and antimicrobial activity of diastereomeric difluoroindanediols 2.

entry	inhibitor	MenE IC_{50} [μM][a]	*B. subtilis* MIC [μg/mL][b]	MRSA MIC [ug/mL][b,c]	*M. tuberculosis* MIC [μg/mL][b]
1	**5**[d]	18.3 ± 3.7[e]	15.6 (62.5)	15.6 (62.5)	15.6 (62.5)
2	(1*R*,3*S*)-**5**	5.0 ± 1.0	15.6 (31.2)	15.6 (31.2)	15.6 (62.5)
3	(1*S*,3*R*)-**5**	> 200	15.6 (31.2)	31.2 (31.2)	31.2 (62.5)
4	(1*R*,3*R*)-**5**	> 200	15.6 (15.6)	15.6 (15.6)	15.6 (31.2)
5	(1*S*,3*S*)-**5**	> 200	15.6 (15.6)	15.6 (15.6)	31.2 (31.2)
6	AMS[f]	n.d[g]	3.9 (3.9)	1.9 (1.9)	0.16 (0.32)

[a] *E. coli* MenE. [b] MIC values in parentheses determined with addition of exogenous menaquinone-4 (10 mg/mL). [c] MRSA = methicillin-resistant *S. aureus*. [d] Equimolar mixture of four diastereomers, prepared by the original synthetic route.[3] [e] This IC_{50} is higher than the 1.5 mM that we reported previously,[3] due to batch-to-batch variability of the enzyme; IC_{50} values reported herein were all determined with the same batch of enzyme. [f] 5′-O-sulfamoyl-adenosine. [g] n.d. = not determined.

We then began exploring the structure–activity relationships (SAR) of the acyl-sulfamate region of OSB-AMS. We anticipated that efforts in this area would increase favorable physicochemical properties while simultaneously decrease the inherent toxicological liability of the acyl-AMS motif and move our MenE inhibitor platform into more favorable drug-like space.

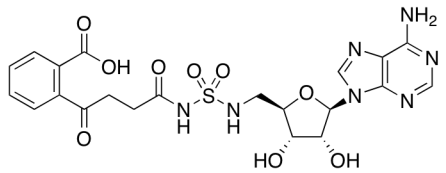

OSB-AMS (1)
ecMenE IC_{50} = 0.025 μM

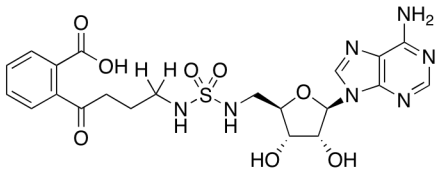

6
ecMenE IC_{50} = 35 μM

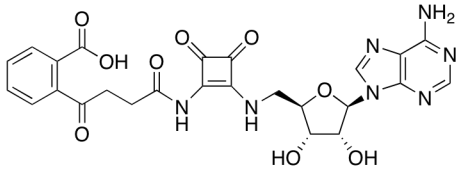

7
ecMenE IC_{50} > 250 μM

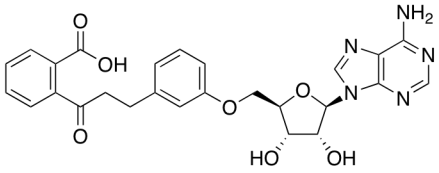

8
ecMenE IC_{50} = 8 μM

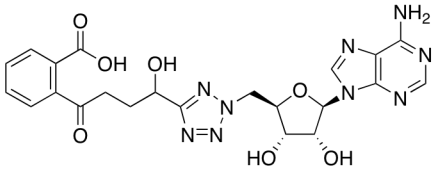

9
ecMenE IC_{50} = 53 μM

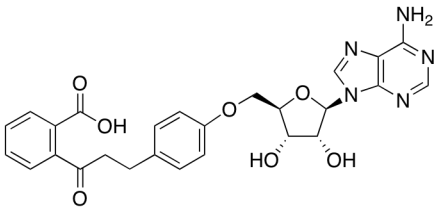

10
ecMenE IC_{50} > 200 μM

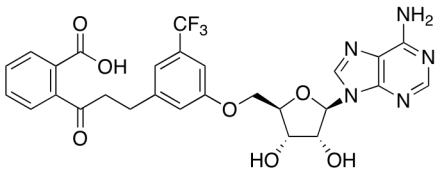

11
ecMenE IC_{50} = 28 μM

Figure 5.2. Biochemical activity of OSB-AMS linker analogues.

We reasoned that conducting a virtual screen of rationally designed OSB-AMS linker analogues using our previously reported docking construct of MenE could narrow a large swath of chemical space within this region. We proposed this would also potentially increase the relative rate of new biochemically active lead compounds. Guided by the results from the docking study, we synthesized a series of OSB-AMS linker analogues before testing

them in biochemical activity assays against MenE (Figure 5.2). Interestingly, more than half of the analogues exhibited activity against MenE. The most promising hit from our first-generation library was the *m*-phenolic linker analogue **8**, which although it substituted nearly the entire acyl-sulfamate for a simple aromatic ring, only exhibited a ~2-log loss of activity versus that of OSB-AMS. While the biochemical activity of early iterations of the aromatic linker analogues is ~2-log worse than that of OSB-AMS, the aromatic linker region presents an excellent platform for extensive diversification and functionalization which will allow for a great breadth of SAR to be performed, giving ample opportunity for increasing potency. Importantly, the aromatic linker analogues are significantly less polar and more stable than OSB-AMS, which offers a possible solution to the ADME and stability problems inherent with OSB-AMS and similar acyl-AMS scaffolds.

5.2. Future Directions

The research reported thus far has highlighted a number of different discovery avenues toward new analogues with improved antimicrobial activity. The difluoroindanediol analogue exhibits improved activity against bacteria versus OSB-AMS, but (as was discussed in Chapter 3) the lack of specificity between the diastereomers in antimicrobial assays suggests a potentially complex or non-specific mechanism of action. When combined with what is only modest activity against bacteria compared to other acyl-AMS based analogues explored by our laboratory, and the relative instability of the difluoroindanediol analogue, which raises significant toxicological concerns, this avenue of further exploration is less attractive than other approaches.

However, these highlighted examples address several areas in which significant improvements can be made to our current line of MenE inhibitors.

5.2.1 Future Directions: SAR of the OSB binding pocket

Although we have explored the SAR of the OSB carboxylate and found it to be relatively intolerant to modification, there is potentially significant work that can be done in this area of the molecule. We have determined that the keto-acid form of OSB-AMS is the active pharmacophore of MenE, but that does not preclude our use of the lactol form to decrease overall polarity of the molecule with the goal of increasing cellular accumulation and antimicrobial activity. A number of different modifications can be considered to the OSB scaffold that would reversibly favor the lactol form in solution (Figure 5.3).

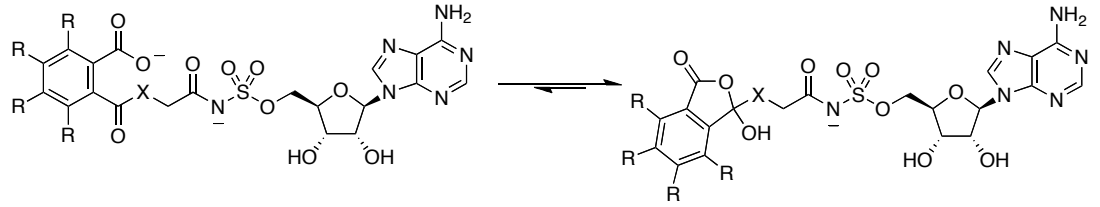

R = H, Me, *t*Bu, OH, OMe, NH_2, NMe_2
X = CH_2, CHF, CF_2

Figure 5.3. Proposed OSB functionalized analogues of OSB-AMS.

One way to potentially favor the lactol form would be by inductively decreasing the acidity of the carboxylate through the use of electron donating substituents on the OSB ring. This would functionally increase the pK_a of the carboxylate, thereby increasing the fraction of OSB-AMS existing as the lactol form at physiological pH. This approach would also open the possibility of gaining additional hydrogen-bonding or hydrophobic interactions between the

scaffold and MenE. Alternatively, the electrophilicity of the *o*-ketone could be increased through a number of different means such as addition of fluorine to the α-keto position of the succinyl chain, which could increase the relative fraction of OSB-AMS existing as the lactol form at physiological pH.

Alternatively, a pro-drug approach where the carboxylate is temporarily masked could be explored. Although we have seen in previous studies that the OSB-carboxylate itself is too hindered to allow for enzymatic cleavage of a simple ester derrivative,[4] other pro-drug strategies could reasonably be employed to temporarily mask the carboxylate, allowing for increased cellular permeability and cleavage after entering the bacterial cytosol.[5-8] When combined with linker analogues discussed in Chapter 4, this could allow for significantly decreased polarity and greatly improved ADME of our MenE inhibitor platform.

5.2.2 Future Directions: SAR of the acyl-phosphate binding pocket

Another area of further exploration is the linker region of the OSB-AMS scaffold. While we discussed a number of analogues in Chapter 4, there is extensive remaining SAR to be performed in this area of the scaffold (Figure 5.4). Although the aromatic and heteroaromatic linker analogues provide the greatest opportunity for diversification and improvement for ADME of the inhibitor scaffold, there are also a number of different analogues from the first-generation docking study that are yet to be explored.

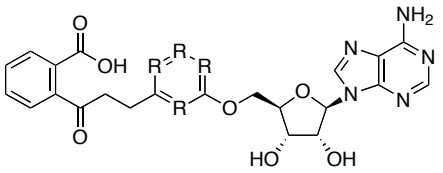

R = CH, N, C-alkyl, COH, COMe, CNH_2, $CNMe_2$, CCN, CCl, CF, CCO_2H, CCO_2Me, CCO_2H, CCO_2NH_2, CO_2NMe_2

Figure 5.4. Proposed aromatic and heteroaromatic OSB-AMS linker analogues.

Additionally, once a new lead inhibitor is found, the designed docking model will allow for rapid screening of second and third-generation virtual libraries to assist in the exploration of each new scaffold. Critically, this work has broad implications across all acyl-AMS inhibitors and could potentially be widely applicable to the field of adenylate-forming enzyme inhibitors.

5.2.3 Future Directions: SAR of the adenosine binding pocket

The last major area of exploration and possible optimization in the OSB-AMS scaffold is the adenosine portion of the molecule. As has been demonstrated with the exponential growth of kinase inhibitors, the adenosine binding pocket of many enzymes is open to a large variety of different scaffolds if properly designed and explored (Figure 5.5A).[9-10]

Returning to the computational docking model of MenE may greatly assist in the probing of the adenosine-binding pocket. Although the adenosine-binding pocket has been examined by other groups exploring other members of the ANL family, in MenE this area is largely unexplored despite it accounting for over half of the mass of the scaffold. Therefore, the first-generation virtual library of analogues to probe this binding pocket would need to be much larger than the one used to originally explore the linker region. The library could focus on any number of substitutions for the adenine ring (Figure 5.5B), or could fully substitute the entire adenosine structure for a

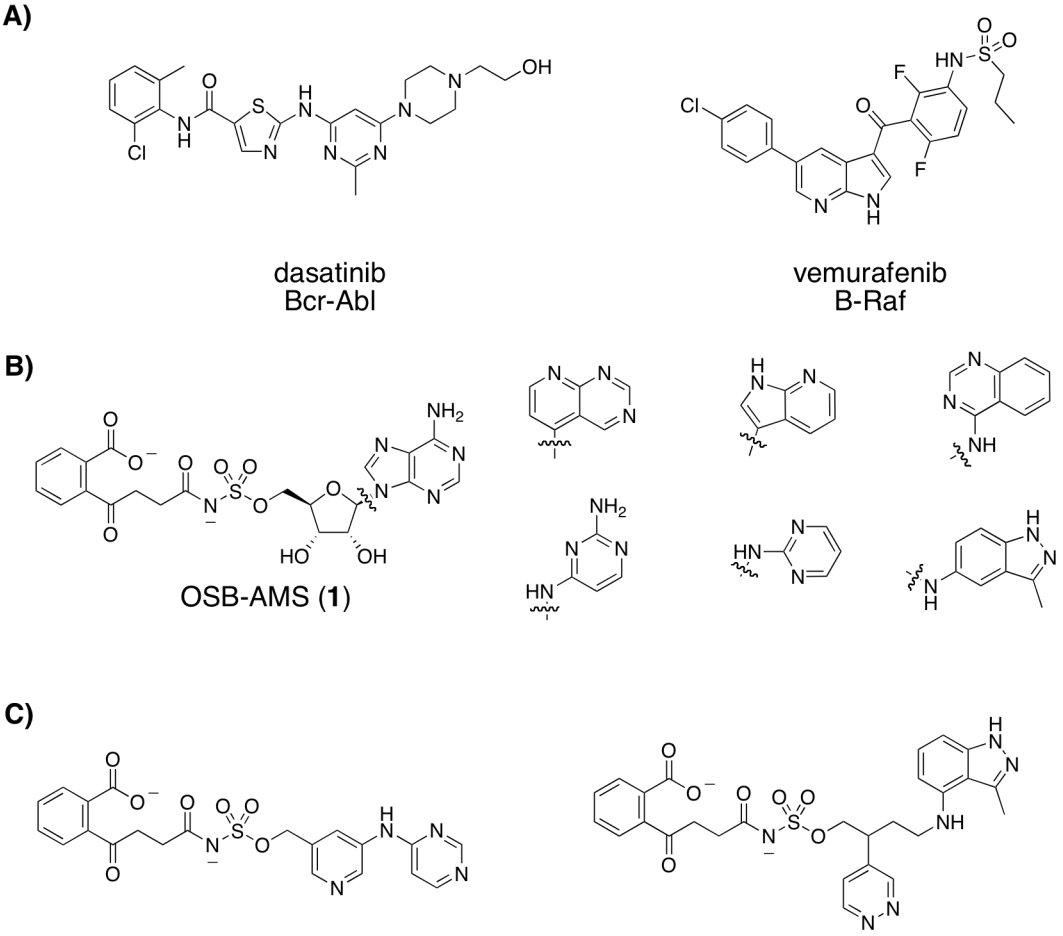

Figure 5.5. Modification of the OSB-AMS adenosine region A) Examples of approved kinase inhibitors B) Examples of substitutions for the adenine region of OSB-AMS. C) Examples of substitutions for the adenosine region of OSB-AMS.

larger variety of aliphatic, aromatic, heteroaromatic, and heterocyclic substituents (Figure 5.5C). Alternatively, the use of automated ligand design as proposed by Professor John Chodera at Memorial Sloan Kettering Cancer Center could generate proposed analogues that might have been overlooked by the *in silico* rational design approach.[11] Once work has been completed in the linker region of the scaffold (Section 5.2.2), the adenosine analogues could easily incorporate bioisosteres from that work into the scaffold to take the place of the current acyl-sulfamate.

Examination of the docking structure of OSB-AMS to MenE (Figure

5.6A) suggests that, as has been seen with kinase inhibitors, future inhibitors could also omit or circumvent the relatively polar ribose binding pocket all together and instead focus on transitioning from the linker region directly into

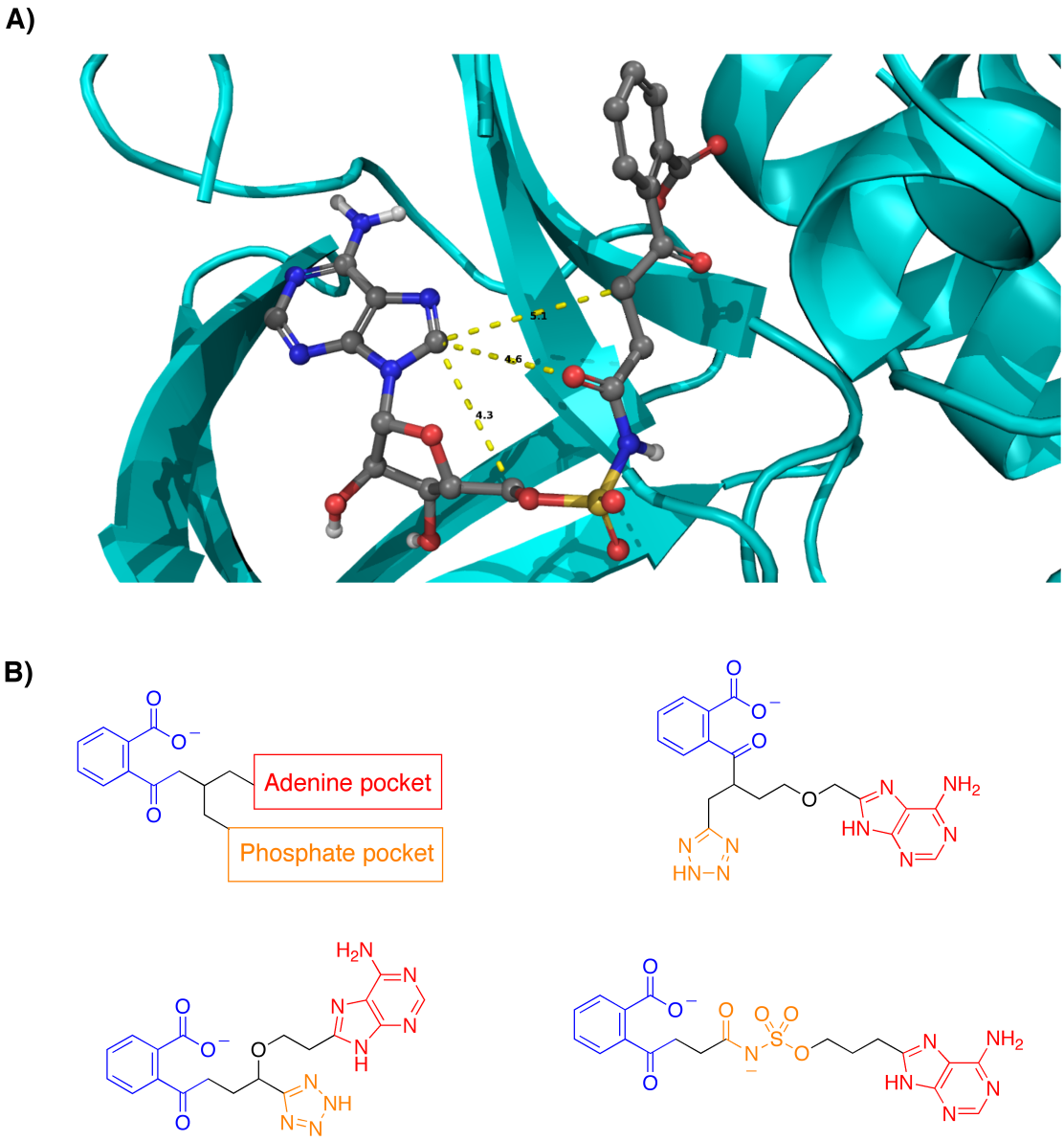

Figure 5.6. Proposed elimination of ribose in MenE inhibitor platform A) OSB-AMS liganded *E. coli* MenE crystal structure with distances between key points. B) Examples of proposed "ribose free" MenE inhibitors.

the adenine binding pocket (Figure 5.6B).[12] There are three key points in the

OSB-AMS scaffold that both present themselves directionally towards the adenine ring and are in close proximity. While these analogues would lose favorable hydrogen bonding interactions present in the ribose binding pocket, the entropic gain through decreased desolvation penalties associated with the polar ribose region may more than compensate for the loss of enthalpic binding in that region. These analogues could also greatly benefit from the work performed in the linker region (Section 5.2.2) to access the optimal bioisostere of the acyl-phosphate, and could then incorporate that structure in the phosphate binding pocket region of the scaffold.

5.2.4 Future Directions: Final words

The work described herein has focused on efforts to optimize the parameters of our current lead MenE inhibitor, OSB-AMS. During our efforts we aimed to increase antimicrobial activity and favorable ADME properties while reducing the toxicological liability inherent in the scaffold. We have garnered important SAR about our scaffold through exemplary studies, which include: the keto-acid/lactol equilibrium of the OSB scaffold, the elucidation of the difluoroindanediol and its antimicrobial activity, and exploration of the linker region of OSB-AMS. Future work will focus on exploration of the SAR around the three key areas of the OSB-AMS scaffold, while attempting to optimize a variety of physiochemical and physiological properties. Ultimately, this research will address and optimized inhibitor of MenE with high selectivity that can someday be used to treat patients suffering from antibiotic-resistant bacterial infections.

5.3 References

1. Matarlo, J. S.; Lu, Y.; Daryaee, F.; Daryaee, T.; Ruzsicska, B.; Walker, S. G.; Tonge, P. J., "A methyl 4-Oxo-4-phenylbut-2-enoate with in vivo activity against MRSA that inhibits MenB in the bacterial menaquinone biosynthesis pathway." *ACS Infect. Dis.* **2016,** *2*, 329–340.

2. Evans, C. E.; Matarlo, J. S.; Tonge, P. J.; Tan, D. S., "Stereoselective synthesis, docking, and biological evaluation of difluoroindanediol-based MenE inhibitors as antibiotics." *Org. Lett.* **2016**, 6384–6387.

3. Matarlo, J. S.; Evans, C. E.; Sharma, I.; Lavaud, L. J.; Ngo, S. C.; Shek, R.; Rajashankar, K. R.; French, J. B.; Tan, D. S.; Tonge, P. J., "Mechanism of MenE inhibition by acyl-adenylate analogues and discovery of novel antibacterial agents." *Biochemistry* **2015,** *54*, 6514–6524.

4. Lu, X.; Zhang, H.; Tonge, P. J.; Tan, D. S., "Mechanism-based inhibitors of MenE, an acyl-CoA synthetase involved in bacterial menaquinone biosynthesis." *Bioorg. Med. Chem. Lett.* **2008,** *18*, 5963–5966.

5. Shan, D.; Nicolaou, M. G.; Borchardt, R. T.; Wang, B., "Prodrug strategies based on intramolecular cyclization reactions." *J. Pharm. Sci. 86*, 765–767.

6. Kevin, B.; Robert, W.; Iain, G.; Kevin, D., "Design of ester prodrugs to enhance oral absorption of poorly permeable compounds: challenges to the discovery scientist." *Curr. Drug Metab.* **2003,** *4*, 461–485.

7. Yuan, L.; Binghe, W., "Substituted coumarins as esterase-sensitive prodrug moieties with improved release rates." *Bioorg. Med. Chem. Lett.* **1999,** *9*, 1795–1800.

8. Maag, H., "Prodrugs of carboxylic acids." In *Prodrugs: Challenges and Rewards Part 1*, Stella, V. J.; Borchardt, R. T.; Hageman, M. J.; Oliyai, R.; Maag, H.; Tilley, J. W., Eds. Springer New York: New York, NY, 2007; pp 703–729.

9. Dar, C. A. S., M. Kevan, "The evolution of protein kinase inhibitors from antagonists to agonists of cellular signaling." *Annu. Rev. Biochem* **2011,** *80*, 769–795.

10. Roskoski, R., "Classification of small molecule protein kinase inhibitors based upon the structures of their drug-enzyme complexes." *Pharmacol. Res.* **2016,** *103*, 26-48.

11. Nilmeier, J. P.; Crooks, G. E.; Minh, D. D. L.; Chodera, J. D., "Nonequilibrium candidate Monte Carlo is an efficient tool for equilibrium simulation." *Proc. Natl. Acad. Sci.* **2011,** *108*, E1009–E1018.

12. Zhang, J.; Yang, P. L.; Gray, N. S., "Targeting cancer with small molecule kinase inhibitors." *Nat. Rev. Cancer* **2009,** *9*, 28–39.